SEISMIC CHARACTERISITION OF FLUID LEAKAGE IN MARINE SEDIMENTS

Muhammad Iqbal Hajana

Submitted in partial fulfilment of the requirements for the degree of Ph.D.

Cardiff University

April 2015

DECLARATION OF WORK

This work has not been submitted in substance for any other degree or award at this or any other university or place of learning, nor is being submitted concurrently in candidature for any degree or other award.

Signed …… (candidate) Date ……

STATEMENT 1

This thesis is being submitted in partial fulfilment of the requirements for the degree of ……(insert MCh, MD, MPhil, PhD etc., as appropriate)

Signed …… (candidate) Date ……

STATEMENT 2

This thesis is the result of my own independent work/investigation, except where otherwise stated.

Other sources are acknowledged by explicit references. The views expressed are my own.

Signed …… (candidate) Date ……

STATEMENT 3

I hereby give consent for my thesis, if accepted, to be available for photocopying and for inter-library loan, and for the title and summary to be made available to outside organisations.

Signed …… (candidate) Date ……

STATEMENT 4: PREVIOUSLY APPROVED BAR ON ACCESS

I hereby give consent for my thesis, if accepted, to be available for photocopying and for inter-library loans **after expiry of a bar on access previously approved by the Academic Standards & Quality Committee.**

Signed …… (candidate) Date

……

Acknowledgements

First of all I am greatful to the Almighty Allah who enabled me to accomplish and present this research work. No expression, verbal or written can truly interpret and acknowledge the tremendous amount of debt of feelings that I have for my research supervisor, family, friends, lab fellows and support of a great number of people who, directly or indirectly, helped me during this project.

I have no words to extend thanks to my research main supervisor Dr. Joe A. Cartwright who provided me a lucky chance to undertake this PhD research project under his excellent supervision overwhelmed with his stern subject knowledge, enormous support and invaluable guidance. Special thanks go to Cardiff University and Caprocks Project for partially funding the project.

I include my mother among the galaxy of my teachers. However, I am truly out of words to acknowledge her love, guidance and prayers. My humble love goes for my father Late Sahib Khan Hajana though, he is not alive but whatever I am today is because of him and my mother who has been a great inspiration and symbol of love for me. Thanks Amma for providing me a chance to follow my choices and ambitions in life. I believe whatever I achieved in life is due to her love, sacrifices, endless prayers, optimism and continuous support through all of my life particularly during the hardest times along my PhD.

My deepest gratitude goes to my wife Nazia Rafiq; she has always being encouraging, considerate and accommodating in the last four years. It is all because of her prayers and moral support that I could complete my work. I am thankful to her for being with me during all the ups and downs of life. I am also thankful to my son Ali Sahib who patiently bore my absence and parental lapses since his birth for my studies sake. Furthermore a mention goes for my sister for her good wishes and love.

At Cardiff University I would like to thank Gwen for her technical support and other members of the 3D Lab with particular Martino, Duarte, Aldina, Usman, Daniel, Ben, Chris[2], Hamood, Oluchi, Pete, Ana and Davide for their cooperation, valuable interactions and academic help.

I would like to extend special thanks to my friend Daniel Currather, Kamal and Tuvie for their unconditional technical and moral support for proof reading my thesis. Furthermore I would like to acknowledge the concerns and motivation by one of my friend from Pakistan for cheering me up and keeping a continuous inquiry related to my work.

In the end I must say sincerity has its own ways of assurance. Nevertheless, I am forever grateful to God, my parents, my supervisor, family and friends for the enormous amount of support and love they have given me.

ABSTRACT

Hydrocarbon migration is one of the key processes that takes place in the development of a successful petroleum system. Understanding when fluids migrated, how they migrated and which routes they took either into primary reservoirs or via transient seals into shallow reservoirs is paramount for successful extraction. Fluids in the sub-surface can be imaged in seismic reflection data as anomalously high reflection amplitudes owing to their contrasting acoustic properties (density and p-wave velocity) with sedimentary rocks. This thesis uses 3-Dimensional seismic reflection data from the Møre Basin, offshore mid-Norway and the Lower Congo Basin, West African margin to investigate the migration of fluids from primary reservoir intervals through overlying successions of fine-grained sediments. These shallow intervals are typically considered as regional seal layers and understanding how seals were breached and fluids migrate through them is vital to risking exploration targets.

The Møre Basin case study investigates a gas-associated amplitude anomaly at the crest of a domal structure cored with alternating fine-grained biosiliceous and calcareous ooze sediments. The anomaly has a rather unique convex-upward basal contact which is explained by the superposition of lateral velocity variations through the gas-filled dome. The centre of the dome has more gas than the flanks resulting in a lower velocity which pushes the basal contact to deeper positions with respect to the flanks. The domal trap was charged from gas migrating from depth via capillary entry pressure and possibly via sub-vertical pathways created by compaction-derived polygonal faults which pervasively deform the host stratigraphy.

The Lower Congo case study investigates a range of high-amplitude seismic amplitude anomalies in a thick sequence of hemipelagites (the waste zone) above a deep-seated turbidite reservoir. Anomalies take many forms and include; Linear anomalies, Sub-circular anomalies, Patchy anomalies at which finger-shaped anomalies emanate from their lateral edges, and Discrete filamental anomalies. The Sub-circular and Patchy anomalies were interpreted as being related to the presence of hydrocarbons. Detailed analysis of a sub-set of the hydrocarbon-bearing amplitude anomalies suggest leakage occurred through two means; 1) vertical leakage through feeders and 2) via deep-seated extensional faults formed during gravity-driven gliding of

an underlying salt detachment. Vertical leakage is expressed in the form of Vertical Anomaly Clusters which comprise vertically stacked assemblages of high-amplitude anomalies.

A common aspect of the two case studies are that high-amplitude anomalies within fine-grained sedimentary successions are linked to vertical or sub-vertical migration pathways provided either by faults or pipe-like structures formed during overpressure. These results have implications for our understanding of how seals are breached when reservoirs are overpressured.

Table of Contents

Table of Contents

Table of Contents

Table of Contents

Table of Contents

Table of Contents

Table of Contents

Table of Contents

Table of Contents

Table of Contents

Table of figures

Table of figures

Table of figures

Table of figures

Table of figures

Table of figures

Table of figures

Table of figures

Table of figures

Table of figures

Table of figures

Table of figures

Table of figures

Table of figures

Table of figures

Table of figures

Table of figures

Table of figures

Table of figures

Table of figures

Table of figures

Table of figures

Table of figures

Table of figures

Table of figures

CHAPTER 1

Introduction

CHAPTER ONE

1.1 Rationale

High Amplitude Anomalies (HAAs) are any abrupt increase of seismic amplitude that contrasts with the background amplitude. HAAs can represent the presence of hydrocarbons, processing artifacts, geometric/velocity focusing and/or changes in lithology (Hovland and Judd, 1988; Cartwright et al., 2007; Huuse et al., 2010). Amplitude anomalies that indicate the presence of hydrocarbons are referred to as Direct Hydrocarbon Indicators (DHIs) and commonly take the form of flat spots, bright spots, dim spots, velocity push downs and zones of seismic blanking. They reveal sharp variations in acoustic impedance of subsurface strata, such as when gas-saturated sand underlies shale. High amplitude anomalies such as bright-spots, dim-spots and polarity reversals/shifts can represent different degrees of fluid flux reflecting fluid migration pathways in the subsurface (Berndt, 2005; Cartwright *et al.*, 2007; Gay *et al.*, 2007). Fluid-flow anomalies are generated during past and present subsurface fluid migration (e.g. Cartwright et al., 2007; Løseth et al., 2009). The occurrence of high amplitude anomalies (HAAs) is controlled by the geological setting and the nature of the host lithology (Andresen, 2012)

Evidence of fluid flow can also exist in the form of pockmarks, pipes, gas chimneys, gas hydrates, sediments injections, carbonate mounds, seeps, mud volcanoes, volcanic sills, and related diagenetic phenomena (Cartwright *et al.*, 2007; Løseth *et al.*, 2009; Weibull *et al.*, 2010; Andresen & Huuse, 2011; Andresen *et al.*, 2011; Andresen, 2012; Ho *et al.*, 2012). These acoustic expressions on seismic data are related to the mode of fluid escape/expulsion. Their seismic expression is closely related to their provenance, source of fluid, flow type,

structural setting and nature of the host sediment (Van Rensbergen & Morley, 2003; Cartwright *et al.*, 2007; Huuse *et al.*, 2010).

The question of how the fluid evolves from the immediate subsurface over time i.e. migration phenomena has only rarely been addressed and requires further work in order to improve our understanding of fluid leakage and migration in sedimentary basins. Hence, the study of high amplitude anomalies and other focussed fluid flow is imperative in basin analysis, especially for understanding petroleum systems, trapping and leaking mechanisms (Andresen, 2012). Ever since the first observation and recognition of focused fluid flow features by Newsom (1903) and King and MacLean (1970), the interest of exploration and production companies has amplified in the past decades due to growing quality of 3D seismic data and the realization of the impact of fluid flow features on hydrocarbon plumbing systems (Cartwright *et al.*, 2007; Huuse *et al.*, 2010). The relationship of hydrocarbon leakage flux to different leakage indicators and sedimentary structures has become an increasingly popular research theme in the last few decades (*cf.* Hovland, 1981b; Heggland, 1997; Roberts, 2001; Gay et al., 2003; Cartwright et al., 2007). Apart from the impact on hydrocarbon plumbing systems, the occurrence of fluid flow features may also have implications for the extraction of groundwater, geothermal energy, storage of CO_2 and nuclear waste, and global organic carbon cycle of the Earth (Andresen, 2012).

The migration of hydrocarbons through fine-grained sediments is still not well understood and many questions remain unanswered because of the high number of uncertainties to reproduce and understand the phenomena in deep basins and reservoirs. The main aims of this research are to provide a detailed description of the fluid systems and propose some fluid flow mechanisms that can justify the position of the gas in the analysed basins and improve the

knowledge about how fluid flows in fine-grained sediments in the deep marine basins and delineate new fluid flow feature that are observable on seismic scale.

1.2 Overview

A succinct review of literature is provided as to what DHI's are, their detection and recognition on seismic data, their mode of formation and examples from different sedimentary basins and geologic settings. The aim of this section is to review what is known on (DHI's) and how they are expressed in seismic data. The key objectives of the review are as follows;

1. To undertake a detailed study of different types of DHIs and highlight the analytical capabilities of high amplitude anomalies in the context of this research.
2. To describe the geological setting and host lithology in which DHIs are developed.
3. To describe geophysical expression of DHIs.
4. To provide an overview of fluid flow processes in the context of reservoir seal failure and secondary migration phenomenology.
5. To outline the pitfalls in DHI interpretation.
6. To discuss how DHIs can be validated.

1.2.1 Direct hydrocarbon indicators

Direct hydrocarbon indicators are seismic amplitude anomalies, seismic events or characteristics of seismic data by which presence and/or absence of hydrocarbon accumulation can be interpreted (Brown, 2004). These indicators include amplitude anomalies (bright or dim spot), phase change, flat spot, frequency attenuation, velocity anomalies (pull up or push down), variations of amplitude vs. offset and S-wave or P/S waves ratio (Brown *et*

al., 1984; Enachescu, 1990; Brown, 2004). About Eighty percent (80%) of petroleum found in deep water (500–2000 meters) have some sort of DHI associated with them (Brown, 2004; Weimer & Slatt, 2004; Arntsen *et al.*, 2007; Frey-Martnez *et al.*, 2007; Andresen *et al.*, 2011; Foschi *et al.*, 2014).

DHIs on seismic data are directly related to the presence of hydrocarbons and changes in both compressibility (bulk modulus) and density resulting from the substitution of pore fluid by hydrocarbons. Direct hydrocarbon detection is direct in the real sense; it relies on the identification of acoustic contrasts associated with the presence of hydrocarbons. Careful interpretation and analysis is required in order to validate DHIs. Because the acoustic response of DHI's, due to presence of hydrocarbons, are dependent on temperature, pressure and lithology of the reservoir, reliable interpretation of DHIs is problematic in the deeper sections of basins. Usually, bright spots can be authentically identified at shallow depths and are helpful in delineation of gas fields. Even though shallow gas fields may not be commercial, these observations may help to mitigate drilling hazards and are an important element of site survey workflows.

Brown (2004), stressed that for DHI validation, true amplitude must be preserved and the wavelet shape should be as close as possible to zero-phase. Two empirical rules are important to keep in mind before interpretation of seismic amplitudes on seismic data; (1) DHIs have a direct relationship with depth, so the effect of the DHI decreases drastically with increasing depth, and (2) DHIs relate primarily to gas in clastic sediments. Therefore; amplitudes associated with presence of gas, contrasts in elastic properties between individual layers from the back ground lithology, that directly depends on the porosity, pore-fluid type and saturation as well as pore pressure (Avseth *et al.*, 2005).

1.2.1.1 Flat spots

A flat spot is a reflection relating to a hydrocarbon contact, usually between gas and water (Fig. 1.1) but occasionally between gas and oil (GOC) or oil and water (OWC). Flat spots are the most direct indicators for the presence of hydrocarbons and are used universally by geophysicists in hydrocarbon exploration to support the case for drilling prospects. Examples of true flat spots (calibrated, uncalibrated but supported by AVO analysis) and pitfalls of interpretation (false flat spots due to diagenesis) are shown in the Fig.1.1, Fig. 1.2 and Fig. 1.3).

A flat spot results from the increase in acoustic impedance when a gas- or oil-filled porous rock (with lower acoustic impedance) overlies a liquid-filled porous rock (with higher acoustic impedance). Flat spots may stand out on a seismic image because it is flat and will contrast with surrounding dipping reflections. The gas-liquid contact is always a positive reflection and is an excellent reflection for assessing the phase of any seismic data (Brown, 2005).

In the case of dynamic flow, the hydrocarbon fluid contact can be inclined and/or irregular. Flat spots are generated by the acoustic impedance contrast over fluid contacts. They are not only restricted to siliciclastic deposits, but also other lithologies like limestone. It is perfectly possible to have a flat spot in a homogeneous carbonate reservoir as the difference between gas and water can generate sufficient acoustic contrast (Fig. 1.4). In such cases, the background velocity and density values are relatively high compared to presence of hydrocarbon.

Flat spots are not necessarily always flat; a gas-liquid contact need not necessarily be either flat or horizontal in time. For example, tilted hydrocarbon contacts can be related to

compartmentalisation by minor faults or may be related to changes in permeability, of the host sediments. Hydrodynamic conditions can result in tilted contacts (groundwater flow due to differences in pressure) (Dennis *et al.*, 2000; Dennis *et al.*, 2005), dynamic filling (where the fluid phase migrating has not reached equilibrium based on buoyancy and regional pressure) can also result in irregular fluid contacts (Brown, 2005; Chadwick *et al.*, 2005). In addition, many flat spots may be reflected as a sloping contact in time sections but on applying the correct depth conversion will become flat. The critical parameters determining the reflection on the gas/oil-water contact are the velocities and densities of the different lithological units.

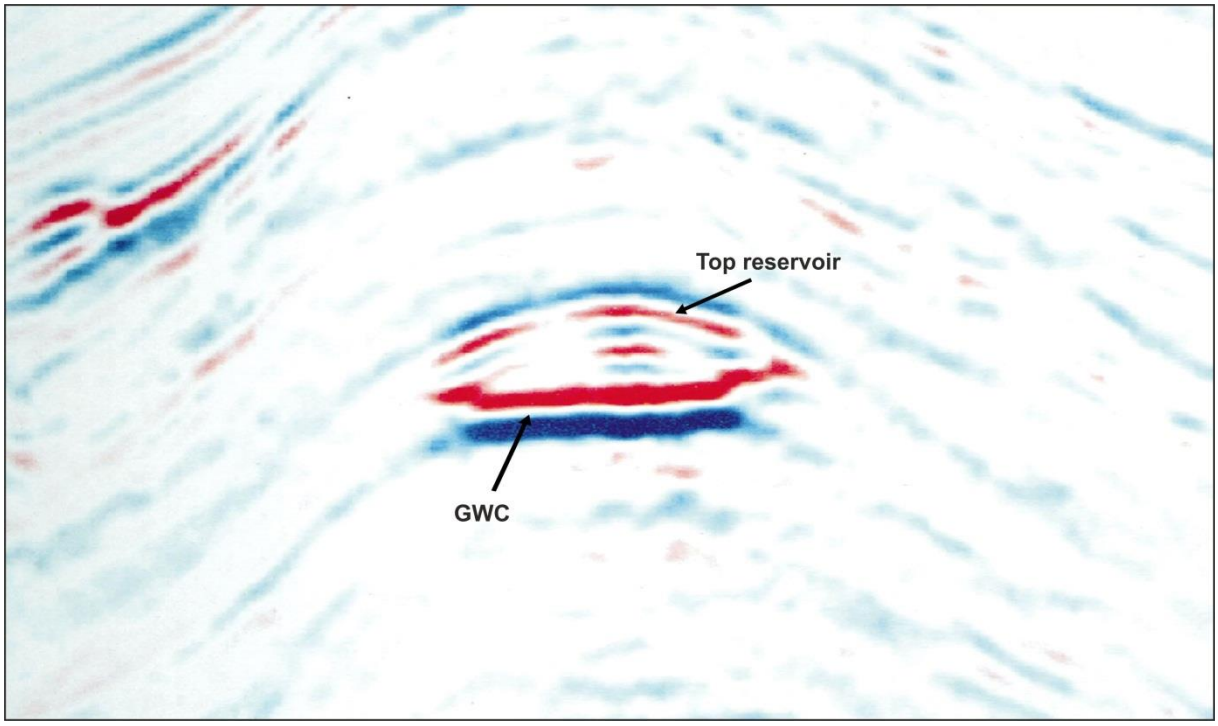

Figure 1.1: Flat spot seen on 900 phase seismic data from the Gulf of Mexico. The 900 phase display can be inferred from the approximately equal energy (amplitude) seen in the red and blue loops. Flat spot is developed at the anticline crest, GWC= gas water contact. Scale is not available (Brown, 2001).

For example, if there is gas instead of water in a rock, the velocity will be considerably reduced. The velocity of a sound wave in gas is typically much lower than it is in liquid, depending on the composition; temperature and pressure (Knight *et al.*, 1998). The boundary between gas-bearing and water-bearing rocks may produce a strong reflection because there is a large difference in impedance between the two layers. For this reason the boundary between gas/water and oil/water is often revealed as a strong reflection because it is close to horizontal and does not lie concordant to reflections from strata (Yilmaz & Doherty, 1987; Brown, 2004; Løseth *et al.*, 2009; Foschi *et al.*, 2014).

The gas/water contact (GWC) is positioned at the zero crossing between these two loops). the top reservoir reflection softens down flank into the water leg. The subtle staircase-like geometry of the GWC reflection as it approaches the top reservoir contact on both flanks is probably due to tuning and interference, but could be due to internal layering within the reservoir package.

Brown (2004) strongly recommends that interpreters assess the phase of their seismic data using reflections from the seabed and from any GWCs. During interpretation of flat spot, (Fig. 1.2) then there is mandatory to judge phase of seismic data.

Flat spots often are not developed as single feature. In some cases, particularly for anticlinal structures, flat spots may be interpreted at different levels of the anticline. For example, a series of structurally-confined flat spots are associated with anticlines from a deep water basin offshore Cyprus (Fig.1.3). Four flat spots can be identified at different stratigraphic positions and with different degrees of confidence. The non-horizontal attitude of these flat spots can be caused by a tilted seabed towards the east direction. Amplitude anomalies observed at the top of anticline are interpreted as leakage from the main reservoir. HAAs above the structure had are associated with a flat spot that helps to validate the presence of hydrocarbon in the structure.

Furthermore, flat spots are not always developed as a single feature on hydrocarbon-water contact. A series of GWCs due to presence of minor gas accumulations (under filled traps) observed from the Eastern Mediterranean (Fig.1.4). Deep water sand-dominated fans on the top of a structure (hence some of the gaps between the amplified reflections). It is interpreted as a several gas accumulations, sealed by deep water claystones. There is a HAA above the flat spot that indicates minor leakage in overlying sediments. The traps are defined by a major erosional surface. The GWC for different traps are at different levels. Although the GWC appears tilted here, this is due to the tilt of the seabed (not seen here). The tilted seabed produces a tilt in a geologically horizontal surface due to the display in the time domain. Depth conversion is therefore essential for the best interpretation of hydrocarbon-water contacts.

Flat spots can be easy to recognise on seismic data in areas where background stratigraphy is tilted (Avseth *et al.*, 2005). Flat spots stands out from strata but it is difficult to detect a flat spot when the stratigraphy is more or less horizontal (Fig.1.3 and Fig.1.4). Quantitative

methods like AVO analysis can help to discriminate between fluid-related flat spots and flat-lying stratigraphy.

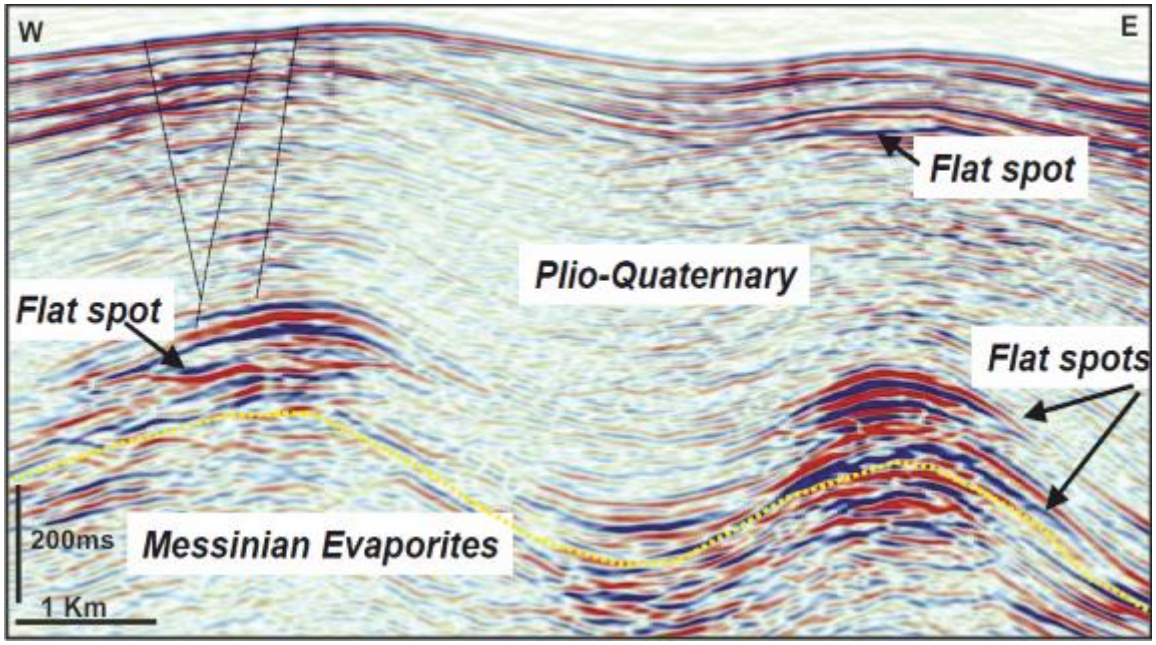

Figure 1.2:A series of flat spots developed at different levels of the crest of anticlinal structures from a deep water basin from offshore Cyprus (http://www.mcit.gov.cy).

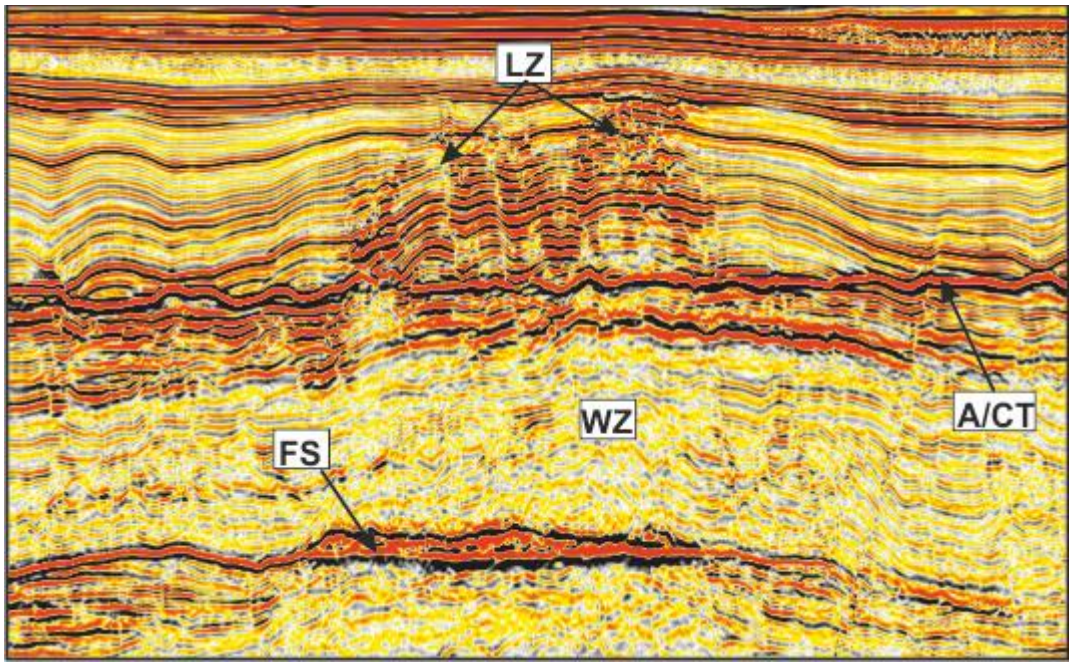

Figure 1.3: NW-SE seismic profile showing a 6 km long flat spot confined by an anticline. Leakage above the flat spot is revealed as cluster of high amplitude anomalies. Blanking of seismic reflection below the cluster of high amplitude anomalies is due to presence of gas in the strata (confidential data). FS: Flat spot, LZ: leakage zone. WZ: wipe out zone and A/CT: Opal A to CT boundary.

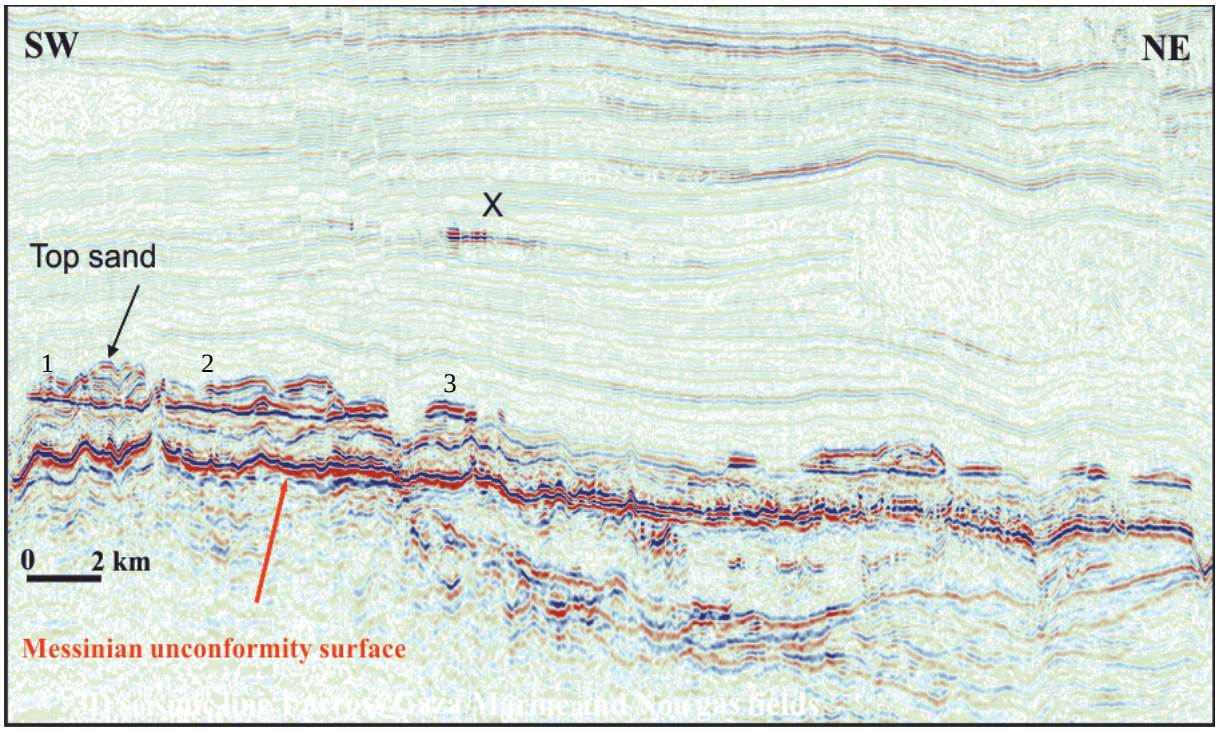

Figure 1.4: Series of GWC related to minor gas accumulations (under filled traps) from the Eastern Mediterranean. There are some minor leakages at point X (Modified after Frey-Martnez et al., 2007).

The flat spot surface does not always have to be a flat. In many cases it is titled due to factors such as hydrodynamics, water flow, and tilted structures. There are many examples of flat spot anomalies from different basins in the Barents Sea (Fig.1.5). Two anomalies have been drilled resulting in one success and one false positive due to amorphous silica transformation. The third anomaly is a potential prospect to drill in the future (Selnes *et al.*, 2013).

Another example (Fig.1.6) shows that the recognition of flat spots can be an aid to interpretation of mounded structures and delineation of high N/G intervals in those mounds (Frey-Martnez *et al.*, 2007). The two mounded structures are delimited here by a relatively concordant, continuous, and flat-lying lower boundary and by a convex-upward and discontinuous upper boundary (Fig.1.6). The two boundaries correspond to the base and top of the Yafo Sand Member, respectively. The internal parts of the mounded structures show

chaotic seismic reflections in the cores (enclosed by dashed black lines) and more continuous seismic reflections in the flanks and crests (marked X). Note the presence of flat spots crosscutting the flanks and pull-up features underlying the cores of the structures (Fig.1.6). There is a prominent amplitude enhancement of the upper boundary over the crest of both mounds due to gas filling the reservoirs. A high-amplitude anomaly at the top of the mounded structure indicates that the reservoir has leaked into overlying sequence. There is a subtle push down effect where the gas-water contact (GWC) dip inwards towards the core of the mounds from both flanks (Fig.1.7). This arises simply because of the slower velocity in the gas relative to the water leg of the reservoir.

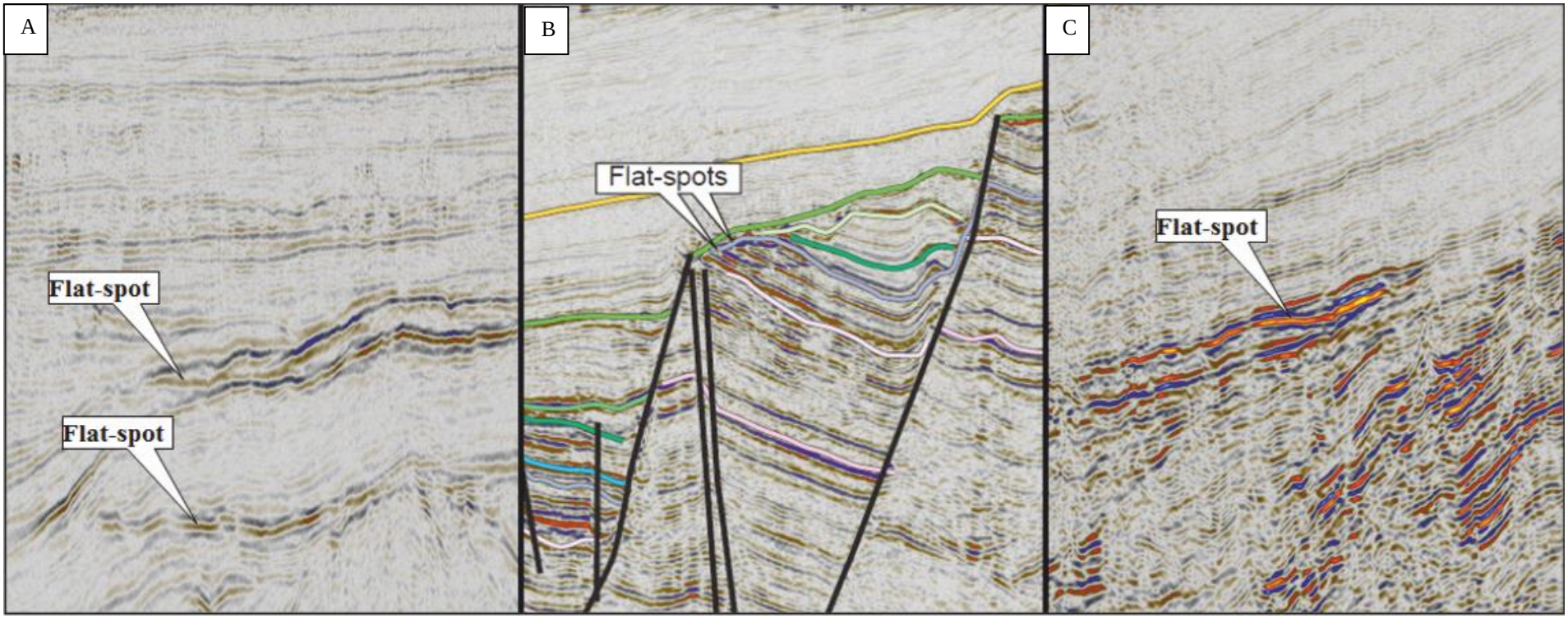

Figure 1.5: A selection of flat spots observed on seismic with different display parameters and potential trap types from the Barents Sea. A) two flat spots are interpreted with distinct features, B) Flat spots developed very close to others bounded by faults on left hand side and C) A flat spot developed at a stratigraphical trap due to pinch-out feature (Selnes *et al.*, 2013)

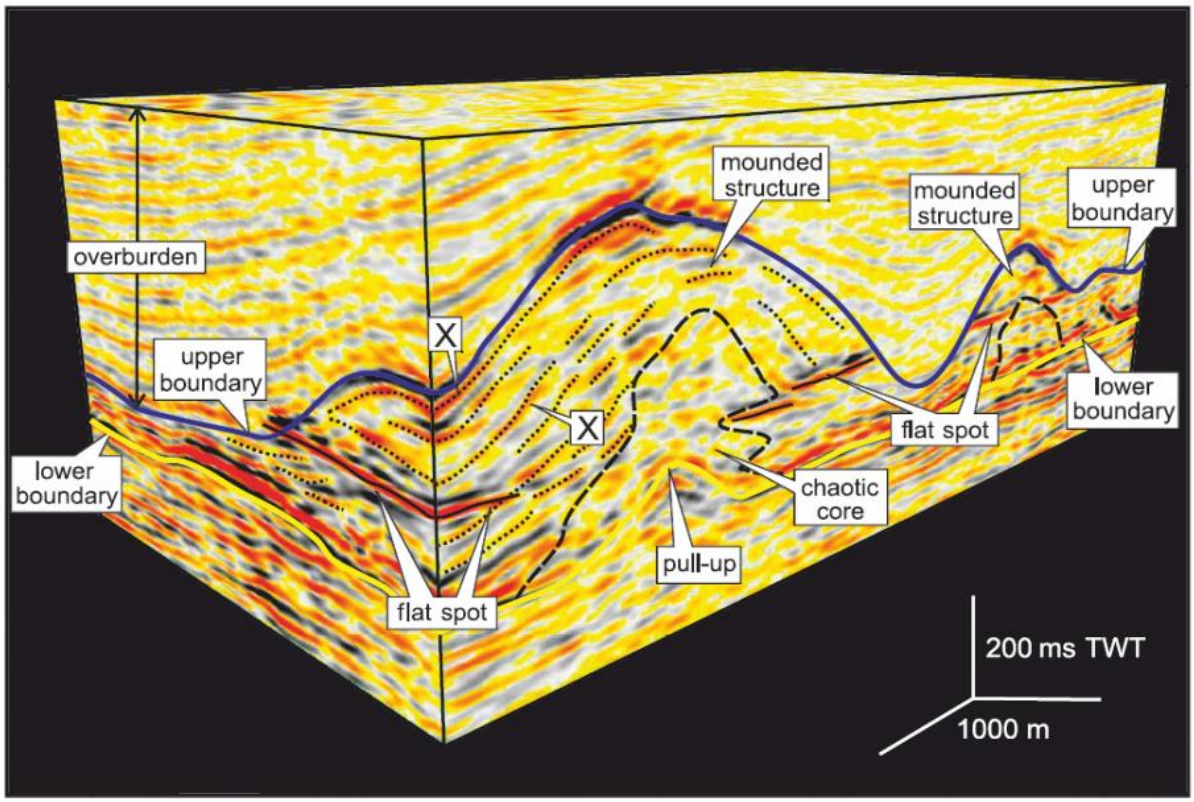

Figure 1.6: Seismic cube from SE Mediterranean displayed here three-dimensional visualization of two representative mounded structures from a Pliocene deep water sand play. Vertical and horizontal scale is 1000m (Frey-Martnez *et al.*, 2007).

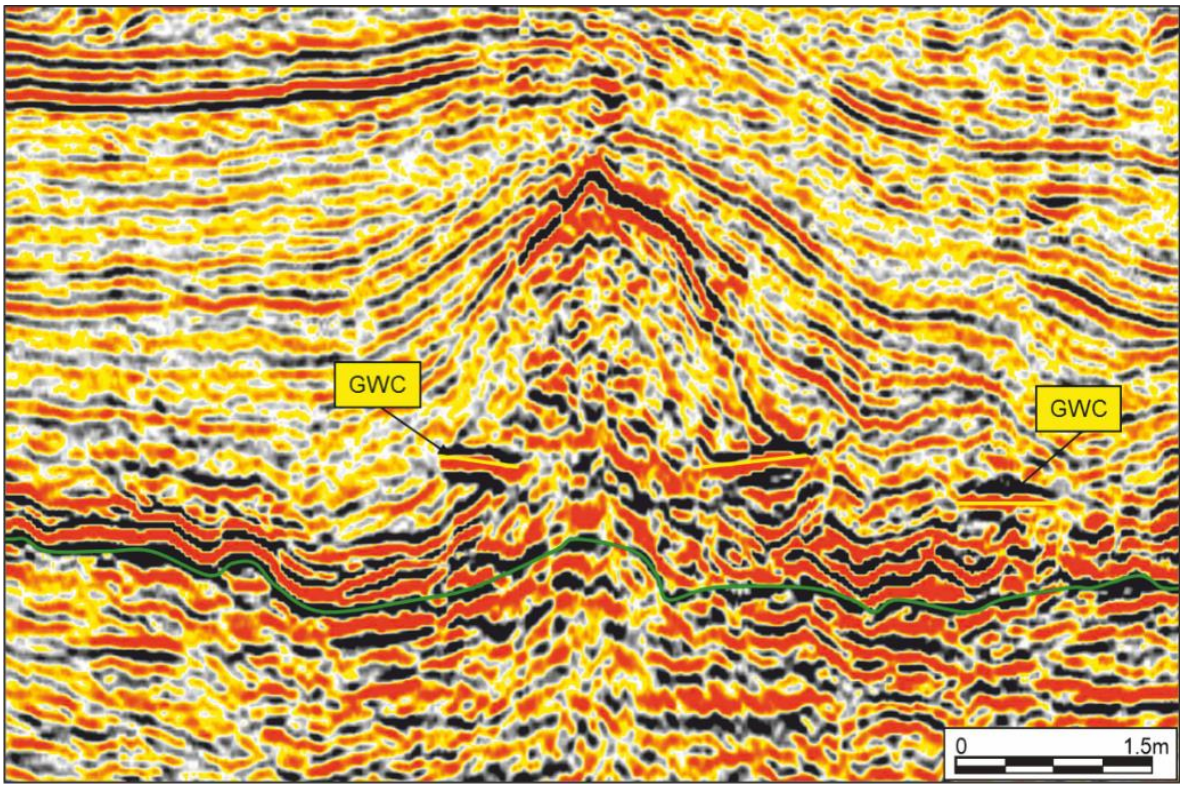

Figure 1.7: Example of interpreted gas-water contact (GWC) as a flat spot from the SE Mediterranean. Seismic profile across the mounds shown in the previous section (modified from Frey Martinez et al. 2007).

1.2.1.2 Pitfalls in flat spot interpretation

Seismic flat spots occur at the reflective boundary between two different types of fluids in a reservoir, gas-oil, gas-water, or oil-water contact (Fig.1.4 and Fig.1.7). They can be easy to detect in areas where the background stratigraphy is tilted, forming cross-cutting seismic events. They are recognisable when the reservoirs are more than twice the seismic tuning thickness and acoustically, relatively soft. This phenomenon is frequently used as a (DHI) in exploring for hydrocarbons. However, one should be aware of several pitfalls when using flat-spots as hydrocarbon indicators. Flat spots can be related to diagenetic events that are depth-/temperature-dependent, such as cross-cutting boundaries of amorphous silica in the form of Opal A and Opal CT and also gas hydrates shown as BSR (Bottom Simulating Reflectors) on seismic data.

The examples in figure 1.8 and figure 1.9 show seismic data where flat spots have been interpreted erroneously as due to hydrocarbons and used as a basis for drilling decisions or other exploration planning. In one example, it was recognised that a possible flat spot/amplitude anomaly might in fact be due to diagenesis and a huge reprocessing effort was instigated to try to differentiate the cause and effect.

The Qulleq well is a classic example (Fig.1.8), where in spite of considerable geophysical analysis; the drilling showed that the flat spot was a false DHI. The well encountered only mudstones in this interval and no gas or oil. Although the nature of the cross-cutting reflection (CCR) is not fully understood, X-ray diffraction analysis suggests that it probably is related to a phase-change transition from Opal-CT to quartz transformation.

Great care has to be taken not to confuse diagenetic effects with true hydrocarbon effects when the diagenetically altered sequence thins to the point where tuning effects kick in. In

this case, a large effort went into reprocessing and quantitative geophysical analysis to discriminate between possible hydrocarbon effects and silica diagenesis (Fig. 1.10). The conclusion was that this amplitude modification was due to tuning and diagenesis in a sequence that was progressively thinning onto a structure (Dart et al. 2010). There are other examples of pseudo flat spots that were previously interpreted as hydrocarbon related flat spots (Fig. 1.11 and Fig. 1.12)

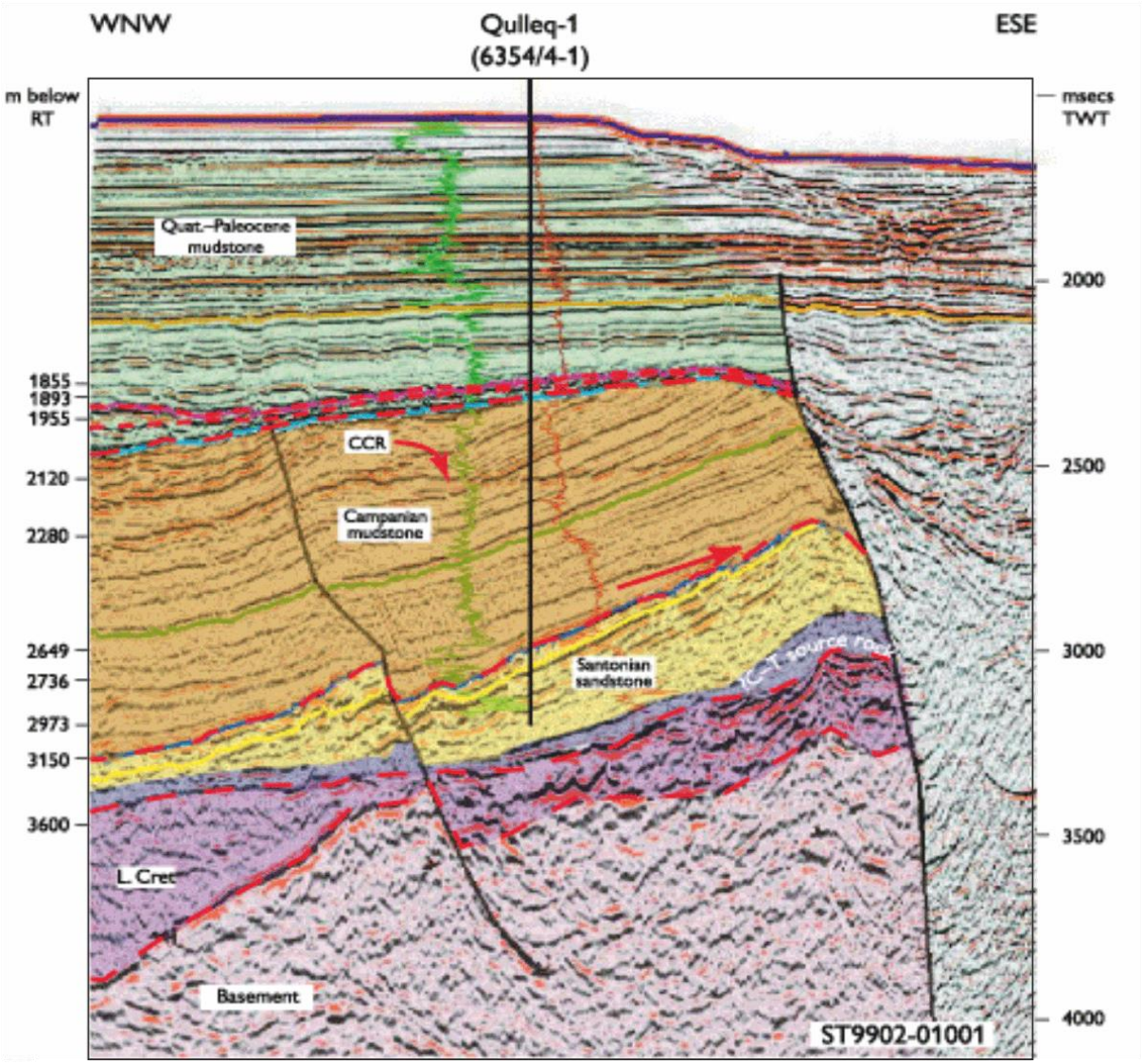

Figure 1.8: The example is from a petroleum exploration borehole drilled in West Greenland. The main target of the Qulleq-1 well was the prominent cross-cutting reflection (CCR) which can be seen on the seismic data around 2550 ms TWTT. Extensive analysis of all data available before drilling (including AVO analysis of the seismic data) suggested that this reflection represented a gas–water contact (from http://www.geus.dk/ghexis/ghexis-19.htm).

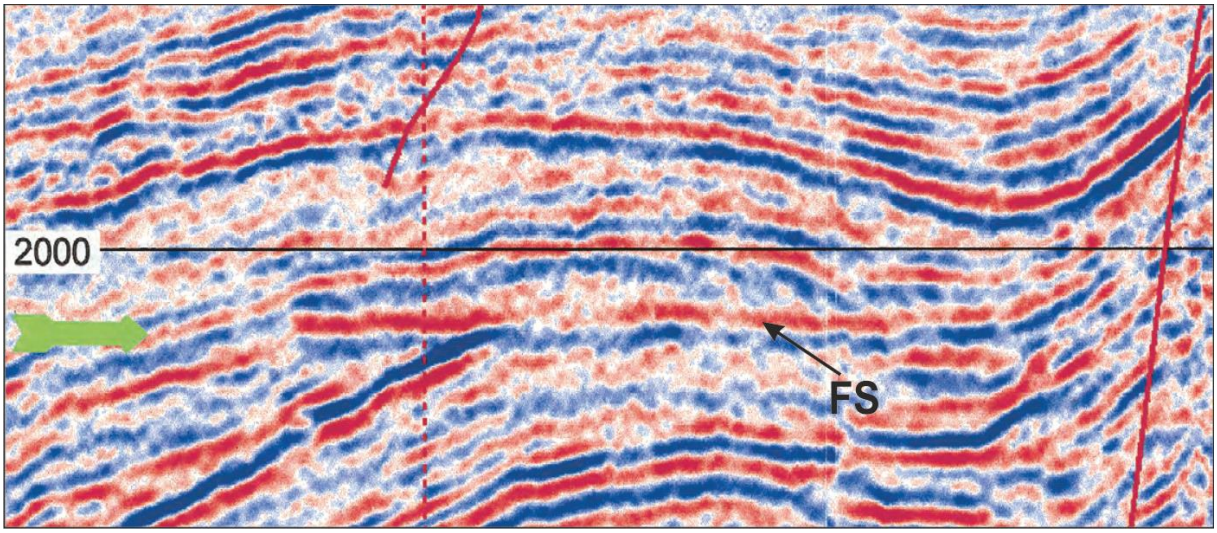

Figure 1.9: A seismic profile shows a flat spot from the Northwest Shelf of Australia. Pre-drilling studies were confirmed as a prospect but the well was dry and the post-mortem report of the well interpreted as a paleo-contact expressing diagenetic effects. (Brown, 2004)

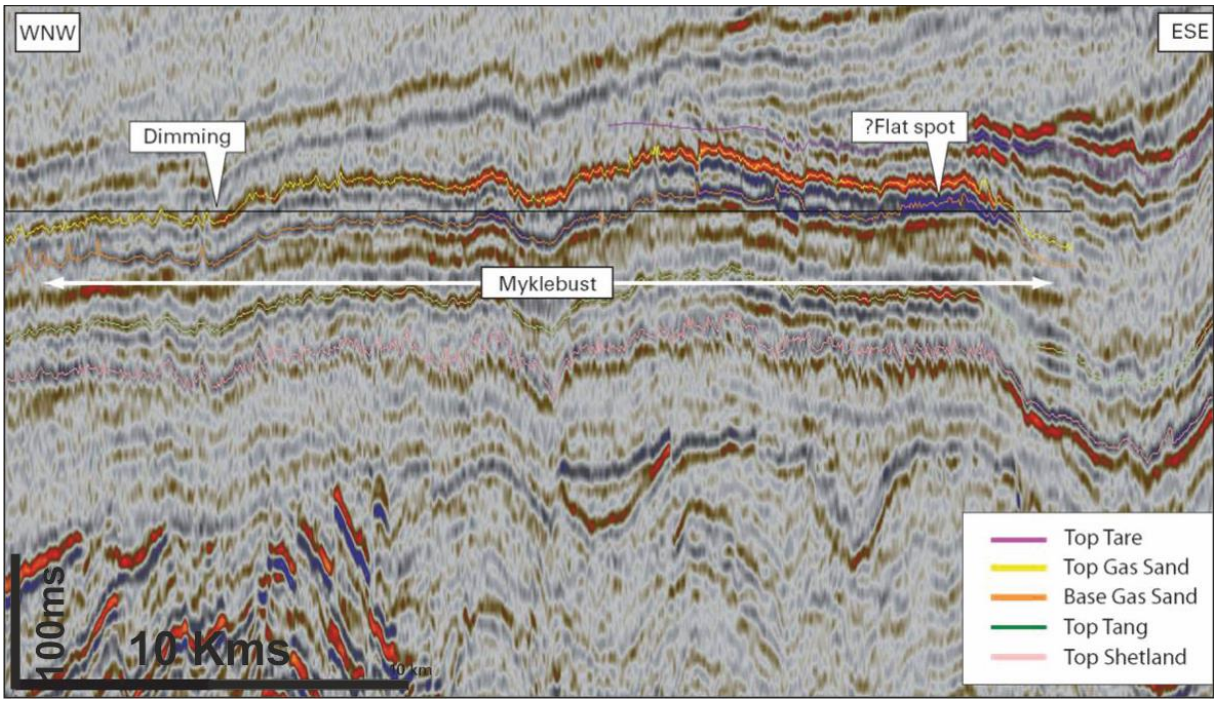

Figure 1.10: A seismic example that was mis-interpreted as a flat spot that developed due to possible hydrocarbon accumulation (Dart et al. 2010)

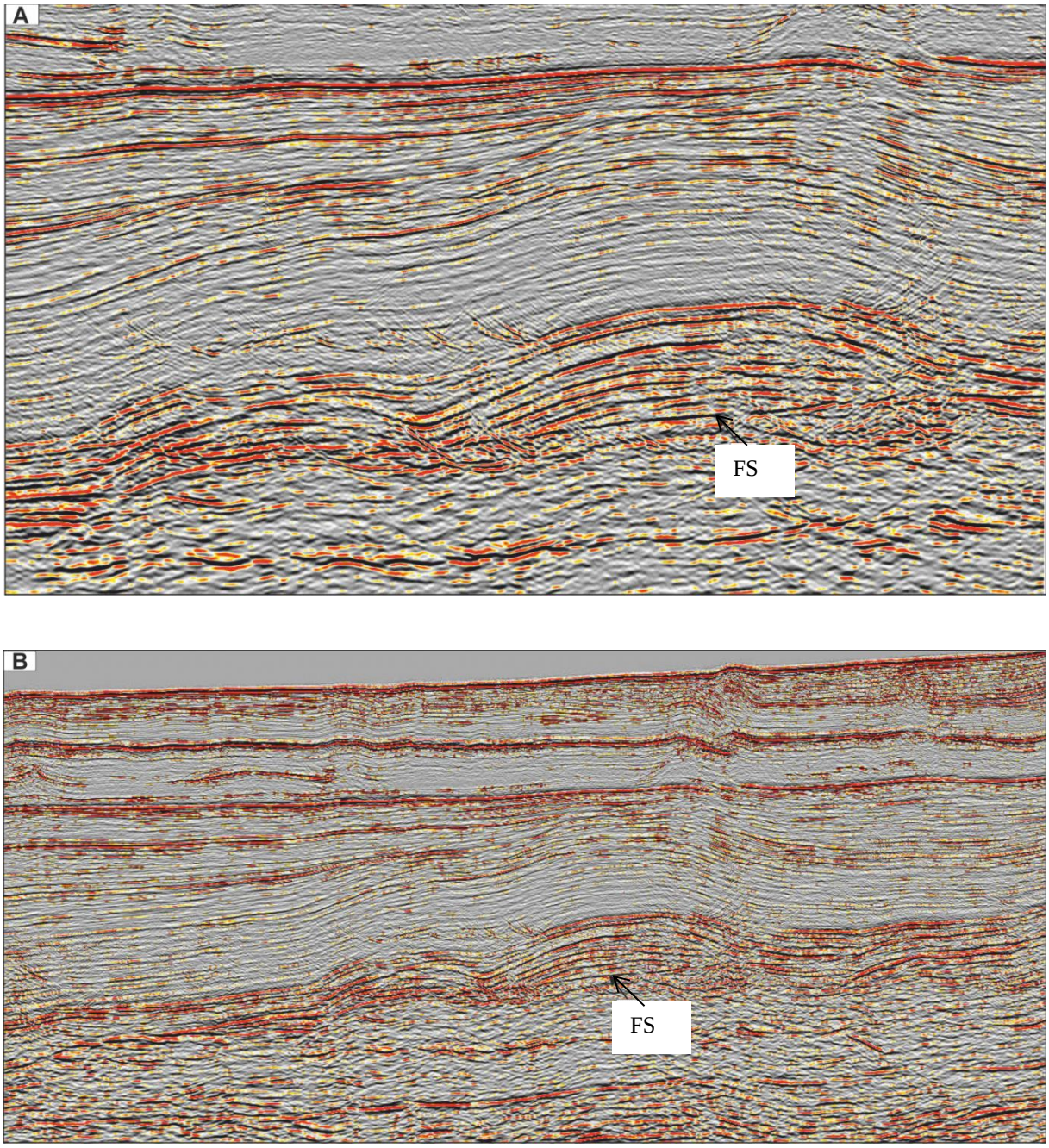

Figure 1.11: There are two seismic profiles (A and B) from same pseudo flat spot (FS) (location and dimensions are not described due to data confidentiality). The features were interpreted as a flat spots but they have the same polarity with seabed.

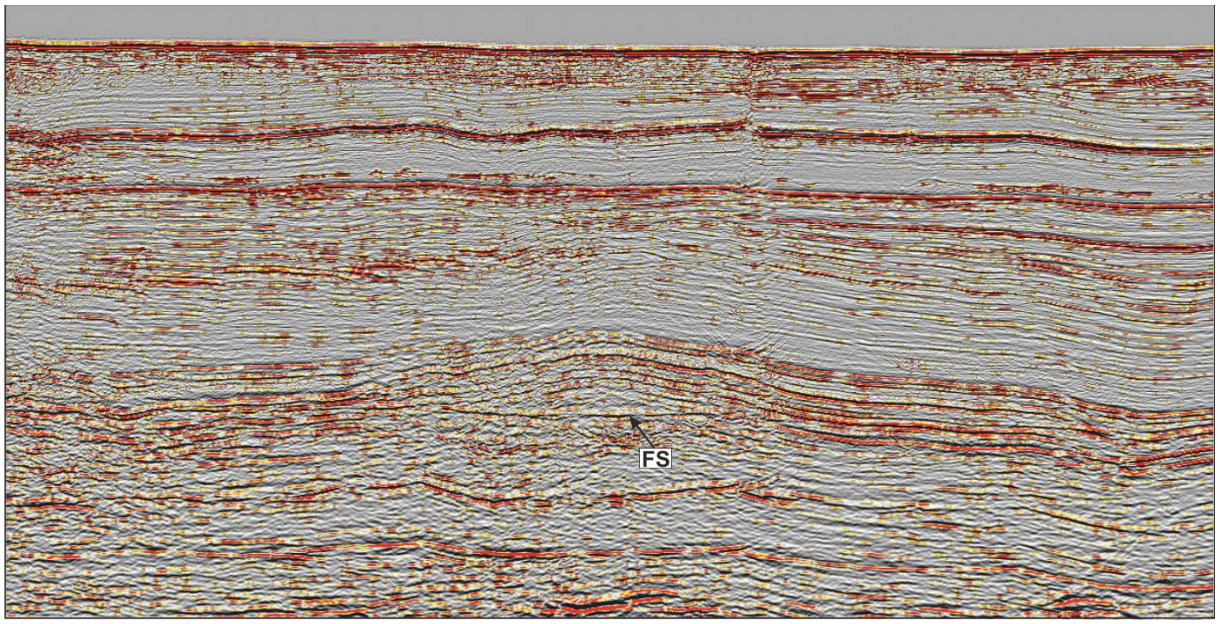

Figure 1.12: Flat spot (FS) is observed on this seismic section. It has the same polarity (hard reflection) as the seabed, but it occurs at almost exactly twice the seabed two way travel time value. Apparently a pushdown effect is also observed below observed flat spot.

1.2.1.3 Summary of flat spot pitfalls

1. The main pitfalls in false flat spot into oil and gas exploration are due to diagenetic boundaries (particularly Opal A-CT-quartz systems).
2. Residual hydrocarbons can also give flat spots.
3. Multiples can occasionally confuse flat spots interpretation.
4. There is not always true that flat spots are developed due to presence of hydrocarbon.

1.2.2 Bright and dim spots

1.2.2.1 Bright spots

A bright spot is interpreted as a local high amplitude anomaly on the seismic reflection data (Fig. 1.13 and Fig. 1.14) that can indicate the presence of hydrocarbons and is therefore known as a DHI. Bright spots were not commonly identified in older vintages of seismic data (pre-1970s). This problem was mainly due to the extensive and industry-wide use of automatic gain control which obscured the amplitude effects of hydrocarbon accumulations (Brown, 2001; Hilterman, 2001; Ren *et al.*, 2006).

A bright spot DHI primarily results from the increase in acoustic impedance contrast when a hydrocarbon (with a lower acoustic impedance) replaces the brine-saturated zone (with a higher acoustic impedance) that underlies a shale (with a higher acoustic impedance still), increasing the reflection coefficient (Fig. 1.15). The effect decreases with depth because compaction for sands and shales occurs at different rates and the acoustic impedance relationship stated above will not hold after a certain depth/age. Beneath this notional depth, there will be a crossover of shale and sand acoustic impedances and a dim spot is more useful to hydrocarbon exploration.

Bright spots are observed at the base of gas hydrate stability zone (BGHS). The upper terminations of high amplitude troughs (red amplitudes) indicate the (BGHS). Some horizons show polarity reversal at the BGHS, below which the pore spaces contain free gas, and above it, frozen hydrates, such as the Blue and Orange horizons (Fig. 1.16).

The relationship between hydrocarbons and direct hydrocarbon indicators such as bright spots is not straightforward and not all bright spots are caused by the presence of hydrocarbons and therefore they should not be treated as conclusive evidence of hydrocarbon accumulations.

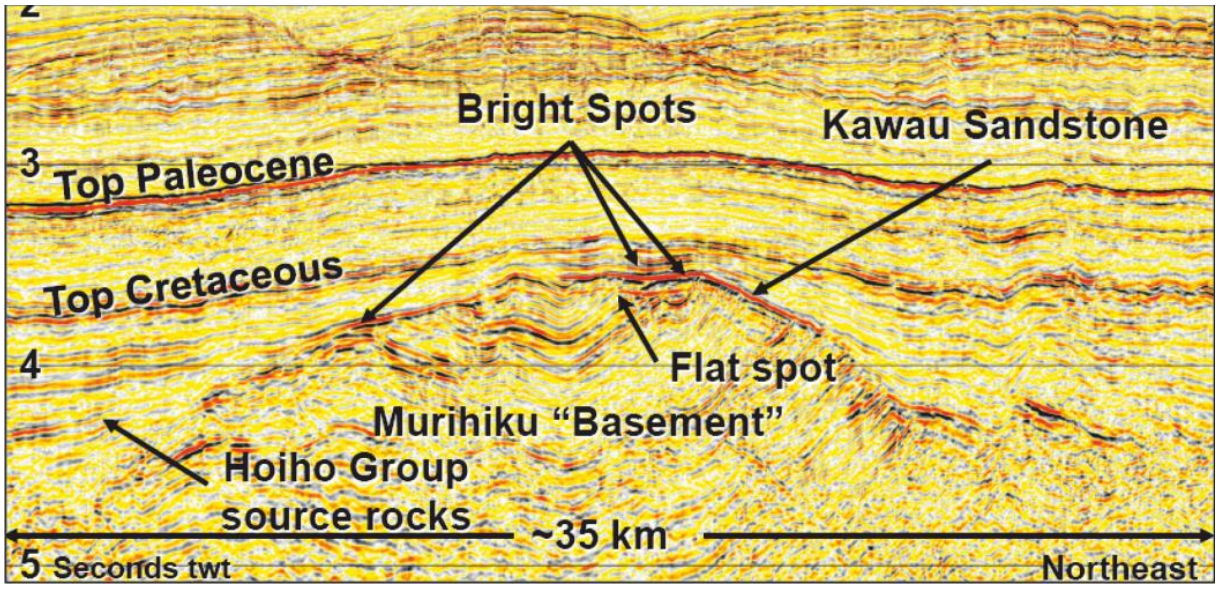

Figure 1.13: The seismic profile shows a bright spot associated with flat spot from South Great Basin, New Zealand. The high amplitude anomaly is developed in the Kawau sand unit of Cretaceous age. The bright spots occur on the crest and flanks of the anticline. These anomalies could be due to tuning, since sequences thin onto the flank and crest of the structure (Geo Expro 2011)

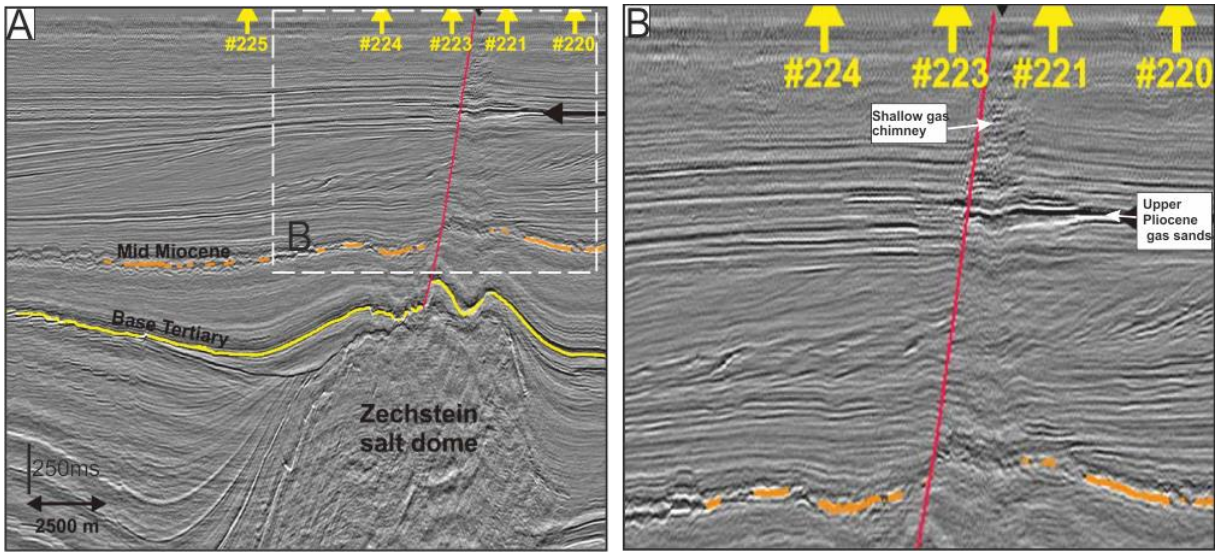

Figure 1.14: Part of seismic profile inline 190 showing the high amplitude anomaly as a bright spot associated with a chimney. The bright spot is developed at the top of the salt dome (Schroot & Schuttenhelm, 2003)

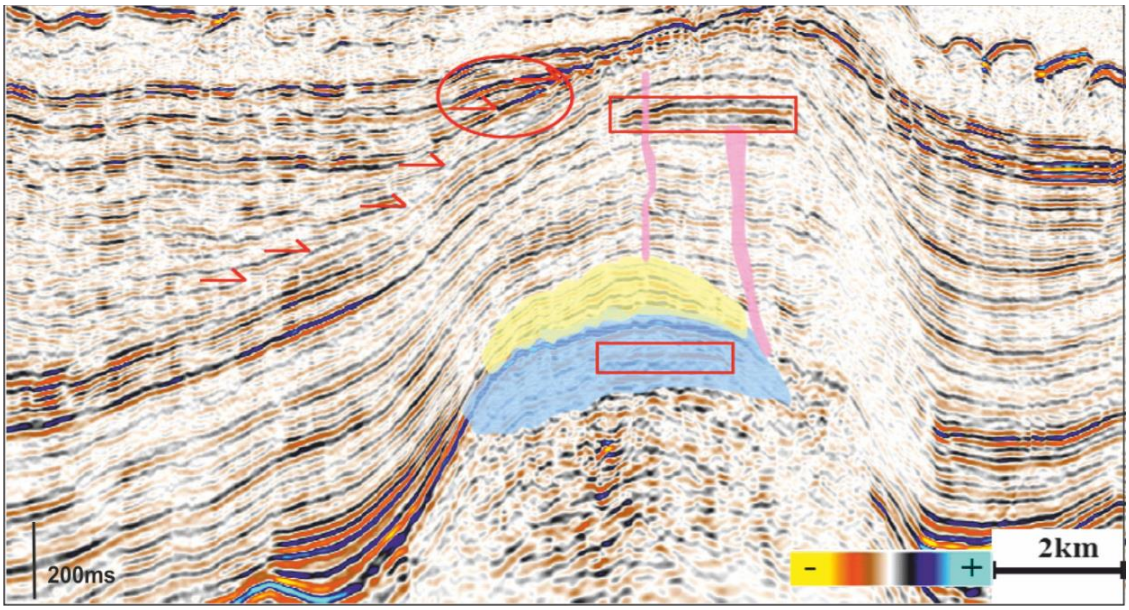

Figure 1.15: Potential DHIs including flat spots, amplitude anomalies and gas chimneys. Seismic profile shows bright spots, flat spots and gas chimneys within an anticline closure (Lie & Trayfoot, 2009)

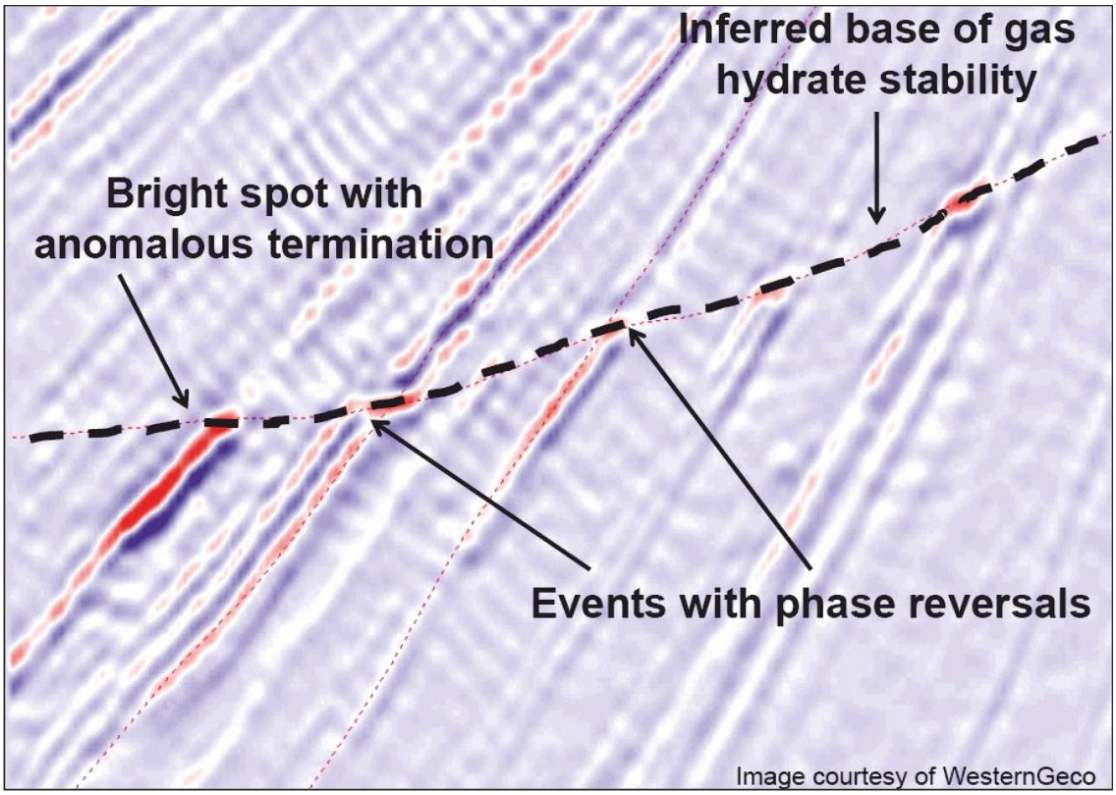

Figure 1.16: Seismic profile is an example from Gulf of Mexico Walker Ridge and Green Canyon showing high amplitudes (bright spots). (Shelander *et al.*, 2010).

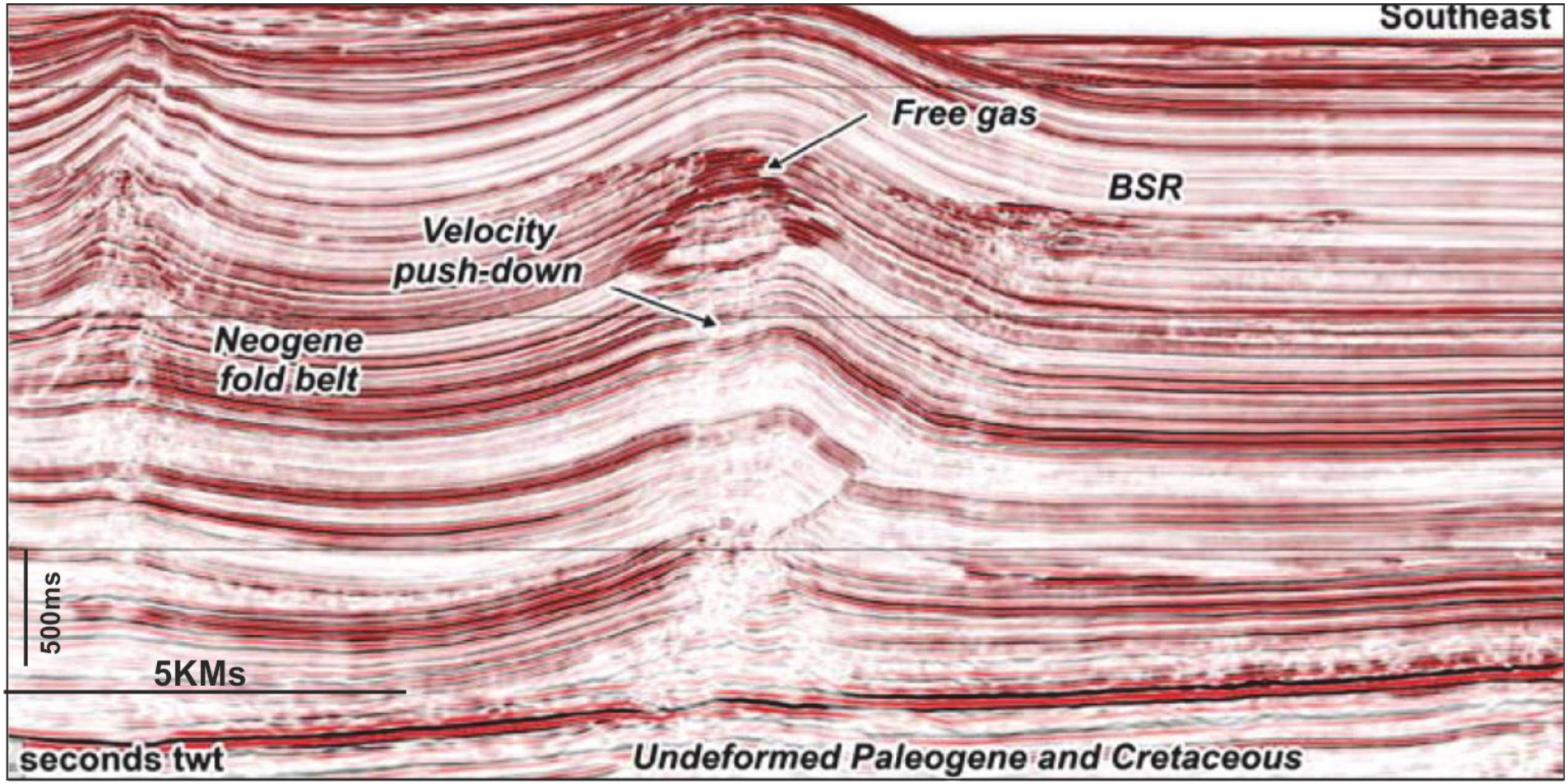

Figure 1.17: Seismic profile showing a example of direct hydrocarbon indicators associated with large, gentle folds; in places a bottom-simulating reflector inferred to represent gas hydrates from Pegasus Basin New Zealand. High amplitude anomalies are clustered below BSR (as a seal). The stepped anomalies suggested possibility of small faults at the crest of anticline. There is a velocity push done effect under the directly below the cluster of anomalies due to the presence of free gas (Geo Expro, 2011)

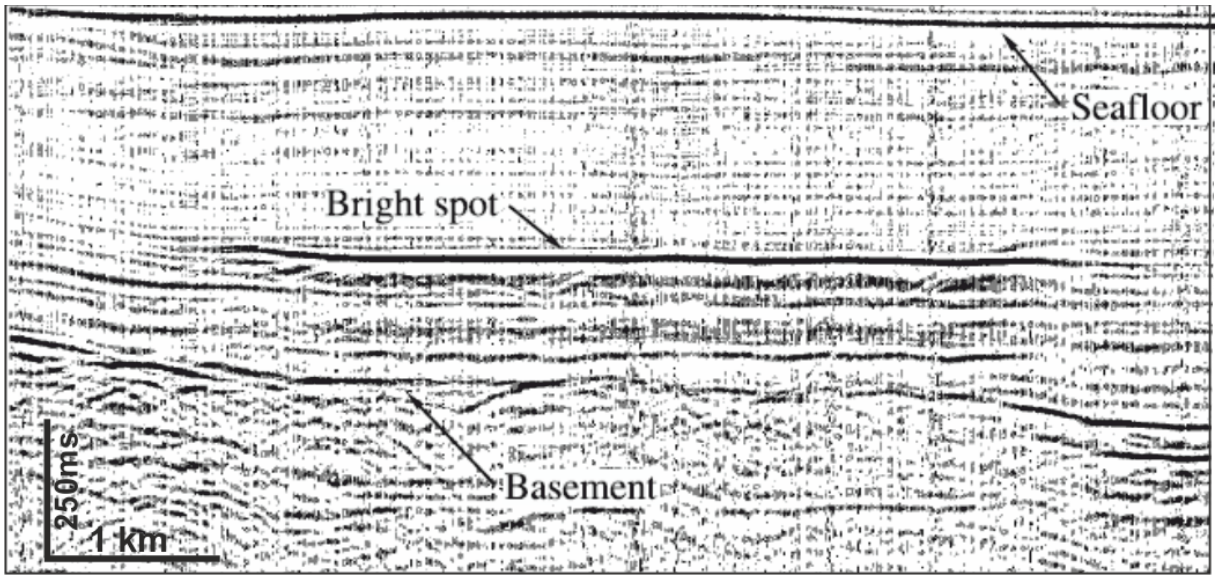

Figure 1.18: Bright spots having polarity reversal are observed at very dense grid of 2D seismic lines below 300-800 ms TWTT below seafloor in water depth of 3800 m in the sedimentary column of the southern Canary Basin (Müller *et al.*, 2001).

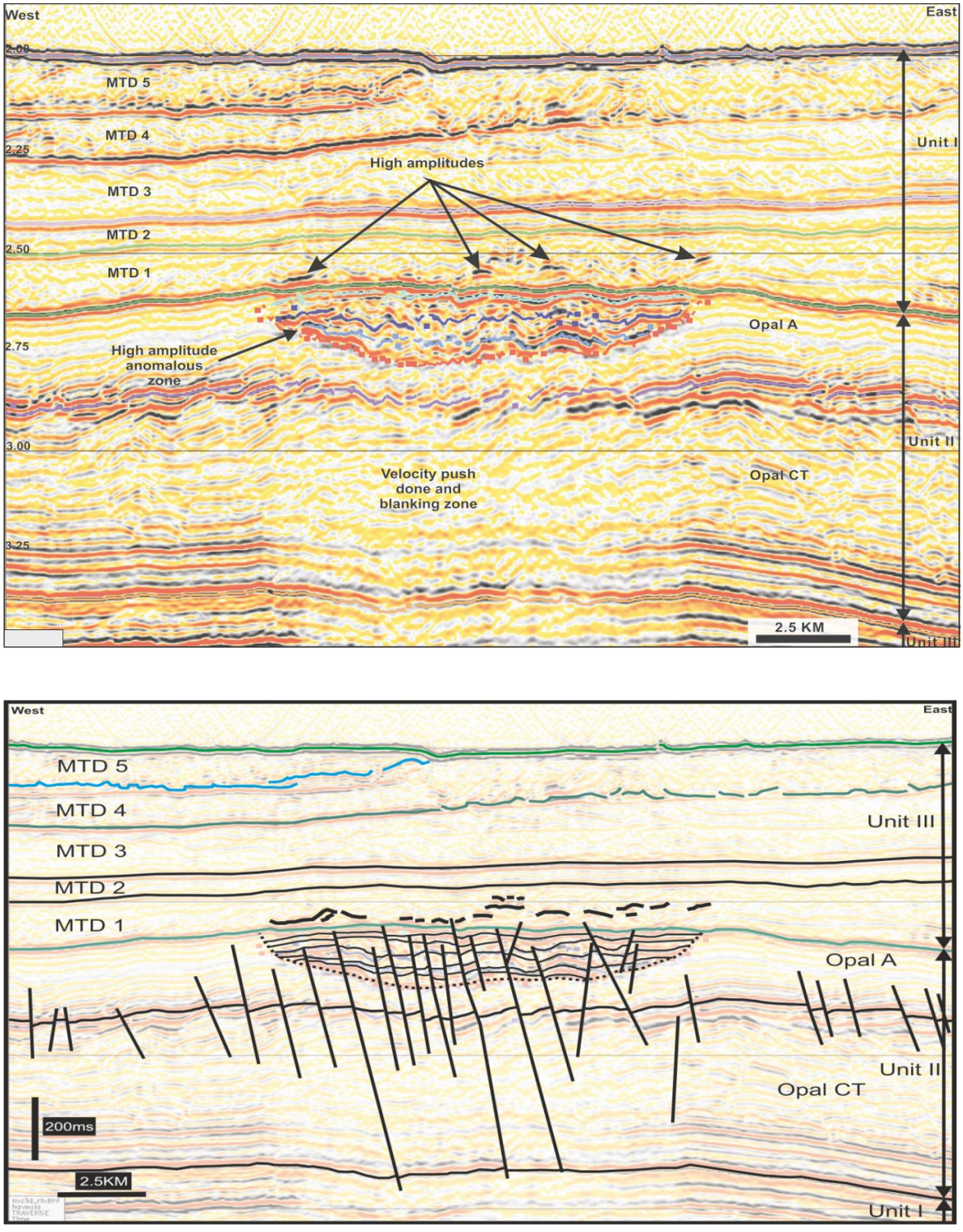

Figure 1.19: Free gas can be detected on the seismic data by the change in seismic velocity that results from gas in the pore spaces of the sediments. This leads to a stronger amplitude reflection than would result from a purely water filled pore volume, and is visible on seismic data as an amplitude anomaly. This study focuses on a description of seismic amplitude anomalies from a 3D seismic data set located in the Norwegian Sea. (For more detail see chapter 3).

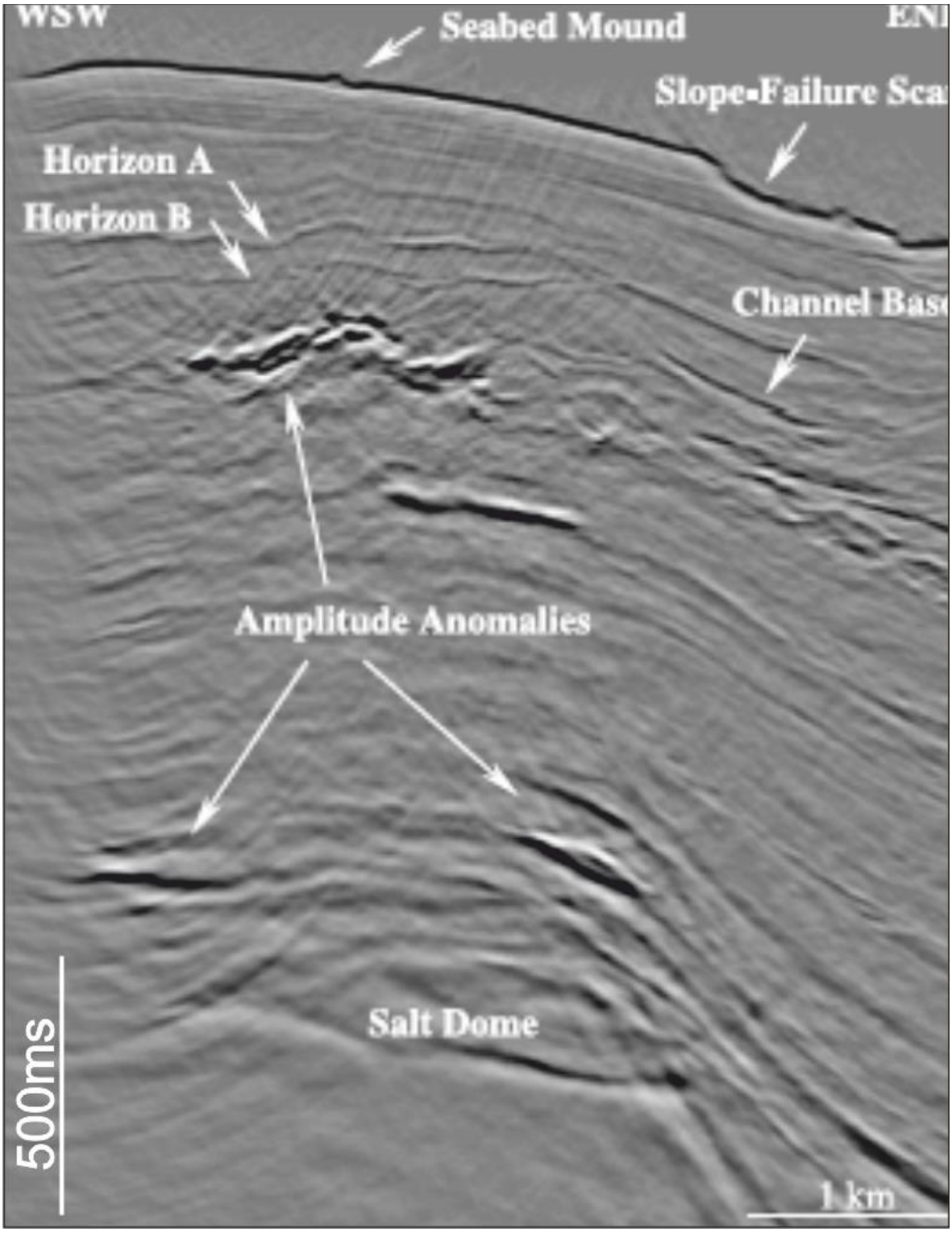

Figure 1.20: 3-D seismic section from deep-water Green Canyon displaying the different features of interest in the geohazards evaluation. At the upper right, a seabed slope-failure scar can be seen (Heggland, 2004).

1.2.2.2 Dim Spots

A dim spot is a locally developed, low seismic amplitude anomaly (Brown, 2004; Brown, 2012) that can indicate the presence of hydrocarbons and is therefore known as a direct hydrocarbon indicator. It primarily results from the decrease in acoustic impedance contrast when hydrocarbons (with a low acoustic impedance) replace the brine-saturated zone (with a high acoustic impedance) that underlies a shale or other caprock unit (lowest acoustic impedance of the three), decreasing the reflection coefficient.

For a dim spot to occur the shale, it has to have a lower acoustic impedance than both the water sand and the oil/gas sand, which is the opposite situation required for a bright spot to occur. This is possible because compaction causes the acoustic impedances of sands and shales to increase with age and depth but it does not happen uniformly – younger shales have higher acoustic impedance than younger sands but this reverses at depth, with older shales having lower acoustic impedance than older sands.

Similar to bright spots, not all dim spots are caused by the presence of hydrocarbons and therefore they should not be treated as conclusive evidence of hydrocarbon accumulations. There are many geophysical techniques to differentiate true and false DHI. A generalized curves showing how the acoustic impedances of gas sands, water sands and shales increase with depth (Fig. 1.21). There are three different stages with respect to depth for development of bright spots occurs above depth A, where dim spots occur below depth B, (Left) Examples of seismic reflectivity for each of the three sand/shale impedance regimes, (Brown, 2004).

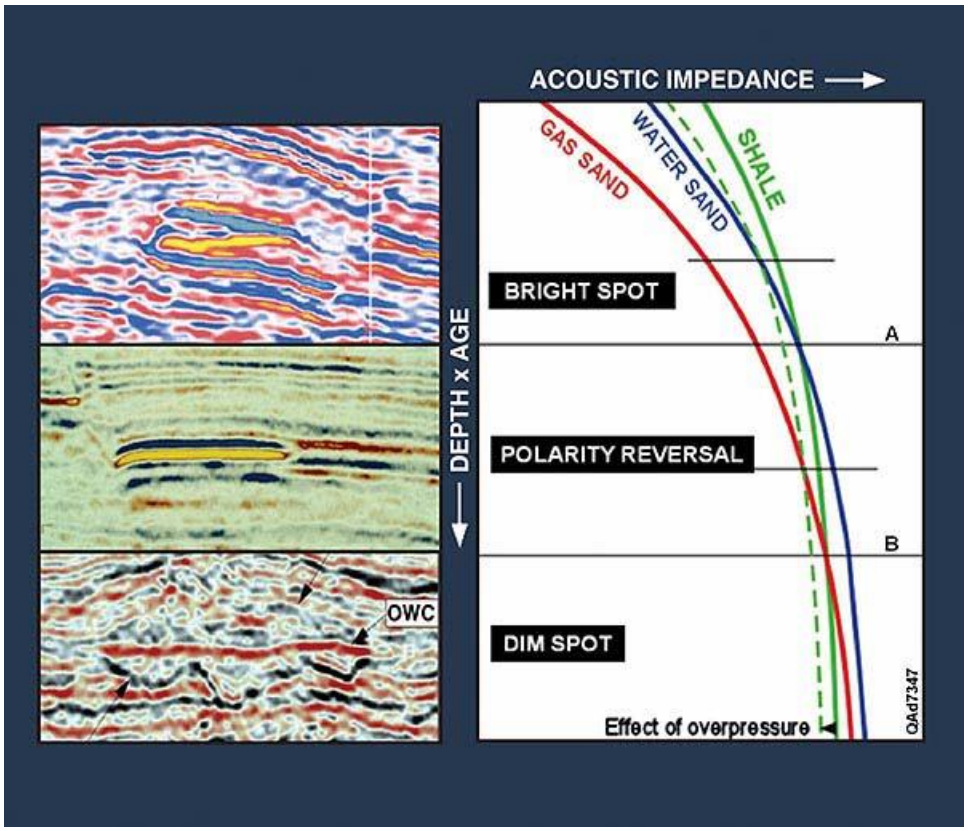

Figure 1.21: A generalized curves showing how the acoustic impedances of gas sands, water sands and shales increase with depth (Brown, 2004)

1.2.3 Gas chimneys

A gas chimney is poorly defined in the literature as a sub-vertical to vertical zone in which there is loss of internal reflection continuity (Aminzadeh *et al.*, 2002a; Heggland, 2004; Cartwright *et al.*, 2007; Løseth *et al.*, 2009). These zones are often seen to overlie a hydrocarbon accumulation (Fig. 1.22). Outside the gas chimney, the reflection continuity is high (Fig. 1.26). The scale of the gas chimney is important for detection and they should be much wider than the lateral resolution limit if the imaging is to be trusted as being truly representative of gas distribution. Some authors (Heggland, 2005; Løseth *et al.*, 2009; Nourollah *et al.*, 2010) implicitly link the presence of the gas chimney to fault and fracture networks.

Seismically defined gas chimneys can be used as evidence of migration paths, seal integrity and hydrocarbon leakage (Aminzadeh *et al.*, 2002a; Aminzadeh *et al.*, 2002b; Aminzadeh *et al.*, 2002c; Alvarado *et al.*, 2003; Alvarado *et al.*, 2005). Gas chimneys are often hosted in low permeable caprocks (Fig. 1.24) (Løseth *et al.*, 2009). The shapes of gas chimneys are highly variable but are generally columnar or ellipsoidal (Fig. 1.25Figure 1.25). Bad seismic velocity determination, poor stacking and loss of reflection continuity may be the result of low background gas saturations (Dvorkin & Nur, 1998; Knight *et al.*, 1998).

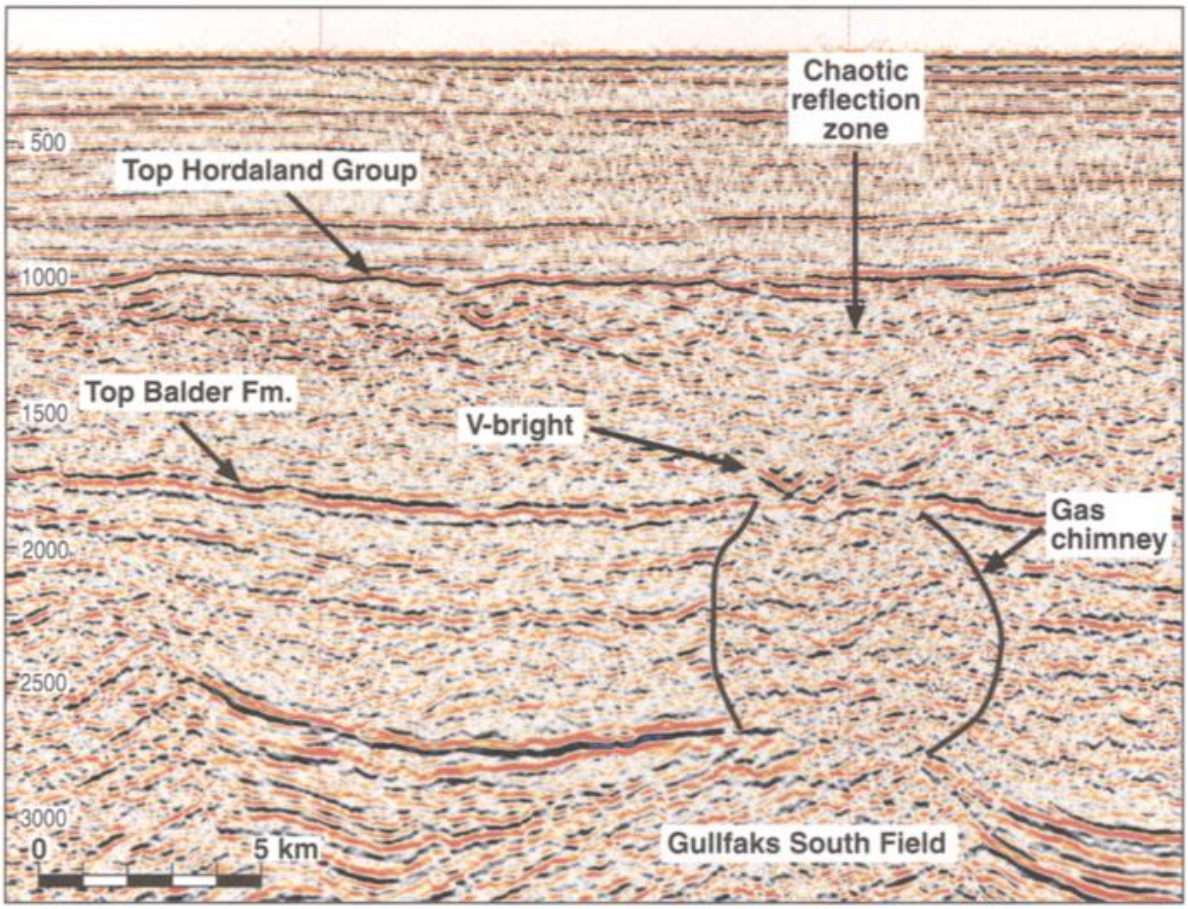

Figure 1.22: A seismic time section from the Gullfaks South Field shows that zones with chaotic reflections in the Hordaland Group are located above V-brights at top Balder level, which again are located above gas chimneys that are rooted in the underlying Jurassic rotated fault block (Løseth *et al.*, 2009)

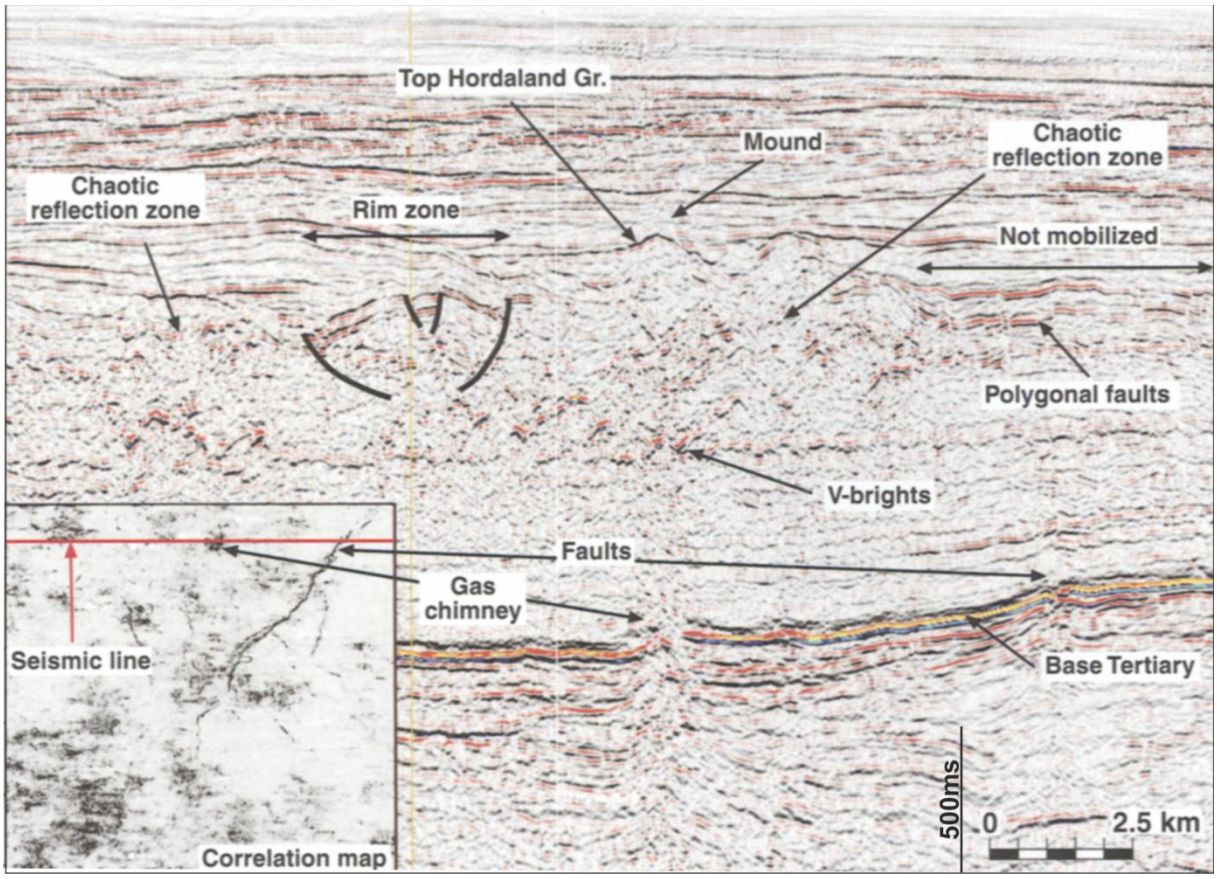

Figure 1.23: A seismic time section from northern part of the Norwegian Block 30/9 that illustrates the chaotic reflection pattern with V-shaped amplitudes and mounds at the top of the Hordaland Group. Note the rim zone with significantly rotated beds on the left-hand side of the figure. A vertical noise zone, which is interpreted as a gas chimney, is located below the chaotic zone. A correlation map demonstrates that the gas chimney, which is a low correlation area expressed with dark colour, has a circular shape while the fault is linear in map view (Arntsen *et al.*, 2007).

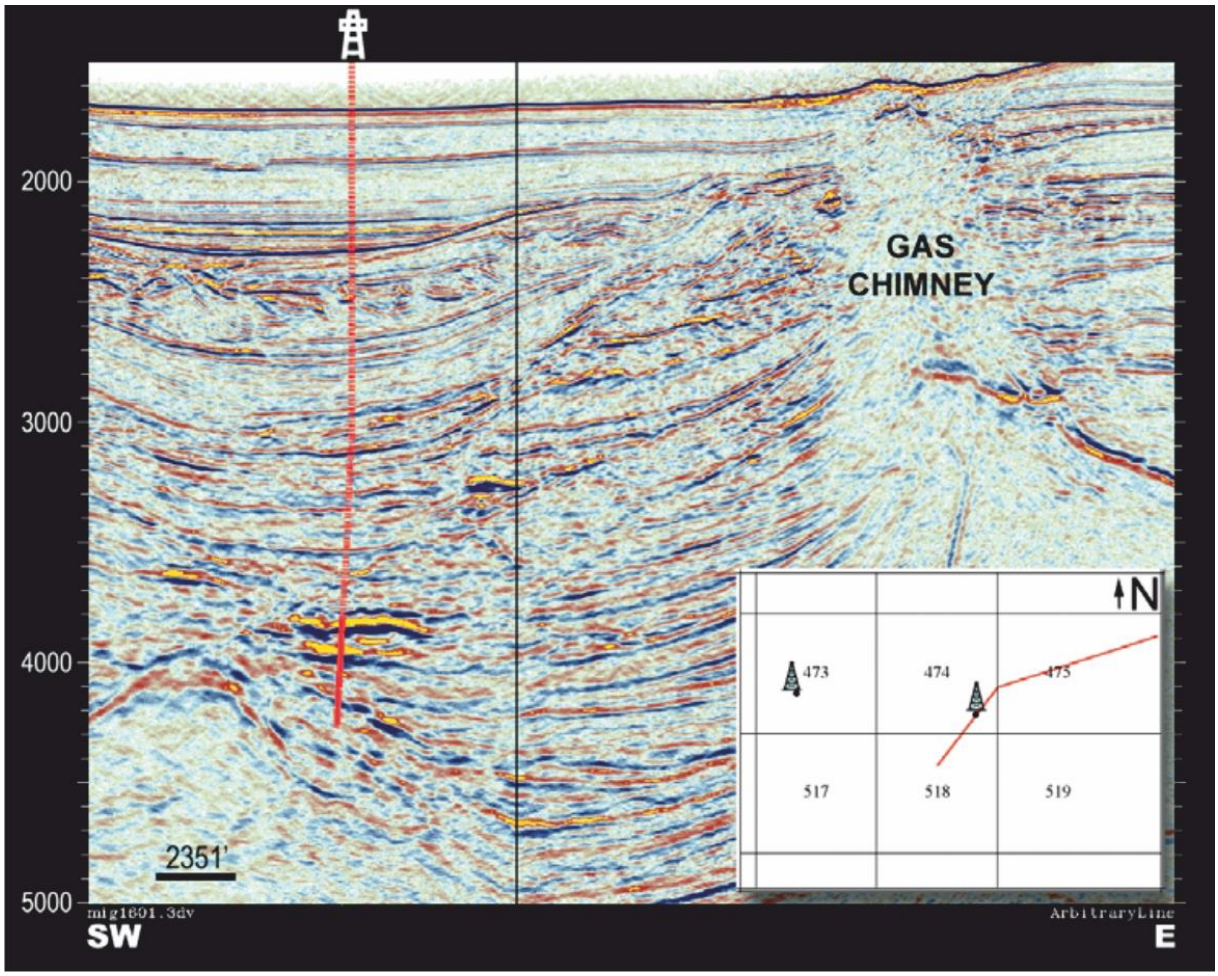

Figure 1.24: A seismic profile illustrating a gas chimney emerging at the crest of an anticline. Gas chimney is about 1 kilometre long and has prominent effect on the sea bed (O'Brien, 2004).

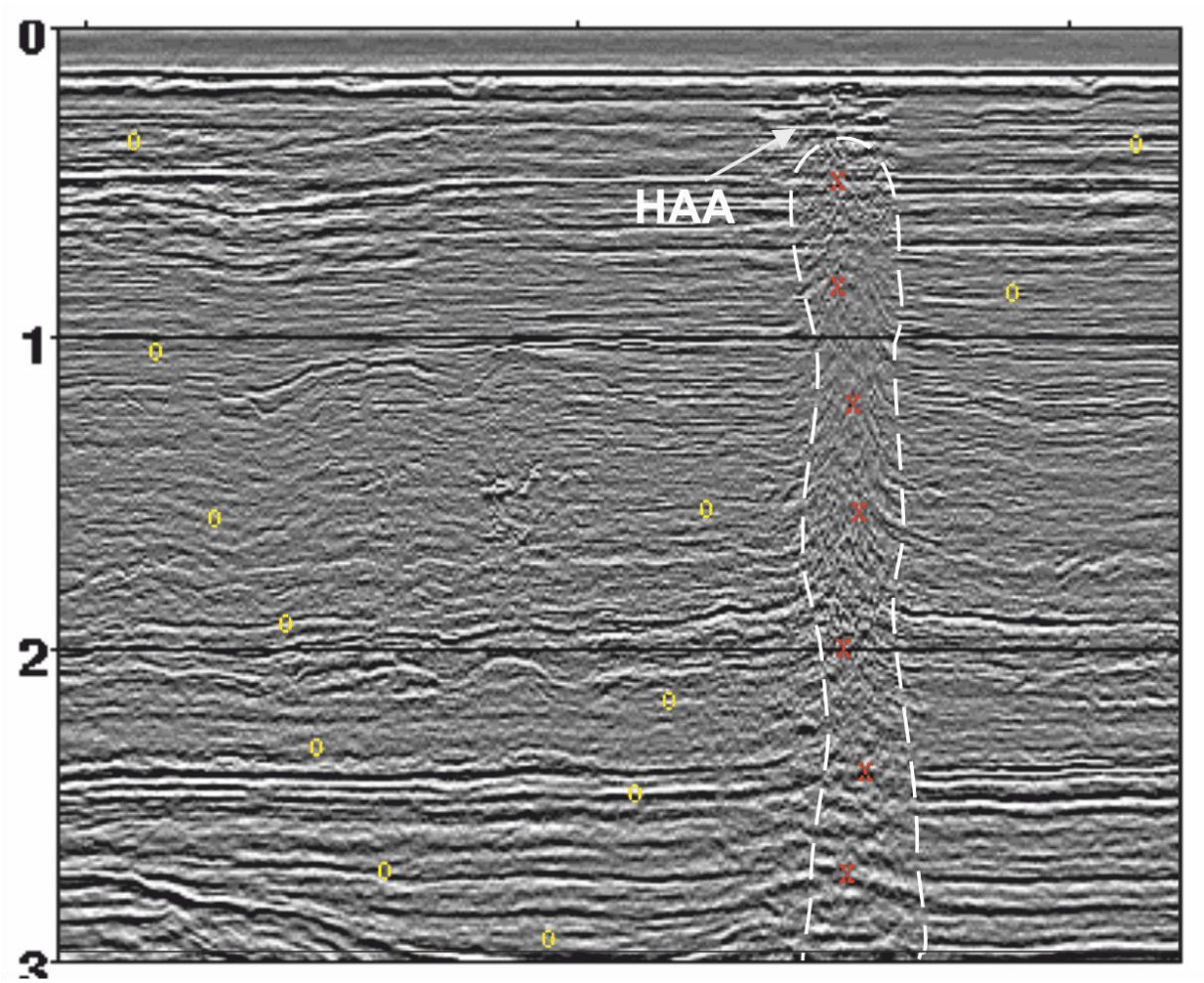

Figure 1.25: Seismic line with seed interpretation showing locations inside a chimney (x) and outside the chimney (0). The dashed line is marking the boundary of the gas chimney. A white arrow is indicating high amplitude anomalies (HAA) developed at the top of gas chimney (Meldahl *et al.*, 2001).

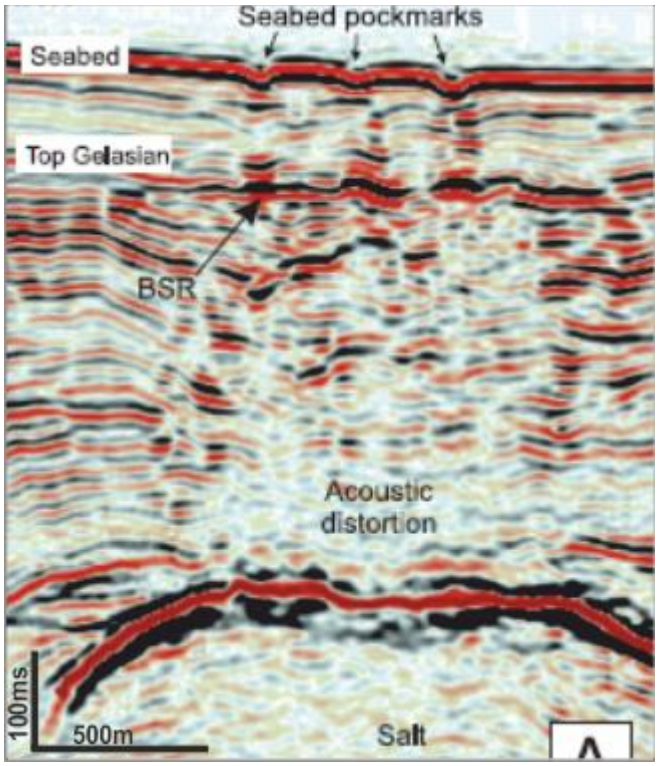

Figure 1.26: Fluid flow mechanism is shown in this seismic profile from offshore Angola. Seabed pockmarks above a salt structure. Below the pockmarks is a shallow bottom-simulating reflector (BSR) (100m sub-seabed) and 1 kilometre wide zone of acoustic distortion interpreted as a gas chimney (Andresen *et al.*, 2011).

In the example shown in figure 1.26 bright spots occur in clusters that are observed above a possible gas chimney located in the underlying Cretaceous succession. Wells penetrating gas chimneys have increased mud gas readings and an increase in heavier hydrocarbons (only hydrocarbons up to C_5 are recorded by mud gas readings) relative to wells drilled outside the gas chimneys. Gas chimneys here, are interpreted as the seismic expressions of zones that have had, or still have focused vertically flow of gas, oil and formation water through fine-grained rock.

In reality, the region denoted as a gas chimney is not fully saturated with gas. The scattering and attenuation of localised gas accumulation can account for the loss of coherent reflection energy in many cases.

This is a really good example (Fig. 1.27) of a misinterpretation of gas chimney. The label ‘gas chimney’ is more realistically a shadow zone of low signal to noise due to attenuation of above enhanced reflections.

A comparison between a well drilled (Fig. 1.29) just outside the chimney, Well 1/9-1, and a well drilled within the chimney, Well 1/9-3R, shows that; 1) the bulk density of the overburden rocks is the same, 2) the sonic velocity of the well within the chimney is significantly less that in the sediments outside the chimney, and 3) the mud gas readings in the sediments within the chimney testify to several intervals with high gas saturations whereas the gas saturations in the overburden rocks of the well drilled outside the chimney are low throughout the section.

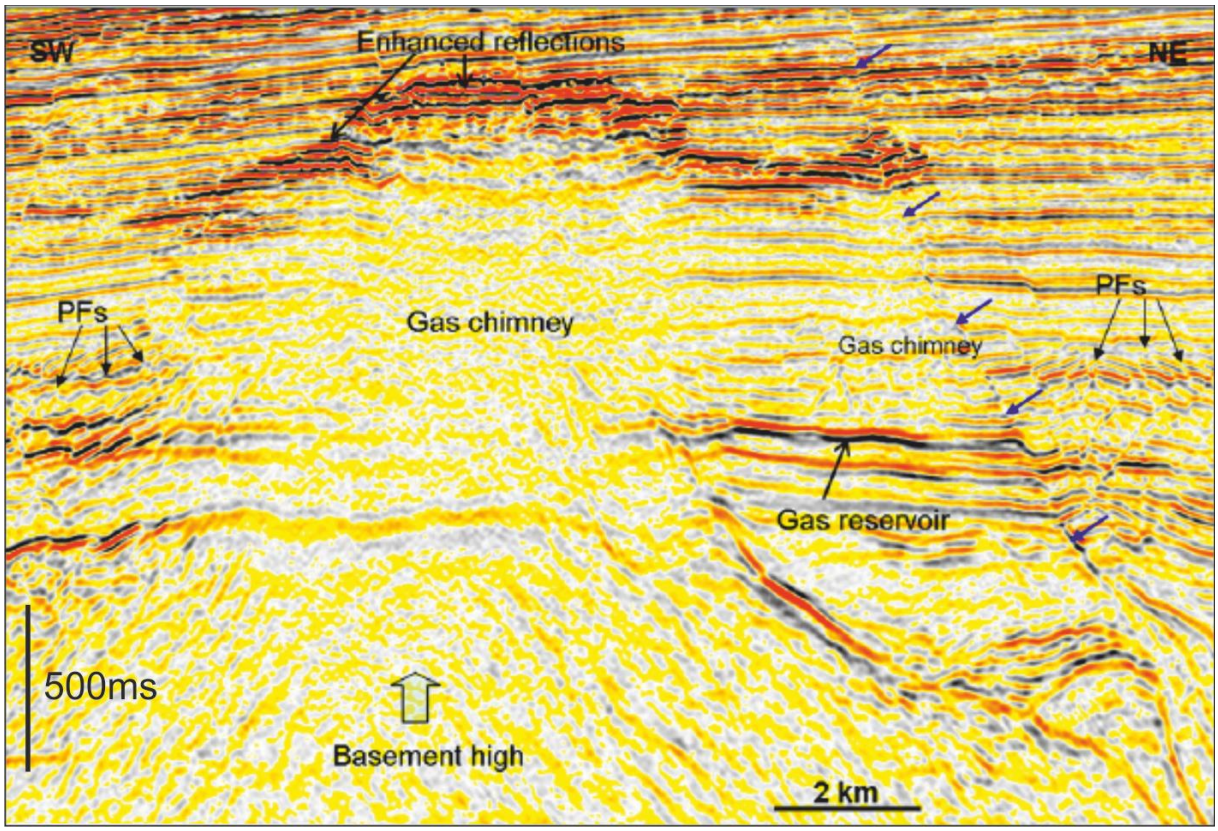

Figure 1.27: A large gas chimney feature has been interpreted with in sub muddy successions above a basement high and obscures the main gas reservoir (late Oligocene sandstone). Enhanced reflections developing at the crest of or around the gas chimney indicate there is important lateral and vertical fluid migration. A large deep-seated normal fault (blue arrows) accompanying a small gas chimney develops in the northeast of the large gas chimney. 'Flag' reflections are present along this fault, indicating that it serves as fluid flow pathway (Sun *et al.*, 2012).

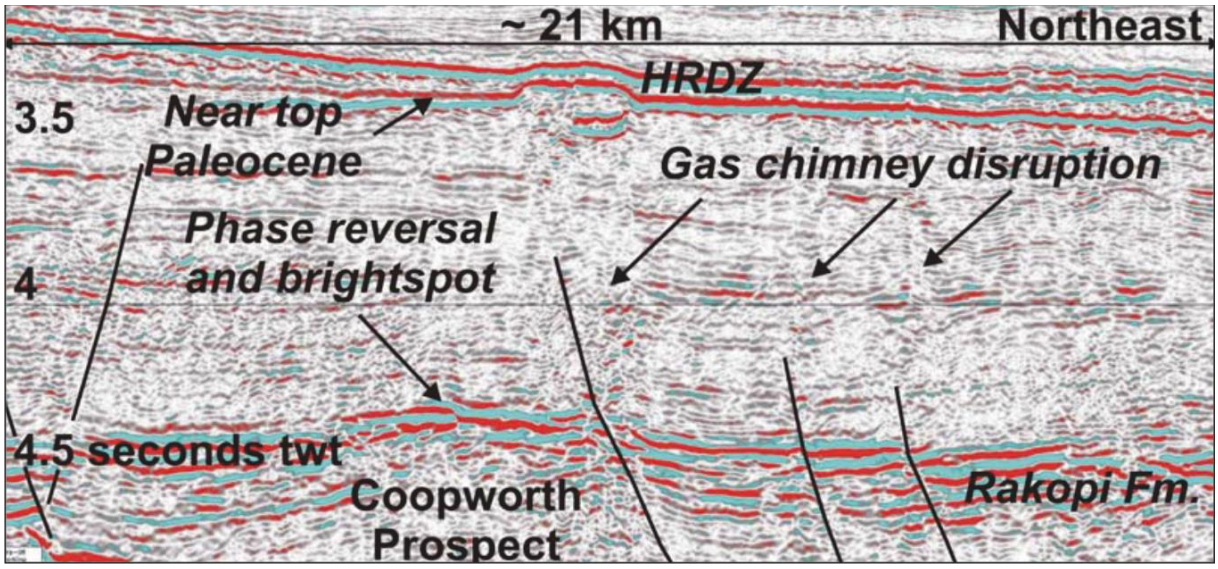

Figure 1.28: Chimneys commonly exploit pre-existing fractures and faults and imply an upward stream of gas, while clouds commonly form above charged reservoirs with imperfect seals, or form closer to the kitchen where migration pathways are limited. Possible gas chimneys are indicated. Seismic panel showing a disrupted zone above a footwall fault block leading to a mounded feature at the near-top Palaeocene reflection. The mounded feature is interpreted as a hydrocarbon-related diagenetic zone (HRDZ) (Chris Uruski and Warburton)

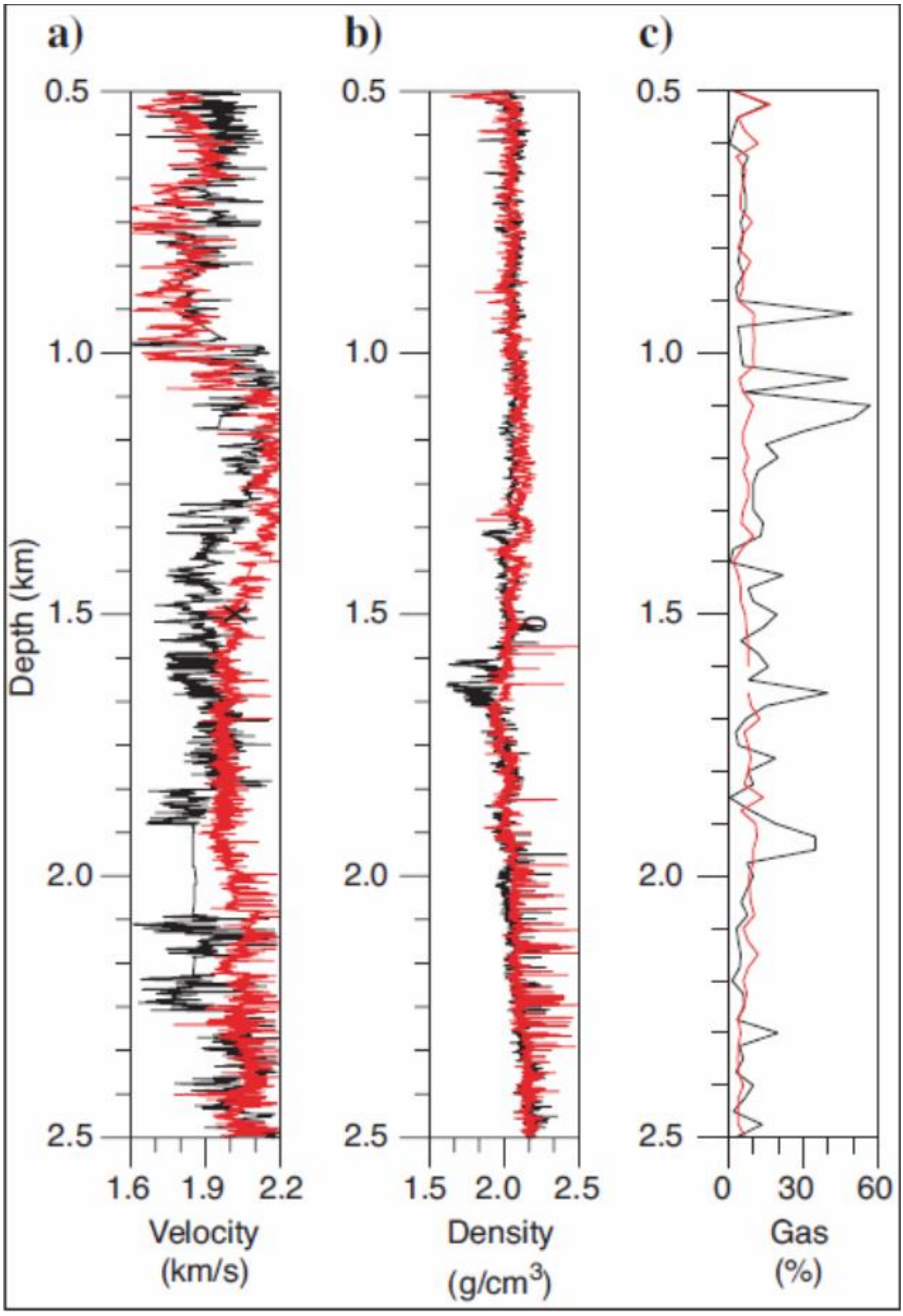

Figure 1.29: a) Sonic velocity, b) density, and c) mud gas readings inside black and red outside the Tommeliten Alpha gas chimney (Arntsen *et al.*, 2007)

1.2.4 Velocity push down

Hydrocarbon accumulations can result in significant velocity anomalies because of difference in the P-wave velocity between gas/oil and oil/water filled reservoirs with background sediments (Brown, 2004; O'Brien, 2004; Prskalo, 2004; Avseth *et al.*, 2005; Calvès *et al.*, 2008; Andresen *et al.*, 2011; Brown, 2012). The magnitude of the velocity anomaly is related to the thickness of the hydrocarbon-filled reservoir (Fig. 1.30 and Fig. 1.34). It is common to observe the most pronounced velocity anomalies beneath gas-filled reservoir. In some cases this can lead to an apparent curvature of gas/water contact as seen on the section (Fig. 1.32).

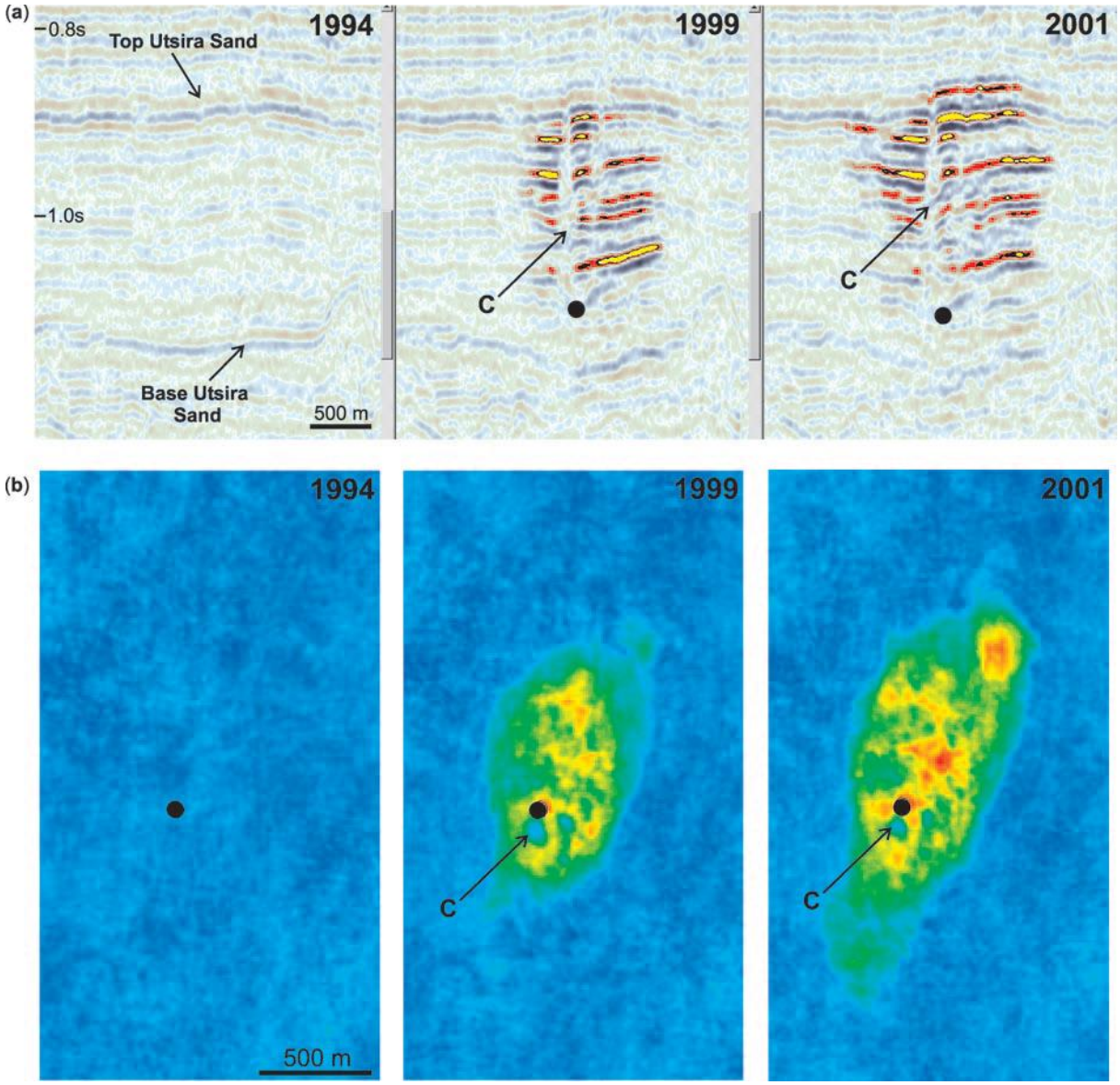

Figure 1.30: Time-lapse seismic images of the CO2 plume (a) N–S inline through the 1994 dataset prior to injection and through the 1999 and 2001 datasets. Enhanced amplitude display with red/yellow denoting a negative reflection coefficient. (b) Maps of integrated absolute reflection amplitudes calculated in a TWT window from 0.84 to 1.08s. Blue, low reflectivity; red, high reflectivity. Black disc denotes injection point. C denotes the main chimney. (Chadwick *et al.*, 2005)

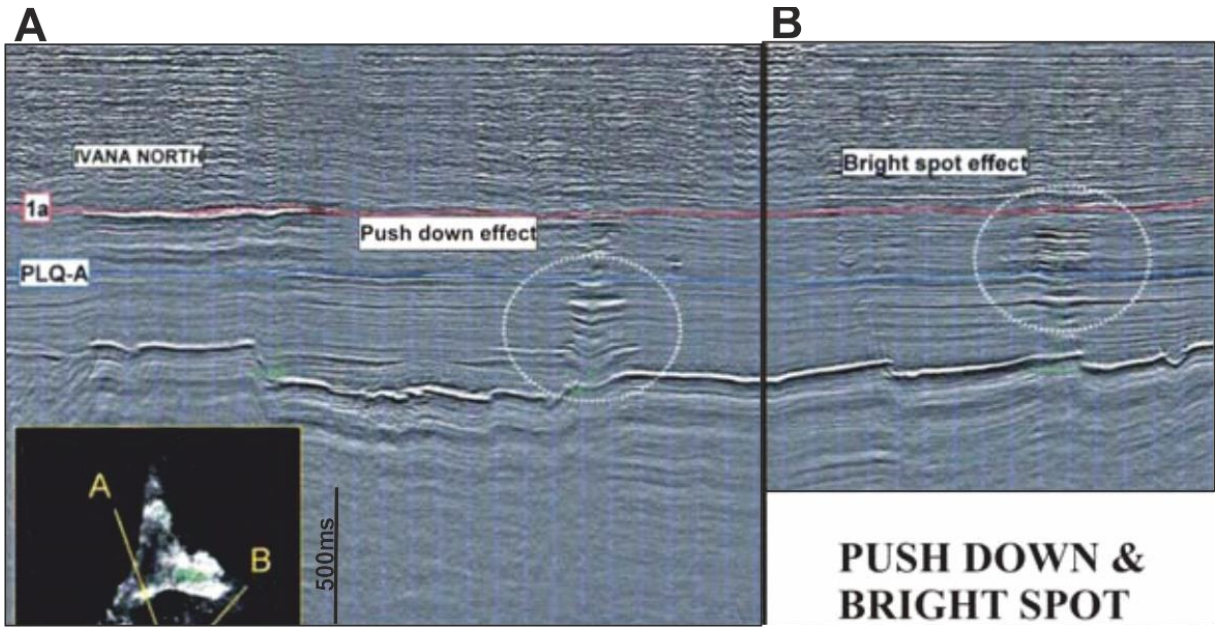

Figure 1.31: Two seismic lines with characteristic bright spot and pull-down phenomena are presented. Very pronounced faulting on strong reflection bellow the areas with these effects shows that the bright spot, as well as the push down effects, were formed during gas leaking through faults. In the marked areas gas accumulations were found above the deeper located faults (Prskalo, 2004)

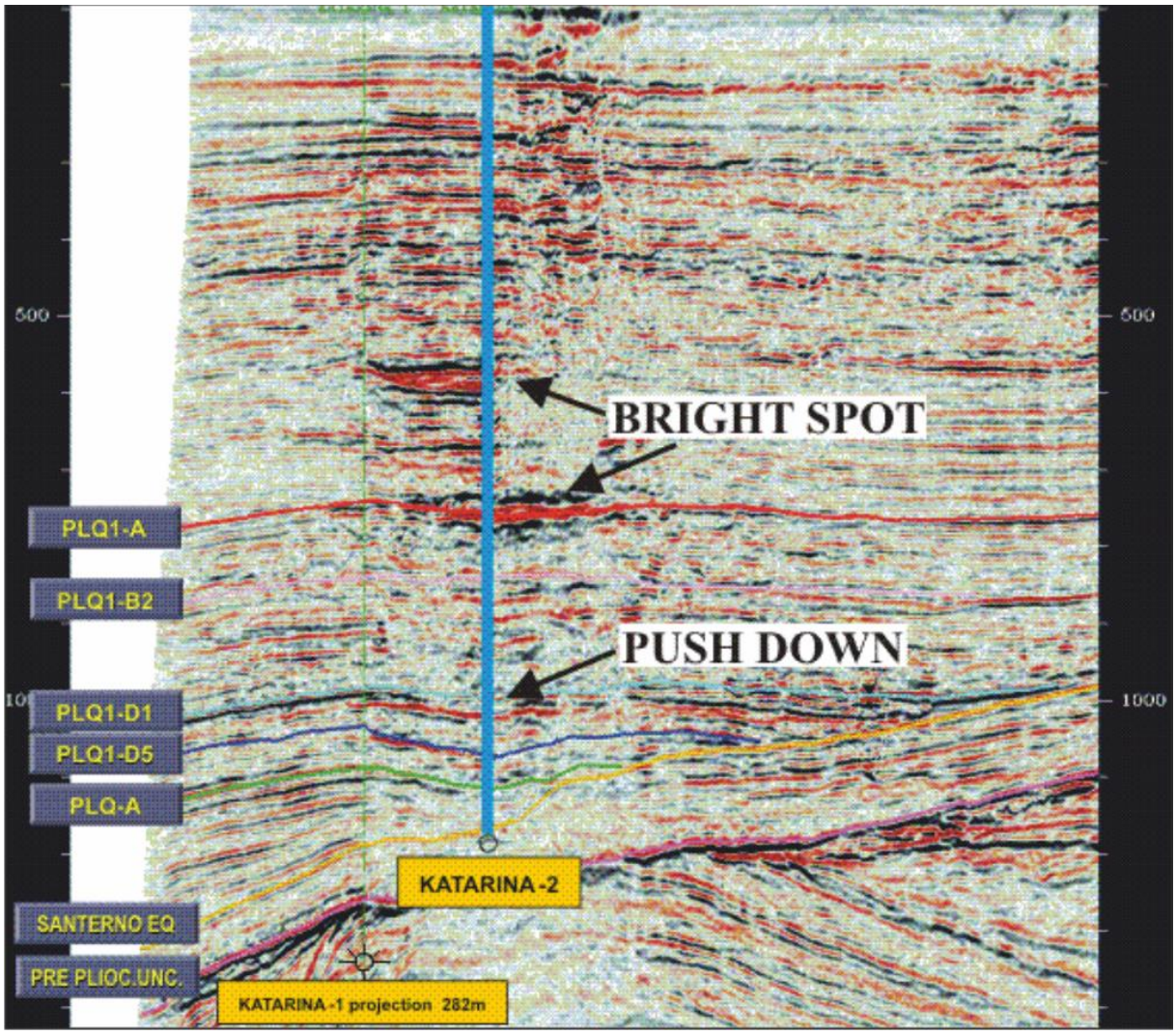

Figure 1.32: The bright spot features with characteristic push-down phenomena creating false syncline structure are clearly visible on the seismic section on example. The well was a success and proved that the presence of gas and confirm that the "bright spot" in north Adriatic Sea area (Prskalo, 2004)

Velocity pushdown effect is a strong evidence of presence of gas. Typically a gas-filled reservoir has P-wave velocity considerably lower compared to the oil-filled case although the magnitude of the difference depends on a depth and saturation of hydrocarbons (See Fig. 1.33 and Fig. 1.34 for a good example of a velocity analysis).

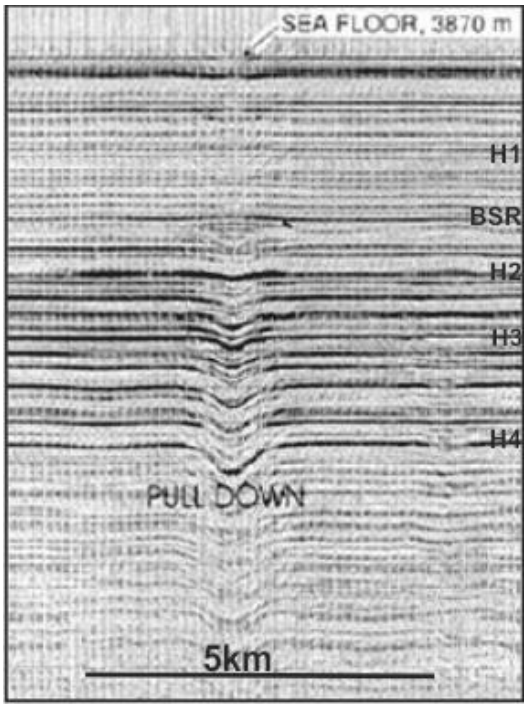

Figure 1.33: A VAMP pseudo structure illustrating velocity pull-up above the gas hydrate BSR and velocity push-down including bow-tie style distortion in a focused gas chimney below the BSR. Migrated stack section of velocity and amplitude structure depicting the prominent velocity pull-downs observed in the Bering Sea Basin. Horizon A marks the velocity pull-up, while horizons B and C show the time-delay effect of an underlying velocity push-down, presumed to be caused by free flow of interstitial gas. Horizon D marks the silica–diagenic boundary of the BSR (Satyavani *et al.*, 2005)

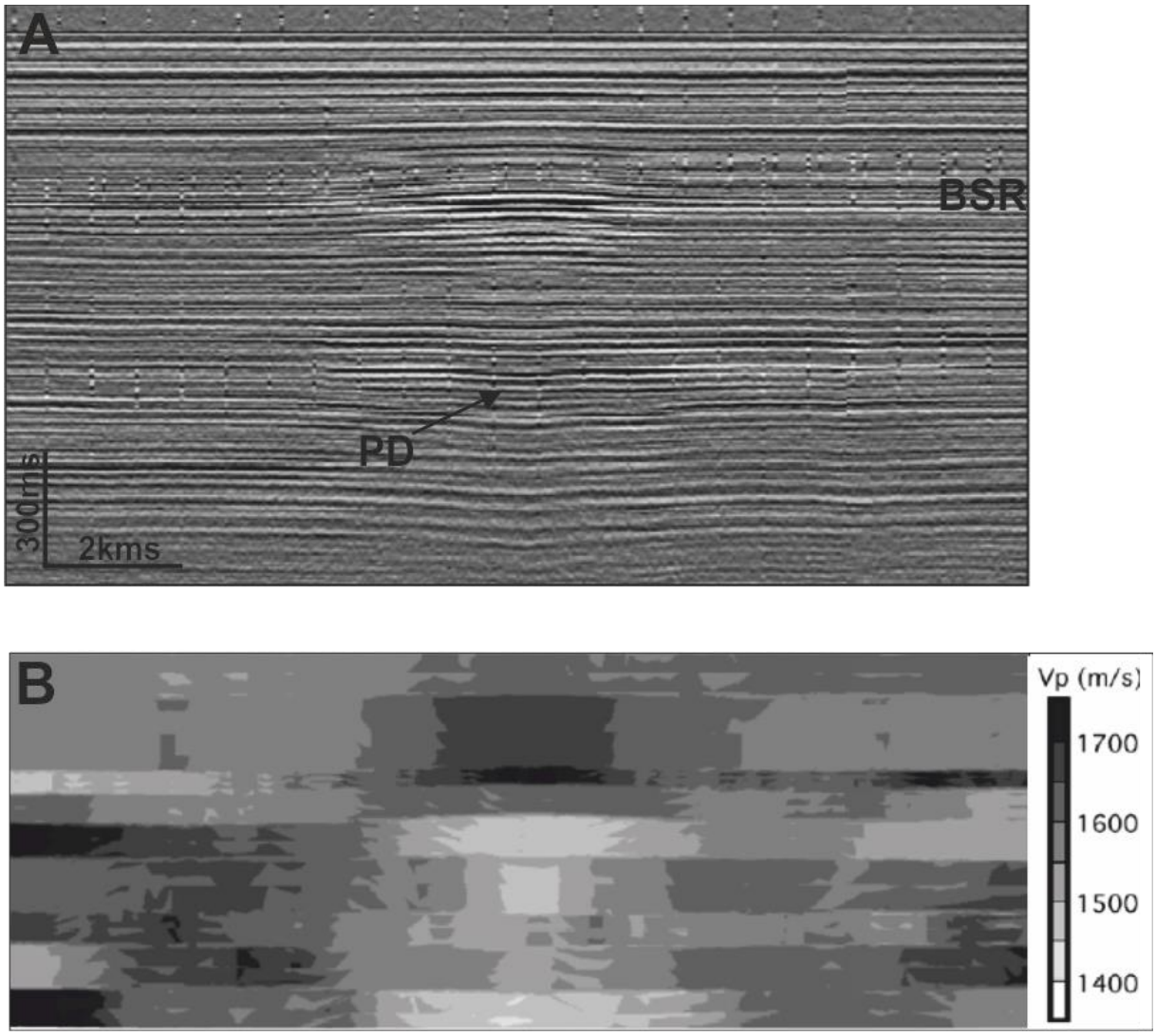

Figure 1.34: Analysis of the travel time anomalies within a VAMP includes (A) identification of key horizons (arrows along right margin), (B) derivation of velocity structure based upon interval time variation between picked horizons and interpretation of the anomalies in terms of equivalent volume of hydrate and gas within the section. Background velocity in the upper section is taken as constant at 1600 m/s. In this example, free gas content is <2% everywhere and maximum hydrate concentration implied is ~20% of pore space. If the profile is a slice through the midpoint of a structure of cylindrical geometry, the hydrate zone alone contains ~0.87 Tcf of natural gas (Barth *et al.*, 2004).

The final result is a reflection with a very strong amplitude and negative polarity ending with diffractions, as presented on the left hand side of the Fig. 1.32 well known as bright spot anomaly. Obviously such features on seismic profiles and isochron maps were caused by bright spot phenomena and not by poor data acquisition and processing, and definitely not by some locally developed small scale tectonic movements.

1.2.5 Vertical anomaly clusters (a new type of DHI)

Here we introduce a new type of direct hydrocarbon indicator, "Vertical Anomaly Clusters (VACs)". VACs are formed due to hydrocarbon leakage from main reservoir to overlying sediments through different migration routes. Hydrocarbon leakage patterns in VACs are irregular to regular and systematically stacked in a way that directly points to vertical migration or leakage. They can originate from the main leakage point and spread laterally by flow of hydrocarbons and are mostly related to gas (Fig. 1. 35 and Fig. 1.37)

A series of amplitude anomalies are observed within the biosiliceous Miocene sediments beneath a regional claystone seal of Pliocene age (Fig. 1.19). These anomalies have an extraordinary geometry: they cluster beneath the crest of a large domal anticline and have a basal boundary that is strongly cuspate with a concave upwards shape (see the Norwegian case study chapter 4 for further details).

This cluster of anomalies (Fig. 1.19) is attributed to free gas from several observations: (1) the location at the crest of a structure, (2) the geometry of the host sediments, (3) the presence of pronounced velocity push down, and (4) the presence of anomalies in the seal immediately above the cluster.

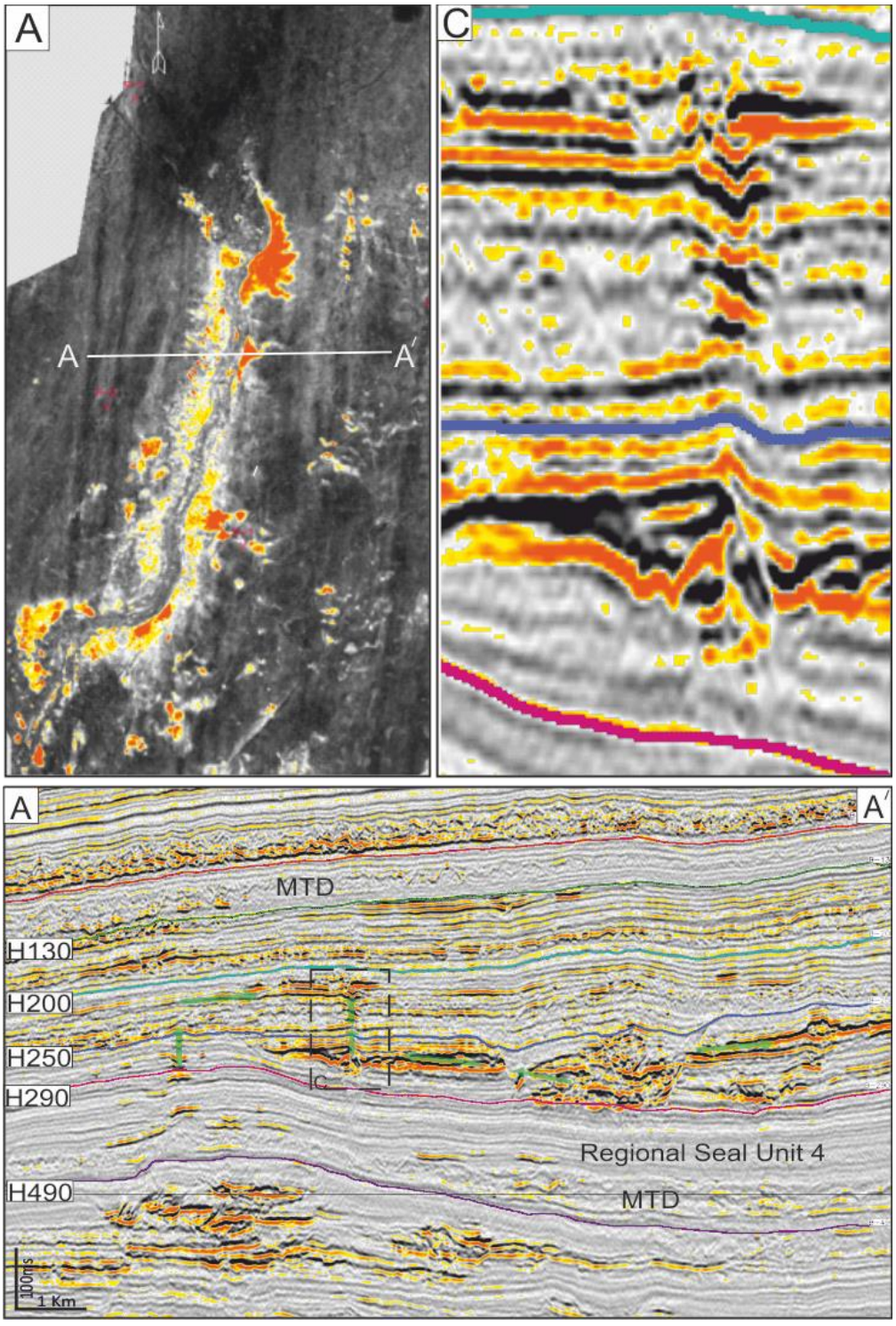

Figure 1.35: A) RMS amplitude map showing distribution of high amplitude anomalies along the mud filled channel levee system lying in waste zone of case study A, above the main Miocene turbidites reservoir B) East west seismic profile indicating main context of HAAs and green arrows showing possible leakage paths C) Zoomed part of vertical anomaly clusters (VACs) connecting HAA to main reservoir.

There are different types of VACs observed as an amplitude anomaly (Fig. 1.36) in the East Falkland basin. VACs form by strongly focused vertical hydrocarbon migration in a heterogeneous stacked sequence of poor-quality reservoirs interbedded with layers with lower permeability, and where the necessary bottom-to-top cross-stratal flow (Fig. 1.37) exploits a well-developed fault and fracture network. Similar vertical associations of gas-related amplitude anomalies could be expected in many other basins so VACs may be useful direct hydrocarbon indicators with specific genetic significance for hydrocarbon migration mechanisms.

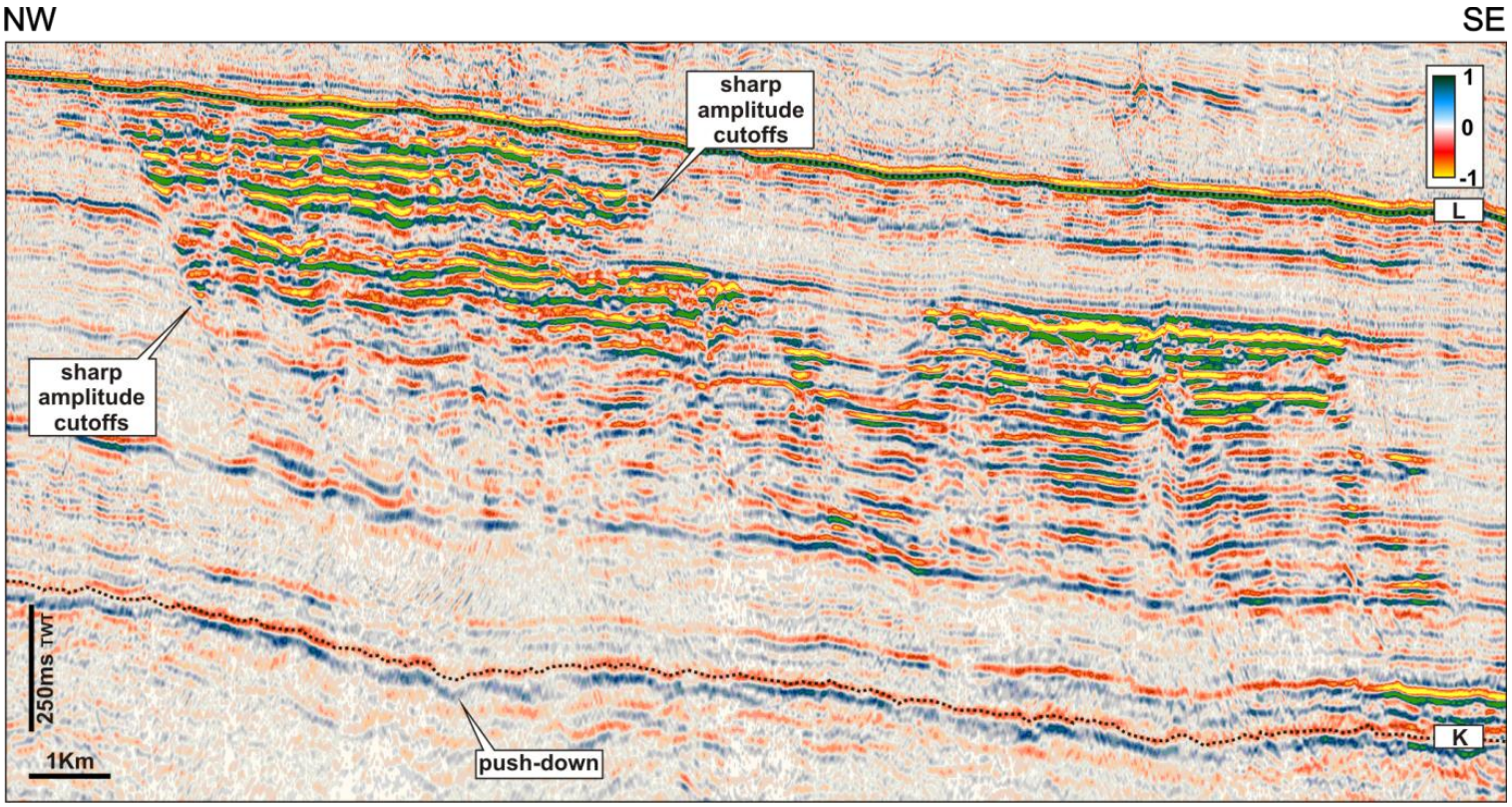

Figure 1.36: Two-dimensional seismic section showing detailed imaging of a vertical anomaly cluster (VAC). The amplitude anomalies (AAs) comprising the VAC are truncated generating sharp seismic cutoffs. The truncation position is interpreted as being demarcated by a fault plane. The VAC is associated with a strong push-down clearly recognizable on K. Other sharp AA cutoffs are present at the other margin of the VAC. Internally, a series of deformed convex-up distortions stack vertically, and can be interpreted as a pipe (Foschi et al., 2014)

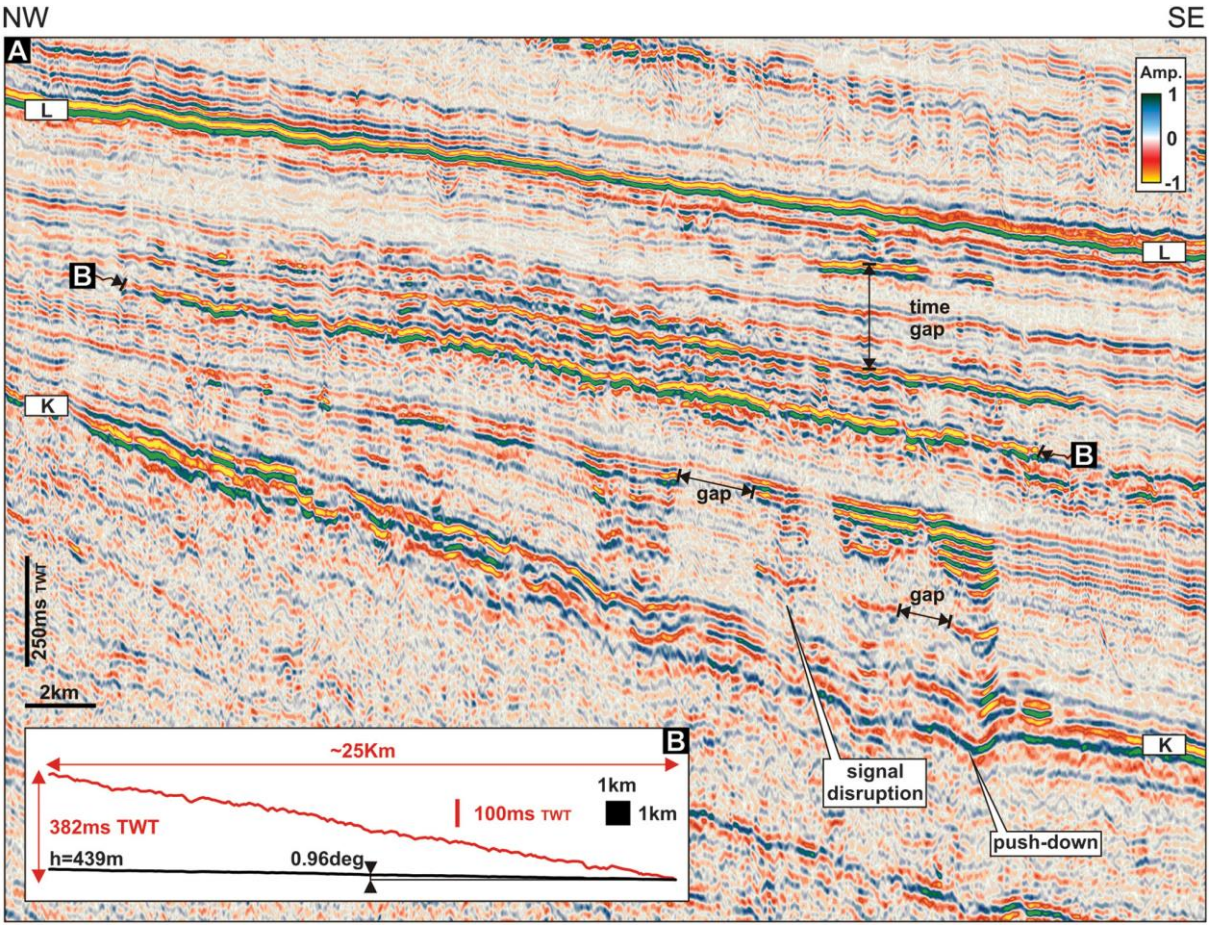

Figure 1.37: (A) Two-dimensional seismic section showing a vertical anomaly cluster (VAC). The line presents the longest amplitude anomaly (AA) discovered in the study area with an approximate length of 25 km (15.5 mi) and many shorter AAs. All AAs are soft reflections (red-yellow). These shorter AAs are separated by gaps occurring along the hosting horizons and time gaps observed as vertical non-amplified horizons. (Foschi *et al.*, 2014)

1.3 Fluid migration pathways

Fluid flow features observed in seismic data are represented in a variety of forms including pockmarks, pipes, gas chimneys, gas hydrates, sediment injections, carbonate mounds, seeps, mud volcanos and related diagenetic phenomena (Huuse et al., 2010, (Cartwright *et al.*, 2007; Løseth *et al.*, 2009; Weibull *et al.*, 2010; Andresen & Huuse, 2011; Andresen *et al.*, 2011). Their specific seismic expressions provide some indication of the migration history of fluids in marine sedimentary basins. All these type of fluid flow features represent subsurface fluid movement during past and present (oil, gas, brine, groundwater, mud and magmatic fluids) from source to the overlying sediment and which sometimes reached the seabed (Yilmaz & Doherty, 1987; Robinson, 1988; Brown, 2004; Gluyas & Swarbrick, 2009; Mavko *et al.*, 2009).

The types of structures generated due to focused fluid flow depends on a variety of parameters such as source of fluid, the flow type, the structural setting (Fig. 1.38) and nature of the host sediments (Van Rensbergen *et al.*, 2003; Cartwright *et al.*, 2007; Huuse *et al.*, 2010). Since the first observation and recognition of focused fluid flow features by Newsom, 1903; King and MacLean, 1970, interest in them has increased over the past few decades due to; (a) a growing quality of 3D seismic data, and (b) the realization of the impact of fluid flow features on hydrocarbon plumbing systems particularly concerning reservoir connectivity, migration and risk assessment (Cartwright *et al.*, 2007; Hurst & Cartwright, 2007; Huuse *et al.*, 2010).

Rocks with low porosity and permeability are normally considered as hydrocarbon seals (Løseth *et al.*, 2009). These so-called seal rocks behave differently and sometimes can host hydrocarbons (Jarvie *et al.*, 2007). Low permeable rocks are reported as seals in many case studies but rarely described as a reservoir rocks (Cartwright *et al.*, 2007; Imbert, 2009).

Faults are the main conduits for fluids in many basins worldwide, especially in the deeper subsurface where sediments are more consolidated and lithified.

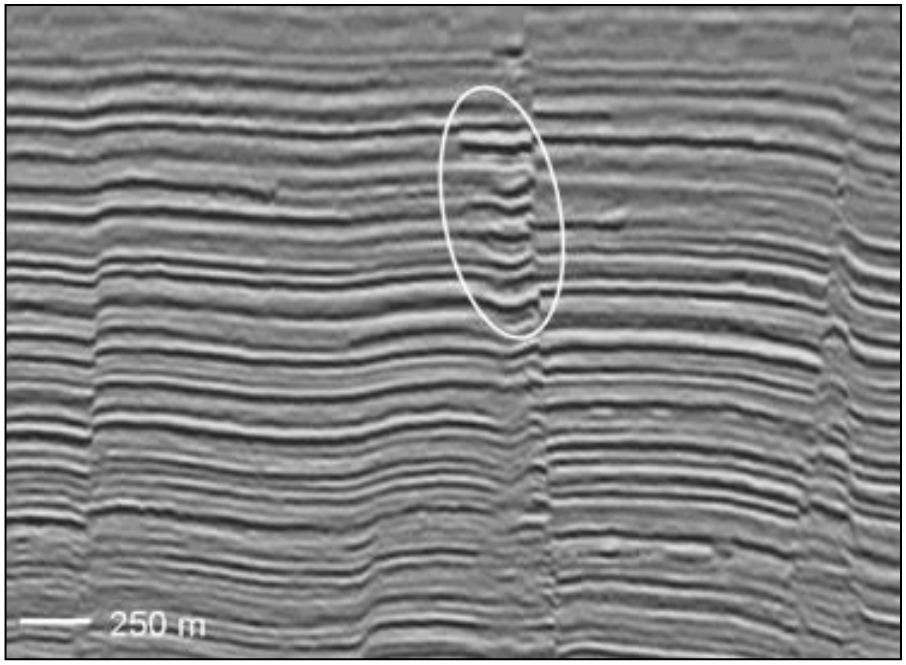

Figure 1.38: Direct hydrocarbon indication by bright spots located along leaking fault. Amplitude anomalies cluster is indicated by white ellipse. (Ligtenberg, 2005)

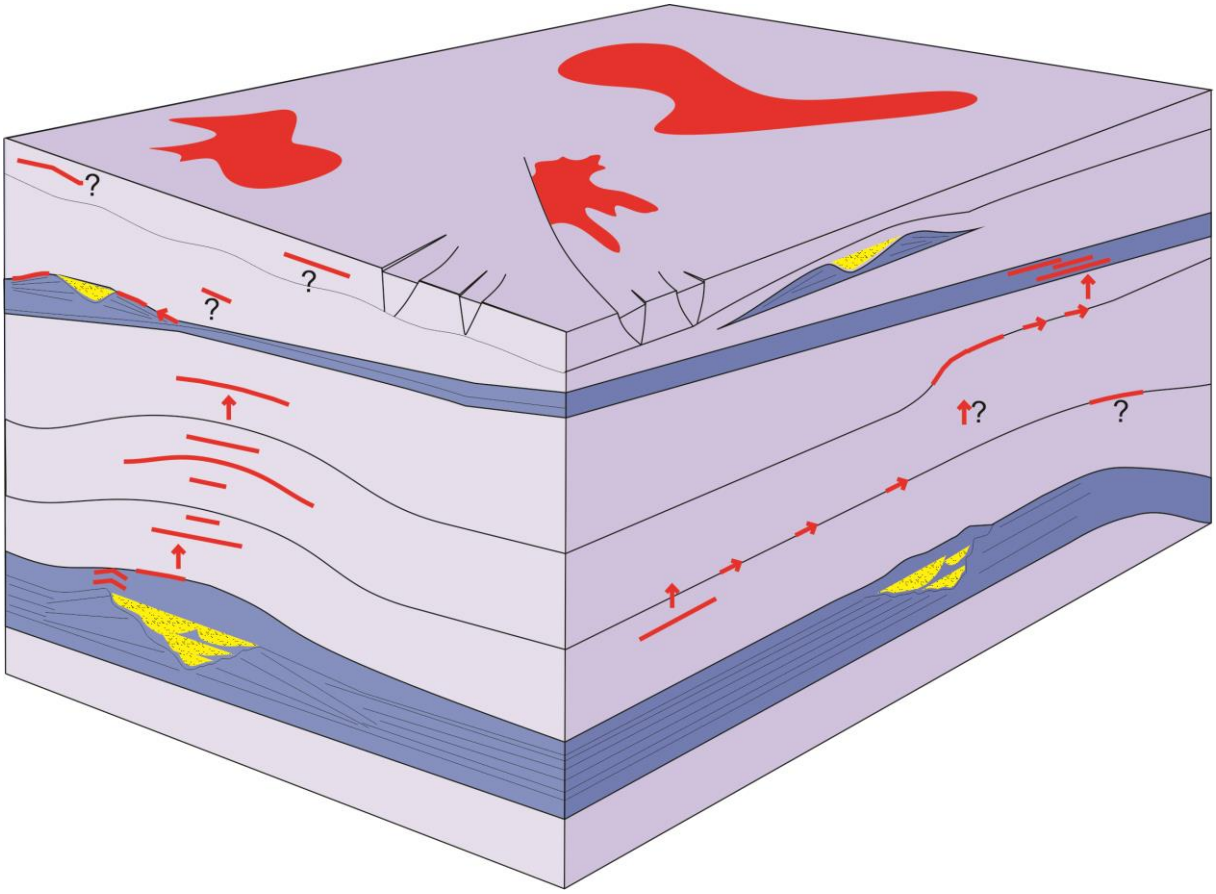

Figure 1.39: A hypothetical leakage model of and associated amplitude anomalies that can be characterised as due to hydrocarbon substitution, There are possible flow pathways from the shape, context, cross-sectional form, and context of the anomalies, and their spatial relationships. Groups of anomalies can be linked together in a series of linked anomalies- a stack or cluster. But where anomalies are widely dispersed, there may well be too many potential flow routes to allow a well constrained flow path to be inferred. Vertical stacks or clusters (VACs) are the strongest evidence we have of vertical flow paths. The model is presented in the Caprocks internal meetings)

1.4 Aims and objectives of the thesis

The research presented in this thesis is mainly based on the evaluation of high-amplitude anomalies in seismic data (for more detail chapter 3, 4, and 5). The main questions tackled in this thesis are related to the gaps in the research presented in the previous section. As outlined in the overview sections, the vast majority of research on amplitude anomalies associated with fluids is in porous and permeable sedimentary systems. In this thesis I will focus on amplitude anomalies developed in fine-grained systems. In particular, the general questions of interest are as follows;

- What is the 3-D geometry of amplitude anomalies within seismic units dominated by fine-grained sediments (Fig. 1.39)
- How do fluids flow through and into fine-grained sedimentary units which are conventionally regarded as impermeable seals. In other words, why do HAA's form where they do and how do they evolve into their current geometry?
- What are the role of faults and overpressure in fluid migration?

This thesis is broken down into two sections based on two case studies; a case study from the Møre Basin offshore mid-Norway and a case study from the Lower Congo Basin, offshore western Africa.

1.4.1 Chapter 3: Møre Basin case study

In chapter 3, 3-D seismic data is used to examine a unique gas-associated amplitude anomaly which has a concave-upwards basal contact. There are very few examples of anomalies with this geometry so the first objective of the chapter is to present a detailed description and analysis of

the anomaly and its relationship with the stratigraphic and structural setting of the basin. Subsequent objectives of the chapter are;

1. To establish the composition of the fluids creating the anomalous amplitude zone.
2. To establish the source of the fluids.
3. To explain the extraordinary concave-upwards geometry of the basal contact of the anomaly.
4. To establish how and why the fluid accumulation is trapped and how fluids filled the trap
5. To establish how fluids migrated into the trap

1.4.2 Chapters 4 and 5: Lower Congo Basin case study

In Chapters 4 and 5, high density 3D seismic data is used to examine a host of different amplitude anomalies within a hemipelagic sedimentary succession in the Lower Congo Basin (LCB). This case study area contains abundant evidence of fluid flow and has an active petroleum system. Determining which amplitude anomalies are associated with accumulations of hydrocarbon is a critical task in exploring this part of the basin. There has been a recent in-depth study of the fluid venting structures from the shallow levels in similar stratigraphic areas in the LCB (Andresen & Huuse, 2011; Ho *et al.*, 2012) but there are few studies from the deeper stratigraphic levels (Andresen & Huuse, 2011; Andresen *et al.*, 2011).

In Chapter 4, a detailed description of the amplitude anomalies are presented using a new classification system based on geometry. Using this classification system and traditional analytical methods I will determine which of these amplitude anomalies are hydrocarbon-bearing and non-hydrocarbon-bearing. The main objectives of Chapter 5 are;

1. To establish the relationship of hydrocarbon-bearing amplitude anomalies in fine-grained hemipelagic sediments with underlying turbidite reservoirs.
2. To establish the migration routes between deep-turbidite reservoirs and present-day locations of amplitude anomalies.
3. To go some-way in establishing the mechanism by which fluids migrated into the fine-grained units for example by Vertical Anomaly Clusters (VACs), faults, or other means (Chapter 5).

Collectively, Chapters 3-5 target mechanisms of fluid flow into fine-grained sedimentary series.

1.5 Layout

This thesis is divided into seven chapters. Chapter 1 consists of overview of the research topic covered in this research. This is followed by a overview of the data and methods employed in the research. As such Chapter 2 presents the details of the 3D seismic data, how it was acquired, how the seismic data was interpreted and the workflows used for identification of high-amplitude anomalies and associated fluid flow features. Chapter 3, 4 and 5 present the main results of the thesis. Each of these core chapters focus on various topics associated with identification of high-amplitude anomalies and their fluid flow paths.

Chapter 3 investigates a unique gas-associated amplitude anomaly in the Møre Basin, offshore mid-Norway. Chapters 4 and 5 investigate a range of high amplitude anomalies in seismic data from Lower Congo Basin. Chapter 6 presents a summary of the major findings and discusses the origin of finger-type amplitude anomalies in the Lower Congo Basin. The chapter then outlines

the major implications of the research and areas for further research. The main conclusions drawn from the research project are presented in chapter 7.

CHAPTER 2

Data and methods

CHAPTER TWO

2.1 Introduction

The research presented in this thesis is largely based on the observations, interpretations and analysis of high amplitude anomalies that were imaged in 3D seismic data. The aims of this chapter are to 1) give an overview of seismic data with an emphasis on its limitations, 2) description about the specifications and parameters of each of the seismic surveys and how they impact data quality, 3) give an overview of the methods that were used to interpret and analyse different high amplitude anomalies and their possible fluid flow pathways, and 4) outline what limitations the data poses to the project and how these problems are tackled.

2.2 3D Seismic data

The research presented in Chapter three is based on a pre-stack time-migrated seismic survey of the Havsule Dome from the Norwegian Sea. The research presented in Chapter four and five is based on a near offset high density three dimensional time-migrated seismic survey from the Lower Congo Basin (LCB) that contained salt and turbidite channel levee systems and their related structural and stratigraphic features (Fig. 4.6).

Seismic reflection surveying is a well-established technique for imaging subsurface geology. It works on the basis of recording the time taken for a seismic energy pulse to travel from source, reflect from a sub-surface interface, and return to a surface detector (Sheriff and Geldart, 1995; Kearey *et al.*, 2002) that defines a contrast in acoustic impedance and be detected at a receiver.

This is referred to as the two way travel time. Typically with marine 3D seismic, data is acquired using a near surface seismic energy source (air guns) used to generate a seismic source (p-waves) of a given frequency whilst reflected p-waves are detected by a series of hydrophones towed behind a vessel and a series of hydrophones which detect the reflected energy of compressive (P) waves from subsurface physical boundaries (Fig 2.1). The strength of the reflected energy is the result of the acoustic impedance between two different lithologies. Acoustic impedance (Z) is the function of the rock density (p) and the p-wave velocity (v). (Equation 2.1)

$$Z = V * \rho \tag{2.1}$$

Once the data has been acquired the data undergoes a standard set of processing algorithms whereby the two way travel times are stacked and reflections are repositioned as close to their true geometry as possible (Robinson, 1988). A full description of the standard seismic acquisition and processing sequence can be found in Yilmaz and Doherty (1987). The basic processing sequence is often sufficient in settings where strata are sub-horizontal and where ray paths occur at low angles of incident with respect to the strata (Fig. 2.1) however around vertical structures such as salt diapirs and faults additional data processing is required. The cartoon in figure 2.1 illustrates the complexity of the ray paths.

The time from the seismic source to an acoustic impedance boundary and back to the geophone detectors is termed the two way travel time (TWT), it is often given as the vertical scale in a seismic section and may also be converted to a vertical distance with knowledge of wave velocity (Brown, 2004). Equation 2.2 expresses the relation of time (t) that is proportional to the ratio of distance (d) and velocity (v).

$$t = \frac{2d}{V} \tag{2.2}$$

Generally, seismic wave velocity increases with depth as the wave advances through more compacted sediment and rock (Kearey *et al.*, 2002; Brown, 2004). However, other properties of the subsurface can control the velocity of the seismic wave, these include; lithological composition, porosity, density, material texture, elastic modulus and fluid content (Mavko *et al.*, 2009). Two other key properties of a seismic data volume are the wavelength and frequency of the wavelet. Wavelength is the distance from wave peak to peak, while frequency is a measure of how many peaks pass through a point per second. Both are related to wave velocity where wavelength (λ) is the quotient of the velocity (v) of the wave and the frequency (*f*) (equation 2.3), and if assuming a constant velocity, wavelength is inversely proportional to frequency i.e. higher frequencies form shorter wavelengths.

$$\lambda = \frac{V}{f} \tag{2.3}$$

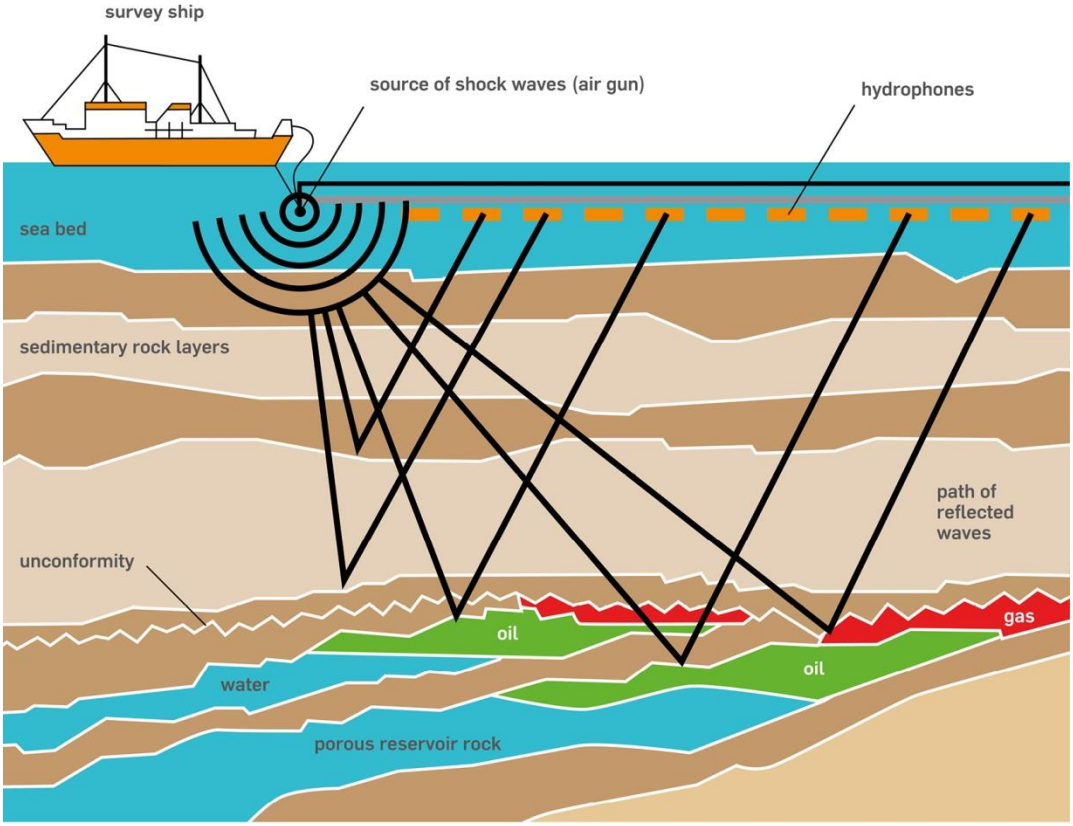

Figure 2.1: Cartoon showing a typical set up for marine acquisition of seismic data. The black lines show typical ray paths for p-waves from an energy source, their reflection at interfaces of contrasting acoustic impedance $v \times p$, of different interfaces and detection at a set of hydrophones (Orange rectangles). (http://www.open.edu)

2.2.1. Colour convention

Seismic sections presented in chapters 3-6 are displayed using a black-white-red or black-white-yellow-red colour schemes. Following the SEG colour convention, positive reflection events are red and negative reflection events are black with white depicting zero-crossings (Fig 2.2A). According to common convention shown in figure 2.2A, seismic data in this thesis is displayed in zero phase SEG (Society of Exploration Geophysicists) normal polarity during processing indicating that acoustic impedance contrasts coincide with the peak of the seismic wavelet and that the wavelets are symmetrical with the peak corresponding to the zone of maximum energy (Yilmaz and Doherty, 1987; Evans and Dragoset, 1997; Brown, 2004) (Fig. 2.2A).

The convention of SEG normal polarity is that an interface defining a positive downward acoustic impedance contrast coincides with peak in the seismic wavelet whilst an interface defining a negative downwards impedance contrast coincides with a trough in the seismic wavelet. The high amplitude events typically occur due to velocity and density contrast at the interface between the sedimentary overburden. The positive amplitude event occurs at with increasing density and velocity contrast (seabed at figure 2.2B). Conversely the interface defining a downward transition from sedimentary overburden to any soft anomaly like gas accumulation represents a negative impedance contrast and is thus defined by a seismic wavelet with negative amplitude (Gas anomaly in figure 2.2B) (Evans and Dragoset, 1997). Despite evaporites having low density with respect to the sedimentary overburden the internal p-wave velocity is significantly higher thus increasing the magnitude of acoustic impedance relative to the sedimentary overburden. Wave amplitude (height of the peak or trough) corresponds to the

magnitude of impedance contrast, higher the impedance contrast leads to high amplitude (Brown, 2004)

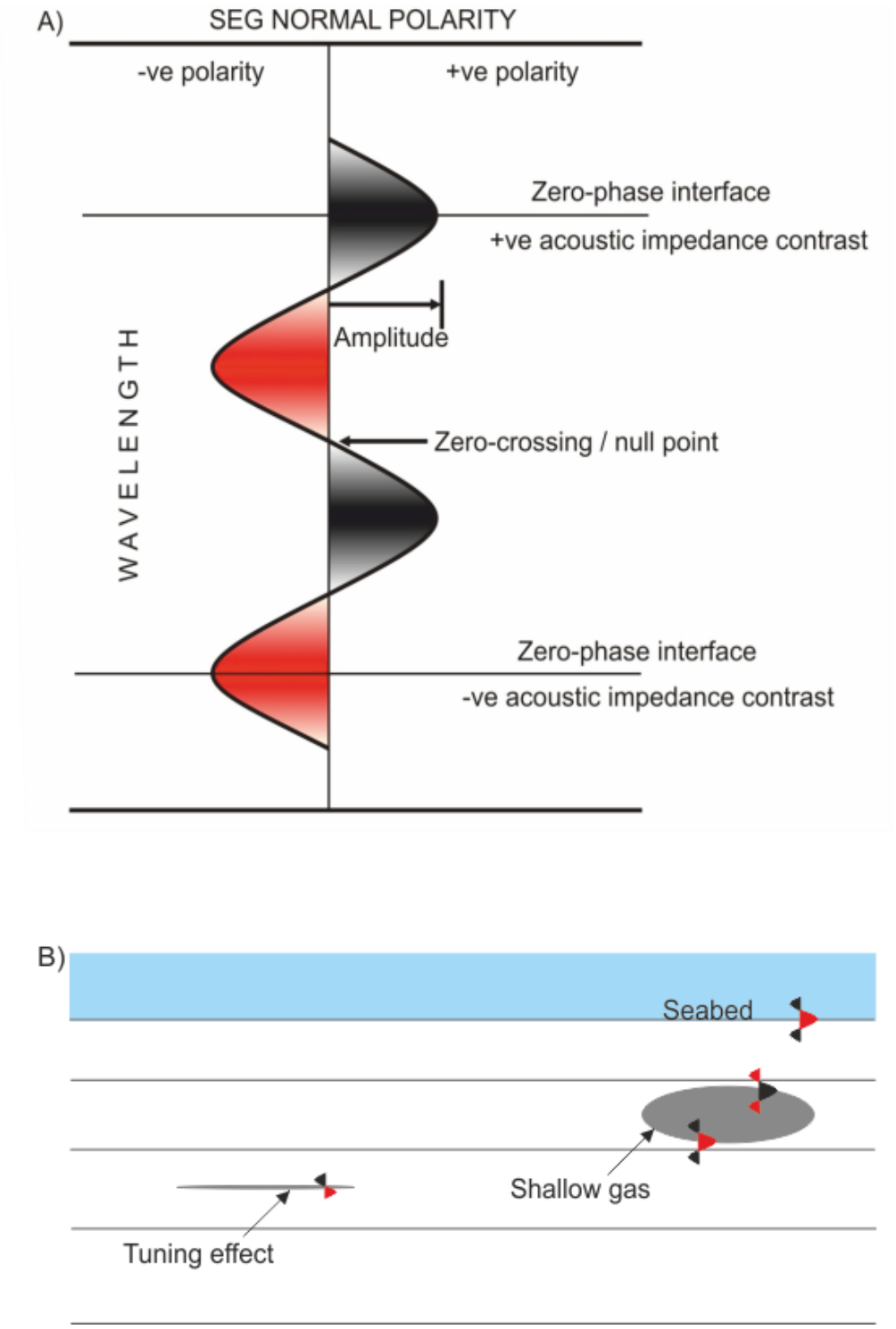

Figure 2.2: A) SEG colour convention for the display of seismic data. Positive impedance contrasts are shown in black. Negative impedance contrasts are shown in red. Zero crossings are shown in white. B) Polarity of reflection events at the interface between water and sediments (seabed), top of gas accumulation (soft reflection), at base of gas anomaly (hard reflection) and paired reflection at the thin bed (tuning effect).

2.2.2. Seismic resolution

Seismic resolution is defined as the ability of seismic data to distinguish between separate features both vertically and horizontally. Resolution relates to the minimum distance that two points can be located to each other and be distinguished on seismic sections (Yilmaz and Doherty, 1987). So one of the main problems in seismic interpretation is to be able to determine how and where to distinguish geological elements that are resolved and unresolved. In other words to enhance seismic resolution in both directions vertical and horizontal (Brown, 2004)

2.2.2.1. Vertical resolution

Vertical resolution or the limit of separability is the limit at which the top and base of bed is no longer detected as a single wavelet (Brown, 2004). Vertical resolution is a function of the dominant wavelength (λ) which is the quotient of p-wave velocity (v) and frequency (f). Generally the internal P-wave velocity of strata increases with depth as the rocks have become progressively more hard and compacted during burial. The frequency range may vary according to specific surveys but low frequency waves generally permeate to greater depths whilst high frequency waves are attenuated at shallow depths due to adsorption (Brown, 2004). Thus, deciding what range of P-wave frequencies should be emitted from the geophone is essential when there is a specific interval of interest in the survey i.e. Cretaceous and Palaeocene plays between 1.5 - 3.5 km depth in the UK Central Graben (Kearey *et al.*, 2002; Brown, 2004). Vertical resolution is typically taken to be ¼ λ. When beds thickness is below ¼ λ the amplitude

of the wavelet becomes progressively attenuated until the limit of visibility is reached and the reflection signal is obscured by background noise (Fig. 2.4).

2.2.2.2. Horizontal resolution

The distance at which two points can be distinguished in the horizontal plane (horizontal resolution) is a function of the hydrophone spacing and the width of the Fresnel zone (Fig. 2.3A). For un-migrated seismic data, the horizontal resolution is equal to the first Fresnel zone (Yilmaz and Doherty, 1987; Sheriff and Geldart, 1995; Kearey *et al.*, 2002) (Fig. 2.3B). The Fresnel zone is defined as 'the portion of the reflector from which the reflected energy can reach the receiver within the first half cycle of the reflection'. 'Amplitudes reaching the detector from this zone constructively interfere to produce a reflection' (Sheriff, 1980). Horizontal resolution is improved during pre-stack migration as diffractions below the first Fresnel zone are resolved. The horizontal resolution of pre-stack migrated data is regarded as ¼ λ.

The horizontal resolution is also restricted by the lateral sampling of the data which is governed by the spacing between individual hydrophones toed behind the acquisition vessel. The reflection points on a surface have a horizontal resolution of equal to half the geophone/hydrophone spacing. The horizontal resolution of the data is equal to the larger of the two values. The detector spacing does not usually affect the lateral resolution for migrated data (Davies *et al.*, 2004; Sheriff *et al.*, 2010). Detector spacing may however influence the lateral resolution where the seismic data has sufficiently high frequency (> 50 Hz) and where the interpreter is concerned with the very shallow subsurface (< 1 s). The horizontal resolution of the seismic data can be assumed roughly constant where the strata are (sub) horizontal but around the diapir where strata

are often steeply inclined the lateral resolution may decrease due to a spreading of the Fresnel zone (Yilmaz and Doherty, 1987).

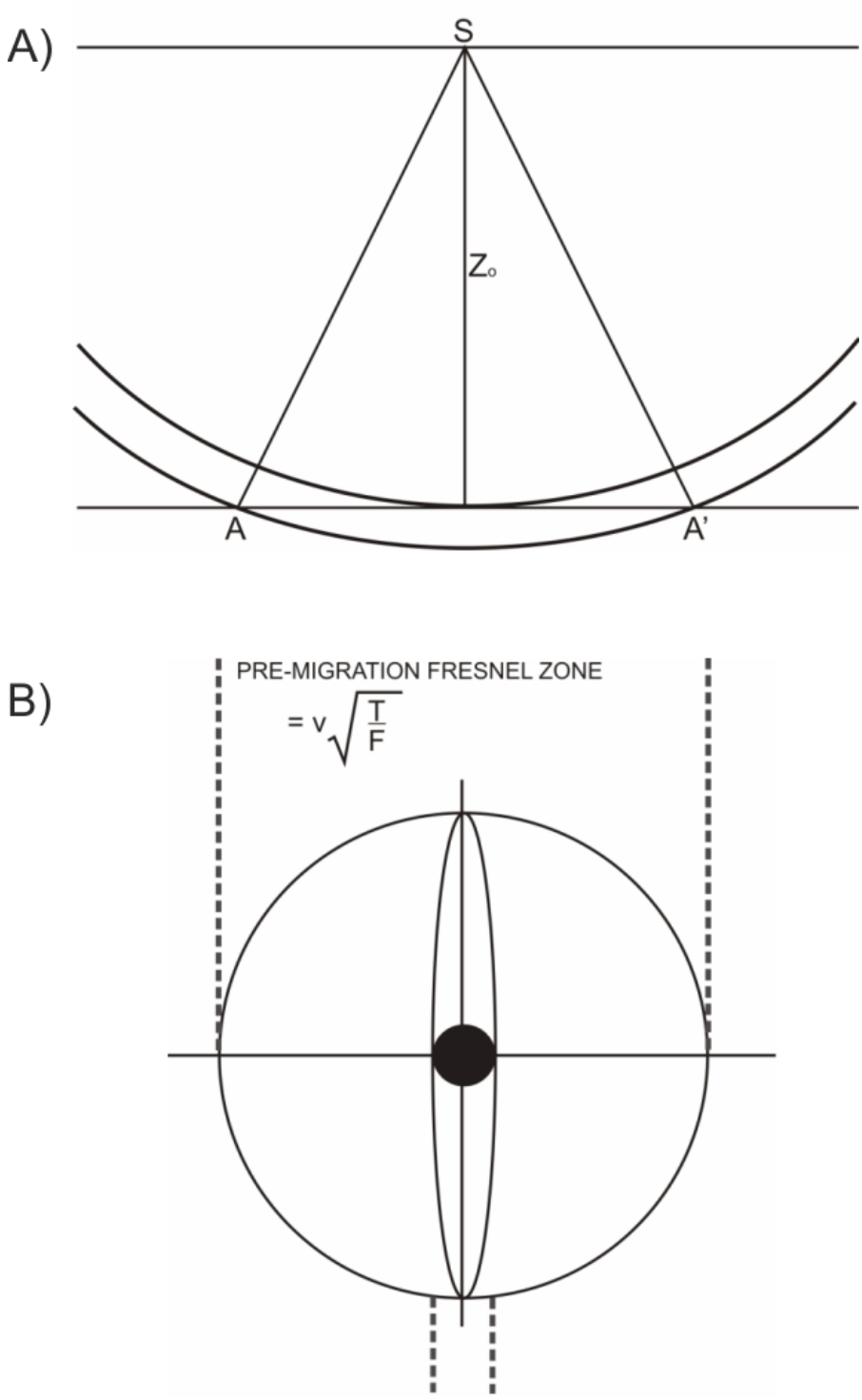

Figure 2.3: Horizontal resolution. A) Fresnel zone A-A' for an energy pulse created at the sea surface (S) and striking a horizontal geological interface at depth Z_0. B) Reduction in the width of the Fresnel zone following migration of seismic data. The post migration Fresnel zone is one quarter of the dominant wavelength.

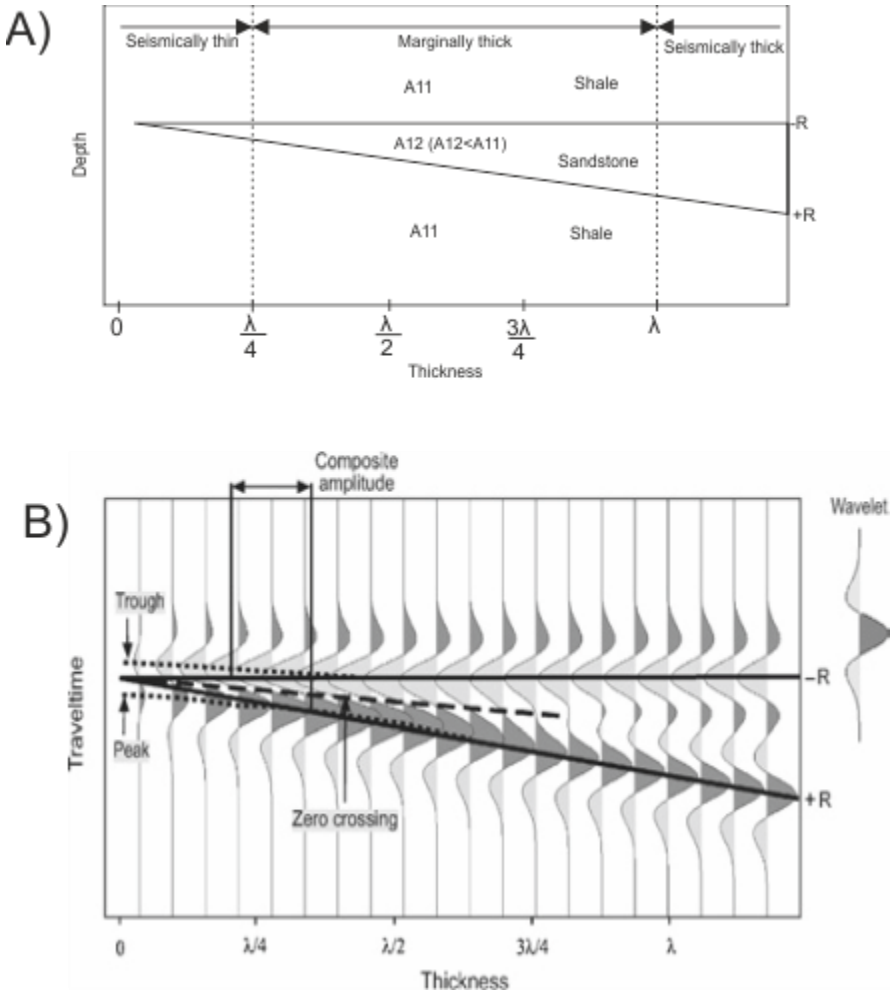

Figure 2.4: A) Wedge acoustic impedance (AI) model of sandstone encased in thick shale. Assuming constant AI in sandstone and shale, R is negative at the top and positive at the bottom, with the same magnitude; λ denotes seismic wavelength. B) Zero-phase Ricker seismic model. Despite the symmetric shape of the Ricker wavelet, composite waveforms are symmetric only in seismically thick beds (>λ). Antisymmetric seismic responses dominate when a bed thins. If the bed is thinner than λ/4, deviation between reflection interfaces and seismic trough–peak measurements (indicated by dashed lines) occurs. Neither polarity nor amplitudes in asymmetric waveforms match wedge geometry (lithology).(modified from (Zeng and Backus, 2005)

2.3 Seismic data

3D seismic survey was carried out to improve imaging through gas clouds, characterize high amplitude anomalies in terms of fluid flow contents and provide clues as to the origin of these anomalous bodies from the back ground (Robinson, 1988).

2.3.1 The Mid Norwegian Sea

3D multi-channel, poststack, time-migrated reflection seismic data used for chapter 3 (Fig.2.5). The seismic data display used here are zero phase, SEG normal polarity, (black peak indicating an increase in acoustic impedance ‘‘American polarity’’). The 3D seismic survey covers an area of 1300 km^2 and is 120 fold with a 4 ms TWT sample rate. The 3D grid is subdivided into inline and crossline directions, spaced at 25 m and 25 m respectively. The frequency range in the shallow subsurface is 7.5–90 Hz with a dominant frequency in the 42–50 Hz range. Assuming a dominant frequency and a velocity of 1600–1900 m/s, the seismic resolution, defined as a quarter of the dominant wavelength, would be 10–15 m. This implies that anomalously high (tuned) amplitude due to constructive interference would occur for thicknesses of 2–9 m, the average thickness depending on the exact frequency and velocity for a given sedimentary layer in the main geological boundary “Brygge Formation". Two nearby wells (6403/10-U1 and 6404/11-1, Fig. 2.5) provide velocity data for the stratigraphic interval and velocity values ranges between 1700 m/s and 2100 m/s. An average interval velocity of 2000 m/s was considered suitable for depth and thickness estimations (1 ms is equivalent to 1 m). The horizontal resolution ranges between 25 and 50 m, and the vertical stratigraphic resolution between 7 m and 14 m.

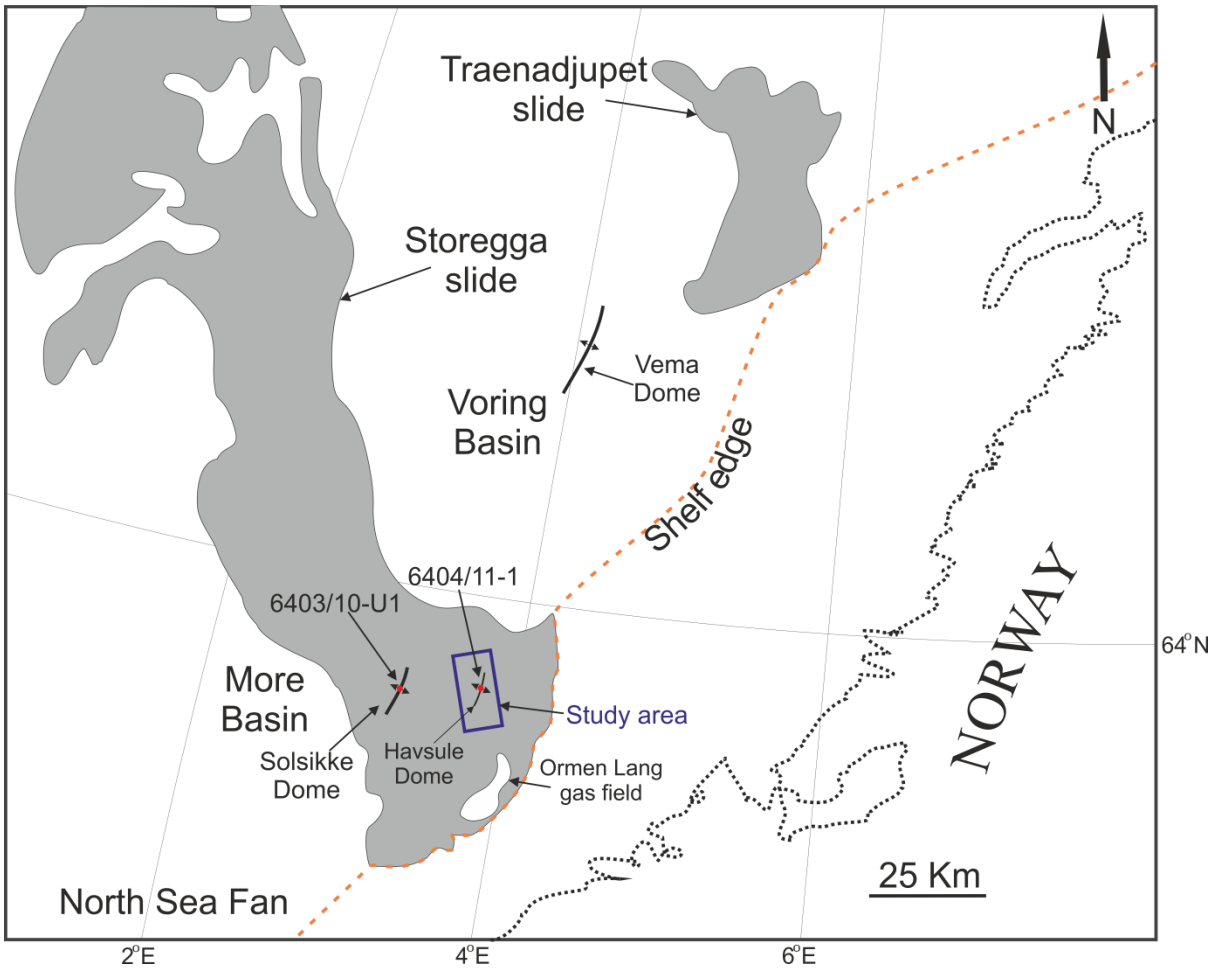

Figure 2.5: Location map of 3D seismic survey in the mid Norwegian Sea. The survey is situated at the south edge of Storegga Slide (modified from (Riis *et al.*, 2005).

2.3.2 The Lower Congo Basin seismic data

The 3D seismic reflection data used for this study were acquired on the outer continental shelf of the Angola margin (Location is not shown due to data confidentiality), in a water depth of 800 to 1300 meters, with a near-seabed velocity of 1700m/s. The survey provided by *"Caprocks project"* for analyses of high-amplitude anomalies that developed in the waste zone above main Oligocene-Miocene turbidite reservoirs. The study survey consists of an area of 1310 km². It has a dominant frequency of about 55 – 60Hz with a main vertical resolution of about 7 ms. Survey extends from the seafloor to sedimentary section with depth of 4.5s two-way travel time (TWT). High density 3D (HD3D) cube has a bin size 6.25 x 6.25 m yielding a horizontal resolution of 6.25 m.

The seismic data is zero phase and the downward increase of acoustic impedance is represented by positive amplitude value, i.e. SEG normal polarity. Three different cubes near, middle and far offset were generated at different processing stages but only the near offset data cube were available for the research of this thesis for chapter five and six. Rock physical analysis of the seismic data was beyond the scope of this study.

2.3.3 Well data

A set of six exploration wells (location of these well are confidential so not showed for the whole thesis) were drilled on the basis of this data set from the Lower Congo Basin. Two exploratory wells were available for the Norwegian case study. Wireline logs and unpublished commercial well reports, mainly based on cutting analyses were available for all the wells. Due to non-availability of check shot or vertical seismic profile (VSP) data therefore well data is not calibrated with seismic data. High-amplitude anomalies are possibly

avoided during well planning due to risk hazards (Cartwright *et al.*, 2007; Andresen, 2012). Therefore, no well directly calibrated high-amplitude anomalies in the two data sets. In the Lower Congo Basin, only three of the well logs (out of six wells) were available for chapter five and six. Only one well W41 out of these three penetrated through high-amplitude anomaly and has been calibrated it well logs for confirmation of presence of hydrocarbons (Chapter 4).

2.4 Seismic interpretation of HAAs

The interpretation of 3D seismic data represents the core method used in this research project. In the past, 2D and 3D seismic interpretation has been used for the analysis of the high-amplitude anomalies and their associated fluid flow mechanism in the Mid Norwegian and Lower Congo Basins. Nonetheless, previous work on this field has been limited to the analysis of relatively low-resolution 2D seismic data (e.g. (Gay *et al.*, 2006). Indeed, the present research project represents the first comprehensive work on the analysis of high-amplitude anomalies using a simple 3D and HD3D seismic data. This has allowed an excellent coverage of the basinal distribution of HAAs in the region and has enabled their associated fluid flow mechanisms to be resolved at the limit of seismic data accuracy. In this section, the methodology used for the interpretation of HAAs in different sedimentary levels on seismic data, coupled with an assessment of their seismic response and imaging problems, are presented.

2.4.1 3D seismic interpretation software

Seismic interpretation provides the main approach for visualising and analysing of high-amplitude anomalies and associated structural and/or stratigraphic features. Seismic interpretation was undertaken on two state of the art software platforms to the project at the 3D Lab in Cardiff University. For the interpretation work, the majority of interpretation was under take on a Sun System with Schlumberger's Geoframe software. Some interpretation work (3D visualization) was undertaken on Schlumberger's Petrel software.

2.4.2 Horizon and fault interpretation

The 3D seismic data was interpreted in the IESX software (Geoframe, Schlumberger) and window based schlumberger's Petrel software. Seismic interpretations included analysis of seismic amplitude maps. The RMS seismic amplitudes were used to map the spatial distribution of enhanced reflections at inferred stratigraphic intervals of free gas accumulations in the form of high amplitudes.

For visualization and interpretation of the 3D seismic data, the IESX software (Geoframe, Schlumberger) seismic interpretation software was used. The Automatic Seismic Area Picker (ASAP) is the software's tool for tracking horizons. It uses the interpretation done within one or more inlines or crosslines as a "seed" and tracks across the surface as we "paint brush" it. Parameters have to be chosen for the ASAP in accordance with part of the seismic wavelet to be tracked along the horizon, that is to follow maximum or minimum amplitude, or upper or lower zero crossing. The quality of the interpretation is very important here, as you interpret quickly through large areas, so it is imperative to specify correct parameters for the quality control of the ASAP, this is done in a set of tabs on the ASAP tool including dip/trace, track

technique and quality, correlation, and snap range. Choosing too strict quality control will lead to many areas being left uninterpreted, while choosing too loose parameters will lead to a lot of "miss-picks". Seismic interpretations included analysis of seismic amplitude maps.

Detailed seismic interpretation is an important step to understand the distribution of high amplitude anomalies. Interpretation is based on careful identification of continue reflections called "seismic horizon" and further more identification of amplitude anomalies. Structural analysis was undertaken using a combination of two traditional seismic interpretative techniques 1) horizon interpretation to understand the planform geometry of faults surrounding salt diapirs and 2) mapping or tracking of fault planes to view how the 3D geometry of fault planes forms (Brown, 2004).

Throughout this PhD thesis seismic sections and maps are displayed in milliseconds (ms) two-way travel time (TWTT). Depths and thicknesses are expressed in metres (m) where time-depth conversion was applied.

2.4.2.1 Horizon interpretation

Seismic horizons were tracked by manually following horizon events or reflections which correspond to key horizons of interest. Most of the time these seismic horizons are continuously traced throughput seismic data sets. Two way travel time maps were extracted through these interpreted seismic horizons. The process of horizon interpretation is summarised as follows but relates to the standard techniques illustrated in Brown, (2004).

1. Horizons were tracked on grids spaced between every 5-50 inlines and cross lines depending on the complexity and lateral continuity of the reflector.

2. Horizons were tracked laterally and where available, well data was used to aid regional scale mapping or horizons which are laterally discontinuous.
3. During tracking, the horizon was snapped to the peak of the horizon event or reflection i.e. positive or negative loops.
4. Horizon maps and surfaces were made by interpolating along horizons events between tracked seed points by using an automated process called ASAP.
5. Steps 1-4 were repeated in a quality control workflow to ensure maps were completed with a desirable level of quality.

2.4.3 Surface attribute analysis

Vertical seismic sections fail to clearly identify some important stratigraphic features because they are typically manifested as subtle variations in amplitude strength, phase shift, or polarity reversal and are easily overlooked by interpreters. Imaging these features in a horizontal view adds additional information of spatial distribution to the typical seismic cross-section geometries used to interpret seismic facies and thus infer depositional pattern that lend insight into the associated reservoir quality. The sinuous nature of these features can only be seen in such a horizontal view and well data from the area, as well as analogs from other fields, indicate that such sinuous features are highly likely to be incised valleys or channel reservoir sands.

Complex trace seismic attributes, including measures of seismic amplitude, frequency, and phase, have been used successfully in mapping seismic lithology changes for almost three decades. Multitrace relationships, including cross correlation techniques, have been used in

the automatic picking of static corrections and 3-D seismic horizons (Haskell, 1995) over the past decade.

Seismic data can elucidate fluid flow in the sedimentary basin if flow related processes affect sediment structure e.g., by creating faults and fractures or sediment physical properties, e.g., by changing porosity which influence density and seismic velocity (Zühlsdorff and Spiess, 2004). The presence of hydrocarbons such as methane may also affect seismic data since a free gas phase attenuates seismic signals (Wood *et al.*, 2002).

Once horizon maps were obtained a variety of seismic attributes were calculated to reveal the aspects of the geometry or physical properties of the surface. A number of different attributes are useful for fault visualisation.

2.4.3.1 TWT and amplitude

The first and most basic maps to be generated from seismic data derived from the geometry of the reflection and the amplitude of the corresponding wavelet, so called, two-way travel time (TWT) maps and acoustic amplitude maps. A TWT map defines the approximate sub-surface geometry of geological interface (when time can be approximated to depth) and are thus useful for imaging faults which have large throws with respect to the regional gradient of the faulted surface (Fig 2.6A). Horizon fault intersections are detected on amplitude attributes by low acoustic amplitudes with respect to that of the host layer. The later is useful for detecting small or densely spaced fault systems such as polygonal faults (Fig. 2.6A and C).

2.4.3.2 Dip

Dip maps are the first derivative of TWT maps. Dip is a particularly useful attribute for imaging fault patterns which are composed of faults with small throws (5-100 m) and intersecting sub-horizontal or gently dipping surfaces (Fig. 2.6E).

2.4.3.3 Petrel generated TWT maps

A blended of two way travel time and vertical relief (Dip) can be created in Petrel by displaying horizon maps in 2D and increasing the vertical exaggeration (Fig. 2.6). This has the potential of understanding how fault geometry relates to the structural relief of a folded or dipping surface.

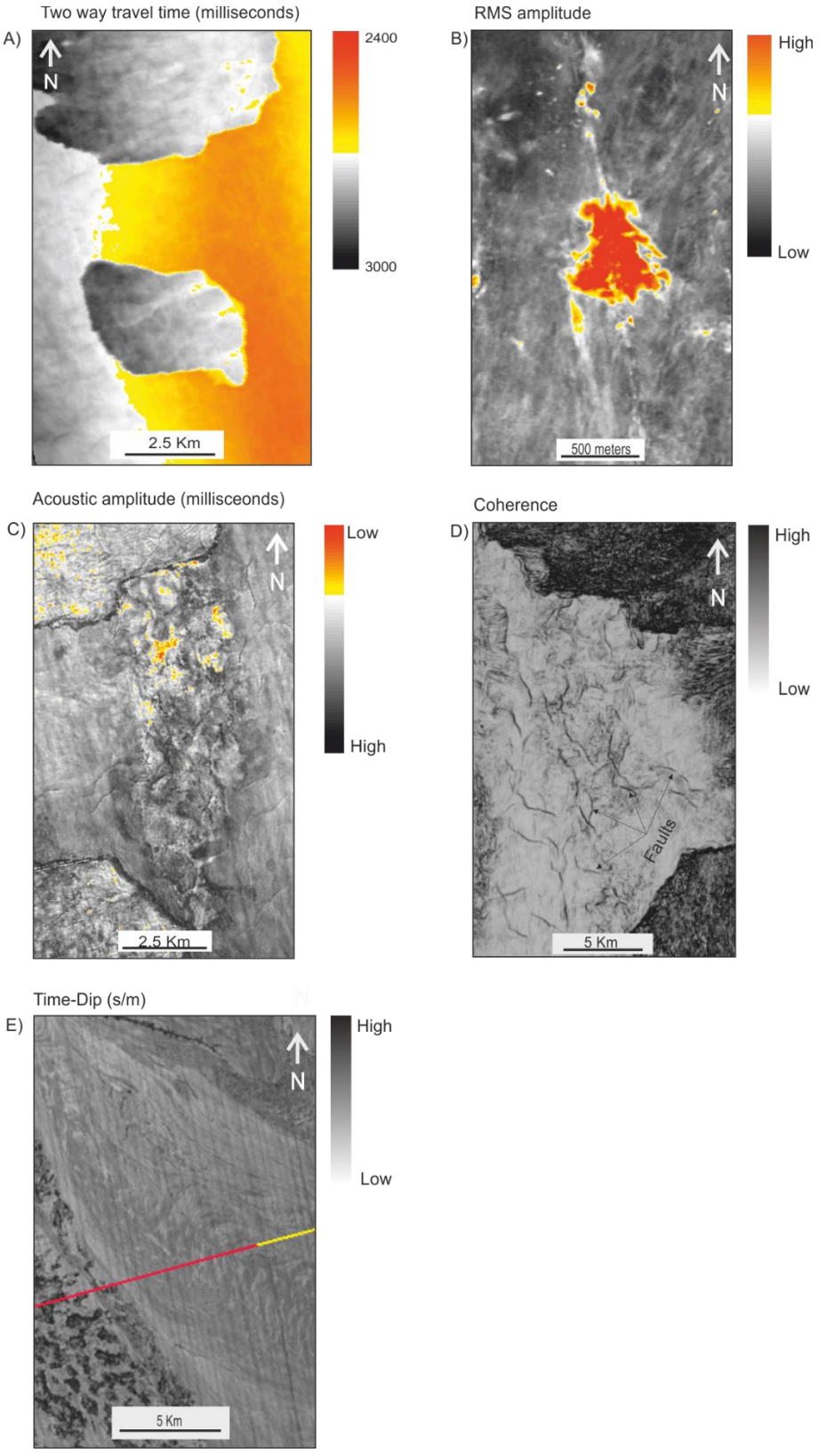

Figure 2.6: Seismic interpretation made through different interpretation methods (tools) to delineate high-amplitude anomalies A) Two way travel time in milliseconds B) RMS amplitude, C) Acoustic amplitude, D) Coherence slice, E) Time-Dip map

2.4.4 Volume attribute analysis

The study and interpretation of seismic attributes give some qualitative information of the geometry and the physical parameters of the subsurface (Taner, 2001). Volume attributes were computed from 3D reflection seismic data sets like coherency, Root Mean Square (RMS) amplitude, Instantaneous phase and Instantaneous frequency. These seismic attributes are used to map the spatial distribution of enhanced reflections at inferred stratigraphic intervals of free gas accumulations in the form of high amplitudes. Seismic attributes are used to enhance recognition of the high amplitudes, coherent events and to emphasize discontinuities, faults, stratigraphic surfaces and unconformities to understand the effect on the amplitude of the reflections of sediment versus fluid charging of the layers (Calvès *et al.*, 2008). The seismic RMS amplitude between horizons was computed and used to detect the occurrence of anomalous amplitudes. Hydrocarbon gas in shallow porous sediments is detected by high-amplitude reflections and the absorption of high-frequency components of the underlying seismic section (Castagna *et al.*, 2003).

2.4.4.1 Coherency

The 3D seismic coherency cube extremely effective in delineating seismic faults when sufficient lateral change in acoustic impedance (Bahorich and Farmer, 1995). The Coherence Cube is essentially a cube of coherence coefficients generated from the input 3D seismic data volume that portrays faults and other stratigraphic anomalies clearly, on time or horizon slices.

Seismic coherency is a measure of lateral changes in the seismic response caused by variation in structure, stratigraphy, lithology, porosity, and the presence of hydrocarbons. Unlike

shaded relief maps that allow 3D visualization of faults and channels from horizon picks, seismic coherency operates on the seismic data itself and is therefore unencumbered by interpreter or automatic picker biases (Marfurt *et al.*, 1998). In the Norwegian study area, for example an anomaly is developed in the Brygge formation and has many polygonal faults inside the anomaly. These faults are not clearly visible due to the presence of enhanced amplitudes with anomaly. So the seismic coherence cube is computed to analyse lithological variation and relationship of polygonal fault to formation of the anomalous zone.

Coherence attributes are calculated based on quantifying the degree of vertical and lateral discontinuity or coherence of reflections in the 3D time volume (Bahorich and Farmer, 1995; Marfurt *et al.*, 1998; Chopra and Larsen, 2000; Brown, 2004). A variety of similar attribute such as variance are also available within the Petrel seismic interpretation software. Figure 2.6D shows an example of faults around an anomaly that developed in the Norwegian Sea data set.

2.4.4.2 RMS Amplitude

Seismic reflection amplitude information can help identify unconformities, reefs, channel and deltaic sands, lithology, and gas/fluid accumulations. Amplitude anomalies may also be attributed to constructive or destructive interference (tuning effect) caused by two or more closely spaced reflectors and/or to variations in net sand within a thin-bed unit (DeAngelo and Wood, 2001).

Many other seismic attributes were test and analysed to understand high amplitude anomalies in the study interval. The root mean square amplitudes observed good to carry forward because it gave the combined effect of positive and negative amplitude that possibly due to

presence of hydrocarbon interested interval. RMS amplitudes are calculated as the square root of the average of the squares of the amplitudes found within an analysis window. The RMS amplitudes are sensitive to sandstone-bearing depositional systems tracts within the reservoir-bearing successions and help define the spatial distribution of genetically related depositional successions. Such RMS amplitude maps may image stratigraphic leads that have been missed by previous exploitation programs (DeAngelo and Wood, 2001).

2.4.4.3 Instantaneous phase and Frequency

The instantaneous phase attribute is considered a good indicator of continuity of seismic data, and so is useful in identifying and interpreting sequence boundaries. Because phase is independent of reflection strength, it often makes weak coherent events clearer. Phase displays are effective in showing discontinuities, faults, pinchouts, angularities, and events with different dip attitudes which interfere with each other (Taner *et al.,* 1979). The instantaneous phase attribute has also been used to define a flooding surface (Lee *et al.*, 2010). Instantaneous phase is a seismic attribute based on the Hilbert transform, and is given by the equation (2.4);

$$\emptyset(t)=\tan^{-1}[(G(t))/Re(G\_K\ (t)))] \qquad 2.4$$

Where $\emptyset(t)$ is the instantaneous phase value at time (*t)*, *arctan* is the inverse tangent, *G(t)* is the value of the seismic trace at time *t*, Re is the real or recorded part of the seismic trace.

The instantaneous frequency attribute is considered a good tool for lateral seismic character correlation (Lee *et al.,* 2010). In the past, a low instantaneous frequency anomaly has been used to predict conventional hydrocarbons (oil & gas) accumulations in the oil industry.

Instantaneous frequency is also based on the Hilbert transform and is given by the derivative of the instantaneous phase (Fig. 2.7 and 2.8).

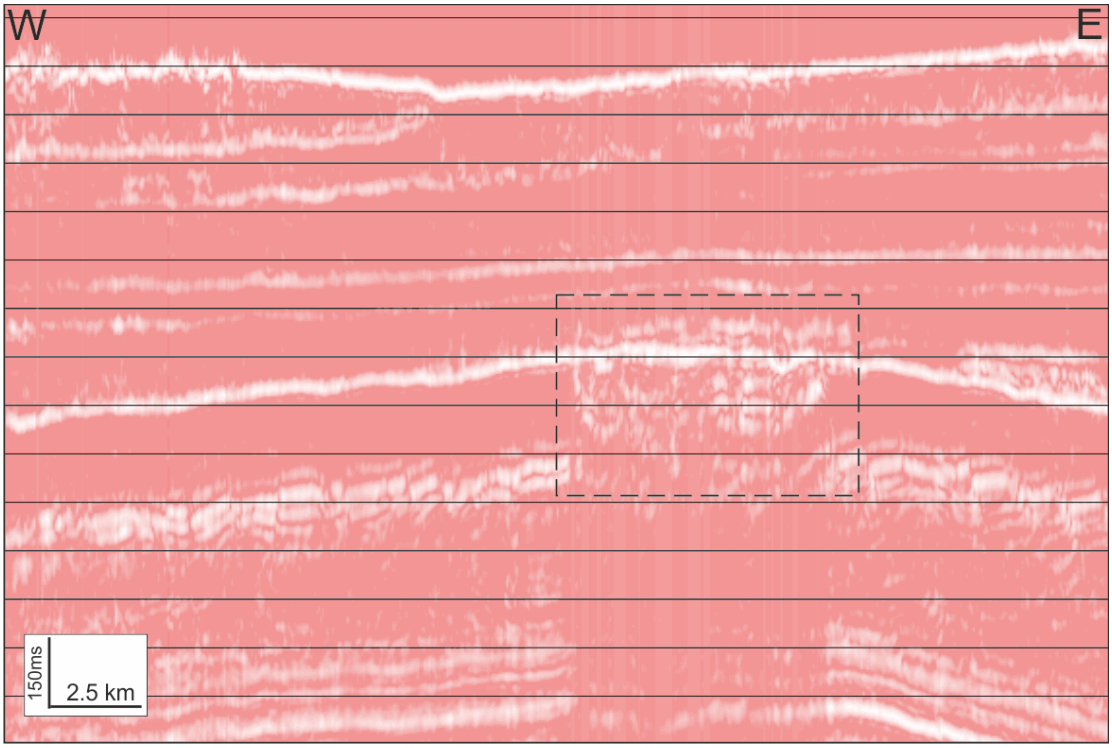

Figure 2.7: A seismic profile from instantaneous frequency data set shows low frequencies in white.

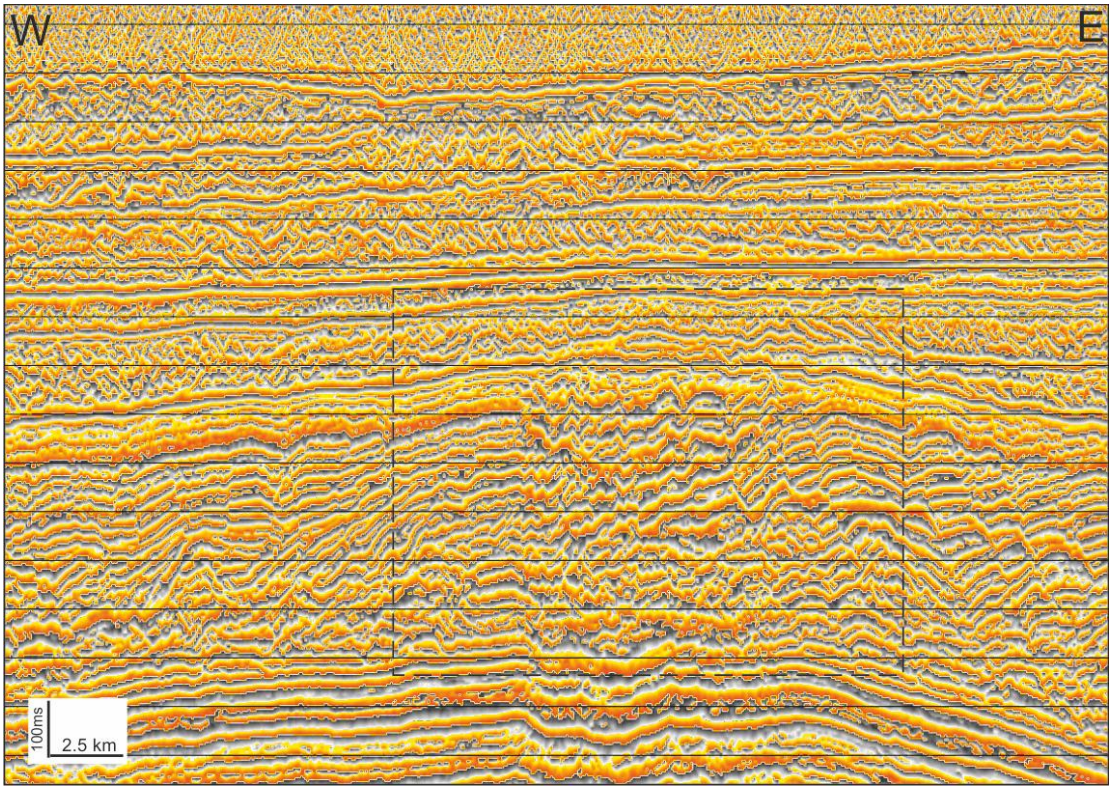

Figure 2.8: Example of instantaneous phase seismic profile that showed continuity of reflections inside seismic anomaly (rectangle)

2.4.5 Advance techniques

As horizon mapping of densely faulted horizons for example polygonal faults is time consuming due to the need for a dense mapping grid, automated techniques are used in some cases. These techniques are based on slicing of amplitude and coherence volumes parallel to underlying or overlying surfaces, a technique referred to as iso-proportional slicing or stratal slicing. Iso-proportional sculpts are generated by creating surfaces which are geometrical averages of reference horizon (Fig. 2.9). At a more simple level coherence slices are generated sub-parallel to stratigraphy by simply flattening horizons at a key horizon and scrolling up and down through the volume.

Stratal slicing had been used to compute of RMS (Fig. 4.7 in chapter 4). E-W seismic profile showing main stratigraphic subdivision to detailed analysis of high-amplitude anomalies, their extent and geometry, for example the Waste zone between H130 to H250 interpreted horizons in the LCB. The upper boundary is marked by H130 seismic horizon below regional seal unit 3 of the Early Miocene to seismic horizon H490 base of seal unit 4 of the Late Oligocene age. The time interval between main reflectors are H100-H130=80 to 90ms, H130-H200= 100 to 120ms, H200-H250= 90 to 150ms, H250-H290= 60 to 150ms and H290-H90= 200 to 250ms.

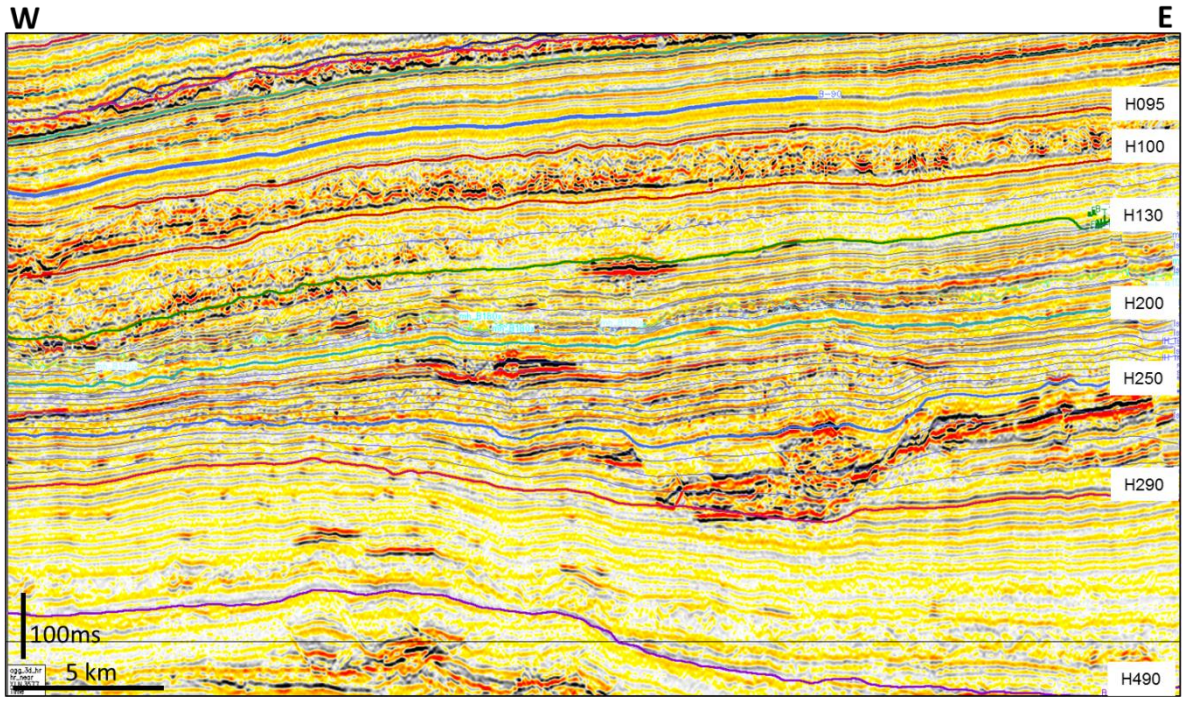

Figure 2.9: Seismic profile showing the iso-stratal methodology adopts for careful and detailed observation of high-high amplitude anomalies and their associated fluid flow mechanisms.

2.4.6 Analysis of fault patterns

A component of the fault characterisation and diapir interpretation involves a basic quantitative analysis based on manual measurements from either maps or seismic cross sections. Measurements types include; spacing and density of fault systems, fault length, spatial variations in fault orientation, fault height, inclination of overburden against salt diapir. Each of the separate methodologies and workflows used to obtain the above measurements are presented in the relevant results sections in Chapters 3-6.

2.5 Identification of HAAs

The simple workflow for identification of high-amplitude anomalies associated fluid flow features used in this study involved a systematic examination of seismic data (Fig. 2.10) for different types of anomalies (for more detail chapter 4 and 5). The identification and analysis of anomalies was done through careful analysis of vertical seismic sections, time maps and slices, surface and volume based seismic attributes. Iso-proportional slices subdividing interval of two interpreted seismic horizon into several sub-intervals for detailed spatial geometrical analysis of anomalies through generating long and short window volume attributes particularly amplitude and coherency. These volume attributes were helpful for detection of fluid flow features. The surface attributes that were extracted of both manually interpreted horizons and derivative iso-proportional horizons.

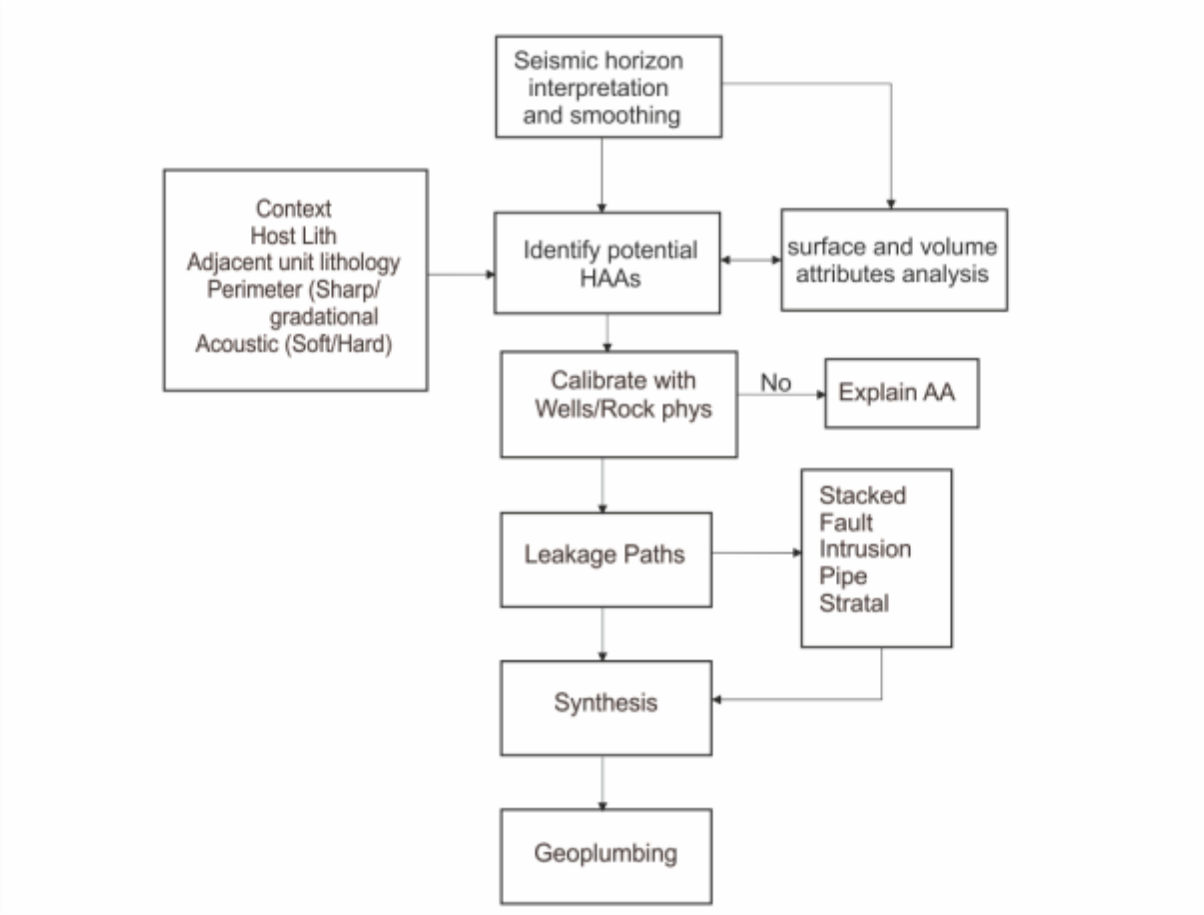

Figure 2.10: Workflow for identification of hydrocarbon related high-amplitude anomalies, their associated fluid flow feature and geoplumbing system.

2.6 Limitations due Seismic quality and availability of well data

The greatest limitation encountered during seismic interpretation is lack of availability of well data to correlate interpretation for age control. Only one well 6404/11 was drilled in the Norwegian case study and 6 exploratory well data from the LCB were available for this research. Only two well data are useful for this study because; (1) the degree to which interpreter depends on sub-surface data (borehole data), (2) the accuracy in the position of seismic reflections with respect to the true geological interface, and (3) seismic resolution. The first two form the main limitations faced during this research. As explained in section 2.3 and 2.4 these occur due to the difficulty to obtain an accurate or clear image of strata adjacent to diapirs or beneath salt overhangs.

2.6.1 Calibration of HAAs on seismic and ground truth

The second major limitation that was encountered in this research was that the interpretation of positive high amplitude anomalies was entirely based on geophysical aspects and on comparison with previous studies. The opportunity of relating seismic amplitude anomalies with ground truth, has not been provided.

2.6.2 Age of seismic stratigraphic units

Confidential well data, mud logs and formation picks were used to calibrate seismic horizons with the regional stratigraphy. Ages for each of these units and their bounding surfaces have been obtained by standard biostratigraphic dating techniques such as identification of specific assemblages of foraminifera (Berggren *et al.*, 1995). Well data and age constraints are sparse

and generally lacking in the shallowest section (Pliocene-Quaternary units). Ages of horizons within these units were estimated by assuming a uniform sedimentation rate and extrapolating ages from known surfaces based on interval thickness. Given that the Pliocene-Quaternary section is largely composed of hemipelagic sediments, the sedimentation rate would not be expected to change to significantly (cf. (Mulder *et al.*, 2010). Thus, I consider the estimations of ages for horizons in this interval as fairly close to their true age.

CHAPTER 3

The Analysis of High Amplitude Anomalous Zone with Concave Upward Base

CHAPTER THREE

3.1 Introduction

High amplitudes anomalies are prominent features usually observed on seismic data. They form in response to a real, physical changes in the subsurface lithology and can also result from various kinds of noise internal to the geophysical equipment, or noise from external sources. Seismic interpreters attempt to understand the nature of the high amplitude anomalies through different geophysical methods.

The aim of this chapter is to analyse the geophysical expression of free gas in marine sediments. Free gas can be detected on seismic data by the change in seismic velocity that results from gas in the pore spaces of the sediments. This leads to a stronger amplitude reflection than would result from a purely water filled pore volume, and is visible on seismic data as an amplitude anomaly (Brown, 2004; Løseth *et al.*, 2009). This study focuses on a description of seismic amplitude anomalies from a 3D seismic data set located in the mid Norwegian Sea. A series of amplitude anomalies are observed within the biosiliceous sediments of the Miocene age beneath a regional claystone seal of Pliocene age. These anomalies show an extraordinary geometry: they cluster beneath the crest of a large domal anticline and have a basal boundary that is strongly cuspate with a concave upwards shape.

The main questions addressed in this chapter are;

1 How these seismic anomalies are developed and what is the source of this high-amplitude anomalous zone? Is the high amplitude anomalous zone a lithological barrier or related to hydrocarbon accumulation?

2 Why does the anomaly have an extraordinary geometry?

3 What are the kinematics that can be derived from the geometry of the anomaly?

A model is proposed to understand the development of the extraordinary shape and geometry of the anomalous zone in very fine clay rich sediments.

3.2 Seismic and well data

3.2.1 Data set

Three dimensional (3D) multi-channel, poststack, time-migrated seismic reflection data is used to describe the high amplitude anomaly developed at the crest of the Havsule Dome (Fig. 3.1) and proposed a model to understand development and explanation about the shape and geometry of anomalous zone in very fine clay rich sediments of the Brygge Formation. Time maps, dip maps, coherency maps and amplitude maps (Brown, 2004) are used to provide much information on the basal surface, internal geometry and fluid flow in and outside the seismic anomaly.

The 3D seismic survey covers an area of 1300 km^2 and is 120 fold with a 4 ms two way travel time (TWT) sample rate. The 3D seismic grid is subdivided into inline and crossline directions, spaced at 25 m and 25 m respectively. The seismic data is displayed in the zero phase, SEG normal polarity, (black peak indicating an increase in acoustic impedance ‘‘American polarity’’ (Brown, 2004). The seismic migration velocities vary spatially, based on normal moveout velocity analysis. Within the study interval (0-1000ms TWT below seafloor) the interval velocity ranges between 1500 and 1750 m/s. The frequency range in the shallow subsurface is 7.5–90 Hz, with a dominant frequency in the 42–50 Hz range. An exploratory well 6404/11-1 provided the

interval velocity of the interested stratigraphic interval described in the geological setting and these velocities are range between 1500 m/s and 1750 m/s. By using the dominant frequency and a velocity of 1500–1750 m/s, the seismic resolution, defined as a quarter of the dominant wavelength is, 10–15 m.

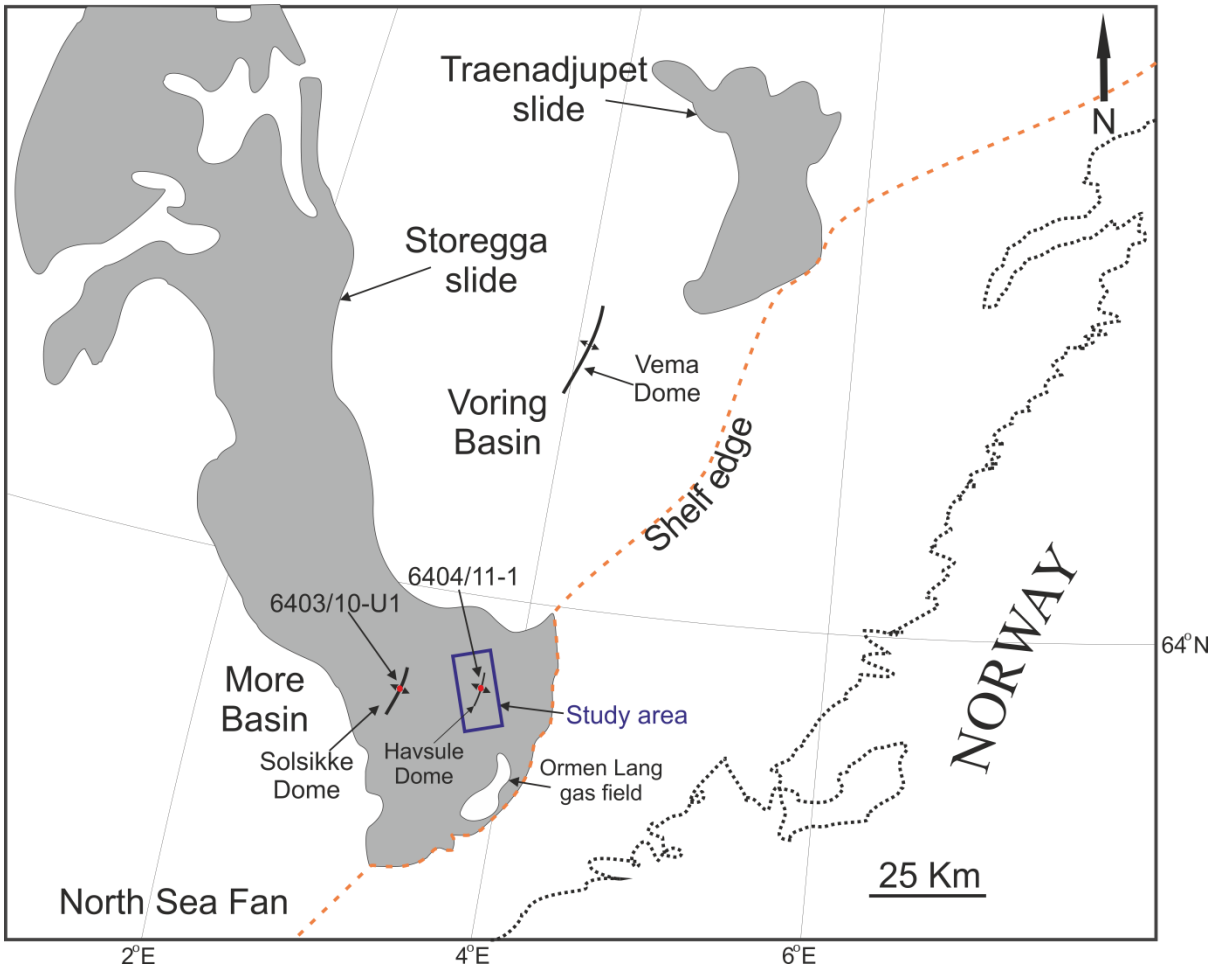

Figure 3.1: Location map of the 3D seismic survey in the mid Norwegian Sea. The survey is situated at the south edge of Storegga Slide. Developed gas -field (Ormen Lang gas filed) is located about 10 kilometres in the south of study area. NE-SW oriented domes developed in the basin (Vema, Hasule and Solsikke domes). Exploratory well 6404/11-1 was drilled in the study area (modified from *Riis et al., 2005*).

3.2.2 Wells in the study area

An exploratory well 6404/11-1 was drilled in the study area (Fig. 3.2). The pre-drill objective of the well was to test the Havsule Prospect. The prospect was a seismically defined north-south trending structural dome located in the north of the Møre Basin in the Norwegian Sea (Doyle *et al.*, 2003; Lawrence & Cartwright, 2010), thought to have developed during the Tertiary Period in response to compression during opening of the North Atlantic Ocean. Three primary reservoir targets were identified: Tare Formation, Early Eocene Turbidite sandstone with 4-way dip closure; Springar Formation, Maastrichtian turbidite sandstone with 4-way dip closure; and The Nise Formation sandstone. An optional secondary target was a 4-way dip closure Coniacian Lysing turbidite.

The targets were directly drilled and passed through five different MTDs, biogenic ooze sediments and diagentic boundary (Opal A to CT boundary) in the Tertiary sequence. The turbidites sandstones of Tertiary and Upper Cretaceous were considered hydrocarbon bearing (Doyle *et al.*, 2003), but at the shallowest primary target (Early Eocene Tare sandstones) was absent at the well location. The primary target of the Upper Cretaceous sandstone was absent and the Nise Formation sandstones were poorly developed. The well was not extended to penetrate the secondary target, the Lysing Formation.

The gas shows were observed during drilling. The gas was composed of C_1 to C_3 with concentration of 0.3% at the Brygge Formation. The Tare Formation was drilled with heavy mud weight to balance gas pressure present at the depth of 2563m. The gas was composed of C_1 to C_3 with concentration reached up to 5.33%. The well was plugged and declared abandoned due to non-commercially production and declared dry well (Doyle *et al.*, 2003).

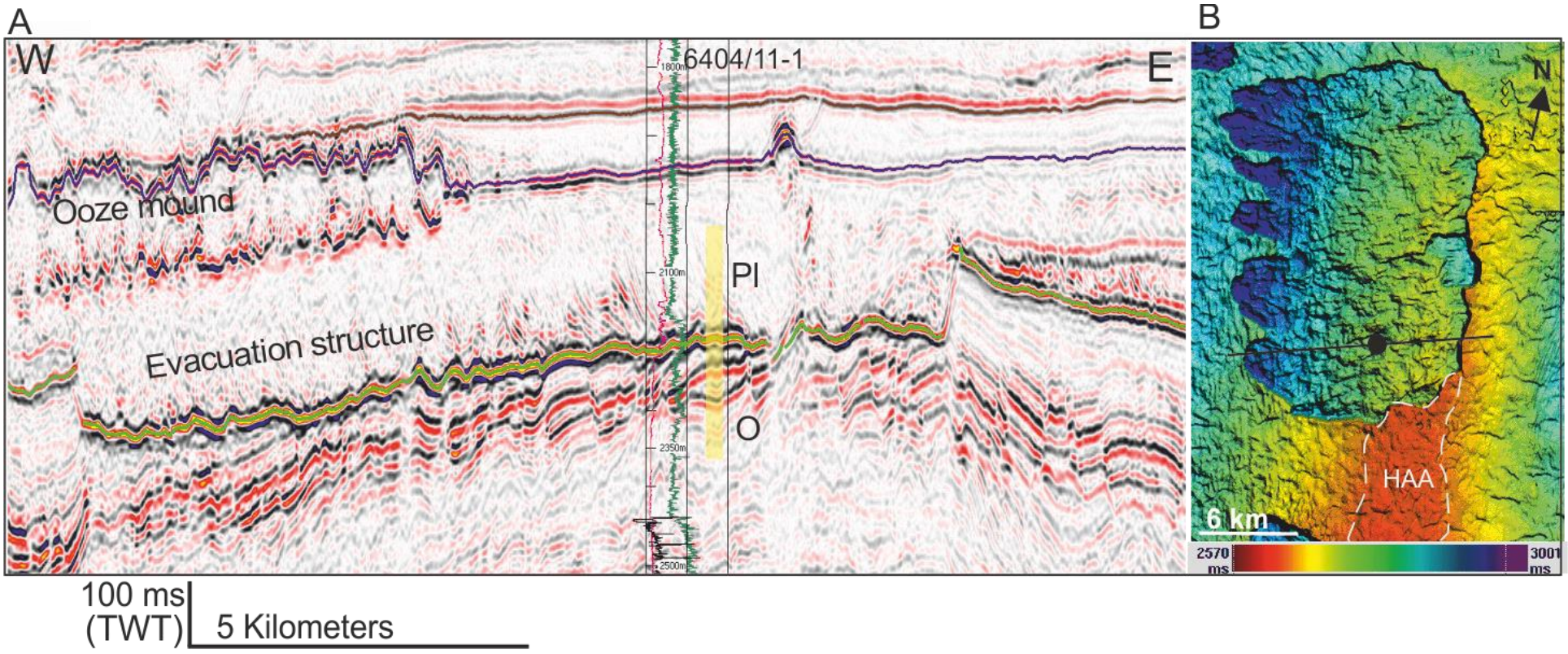

Figure 3.2: A) Seismic profile across the Havsule structure. The yellow bar shows the interval which was sampled in the biostratigraphical study. The top of the ooze is an onlap surface shown by a green line in the seismic section, while the top of the Intra Naust slide and top of the ooze mounds is shown by blue. The arrows point at velocity effects caused by ooze mounds. Pl: Pleistocene, O: Oligocene (modified from *Riis et al., 2005*). B) Well 6404/11-1 shown as black dot in the two way time map of the top of undisturbed Oligocene/Miocene ooze to the right.

3.3 Regional geological setting

3.3.1 Regional tectonic setting

The continental margin of Mid Norway is one of the most unstable margins in the world (Bryn *et al.*, 2005). The Møre Basin is the part of this margin. The Cretaceous the Møre Basin (Rønnevik & Navrestad, 1977; Gabrielsen, 1984; Hamar & Hjelle, 1984; Blystad *et al.*, 1995) is an elongated, wedge-shaped feature, the axis of which strikes in a NE-SW direction (Fig. 3.3). In its axial parts, Cretaceous and younger strata exceed 5000 m in thickness (Grunnaleite & Gabrielsen, 1995). To the southeast and east of the Møre Basin are the Møre-Trondelag and Klakk Fault Complexes. The northern border of the basin is diffuse, but it is separated from the Voring Basin by the Jan Mayen Lineament (Skogseid & Eldholm, 1989; Skogseid *et al.*, 2000) which extends from the Jan Mayen Fracture Zone. To the west the Møre Basin terminates against the Møre Marginal High, the ocean side margin which corresponds to the Faeroe-Shetland Escarpment. The Møre Marginal High, which is underlain by pre-Tertiary rotated fault blocks (Bøen *et al.*, 1984), marked the western margin of the Møre Basin during the Palaeocene(Smythe *et al.*, 1983; Brekke & Riis, 1987; Blystad *et al.*, 1995). To the south the Jurassic-Cretaceous basins, including the Sogn Graben and the northernmost Viking Graben, limit the Møre Basin. This border is diffuse and (Hamar & Hjelle, 1984) included the Sogn Graben extends from the Møre Basin domain.

The structure of the Møre Basin reflects a multiphase rifting event consisted of large-scale volcanism, uplift and inversion doming (Blystad *et al.*, 1995). The multiphase rifting event started during Permian and ended with the arrival of the Icelandic Mantle Plume during the Late Cretaceous. (Weibull *et al.*, 2010). Internally in the Møre Basin, lavas of Cretaceous

(Hamar & Hjelle, 1984) or Paleocene to Eocene ages (Rønnevik *et al.*, 1983) have been identified, and the Cretaceous-Tertiary basin fill is reported to be folded and affected by reverse faults. The reported elongated domal structures in the Cretaceous-Tertiary sequences along the eastern margin of the Voring Basin (Rønnevik *et al.*, 1975), and suggested a strike-slip mechanism for their deformation. Rønnevik and Navrestad (1977) stated that the mid-Cretaceous sequence is strongly disturbed and may be partly folded.

Jørgensen and Navrestad (1981) linked the domal structures with positive inversion, whereas Hamar and Hjelle (1984), who dated the deformation as Late Oligocene-Miocene, suggested these structures were igneous intrusions, pre-Cenozoic evaporates or deep crustal movements. Bukovics and Ziegler (1985) supported the view of (Hamar & Hjelle, 1984) stating that "locally the Møre Basin was also influenced by compressional deformations that can be related to the transform movements along the Jan Mayen Fracture Zone and the Oligocene spreading axes in the Norwegian-Greenland Sea". The most prominent internal features of the Møre Basin are the Vigra High (Hamar & Hjelle, 1984), and the Helland-Hansen Arch.

The overall compressive stress field that gave rise to the Mid-Norwegian dome structures has been explained as a result of the combination of spreading in the adjacent ocean and the distant effects of Alpine tectonics (Doré & Lundin, 1996; Vågnes *et al.*, 1998). The extensional vector at breakup time (early Eocene, 55Ma) was directed NW-SE, more or less parallel to the trend of major transform zones such as the Jan Mayen Fracture Zone. The weakly compressive regime, which is assumed to have been established at the onset of spreading, still exists at the present day. The Møre Basin was compressed at this time (Løseth & Henriksen, 2005) resulting in series of N-S to NW-SE trending anticlines and synclines.

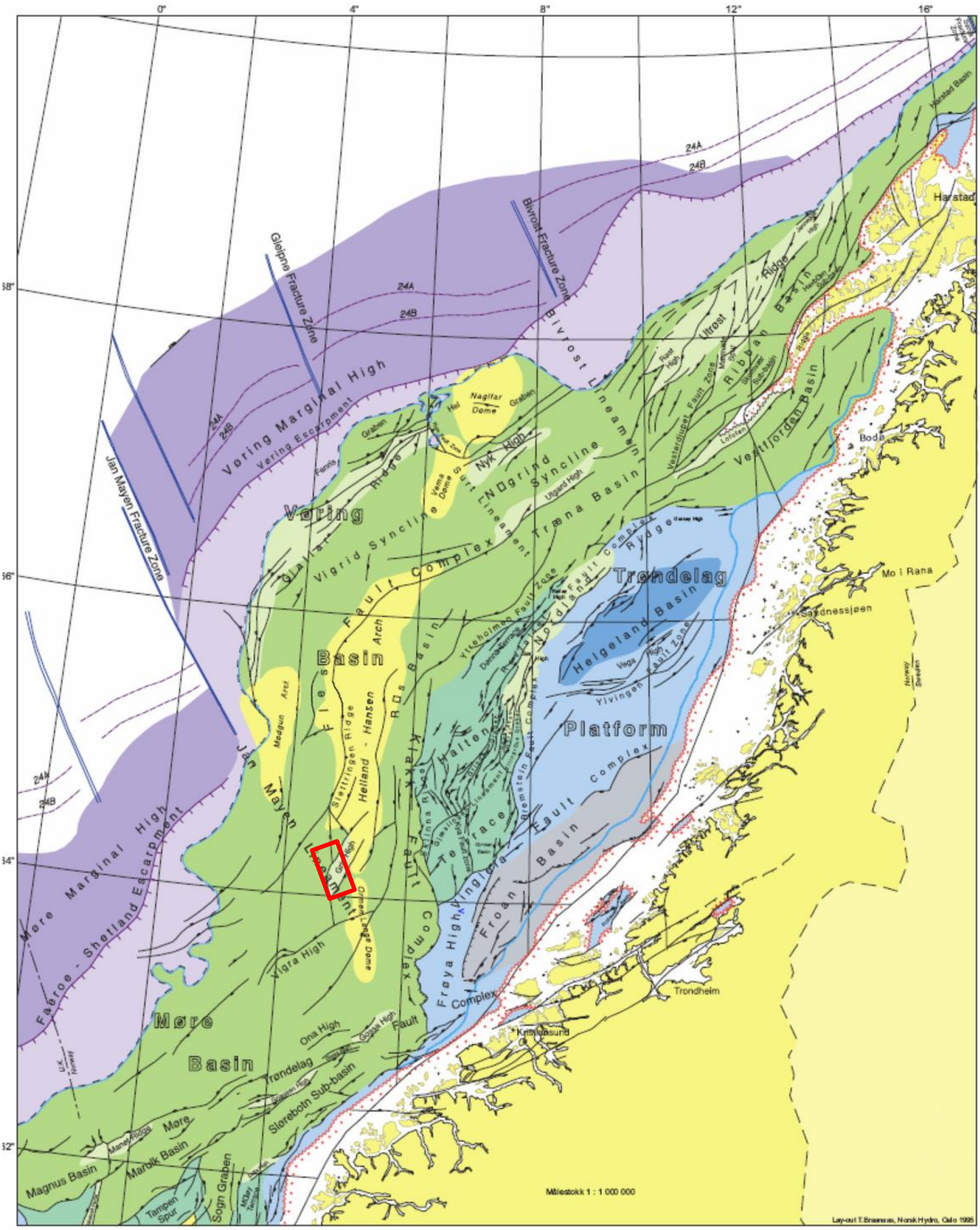

Figure 3.3: Simplified structural map of the Norwegian Sea continental margin. The red rectangle is the location of 3D seismic survey in the study area (Blystad *et al.*, 1995).

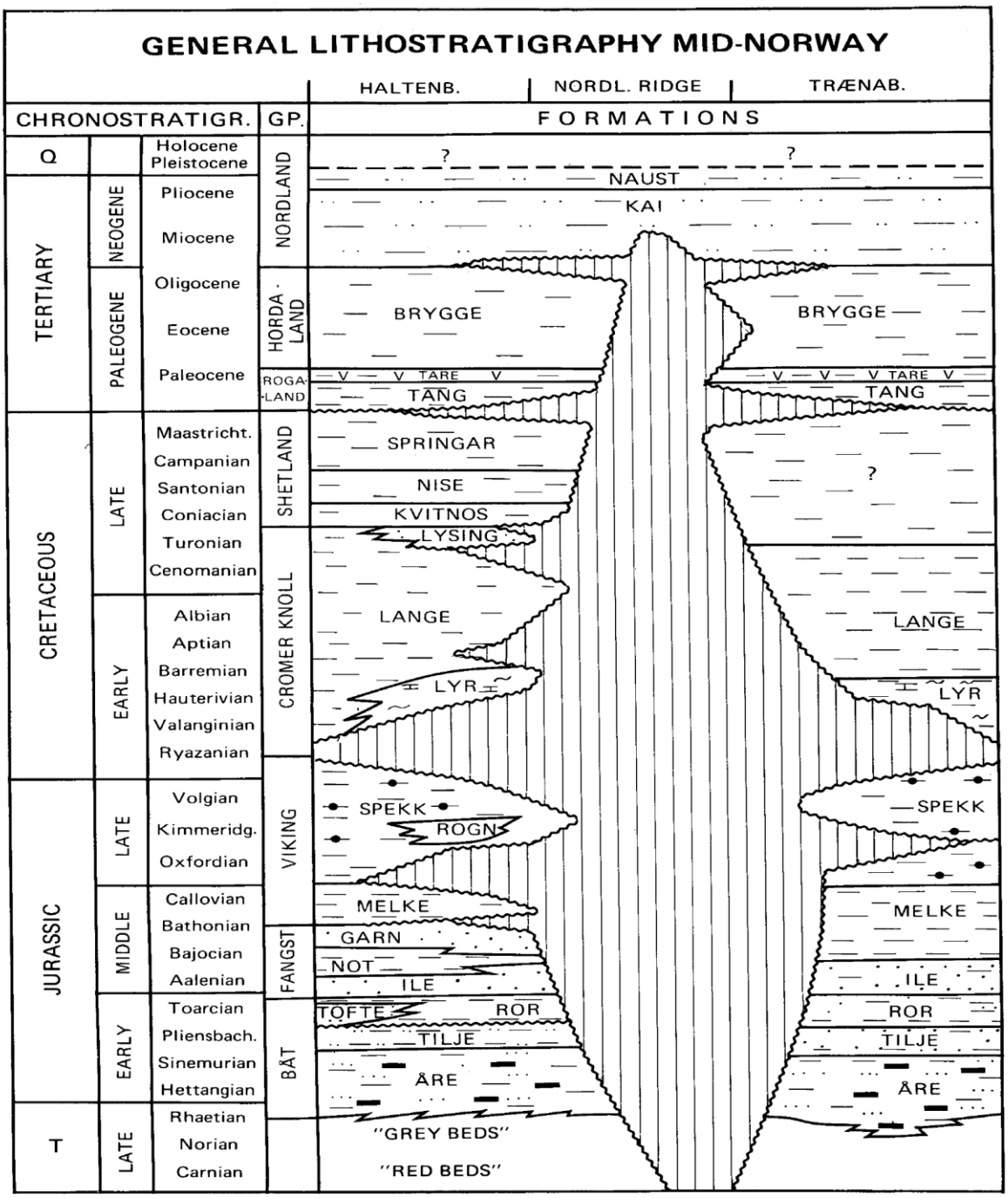

Figure 3.4: A generalized stratigraphy of the Møre Basin in the Mid-Norwegian Sea (Dalland *et al.*, 1988).

Sediment with a high calcareous and siliceous fossil content formed growth packages in the synclines (Løseth & Henriksen, 2005). In the Møre Basin, the Brygge and Kai Formations are deformed by an extensive tier of polygonal faulting (Cartwright & Dewhurst, 1998; Berndt *et al.*, 2003; Hustoft *et al.*, 2010). This polygonal faulting spans an interval from the base of the Brygge Formation to a datum in the Kai Formation (Lawrence & Cartwright, 2009).

3.3.2 Stratigraphy

In the Norwegian Sea, the Palaeocene Rogaland Group (Deegan & Scull, 1977) consists of claystone with minor interbeds of sandstone near the Norwegian continental margin (Dalland *et al.*, 1988). The Rogaland Group is overlain by the Lower Eocene to Lower Miocene Brygge Formation, which is part of the Hordaland Group (Fig. 3.4) (Eocene to Lower Miocene) (Deegan & Scull, 1977; Dalland *et al.*, 1988). Large parts of the Oligocene-Miocene sequence of the western Voring Basin consist of bio- siliceous ooze (Hjelstuen *et al.*, 1997). The Brygge Formation consists mainly of claystone with biogenic ooze and interbeds of sandstone that were not observed in the study area. The Hordaland Group is overlain by the Lower Miocene to recent Nordland Group (Deegan & Scull, 1977), which is subdivided into the Lower Miocene to Upper Pliocene Kai Formation (Dalland *et al.*, 1988) and the Upper Pliocene the Naust Formation (Dalland *et al.*, 1988).The Pliocene part of the Kai Formation is missing in the study area. The Kai Formation consists of alternating claystone, siltstone and sandstone with limestone interbeds. The Naust Formation consists of alternating claystone, siltstone and sandstone.

The seismic data used in this study provide excellent imaging of most of the Cenozoic succession, but only provides limited imaging of the Palaeocene and the Eocene succession because of the volume has been truncated below 3.252s TWT. The horizons mapped for this

study have been dated by correlating the seismic data to the stratigraphy of well 6704/12-1 and correlated with the seismic using the integrated sonic-log data.

For the purpose of the description and arguments presented here, the whole sedimentary succession is divided into three main units (Units I, II and II) based on position of anomalous body above and below from exploratory well 6404/11-1, mass transport deposits, seismic reflection amplitude and continuity (Fig.3.5).

The unit III consists of Naust formation from seabed to the top of the Brygge Formation. The Naust Formation comprises the Late Pliocene-Pleistocene sediments on the Norwegian shelf, forming a thick succession of prograding wedges and flat-lying sheet-like units, mainly of glacial origin (Laberg *et al.*, 2005; Rise *et al.*, 2005). The acoustic character of the unit III appears mainly to be massive, and I infer that various types of mass movements and down-slope gravity currents were responsible for recycling of sediments beyond the palaeo-shelf edge. Some subunits in Naust Formation probably represent glacial debris flows, redistributed beyond the shelf edge during periods of extensive shelf glaciations (Rise *et al.*, 2005).

In order to obtain a detailed description of the stratal relationships of the Cenozoic succession in the study area, eight key seismic reflections at different stratigraphic levels were picked (Fig, 3.6). These horizons represent the top of the Rogaland Group (named Top Rogaland), three separate intra-Hordaland Group reflections (named H8. H7 and H6), the top of the Hordaland Group (named Top Brygge), an intra-Nordland Group reflection (named Top Kai) and finally the seabed (named Seabed or H1) (Fig. 3.6). The principal time structure maps, dip maps and amplitude maps of the Top Rogaland, Top Lower Eocene, Intra-Oligocene and Top Kai horizons are presented in this research, (Fig. 3.5 and Fig. 3.6).

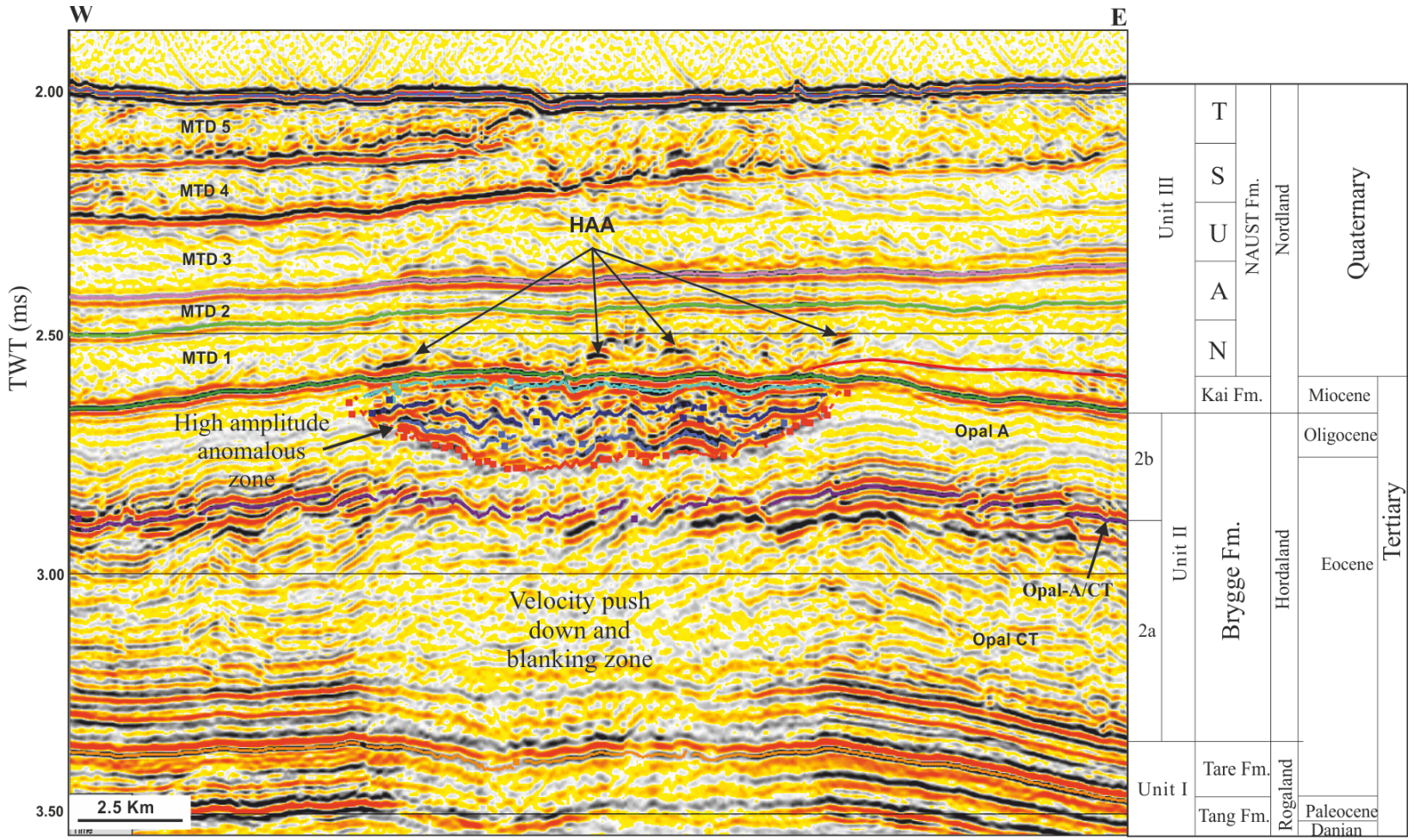

Figure 3.5: A representative seismic profile passing through a high-amplitude anomalous zone that developed at the Havsule Dome structure in the study area (see Fig. 3.7 for location). A series of mass transport deposits (MTD1 to MTD5) have been interpreted in Naust Formation of Quaternary age. A diagenitc boundary (the Opal A/CT boundary) developed in the Brygge Formation of Tertiary age. HAA: High-amplitude anomalies

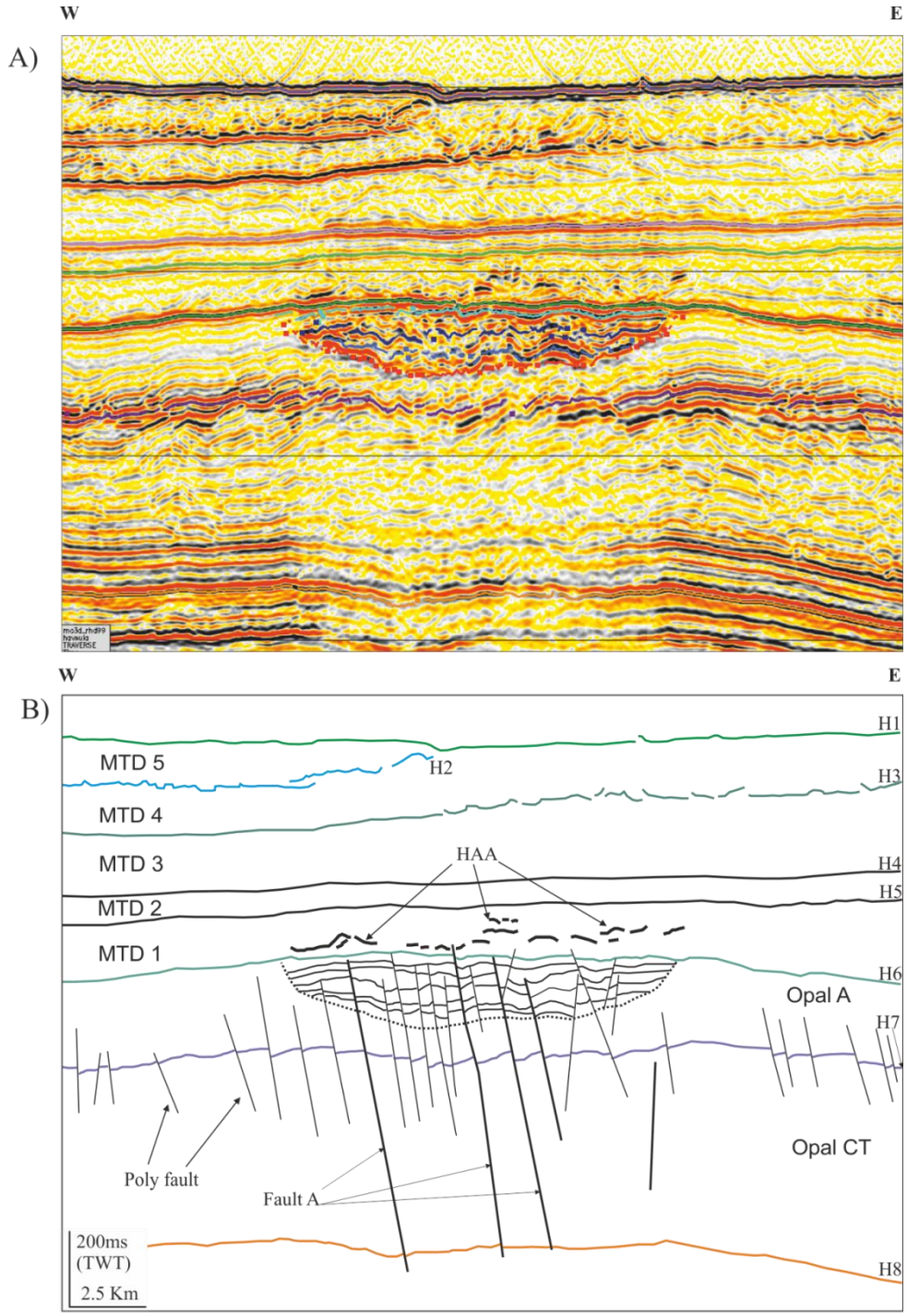

Figure 3.6: A) Uninterpreted Seismic profile through the high-amplitude anomalous zone (see Fig.3.7 for location). B) Interpreted seismic profile showing eight interpreted seismic horizons (H1 to H8) starting from the seabed to a deeper seismic reflector H8 the Tare Formation boundary. Two types of faults are interpreted 1) Regional faults interpreted as fault A and others polygonal faults. HAA: High-amplitude anomalies

3.3.2.1 Naust Formation

The overall seismic stratigraphy covering the last 5 My (Naust Formation) is divided into five main sequences (Naust:- N, A, U, S and T) with boundaries that can be traced throughout the Mid-Norwegian margin (Rise *et al.*, 2005). Berg *et al.* (2005) mentioned the nomenclature of these sequences (Naust W, U, S, R and O). The sequences are linked to the main glaciations, but each sequence may contain more than one shelf glaciation. Naust units S, R and O have been subdivided into a total of 16 subunits in the Ormen Lange area, based on seismic data, and supported by geological and geotechnical analyses of sediment samples, as well as the results of borehole geophysics. The deposits of the Naust Formation overlie the thick siliceous oozes of the Kai and Brygge Formations. The Naust Formation consists of interbedded contourite and mass wasting deposits (Berg *et al.*, 2005; Bryn *et al.*, 2005; Solheim *et al.*, 2005), with its lithology consisting of interbedded claystone, siltstone and sand, with very coarse clastics in its upper part (Dalland *et al.*, 1988).

Hemipelagic and contouritic sedimentation prevailed during interglacial periods, though this sedimentation style was also important during glacial times (Hjelstuen *et al.*, 2004; Laberg *et al.*, 2005). Contourites could act as shallow fluid reservoirs due to their along-slope continuity and high porosity (Bryn *et al.*, 2005; Hustoft *et al.*, 2010). Naust U sediments consist predominantly of (contourites) sediment drift deposits. Glacigenic debris flows (GDF) are derived from destabilization of till sediments at the shelf edge, and were deposited mainly at the upper slope (Hjelstuen *et al.*, 2004) and on top of the sediment drifts (Leynaud *et al.*, 2007; Hustoft *et al.*, 2010). GDFs form relatively thick deposits within Naust S and T (Rise *et al.*, 2005). Several large-scale slides affect the Naust sedimentary records, the last one being the Storegga slide of Holocene age 8.2 ka, (Haflidason *et al.*, 2005). North to the Storegga slide impact area the seafloor is very gentle having a mean slope of approximately 1^0

(Hovland & Svensen, 2006). Boreholes south of the study area in the Ormen Lange Dome show that the Naust Formation consists of illite dominated hemipelagic and glacial sediments (Lawrence & Cartwright, 2010). The bulk density of the Naust Formation in well 6407/1-2 east of our study area is 2.3 g/cm^3 (Dalland *et al.*, 1988).

3.3.3.2 Kai Formation

The Kai Formation is not laterally continuous, but where it accumulates in synclinal lows or as contourites mounds it can be over 400 m thick. In wells 6407/1-2 and 6407/1-3 (east of the study area) the bulk density of the Kai Formation rises from 1.9 g/cm3 at the base to 2.25 g/cm3 at the top (Dalland *et al.*, 1988). The main depocentre of the Brygge Formation, where over 1500 m of thick sediment accumulated, is in the Storegga area immediately west of the Ormen Lange field. In most of the Storegga and the North Sea Fan regions, the Kai Formation has a thickness of 600–1000 m, but on the Vøring Plateau it is less than 400 m thick over extensive areas (Berg *et al.*, 2005).

3.3.3.3 Brygge Formation

The deposition from Eocene to mid-Miocene times of dominantly clays interbedded with biogenic ooze (Bryn *et al.*, 2005), known as the Brygge Formation (Dalland *et al.*, 1988). Deposition of the Brygge Formation was followed in the Miocene by deposition of the Kai Formation (Dalland *et al.*, 1988). Two subdivisions of the Brygge Formation are recognised in the well: Brygge ‘A’ and Brygge ‘C’. Polygonal faults are widely recognised in the interval across the Norwegian basins (Fig. 3.5). The Kai Formation was deposited in synclinal lows between domes (Løseth & Henriksen, 2005) such as the Solsikke Dome and

the Havsule Dome in the study area. The Brygge Formation comprises a thick sequence of mudstones with very rare limestone stringers. During the period from 54 to 2.5 Ma fine-grained oozes and shales of the Brygge and Kai Formations dominated the sedimentation. These sediments were abundant in calcareous and siliceous fossils and rich in smectite (Forsberg & Locat, 2005). The mineralogical analyses of Brygge Formation documented low velocities in the mudstones due to presence of smectite with different content (Storvoll *et al.*, 2005).

A seismic profile showing a series of MTDs overlying the high amplitude zone (Fig. 3.6). The Brygge Formation comprises a thick sequence of mudstones with sparse limestone stringers. These sequences range in thickness from 2 – 9 m averaging at 4.5m (confidential well report). Some of the mudstones are low density ooze sediments.

3.3.3 Petroleum system

The petroleum system of the Mid Norwegian continental margins is well understood, the Jurassic rocks are contributing from two source rocks: principally oil and gas from anoxic marine mudstones of the Upper Jurassic Spekk Formation but also gas from coals of the Lower Jurassic Åre Formation (Möller *et al.*, 2004). Regional studies show that the reservoir is located at the transition zone between the wide shelf of the Halten Terrace/Trøndelag Platform area and the narrow shelf of the Møre Basin. This zone is defined by the Jan Mayen Fracture Zone and its extension towards the Norwegian mainland (Gjelberg *et al.*, 2005). The presence of an active hydrocarbon system in the study area has also been demonstrated by a number of gas and oil discoveries in Cretaceous and Palaeocene sandstones of main turbidite channel systems. Depositional environment mapping suggests that Upper Jurassic source rocks are present throughout the Norwegian Sea region. The depth to the Base Cretaceous

unconformity shows that although deeper parts of the Vøring and Møre basins are over mature. An exploratory well drilled in the Ormen Lange into dome structures that confirmed the presence of hydrocarbon in the sands of Lysing, Nise and Springer Formations of the Cretaceous age.

3.4 Seismic observations

3.4.1 Description of the anomalous zone

A series of high-amplitude anomalies are developed at the crest of the Havsule Dome in the Late Miocene-Oligocene succession in the Møre Basin. The anomalies stand out as a strong localized amplification of very fine sediments of the Brygge Formation. All the high-amplitudes are acoustically negative (Fig. 3.5). The amplitude anomalies are characterised by an anomalous zone of high-amplitude reflections and termed here as "anomalous zone". The anomalous zone is constrained by the top of the Brygge Formation (Fig. 3.7). There are scattered high-amplitude reflections that developed at overlaying the Early Pliocene Naust Formation have strong relation with the anomalous zone. The anomalous zone has an extraordinary concave upward geometrical shape. In cross section, the base of the anomaly is cuspate and concave upwards (Fig. 3.6). In plan-view the anomaly appears is N-S elongated 10.45 km in length and 3.45 km in width, with surface area approximately 30 square kilometres (Fig. 3.7). The maximum thickness of the anomalous zone is 220 ms two way travel time at the centre of the anomaly which equates to 165 metres using an interval velocity of the anomalous zone 1500m/s that was calculated from seismic velocity information from nearby drilled wells in the fields.

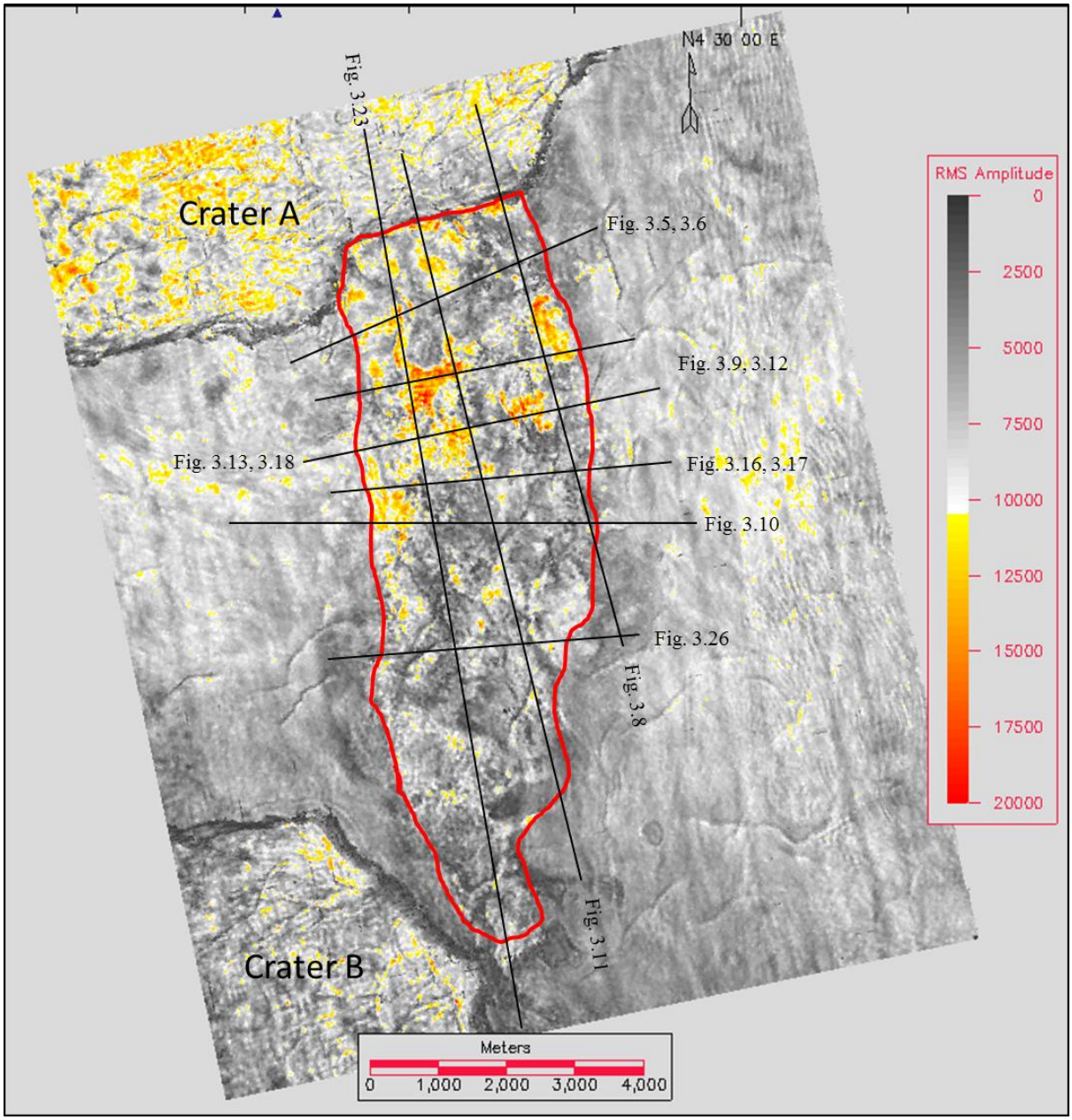

Figure 3.7: RMS amplitude map 20 ms below from top of the Brygge Formation with location of two craters (Crater A and Crater B). Map confirmed that anomaly (red line) is developed at between two craters at the crest of Havsule Dome structure.

3.4.2 Relationship of the crater with anomaly

Two evacuations like structure (craters) observed to the north and south of the anomaly. For ease of understanding, the north crater is named "*Crater A"* and southwards "*Crater B*" (Fig. 3.7). Riis *et al.* (2005) stated that the formation of evacuation structures are created due to mass flows that originating from the slope of the Norwegian Sea margin and formation of an evacuation structure could possibly give the mass flow more energy and initiate a retrogressive slide. The authors did not discuss the formation mechanism of these craters. Lawrence and Cartwright (2010) provided a model for formation of these evacuation structures and concluded that liquefaction and overpressure build up in the Brygge Formation due to presence of methane gas was the main trigging factor for these structures.

Excavation type structures (Crater A and B) that developed at the Havsule structure, the seismic data show clear evidence of high amplitude which were interpreted as gas effects in the top of the ooze. Riis *et al.* (2005) suggest that the presence of high amplitude anomalies possibly due to gas accumulation has a strong association with mechanism of formation of these craters. The authors pointed out that area of craters developed on the crest of Havsule Dom could potentially have been locus of pre-gas migration. Nichols (1995) aslo aided that high pore pressure and gas saturation could facilitate the mobilization of ooze through liquefication, fluidization and gas expension.

Crater A covers an area of c. 273 km^2 having dimensions of 30 X 15 km in length and width respectively and the maximum depth is approximately 150 m with a volume of 68 km^3 (Fig. 3.7) Crater B covers an area of c. 70 km^2, having dimension of 10x7 km in length and width respectively and the maximum depth is approximately 200m, with a volume of 14 km^3 (Fig. 3.7) (Lawrence & Cartwright, 2010). Crater A is adjacent to the anomaly and defines the northern boundary of the anomaly (Fig. 3.8) but Crater B does not coincide with the anomaly.

The base of the Crater A is at 2734 ms while the base of Crater B varies between 2700 ms to 2800 ms. The base of both craters is at 70-100 ms above the Opal A-CT boundary in the Brygge Formation. Crater A eroded portion of the Brygge Formation where the seismic anomaly is developed (Fig.3.8). There are no high amplitude anomalies that possibly indicate fluid leakage (Cartwright *et al.*, 2007; Løseth *et al.*, 2009; Foschi *et al.*, 2014)

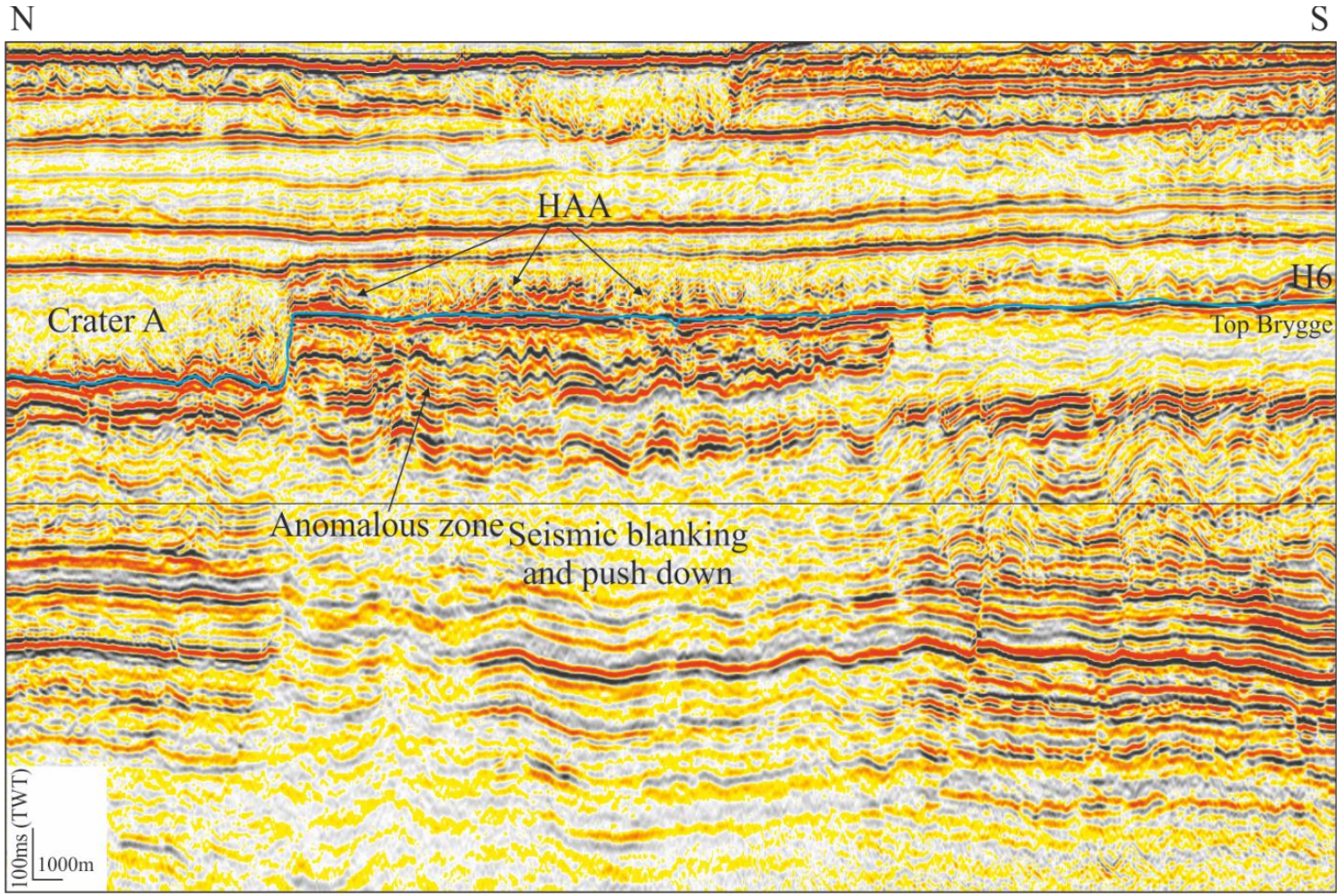

Figure 3.8: Seismic section showing cluster of high-amplitude anomalies (anomalous zone) (see Fig. 3.7 for location). The seismic profile present high-amplitude reflection (HAA) at the top of anomalous zone. The north side crater A filled with sediments of mass transport deposit 1. No high amplitude anomaly observed along the crater. HAA: High-amplitude anomaly.

3.4.3 Relationship of the polygonal faults with the anomaly

A series of the polygonal faults are observed within the Brygge Formation and they have been interpreted as dewatering structures (Cartwright, 1997; Cartwright *et al.*, 2003) possibly acting as the source for fluids that contributed to formation of high amplitudes anomaly at the crest of the Havsule dome. Once created, the faults are considered to act as potential fluid conduits.

A well-developed system of polygonal faults is observed between the Intra-Oligocene reflection and the seabed (Fig. 3.10). The faults exhibit a remarkably steep displacement gradient and sole out just above the Intra-Oligocene horizon. An abrupt upward decrease in fault density is observed at the Opal A to CT reflection, suggesting that part of the polygonal faulting may have occurred in response to the opal A to CT conversion. The Upper Pliocene to Pleistocene interval is almost undisturbed although a few faults penetrate to the present-day seabed (Fig. 3.10). However, indefinite displacement of layers may occur in the lower Naust Formation as an effect of underlying polygonal fault reactivation in the Kai Formation caused by abrupt sediment loading, e.g. by glacigenic debris flows. In the high-density faulted interval, the distance between individual faults is between 100 and 600 m and the throw of the faults is generally between 30 and 50m.

Regionally, the stratigraphic layer containing the seismic anomaly is deformed by a single tier of polygonal faults (Fig. 3.5, Fig. 3.9 and Fig. 3.10). Majority of these polygonal faults tip out at the top of the Brygge Formation and the overlying the Naust Formation. The faults displayed a polygonal pattern on amplitude and coherence slices.

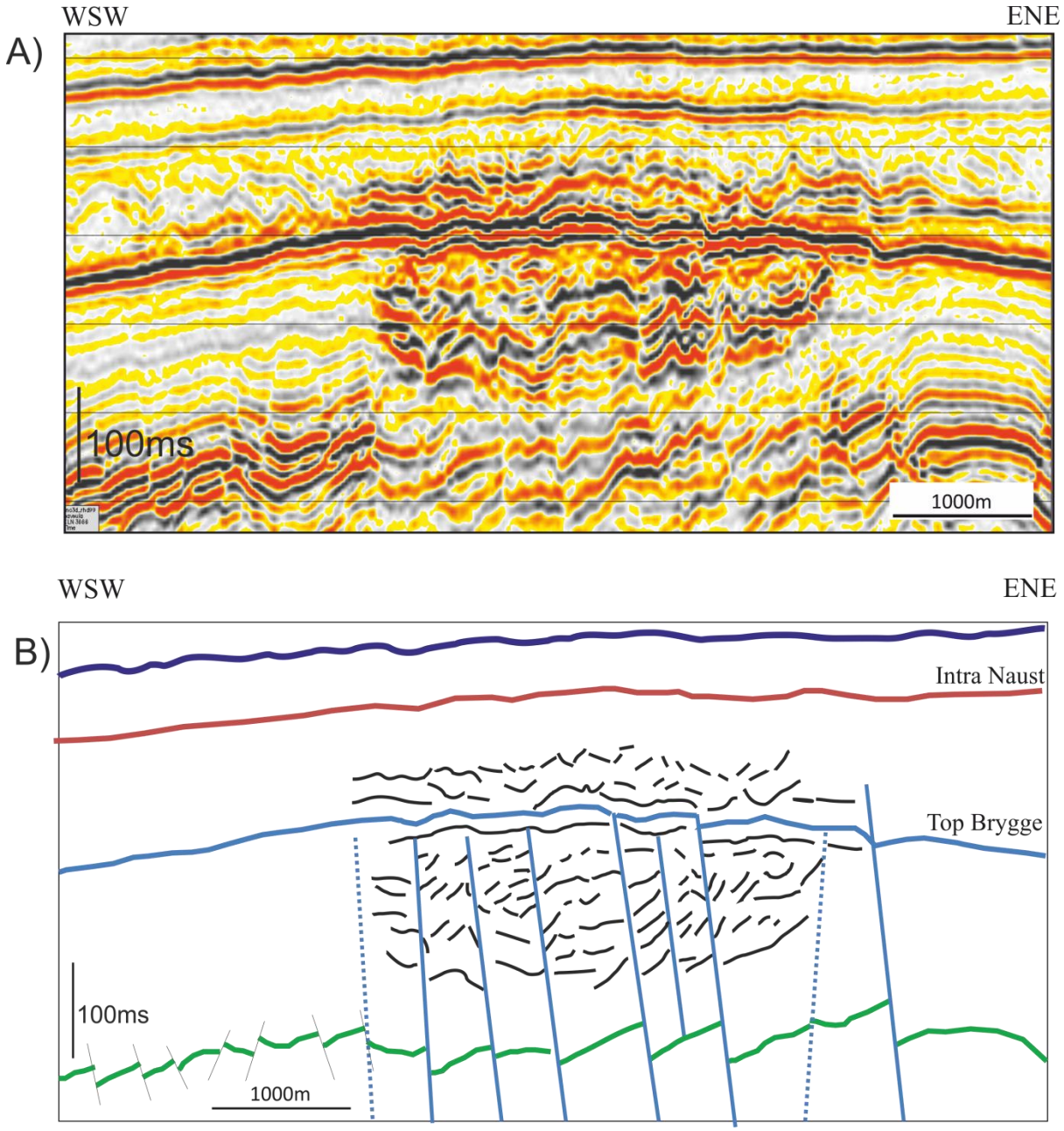

Figure 3.9: Representative seismic profile showing the relationship of polygonal faults with deep seated reservoir (see Fig. 3.7 for location). Faults are interpreted inside of high-amplitude anomalous zone. All the faults tip-out at the top of Brygge Formation except two faults are ended at base of Naust Formation.

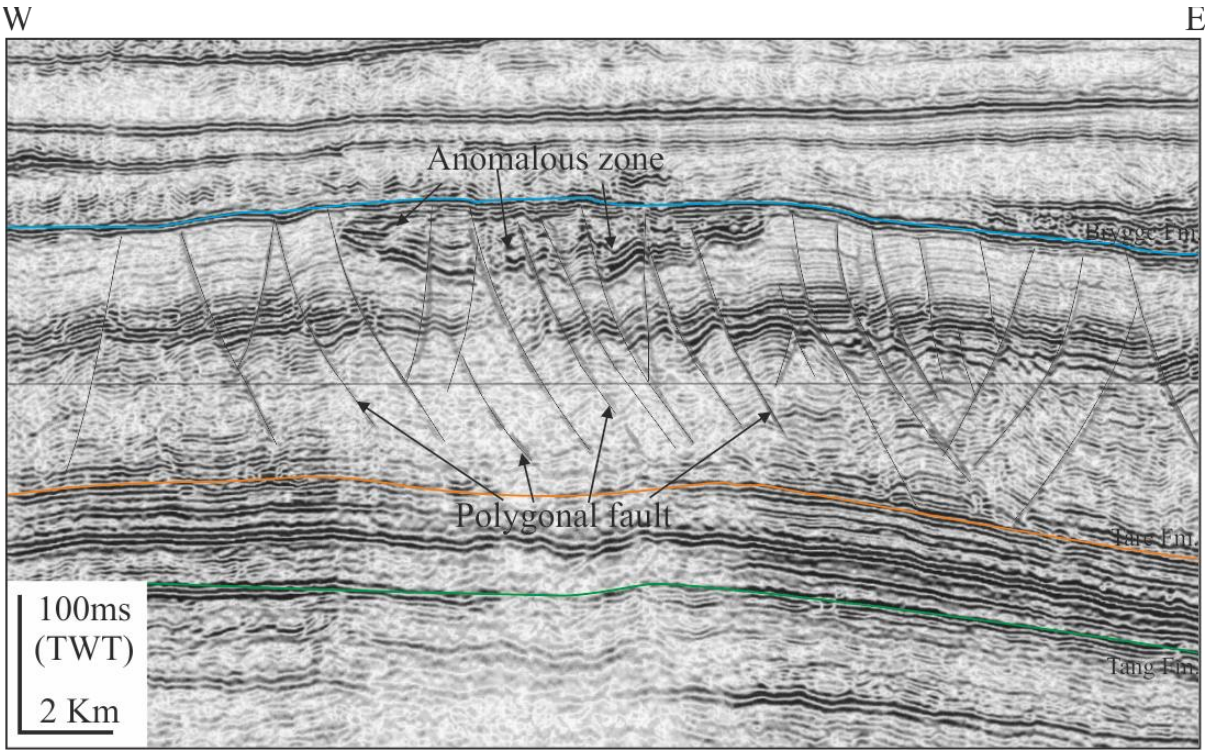

Figure 3.10: Representative seismic profile showing well-developed system of polygonal faults observed in the Brygge Formation of the Intra-Eocene-Oligocene. The faults exhibit a remarkably steep displacement gradient and tip out just at the top of Brygge Formation. See fig.3.7 for location

3.4.4 Extent of high amplitudes

To assess the extent to which high-amplitude reflections or group of reflections in the studied interval might be amplified to form anomalous zone, a careful interpretation was carried out. The interpreted anomalous zone extends 10.45 km along a N-S direction from Carter A, and expands towards up dip direction (Fig. 3.7). High-amplitudes in the anomalous zone are not laterally continuous and are not uniformly distributed within anomalous zone. The highest concentration occurs near Crater A in north direction. All the reflections within the anomalous zone are amplified but the patches are observed between strong reflections. High amplitude reflections are truncated and stop propagating further southwards (Fig. 3.11). Anomaly has sharp cut-offs against fault (Fig. 3.11B).

The development of high-amplitude reflection does not reached up to a spill point towards south direction (Fig. 3.11). It extends 3.45 km along E-W direction. A possible polarity reversal has been observed (Fig. 3.12) and this may be due to presence of small displacement of the strata caused by the presence of polygonal faults that are interpreted in the study interval of the Brygge Formation.

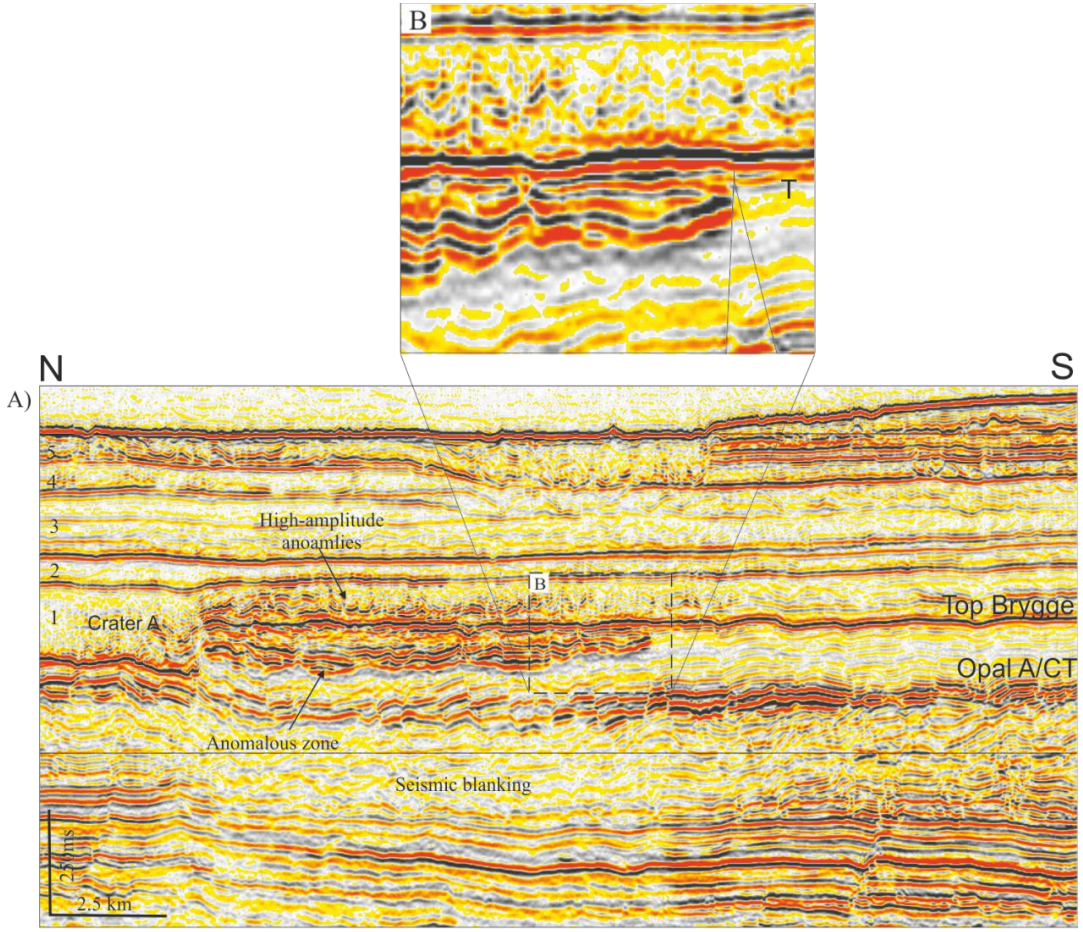

Figure 3.11: A) The interpreted high-amplitude anomalies in the anomalous zone are truncated and stop propagating further southwards possibly against a fault (see Fig. 3.7 for location). B) Zoomed section of seismic profile shows anomaly has sharp cut-off against fault.

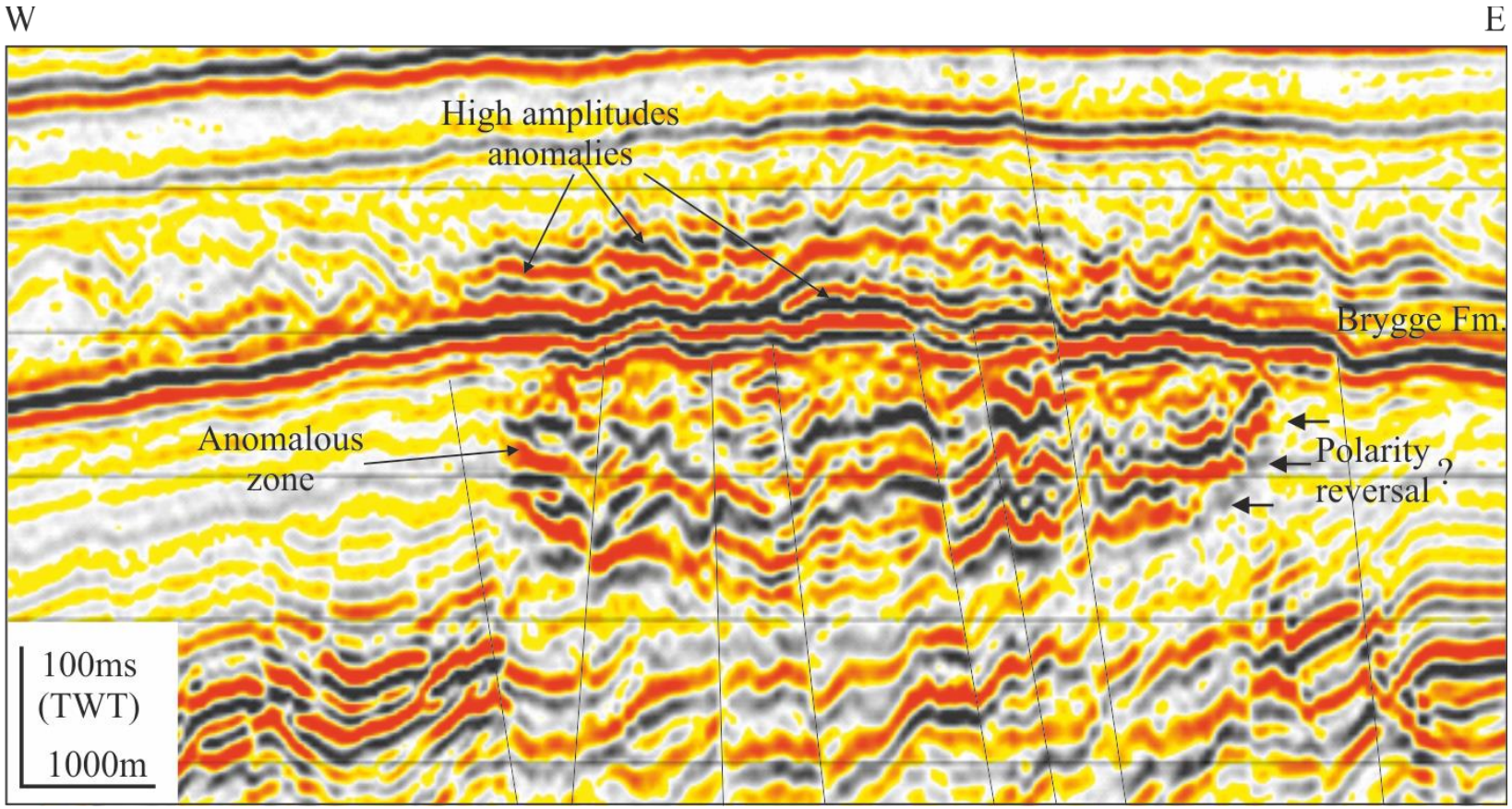

Figure 3.12: Seismic section through high amplitude anomalous body showing equally spaced polygonal faults inside and outside of the body and also high amplitude in the seal unit above indicating leakage of fluid. Polarity reversal observed at the Seismic section through the anomaly displaying polarity reversal at the both sides of the anomaly. See fig.3.7 for location.

3.5 Geophysical observations

3.5.1 Acoustic attenuation and fault associated with anomalous zone

Acoustic attenuation or seismic blank zone is observed beneath high-amplitude anomalous zone (Fig. 3.5). The blank zone is about 4 km in diameter and 500 ms thick below the anomaly within the Brygge Formation. The background amplitude response is regained immediately outside this zone of signal attenuation. Therefor; there is no clear reflection in this blank zone. Blanking zone is transparent at the middle and has vague reflections at the edges. According to Løseth *et al.* (2009) and Foschi *et al.* (2014), the blanking is thought to be related to gas charging, and have widely been interpreted as gas chimneys, and other gas associated structures (Calvès *et al.*, 2008; Hustoft *et al.*, 2010; Andresen *et al.*, 2011; Sun *et al.*, 2013) in different world wide basins (Fig. 1.38, 1.39 in Chapter 1). The strong reflection of Opal A-CT is also fade in this zone of attenuation (Fig. 3.5). The signal attenuation below the anomalous zone seems to apply irrespective of the continuity of high-amplitude anomalies but it is more pronounced in the middle where the anomalous zone is much thicker (Fig. 3.13).

A coherence cube is extracted to analyse the and below high-amplitude anomalous zone. Time slices taken at 24 ms intervals from a coherence cube generated from the 3D seismic data volume (Fig. 3.14A -J) show the presence of fault within the anomalous zone. The less representation of the faults as shown on Fig. 3.14D to Fig. 3.14I might possibly be to the accumulation of fluid in the anomalous zone. At the coherence time slice at 2860ms TWT polygonal faults are again visible because that slice is generated below the anomaly where the anomalous zone effect is not present. Polygonal faults are clearly visible at time

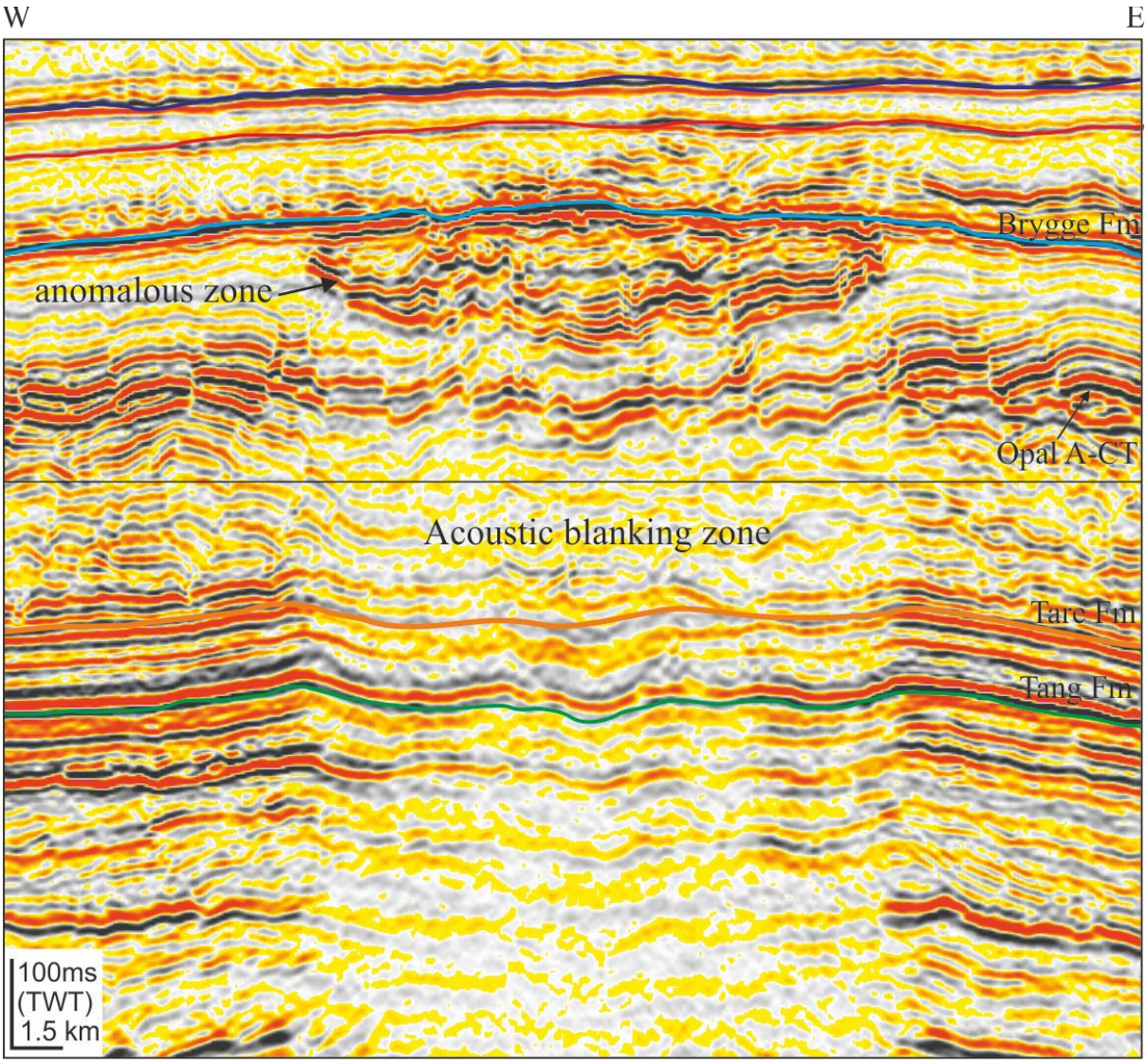

Figure 3.13: Acoustic attenuation observed below up to extends of high-amplitude anomalous zone developed in the Brygge Formation. See fig.3.7 for location.

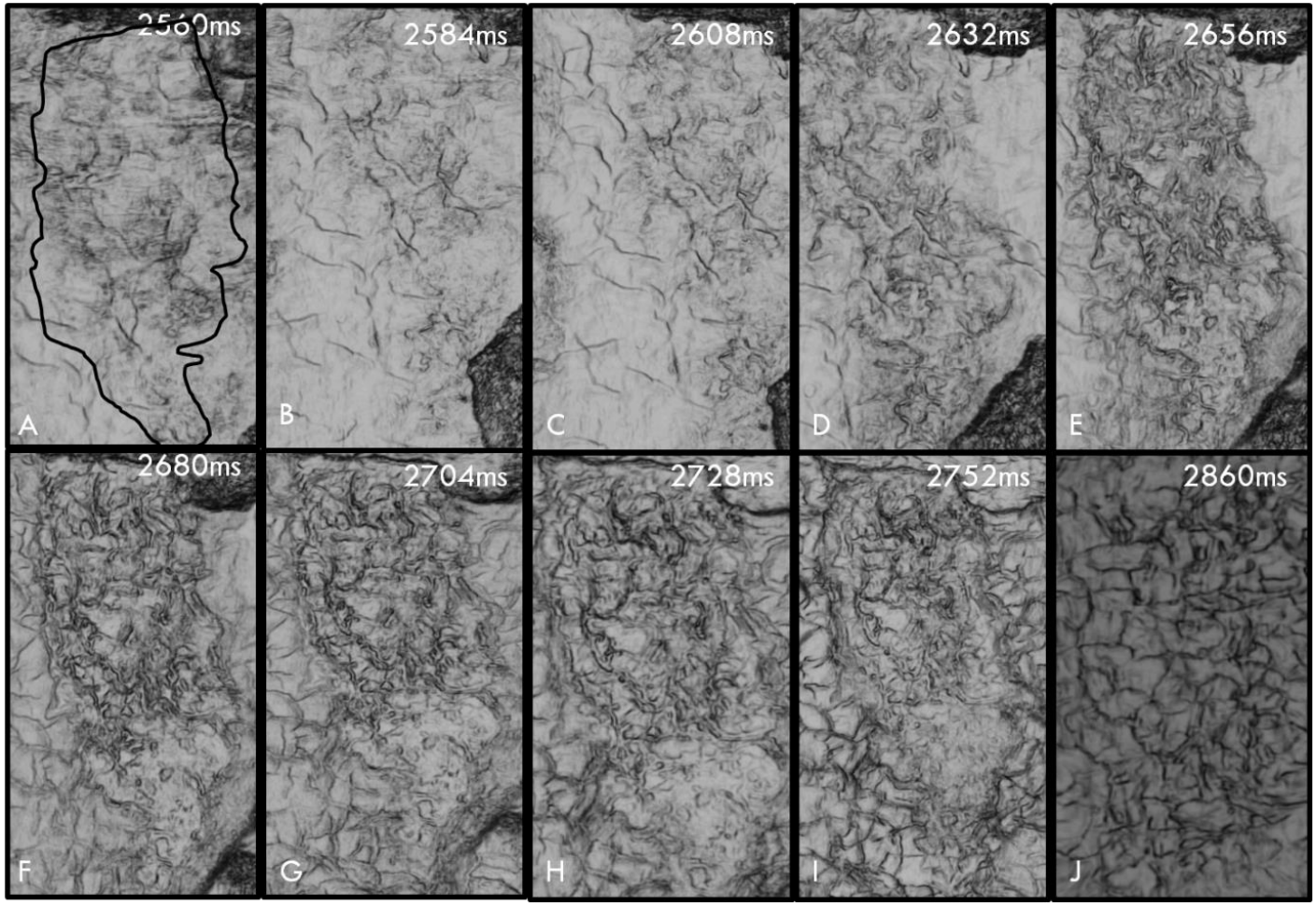

Figure 3.14: Coherence cube time slices at the different time intervals with 300ms TWT thickness. The cube is generated from above the top of the anomaly (2560ms two way travel time and below the base of anomaly 2860ms two way travel time). A black polygone is the trace of anomaly in surface plan-view.

slice at top of Brygge Formation (2560 ms two way travel time) and below the anomalous zone suggest that pattern of the polygonal faults are same and assumed that polygonal faults are present in the anomalous zone.

3.5.2 Vertical distribution of anomalies

Three dimensional analysis of the anomalous zone has been carried out in this study. As earlier stated eight continuous seismic reflections in subsurface were interpreted (Fig. 3.6). Integration of these interpreted seismic horizons with the regional framework shows that these horizons correspond to recent seabed (H1) Paleocene (H8) sediments of the Møre Basin. A series of RMS amplitude extraction (at the interval of 10ms) across the interval in which the anomalous zone is developed shows that the geometry of the high-amplitude anomalous reflections is different from the surrounding background reflections (Fig. 3.15). The RMS amplitude maps show a 10.45 km N-S trending cluster of high-amplitude anomalous zone that confined at the crest of Havsule Dome structure (Fig. 3.7). The high-amplitudes in the anomalous zone are variable in planform, from simple linear to irregular lobate bodies. Anomalies are developed in fine sequence of mudstone with very fine limestone stringers of less than a meter to few meters (Möller *et al.*, 2004) therefore, it is not possible to map these anomalies individually due to tuning effect.

Seven green ellipses (labelled from 1 to 7) are marked on significant occurrence of high amplitude anomalies in order to assess the vertical extent and continuity of amplitude anomalies in the anomalous zone (Fig. 3.15). Each ellipse represents a cluster of enhanced amplitude anomalies. Ellipses 1 to 6 are consistent on all computed maps only ellipse 7 that was observed on figure 3.15C. This observation suggest that continuity of enhance reflection are the possible faults that acts as a routs for fluid migration from the deeper reservoir.

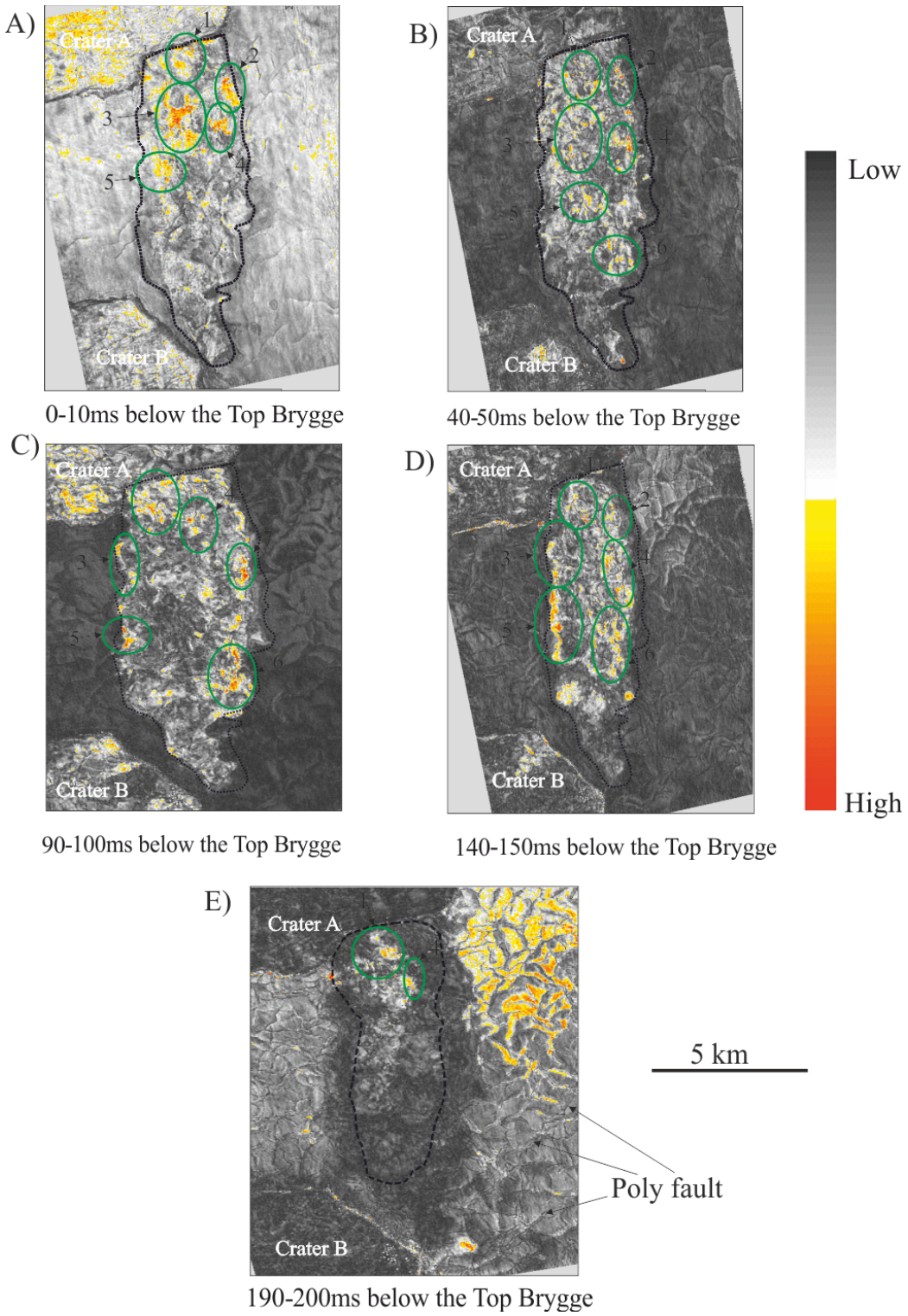

Figure 3.15: RMS amplitude maps extracted from the top to base of the anomaly. Seven green ellipses (Labelled from 1 to 7) are marked representing the location of continuous high amplitudes which may associated with the faults.

3.5.3 Continuity of seismic reflection

Transformations of data from one form to another are common in signal analysis, and various techniques are used to extract significant information from time series (seismic data). Instantaneous phase attribute is used to establish the properties of the host lithology in which the anomaly is developed and frequency attributes used to identify seismic signal attenuation that may be due to gas accumulation and for identifying thin-bed tuning effect on seismic data (Chopra & Marfurt, 2007). In this study, Instantaneous frequency and phase volumes have been generated (Fig. 3.16 and Fig. 3.17 respectively) to analyses the continuity of seismic reflection inside the anomalous zone. Representative seismic profile through the anomalous zone displays continuity of seismic reflection (Fig. 3.16). The white zone on the instantaneous frequency profile indicates low frequency in the anomaly. Observation of low instantaneous frequency has been suggested to imply the presence of gas (Sheriff, 1975; Løseth *et al.*, 2009; Foschi *et al.*, 2014). The continuity of seismic reflection in instantaneous phase data (Fig. 3.17) suggests that high amplitude anomalies developed in the same lithology of the Brygge Formation.

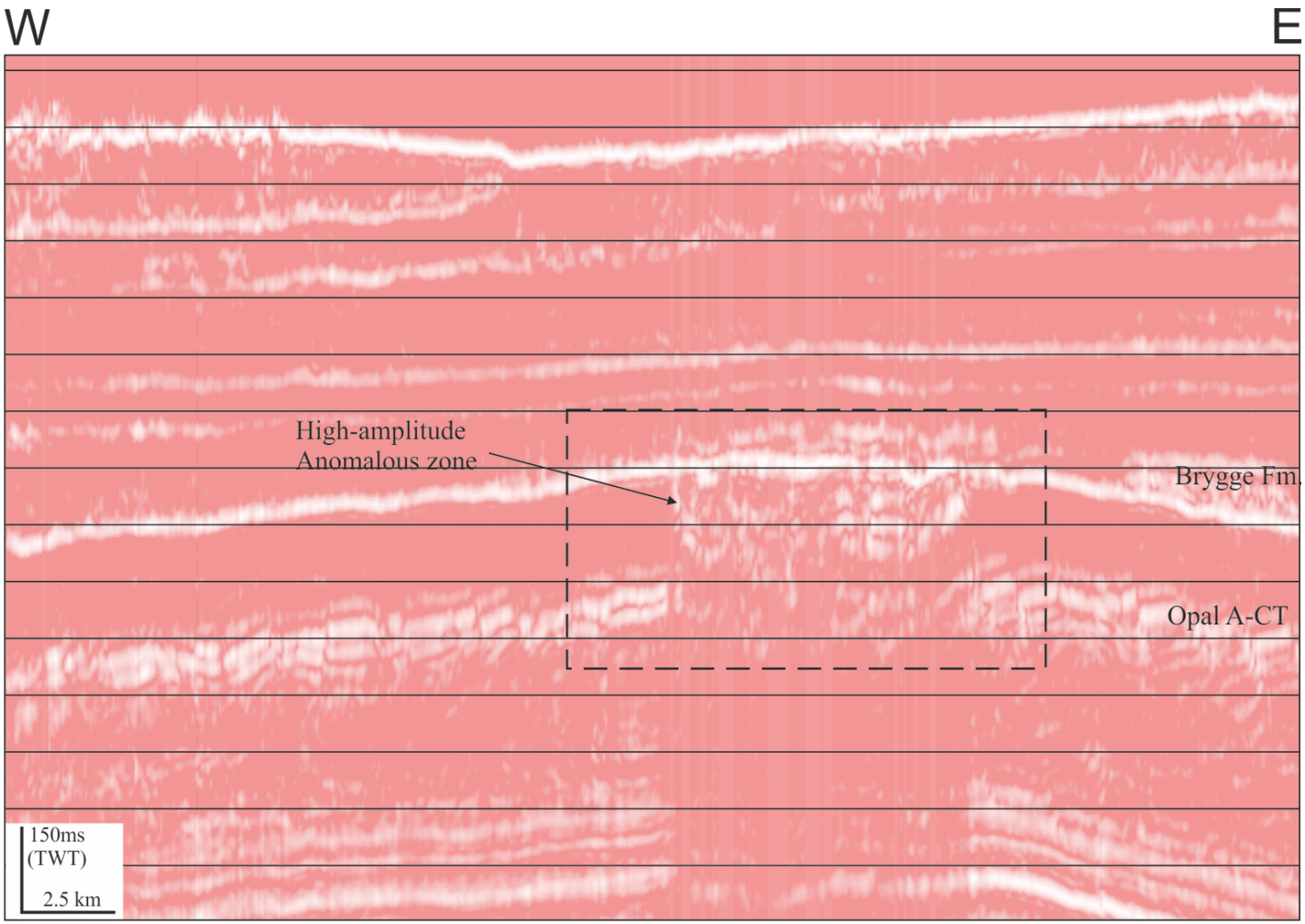

Figure 3.16: Instantaneous Frequency is calculated at NNW-SSE seismic line displaying demonstrates a remarkable decrease in dominant frequencies within and below the high amplitude anomalous zone (dashed rectangle indicates the location of the anomalous zone) of high amplitude at the crest of dome in the Brygge Formation. See fig.3.7 for location.

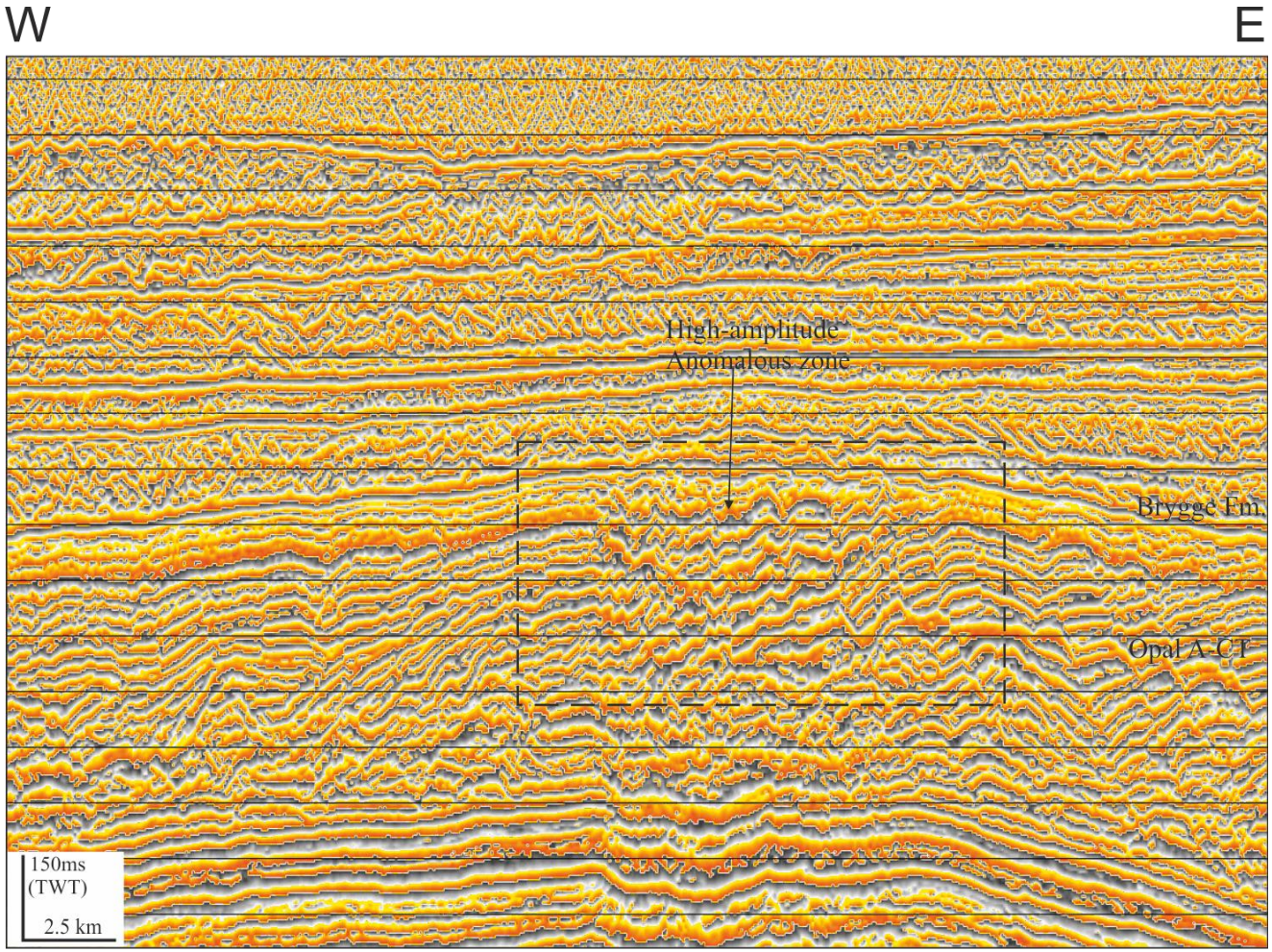

Figure 3.17: Same seismic line in Figure 3.16 with Instantaneous Phase attribute indicates continue reflection in and outside the anomalous zone suggesting that same lithology within the surroundings.

3.5.4 Interval velocity

Seismic acoustic impedance is the product of density and velocity of the sediments. The strength of the reflection of the events depends on the velocity. The base of the anomaly is concave upward and the reflection below the anomaly is consistent with the trend of the base of anomaly (Fig. 3.18). The reflections below the anomaly are bending 30 to 80 ms downward. The push down effect of the reflection is due to the presence of anomaly that has low velocity layer. The 220ms thick anomaly column produces the 30-80ms push down effect below the anomaly.

Well 6404/11-1 in the study area is used to calculate the interval velocity of the anomaly. The well was drilled through Crater A (Fig. 3.17). The Opal-A in the Brygge Formation is eroded due to the slide. The base of the crater is at the 2717ms two way travel time that is equal to 2197.6 meters and the base of the Brygge Formation is at 3065ms two way travel time which is equivalent to 2501 meter in depth, using the interval velocity 1744 m/s of the Brygge Formation (Fig. 3.18). Therefore, it is difficult to incorporate well information directly. Considering the interval velocity of the Brygge Formation (1744 m/s), measured two way travel time at two locations the top (2612ms and 2614ms) and base (3312ms and 3322ms) of the Brygge Formation approximately one kilometre away on the left and right sides of the anomaly and calculated the thickness of the formation that are 610 meters and 617 meters on the both sides respectively. It is assumed that the average thickness of the Brygge Formation is equal to the thickness of the formation at the location of anomaly (Fig. 3.20). Measured the two way travel time of the anomaly (220ms) and below the anomaly to the base of Brygge Formation (514ms) after subtracting the velocity push down effect (70ms). Calculated the thickness of the interval between the base of anomaly and base of the Brygge Formation (448 meters). By subtracting this thickness from the average thickness of the Brygge Formation

gives the thickness of the anomaly (165 meters). From the two way time and thickness of the anomaly, calculated the interval velocity (1506 m/s) within the anomaly.

The range of the interval velocities are used to calculate the interval velocity of the anomaly. The surrounding wells and published material, the interval velocity of the Brygge Formation varies from 1500 m/s to 1900 m/s in the study area (Table 3.1). The calculated interval velocity of the anomaly is plotted against the interval velocity of the Brygge Formation from the 1600 m/s to 1840 m/s, whereas the interval velocity of the anomaly is ranged from 1390 m/s to 1590 m/s (Fig. 3.19).

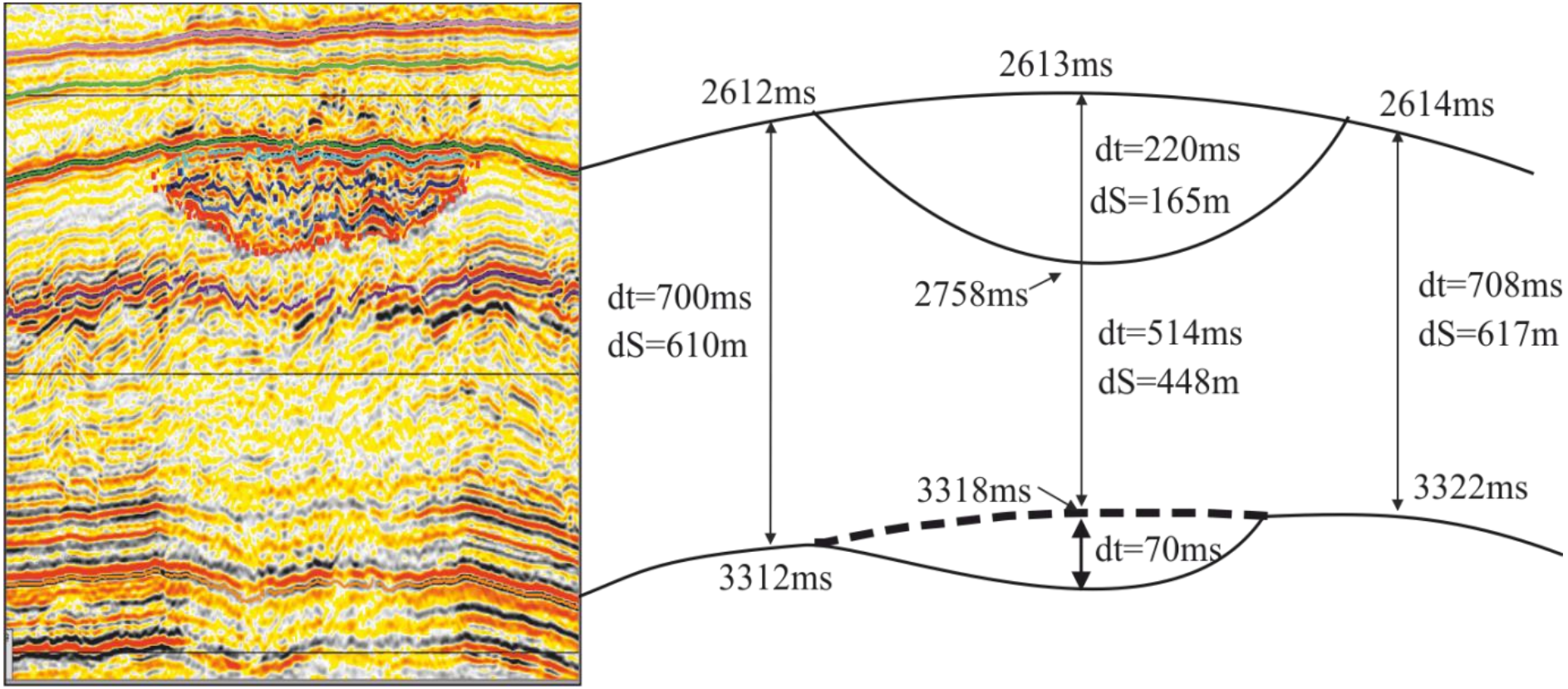

Figure 3.18: Interval velocity of the anomaly is calculated by using the information from Havsule well, the interval velocity of the anomaly is 1506m/s and the interval velocity of Brygge Formation is 1744m/s. This calculation is based on the assumption that thickness of Brygge Formation is almost constant around the anomaly. See fig.3.7 for location.

Table 3.1: Interval velocity of the Brygge Formation in the different well in and near the study area.

Well Name	**Location**	**TWT (ms)**	**TVD (mKRB)**	**Interval Vel (m/s)**
6403/10-1	Solsikke	2745	2091	1662
6403/10-U-1	Solsikke	2753	2074	1532
6404/11-1	Havsule	2717	2501	1744
6305/5-1	Helland Hansen	2065	1720	1804
6405/10-1	Helland Hansen	2228	1867	1894

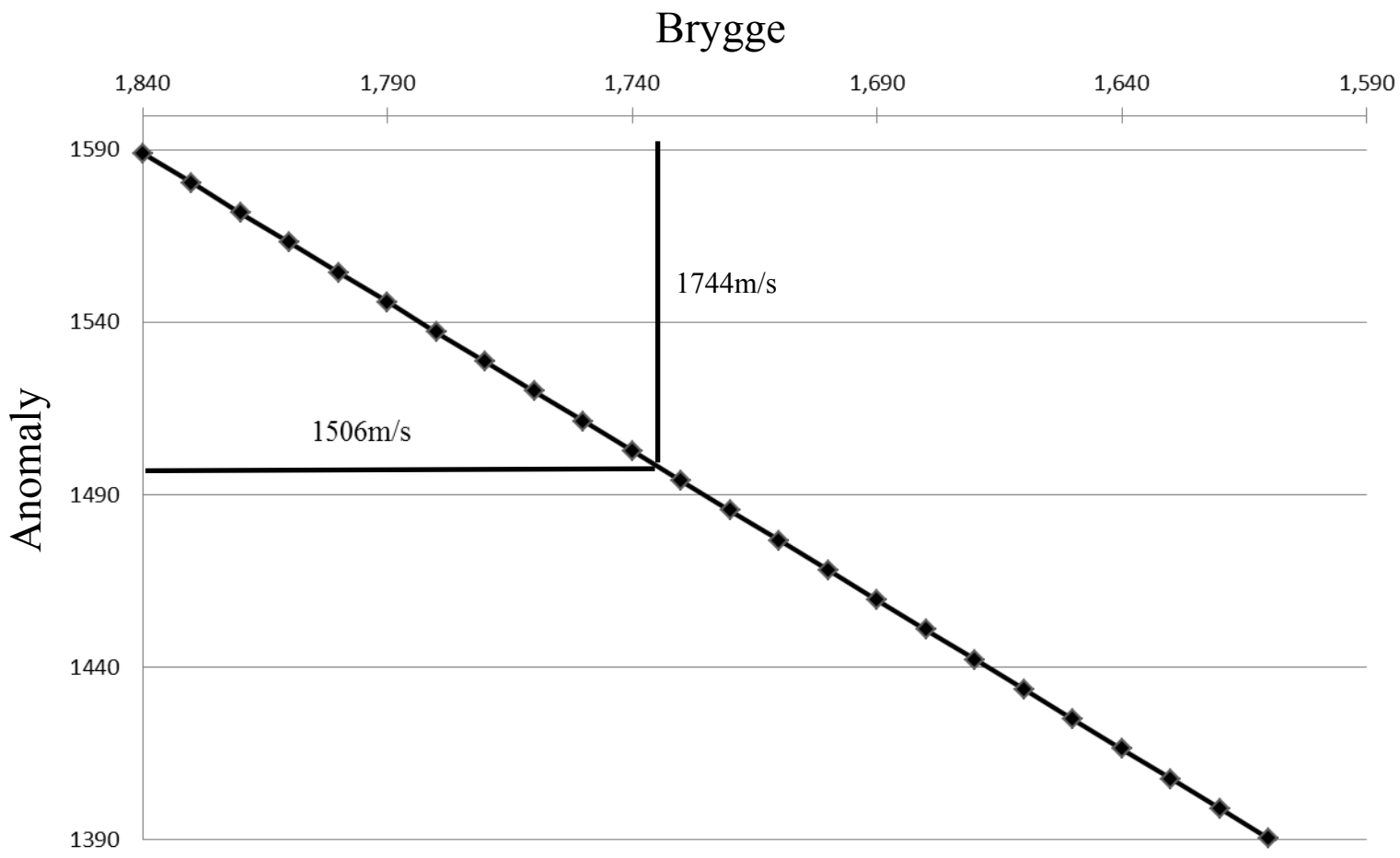

Figure 3.19: A graph showing the interval velocity between the Brygge Formation (Well 6404/11-1) and computed velocity inside the anomalous zone.

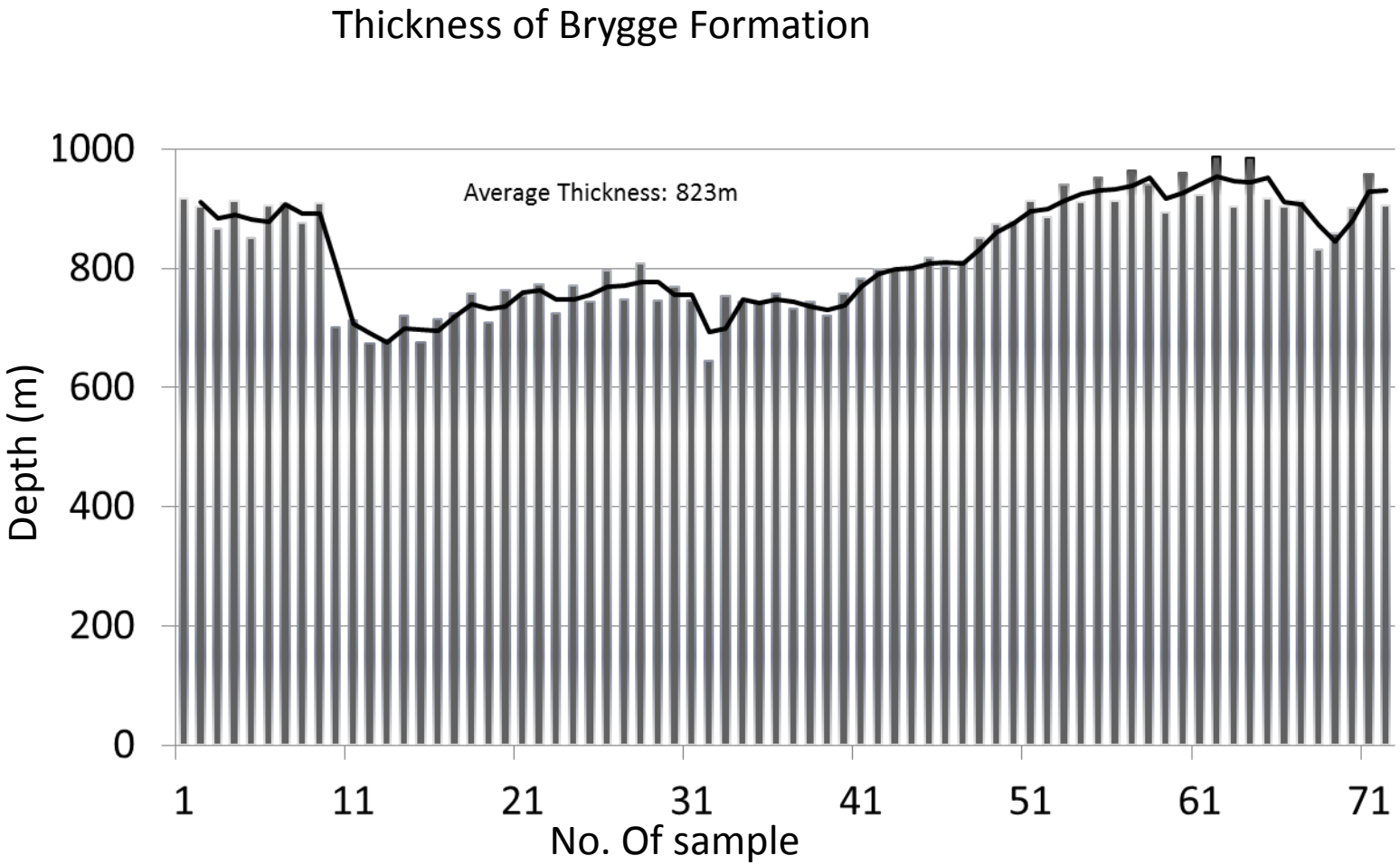

Figure 3.20: Calculated depth of the Brygge Formation in the three dimensional seismic survey acquired at the Havsule Dome.

3.5.5 Leakage indicators from anomalous zone

Fault seals analysis can arise from juxtapositions of reservoir with a sealing lithology or development of a fault rock with high entry pressure for hydrocarbon (Watts, 1987; Smith & Møller, 2003; Stuevold *et al.*, 2003). Smith and Møller (2003) stated that polygonal faults developed in the Ormen Lange field area have considerable influence on the reservoir as polygonal faults transacted main reservoirs in the field. Due to the complexity associated with understanding the sealing behaviour of polygonal faults, leakage through polygonal faults are not fully understood and therefore needs detailed research (Cartwright & Dewhurst, 1998; Cartwright *et al.*, 2003; Forsberg & Locat, 2005; Gay *et al.*, 2006; Cartwright *et al.*, 2007).

The origin of the polygonal faults system in the study area has not been addressed in this study. Rather I focus on seismic observations of leakage through polygonal faults in the anomalous zone. Five different horizons have been mapped in the Naust Formation. On the basis of their internal transparent to chaotic seismic characteristics these mapped reflectors are interpreted as mass transport deposits (labelled 1 to 5 in Fig. 3.5 and Fig. 3.6).

RMS amplitude map generated in a 100 ms interval above the anomalous zone in MTD 1 (Fig. 3.21) shows majority of amplitude reflections developed above the anomalous zone. These high amplitude reflections are not observed in the back ground. The distributions of these amplitudes reflections in the MTD are irregular. This observation suggests that MTD 1 is porous and permeable and that the amplitude reflections could in fact represents possible leakage from the anomalous zone (Fig. 3.22).

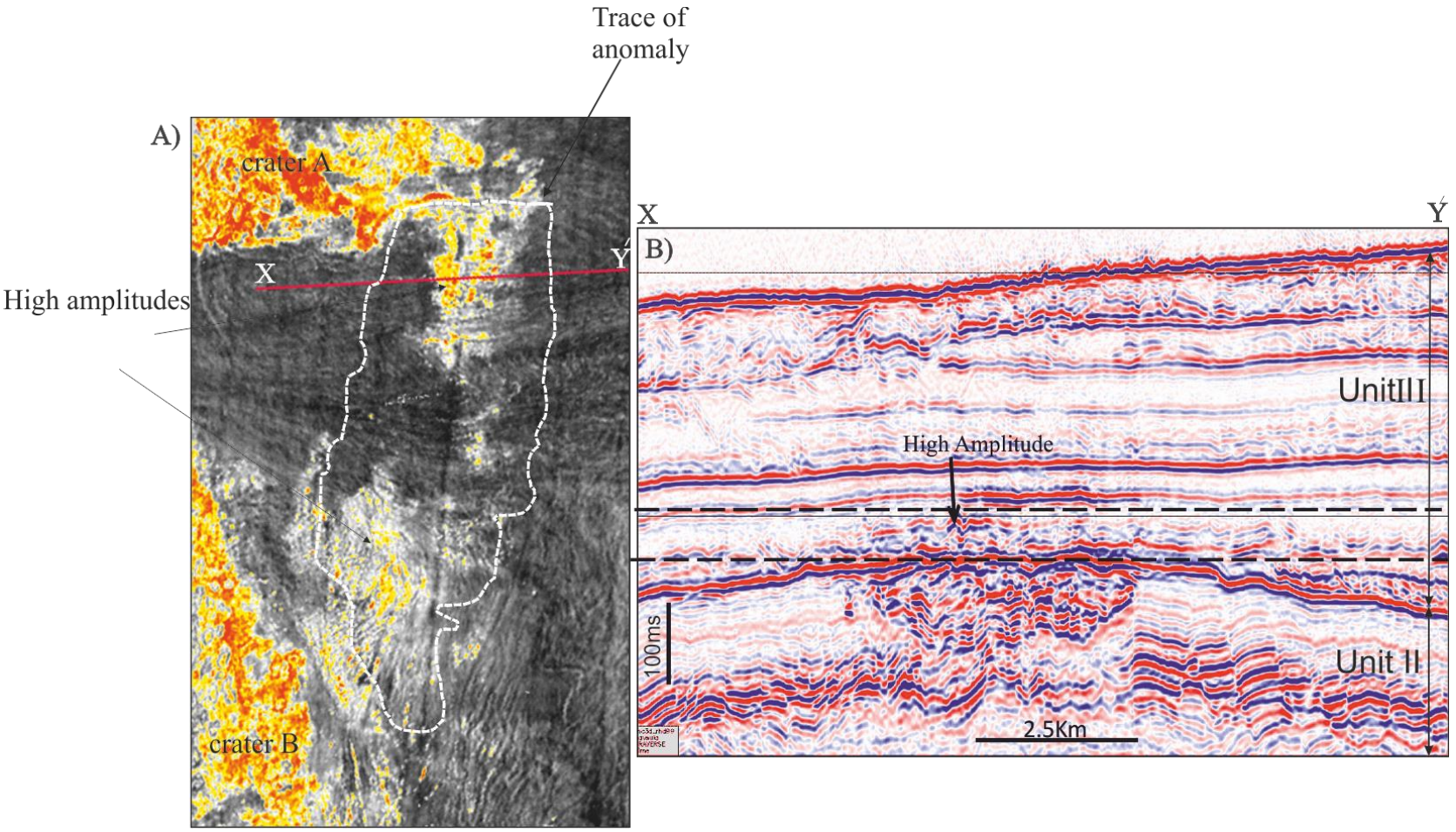

Figure 3.21: RMS amplitude map extracted above the anomaly within a 100ms window to analysis high amplitude pattern in the seal/mass transport deposit that is indicating the leakage from the anomaly.

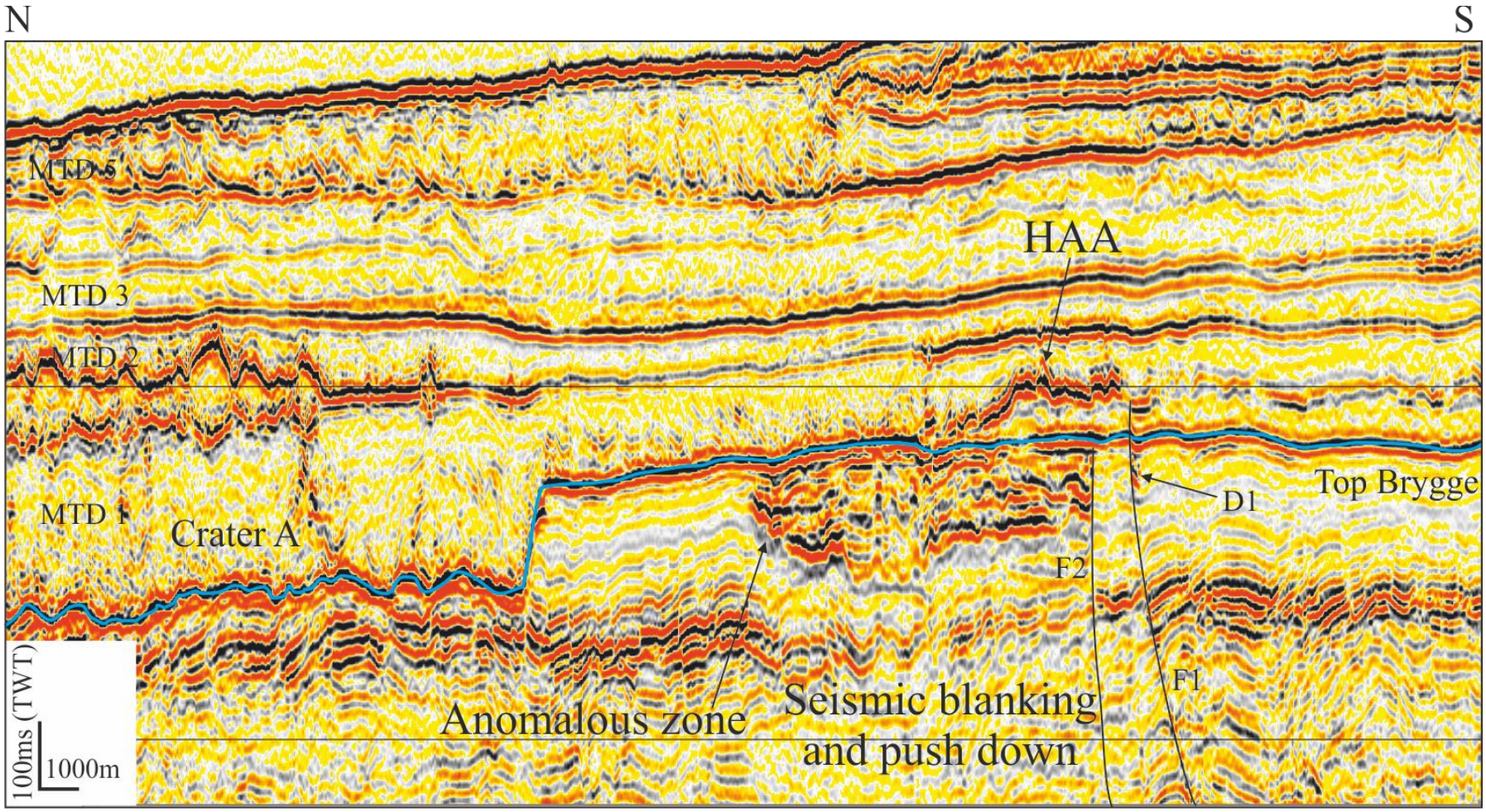

Figure 3.22: Seismic profile shows growth of anomalous zone developed at the Top of the Brygge Formation. A clear vanishing of anomalous zone observed against fault F2 and development of amplitude along fault F1. D1 is indicating the location of new amplitude anomaly. See fig.3.7 for location.

3.6 Discussion

About 165m thick high amplitude anomalous zone observed along the Opal-A sediment of the Brygge Formation that developed at the crest of Havsule Dome. The following observations are made from the previous sections; 1) Amplitude anomalous zone has a negative reflection and sharp change in amplitude from the back ground, 2) Anomaly is developed at crest of Havsule Dome (Fig. 3.7), 3) has significant velocity push down effect ranging from few meters to tens of meters that reduce >20% seismic reflection strength relative to the background (Fig. 3.5), 4) Seismic blanking or attenuation observed below the anomalous zone (Fig. 3.13), 5) Interval velocity of the anomalous zone is less than interval velocity of the host sediments that is 1500 m/sec (Fig. 3.18), 6) Presence of low frequencies in the anomalous zone relative to background sediments (Fig. 3.16), 7) Continuity of sediments reflection in the anomalous zone shows that the anomalous zone was developed in the same type of sediments in the background (Fig. 3.17). All these observations collectively support that the high-amplitude anomalous zone is a direct response to the presence of free gas within Opal-A sediments of the Brygge Formation

The mechanism by which fluids move up in the sediments to a surface is not well constrained in the sedimentary basins (Gay & Berndt, 2007). During burial the sediment porosity decreases because of loading by overlying sediments. The subsequent fluid expulsion due to sediment contraction is referred to as dewatering in fine grain sediments (Cartwright & Dewhurst, 1998) that possibly leads to further development of polygonal faults within the Brygge Formation. Once the polygonal faults are developed, they are considered to be a potential fluid conduit (Hustoft *et al.*, 2007). Vertical migration of fluids through thick (up to 700 m), low-permeability fine grained sediments cannot occur at high enough rate due to low porosity and permeability in fine-grained the Brygge Formation.

3.6.1 Migration and potential origin of fluids

Mapping of the anomalous zone revealed an interesting observation that amplitudes are developed on crest of Havsule Dome conform to the structural closure. The gas fill layers exhibit monoclinal dip towards the south, with a generally low angle (typically less than a degree). The anomalies expand laterally towards up-dip (Fig. 3.7). A possible model is proposed for development of anomalous zone.

The anomalous zone is fed by a conduit or combination of conduits (possibly polygonal and regional faults) from the deeper reservoirs and it charged or filled the lower most layer of the structure (Fig. 3.24) and started expanding by replacing water in that layer up to the spill point or a certain limit where water cannot be replaced due to hydrostatic pressure and then it reached a state of equilibrium. The layer was overpressured due to continuous fluid being feed from deeper reservoir through conduits. At equilibrium state of pressure, there were no further spaces left for fluid to migrate in to this layer so therefore fluid started accumulating in the upper layer and so on up to the present upper layer or even more. (Fig. 3.24)

This model is supported by Carruthers and de Lind van Wijngaarden (2000) "invasion percolation theory". In their model, fluid flow through focused pathways as a function of the rock capillary entry pressure at the timescale of secondary petroleum migration. Gas flow is generally assumed to be controlled by the balance between buoyancy and capillary forces and other minor viscous forces are neglected. Hydrocarbon generation and expulsion from mature source rocks would migrate further through the sedimentary system as a function of hydrocarbon column height and capillary entry pressure that build up due to presence of gas migration and replacement of water until a final balance between both forces is reached (Fig. 3.23). The overpressure in that layer breach the underlying seal and charge/filled the lower layer along the migration paths (Fig. 3.23B and C) to a certain limit and so on at the end of

last layer that is indicated with labelled with 1 to 4 (Fig. 3.23D and E). This process took too much time and indicates the slow and steady gas leakage from deeper reservoir or small quantity of fluid from the deeper reservoir because the exploratory well 6404/11-1 in the study area was dry and abandoned suggesting that the deeper reservoir was not good enough for commercial purpose and just had small quantity of fluid that migrated from it to upper sediments to develop the anomalous zone.

A hypothetical model to understand the development of anomalous zone in very fine sediments is presented in figure 3.25 where vertical permeability is lesser than horizontal (Kv<Kh) as flat stratigraphy with clay rich sediments (very thin layers of ooze material and silt/clay sediments) (Fig. 3.25a). Compaction and capillary entry pressure gas start moving upward due to buoyancy and capillary entry pressure to a certain limit (Fig. 3.25b). Charging of gas through CEP and possibly through faults and trapped at the crest of dome (Fig. 3.23 and Fig. 3.24c). Accumulation and saturation of gas in thin layers generate pushdown effect on underlying layers and this effect increases with high saturation of gas. Fluid filled upward layers, resulting in column height increase and the reduction in pressure in the lower layer due to leakage from that particular layer into upper one (Fig. 3.23).

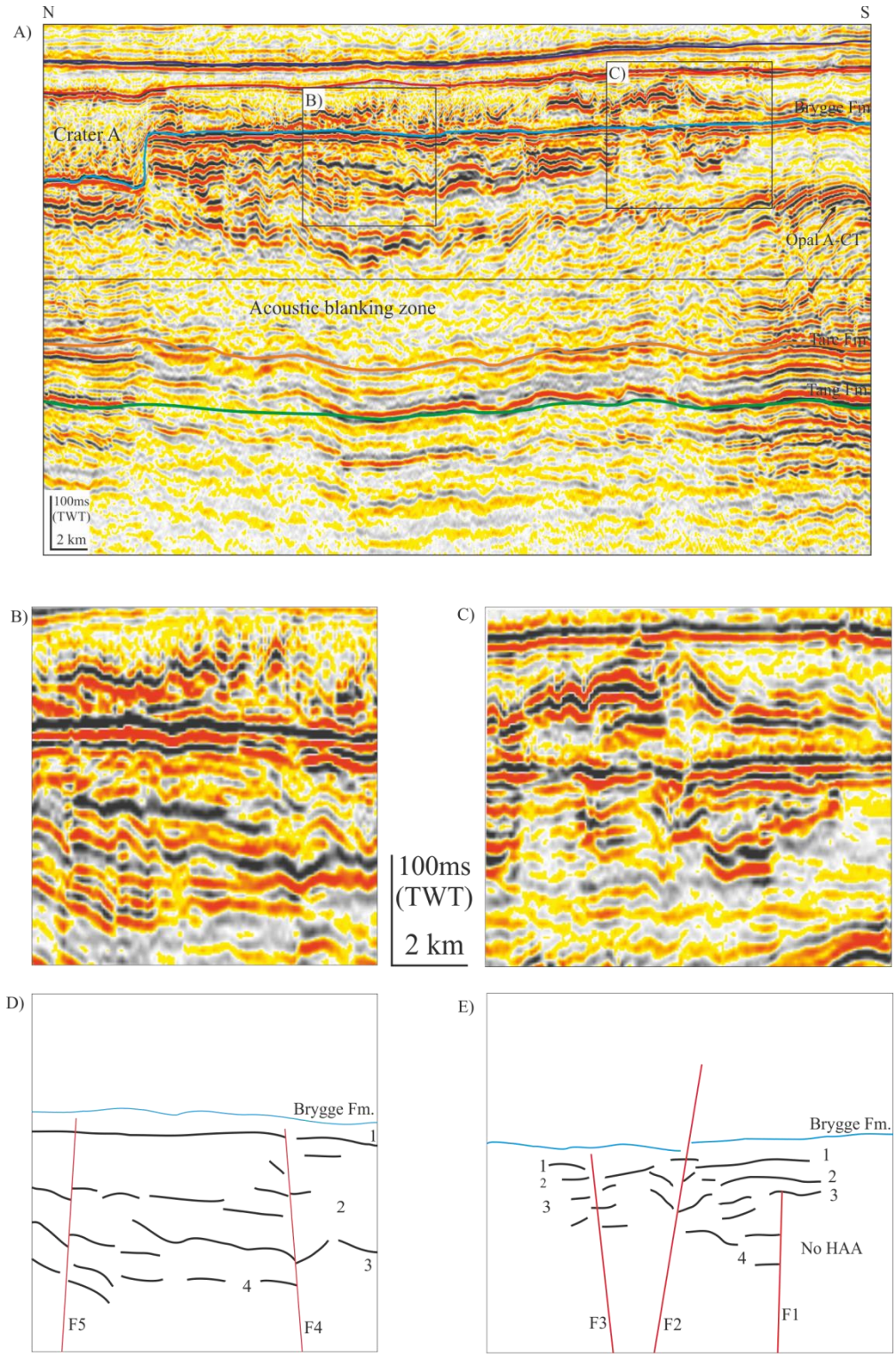

Figure 3.23: Seismic profile through anomalous zone shows development of anomalies in the fine clay/calcareous ooze sediments showing extent of amplitude anomalies towards updip in south direction . D and E are the interpretation of B and C images. See fig.3.7 for location.

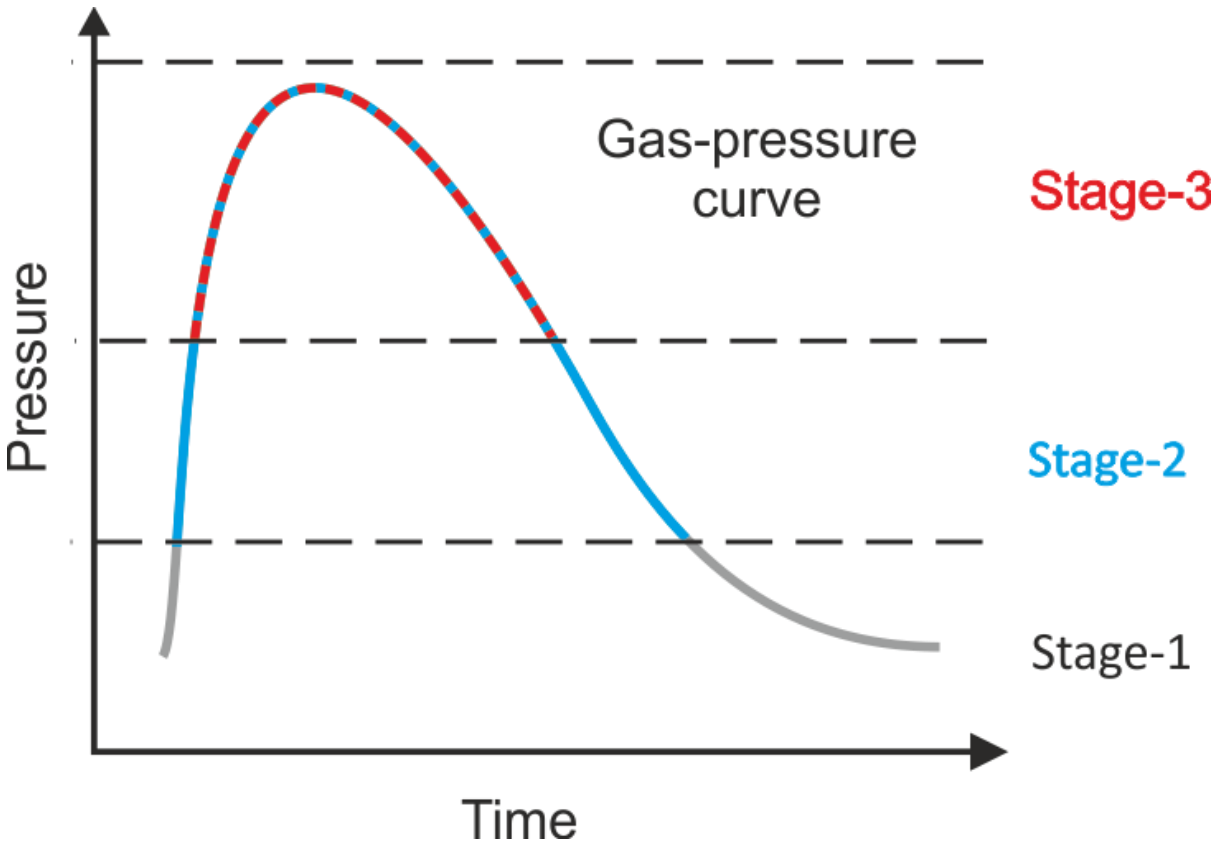

Figure 3.24: The migration model is based on a simplified gas pressure curve composed of a temporary limited peak. Three different stages represent the build-up of high pressure and release of pressure.

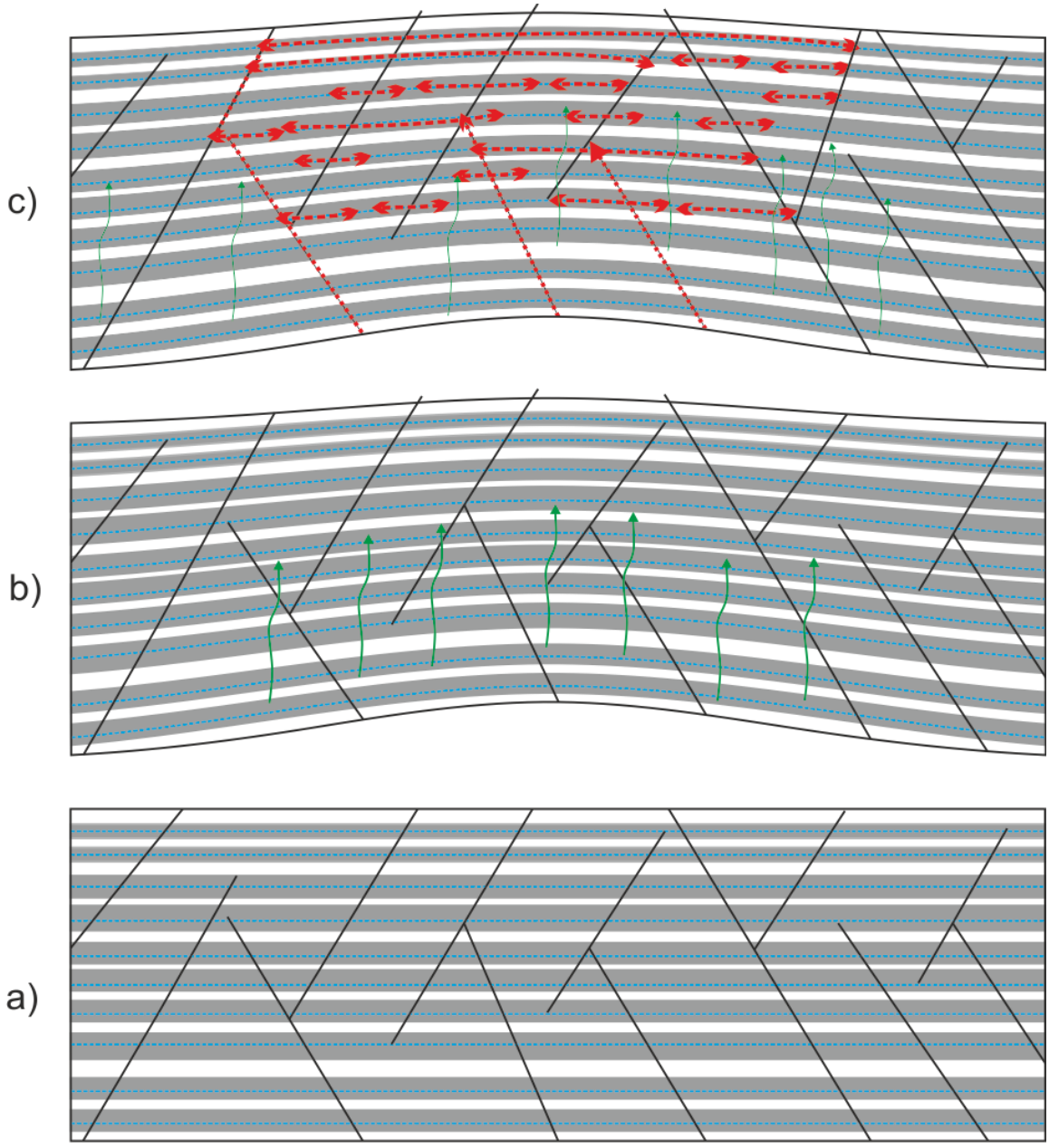

Figure 3.25: A hypothetical model presented here to understand the development of anomalous zone in very fine sediments where Kv<Kh. (a) Flat stratigraphy with clay rich sediments (very thin layers of ooze material and silt/clay sediments). b) Compaction and capillary entry pressure gas start moving upward due to bouncy and due to overburden pressure of sediment load c) Charging of gas through CEP and possibly through faults and trapped at the crest of dome. Accumulation and saturation of gas in thin layers and saturation of gas generate pushdown effect on underlying layers and effect increased with high saturation of gas.

3.6.2 Concave Gas/Water Contact

High amplitude anomaly is developed in fine sediments of the Brygge Formation. Well 6305/1-1 drilled 654 meter thick succession of the Brygge Formation in the Ormen Lange field, south of the study area (Fig. 3.1) provides information about the stratigraphy. 150 intervals of mud/silt and calcareous Ooze sediments of less than 1 m to few meters thick with average thickness of 4.5 m are reported in the well cuttings. Based on this analogy, 165 meter thick anomalous zone has approximately more than 30 intervals of the same lithology like varves deposits. The accumulation of gas in these thin layers acts like a lithogenic reservoir (Fig. 3.26a to f). On the seismic section, only four continuous reflections are mapped due to low seismic resolution. Chopra (2006) suggested that thin bed resolution depends on the presence of noise and consequent broadening of the seismic wavelet during its subsurface (chapter 2 methods, section 2.4). It is widely believed that gas dissolved in water or a few percent of a separate gas phase in water can make the pore fluid mixture very compressible (Chopra *et al.*, 2006). Han and Batzle (2002) defined the fluid bulk modulus (K), the inverse of compressibility, would drop significantly and, in turn, P-wave velocity and impedance will decrease.

As gas migrates upward, it is exposed to lower pressures and temperatures in an open media. In confined reservoir, both density and viscosity of gas decreased as its volume increases. So saturation of gas is directly related to gas volume in the porous media that is also effect on acoustic velocities of the rock (Foschi *et al.*, 2014), 2014). The geometry of a gas in confined reservoir has not any direct relation with in situ pressure that developed due to presence of gas, it only increase the push down phenomenon due to reduction of seismic velocities (Avseth *et al.*, 2005)

The presence of the thin layers filled of gas makes these layers behave as separate reservoirs or compartments for gas accumulation. Each layer has its individual pushdown effect due to presence of gas. So therefore; cumulative effect of the zone of each reservoir makes the shape of the anomaly concave upward instead of the normally flat gas/water contact (Fig. 3.26g) that observed in many sedimentary basins.

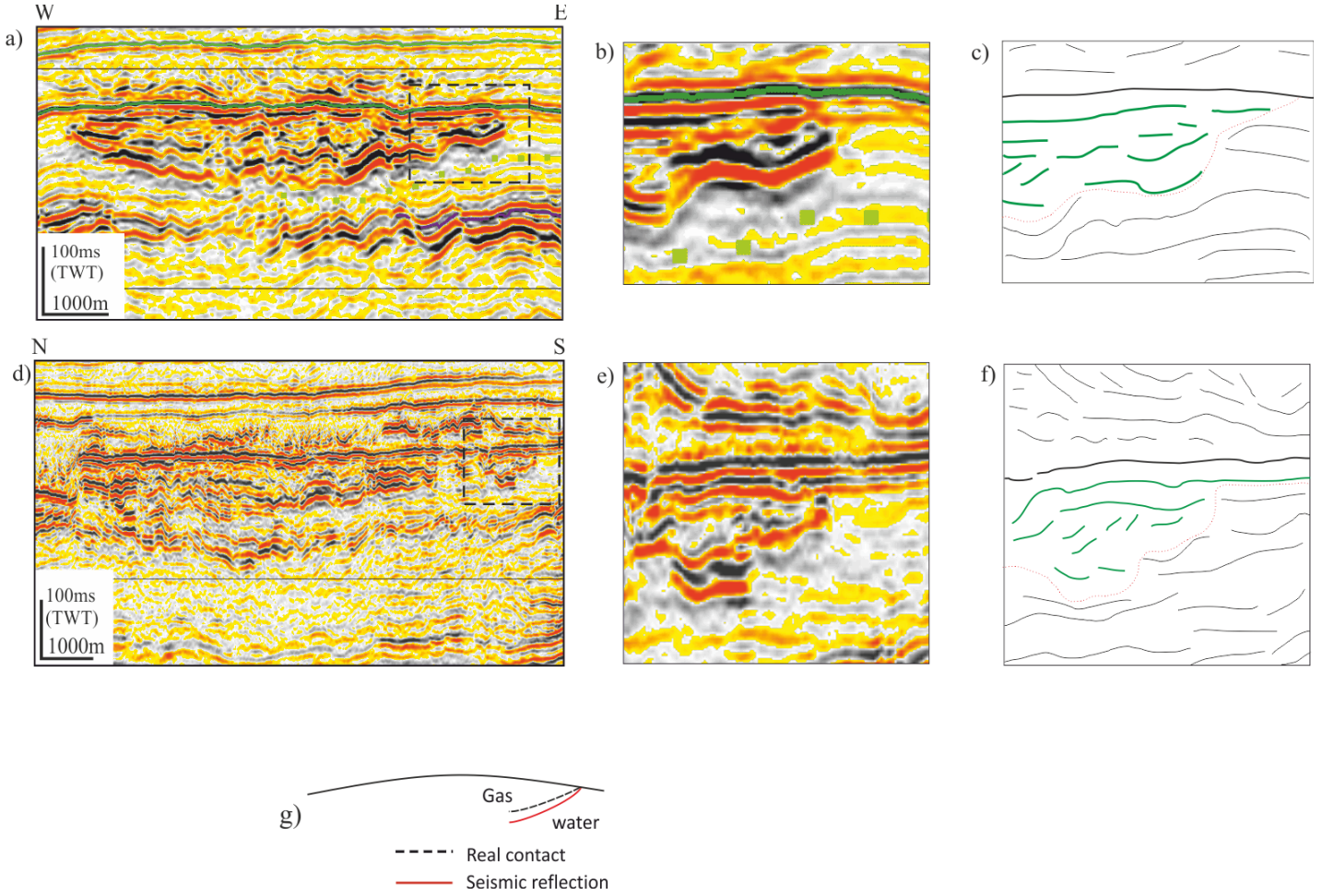

Figure 3.26: Accumulation and saturation of gas in thin layers and saturation of gas generate push down effect on underlying layers and effect increased with high saturation of gas. See fig.3.7 for location.

3.7 Conclusions

This study documents for the first time the occurrence of high-amplitude anomalous reflections with a concave upwards shape geometry in the subsurface of the Møre Basin of Mid- Norwegian. On the basis of seismic attributes analysis of a 3D seismic data set, concluded that the anomalies are related to the occurrence of potential gas accumulation overlying a multiple subsurface landslides mainly the Storegga slide that act as a seal up to sea bed. Simple list of the main conclusions:

- Zone of anomalies is located at the crest of the Havsule Dome
- Polarity reversal is a major indication, the presence of gas in the zone of anomalies
- The velocity push down below the zone of anomalies
- Interval velocity of the zone of anomalies ~ 1506m/s
- Leakage above the zone of anomalies
- High amplitude above the zone of anomalies
- Polygonal faults inside the zone of anomalies
- The deep-seated faults could provide the migration path
- No leakage evidence towards the crater
- The basin is proven as a gas reservoir basin

On the basis of these results, I conclude that

- the HAA is possibly due to accumulation of gas

- The anomalous zone is explained as a dynamic accumulation of free gas that leaked upward through c1000m of polygonally faulted the Brygge Formation and Tare/Tang formation from the deep reservoir.
- Origin of the concave upward gas/water contact is unknown, could be due to leakage or due to low permeability of reservoir diatomites.
- Leakage from deep reservoir in this basin could have been caused by rapid unloading during Pleistocene-Holocene slope failure.

CHAPTER 4

Distribution of HAA in hemipelagite sediments: A case study from LCB

CHAPTER FOUR

4.1 Introduction

High amplitude anomalies are found in the Late Neogene/Quaternary strata in the Lower Congo Basin (LCB) (Gay *et al.*, 2003; Gee and Gawthorpe, 2006a; Anka *et al.*, 2009; Vemba *et al.*, 2011; Andresen, 2012; Ho *et al.*, 2012). These HAAs are identified due to their strong expression on seismic data. To explore the distribution and relationship of these anomalies with possible fluid flow mechanisms. Identified and examined several high amplitude anomalies at different stratigraphic intervals in the basin. The aims of this chapter are: (a) provide an overview of the tectonic and stratigraphic evolution of the Lower Congo Basin (b) summarize the structural elements of the study area (c) take an inventory of high amplitude anomalies at different stratigraphic units (d) classify the high amplitude anomalies (e) differentiate hydrocarbon related anomalies to non-hydrocarbon anomalies and (f) identify mini case studies for further study on fluid flow and possible leakage mechanisms.

4.2 3D Seismic data set

The architecture and stratigraphy of the Congo-Angola continental margins are fairly umderstood because of intensive hydrocarbon exploration activities in the basin (Gee *et al.*, 2006; Anka *et al.*, 2009; Vemba *et al.*, 2011). Hydrocarbon exploration in the Lower Congo Basin is still at its early stage and many areas remain unexplored. However, large oil and gas accumulations have been discovered during recent years and each area represents a prolific region for oil and gas production and focused fluid flow (Davies *et al.*, 2004).

The dataset for this study is a high-density seismic cube (HD3D) acquired in 1999. It is sampled at 6.25 m horizontally and 2 ms vertically for 4.5 s TTWT giving a total volume of

20 km x 24 km x 4.5 s. The dataset is considered one of the best processed 3D cubes worldwide. Six exploration and appraisal wells and three side tracks were available for this study. The wells are composed of traditional well logs such as Gamma, Sonic, Density, Neutron and Resistivity. Most geological reports were extracted from the '*Caprocks*' project. A large number of seismic horizons were supplied by sponsor. A number of these horizons were extended to the entire survey and infill horizons were tracked to enable a detailed stratigraphic slicing of the seals and hemipelagite intervals of the study area.

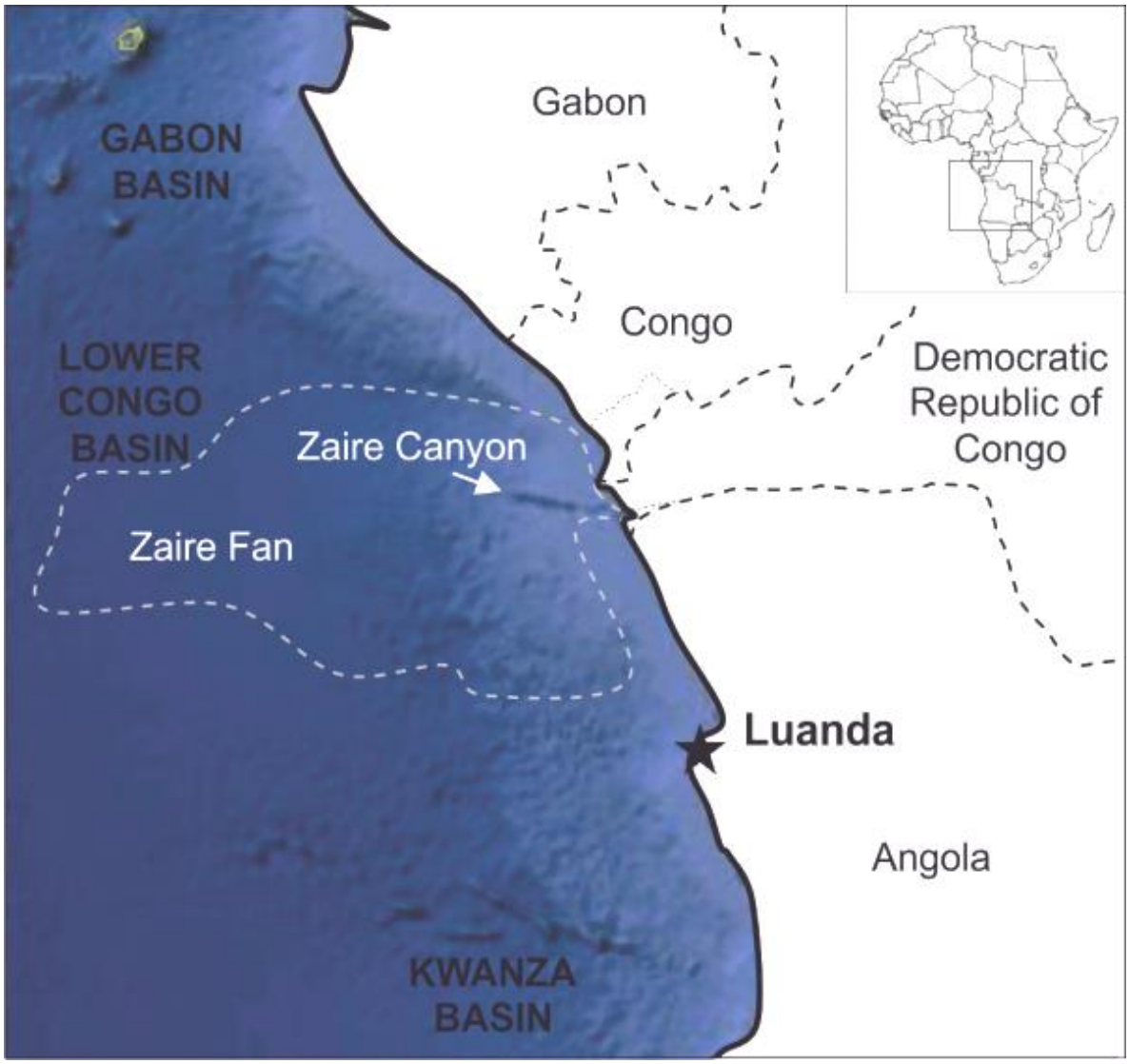

Figure. 4.1: Location map of the study area in the West African Margin (WAM). Exact location of the data set is not mentioned due to data confidentiality (Modified from Ho *et al.*, 2012).

4.3 Geology of the study area

4.3.1 Regional setting

The study area is located on the Congo deep-sea fan on the continental margin of the Lower Congo Basin (LCB) (Fig. 4.1). The LCB is one of the many sub basins along the West African Margin which developed in the early Cretaceous (*c*.130 Ma) during the opening of the South Atlantic Ocean when the southern American plate was separated from the African plate (Larson and Ladd, 1973; Brice *et al.*, 1982; György Marton *et al.*, 2000; Gee *et al.*, 2006; Anka *et al.*, 2010)(Mascle and Phillips, 1972; (Jansen *et al.*, 1984) Karner et al., 1997;Andresen et al., 2010;). The lower Congo Basin is delimited at its northern and southern part by pre-rift basement culminations (Broucke *et al.*, 2004; Standlee et al., 1992). The basin evolved in early Cretaceous (Neocomian) with a continental regime and ended in Tertiary with marine regime (Nombo-Makaya and Han, 2009). The syn-rift sequence is overlain by a succession of evaporites of Aptian age that have correlative on the SE Brazilian margins (Anderson *et al.*, 2000; Broucke *et al.*, 2004). Overlying the evaporites is a thick succession of Albian carbonates and Cenozoic clastic sediments (Lavier *et al.*, 2001; Séranne and Anka, 2005; Liro and Dawson, 2000). The latter strata were deformed by salt-related extensional faults and structures which formed during gravity-driven thin-skinned extension (Duval *et al.*, 1992).

The LCB has a thick, Aptian syn-rift evaporite succession that has led to severe deformation of the overburden and facilitated the development of many minor salt basins (Brice *et al.*, 1982; Andresen *et al.*, 2011; Marton et al., 2000). The rift phase was followed by a post-rift succession, initially dominated by carbonate deposition during Albian and clastic

sedimentation during the Late Cretaceous and Cenozoic (Fig. 4.2) (Seranne *et al.*, 1992). The coarser fraction of the Cenozoic post-rift succession is captured by the submarine Congo (Zaire) Canyon (Fig. 4.1); hence, Cenozoic succession in the basin is comprised of fine-grained mudstones (Pufahl et al., 1998; Uenzelmann-Neben, 1998; Anka et al., 2009).

During Early and Late Miocene, turbidites and coarse-filled submarine canyons occur occasionally and are the main agent transporting coarser clastic sediments across the upper slope on the margin (Anderson *et al.*, 2000). Consequently, Miocene strata were interbedded with hemipelagite and Mass-Transport Deposits (MTD) (Anderson *et al.*, 2000; Sikkema and Wojcik, 2000; Broucke *et al.*, 2004; Andresen *et al.*, 2011). The upper Miocene to lower Quaternary succession in the LCB is deformed by intensive polygonal faulting in most salt mini-basins (Gay *et al.*, 2004; Andresen and Huuse, 2011).

The study interval is chosen in an area where fluid flow features are observed. Pockmarks connected with polygonal faults and underlying turbiditic channels have been previously reported in the basin (e.g. (Gay *et al.*, 2006a; Ho *et al.*, 2012). Gas hydrates, bottom simulating reflections, free gas zones, chimneys and pipes are also frequently reported along the Angolan margin from the Lower Congo and Kwanza Basins (Cunningham and Lindholm, 2000; Gay *et al.*, 2006b).

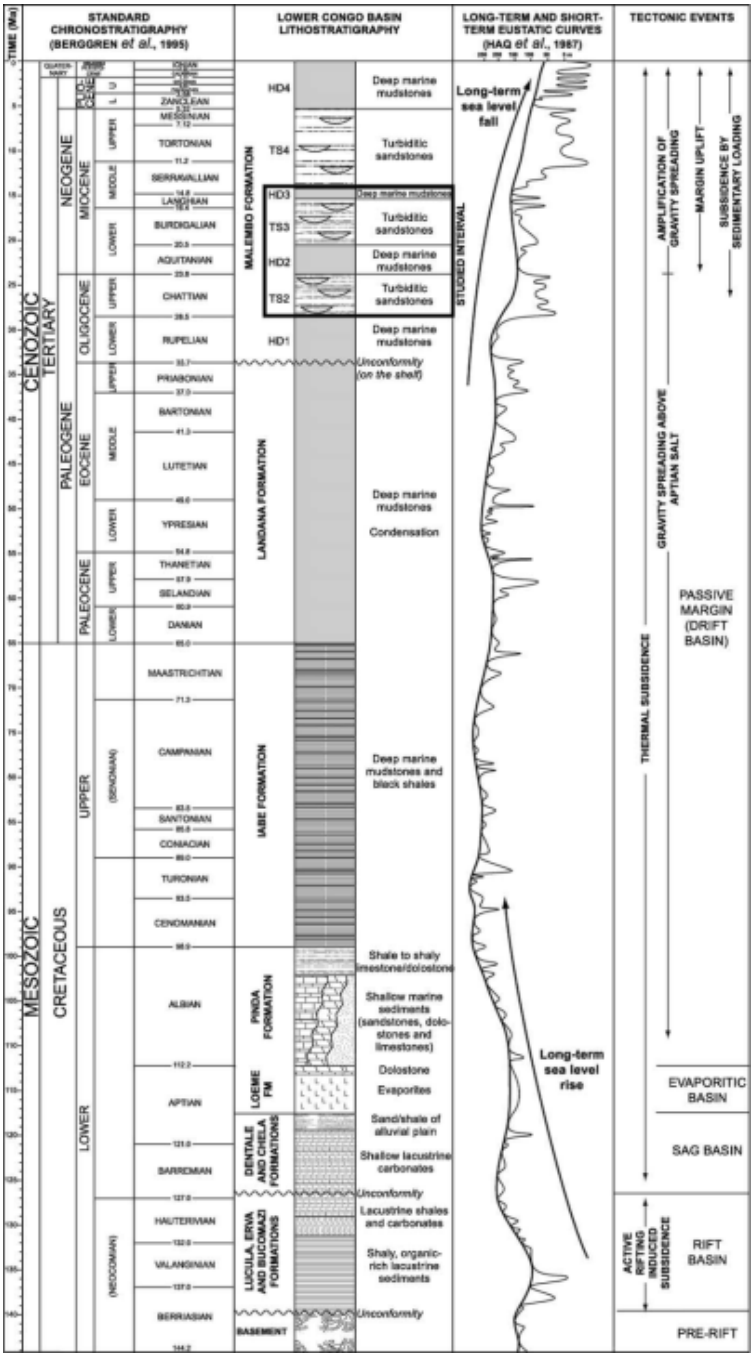

Figure 4.2: Simplified composite stratigraphic chart of the Lower Congo Basin. Note: Black rectangle represents the main interval of interest in this chapter. TS refer to turbiditic system and HD to hemipelagic deposits (from Broucke et al., 2004).

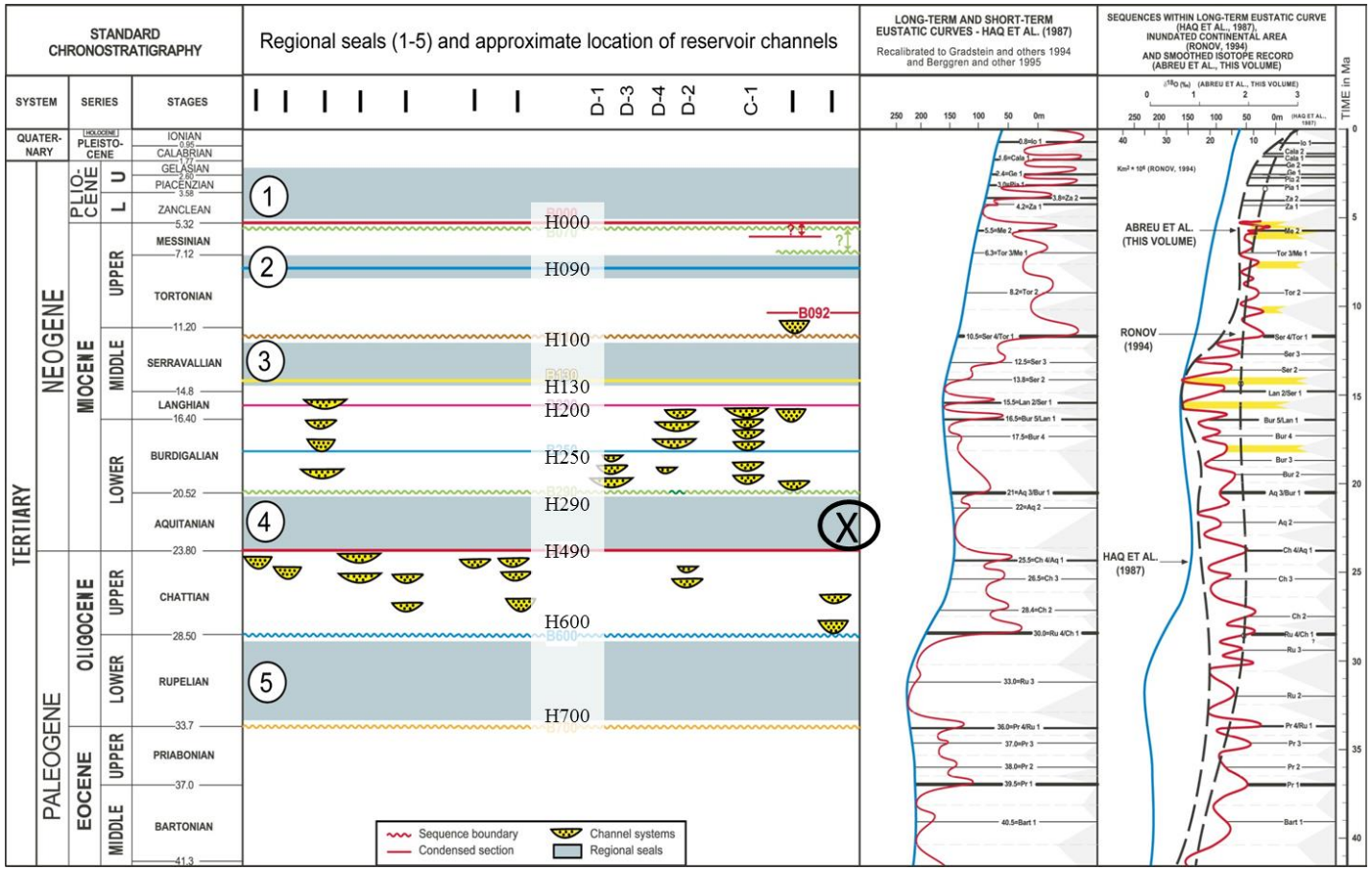

Figure 4.3: Regional stratigraphic framework established by the data provider company. It is based on all data from the study area and surroundings acreages. Five regional seal units (1 to 5) with interpreted seismic horizon to illustrate channels and sequence boundaries.

4.3.2 Local setting of study area

The understanding of the depositional environment has been done through analyses of three dimensional seismic data of the study area. The seismic cube is located in the deep margin of the Lower Congo Basin and shows six structural and depositional elements (Fig 4.4), and related fluid flow features. Six key elements were observed: (1) Complex turbidite channel levees, (2) frontal splays or distributary channel complexes, levees and lobes, (3) Regional hemipelagic sequences (seal units) (4) Debris-flow and Mass transport deposits (5) channel overbank sediment waves that deposited sand lenses/ sheets and (6) faults. The lithology and reservoir architecture of each element depends on the interaction between sedimentary process, paleo sea-floor morphology, and sediment grain-size distribution. The relationship of these elements with development of high amplitude anomalies and related fluid flow features are the main objective of this chapter.

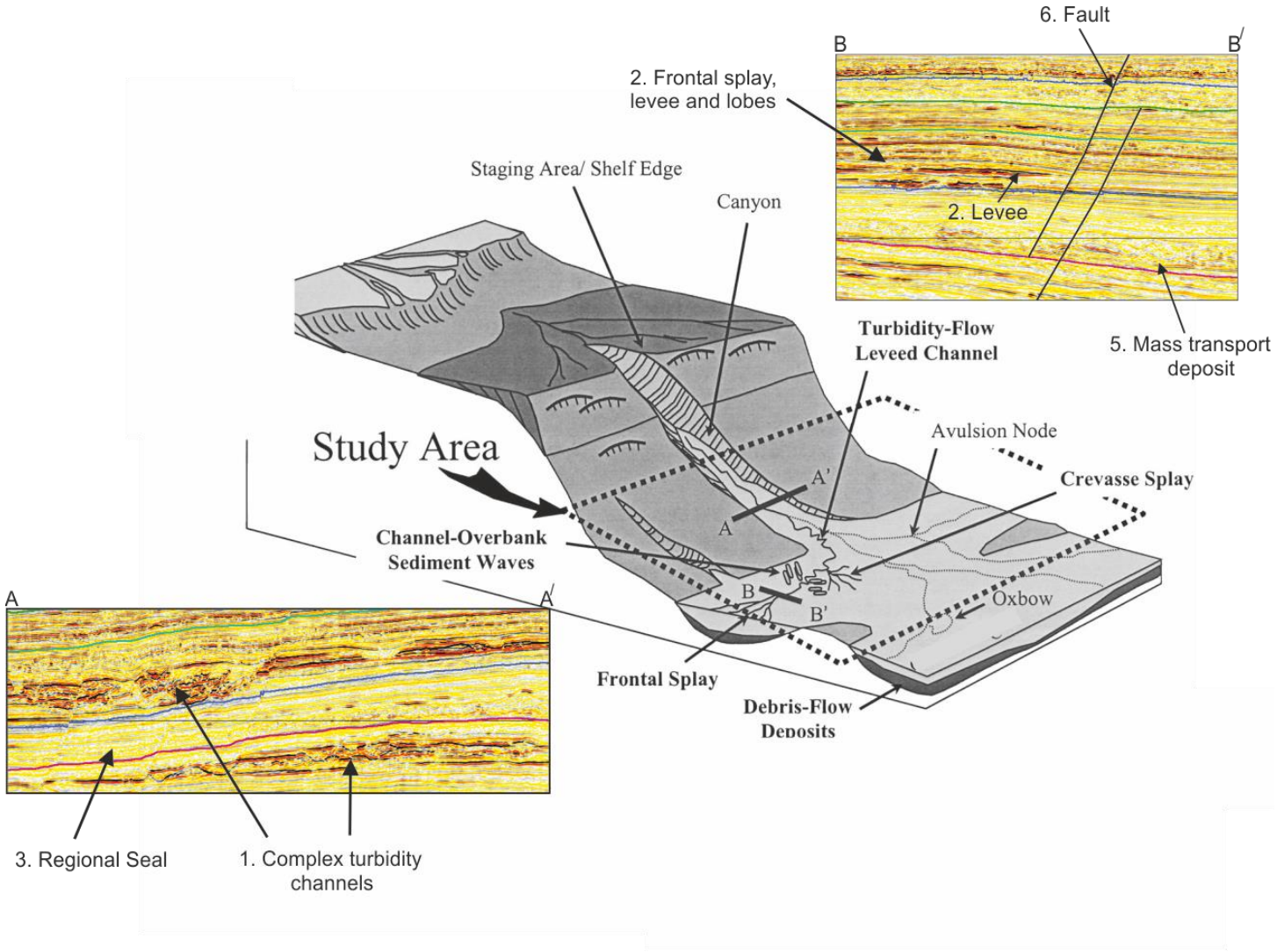

Figure 4.4: Schematic depiction of principal depositional elements of a deep continental margin with examples from the study area (Modified from Posamentier and Kolla, 2003)

4.3.3 Source Rock

Hydrocarbons have been found in onshore and offshore of the Lower Congo Basin (LCB). The best-understood hydrocarbon occurrences in the province are in the Tertiary reservoirs associated with sand distributed by turbidity flows (Brownfield and Charpentier, 2006; Andresen *et al.*, 2011). There are two types of sources rock in the LCB; the Cretaceous and Tertiary source rocks.

The main source rocks are in the Lower Cretaceous bituminous shales of Bucomazi Formation which were deposited during the syn-rift phase. This lacustrine source rocks comprise shales and marls, and are *c.* 1,500 m thick (Cole *et al.*, 2000). The Bucomazi Formation consists of clastic sediments with a high total organic content (TOC) and hydrogen index (HI), mostly oil prone type I Kerogen of >5% to maximum of 20% TOC (Brice *et al.*, 1982; Schoellkopf and Patterson, 2000) On the other hand, the Palaeocene to Eocene Landana Formation is considered as a second source rock. The Formation consists of deep-water shales with a TOC of 3-to-5%, similar to those of the Iabe Formation. The mid-Oligocene to Miocene Malembo Formation generally has TOC contents of 1-2%; the lower and upper parts of the Formation contain from 2-5% of TOC in the form of Type II and Type II/III kerogens mostly considered as oil-gas prone (Schoellkopf and Patterson, 2000).

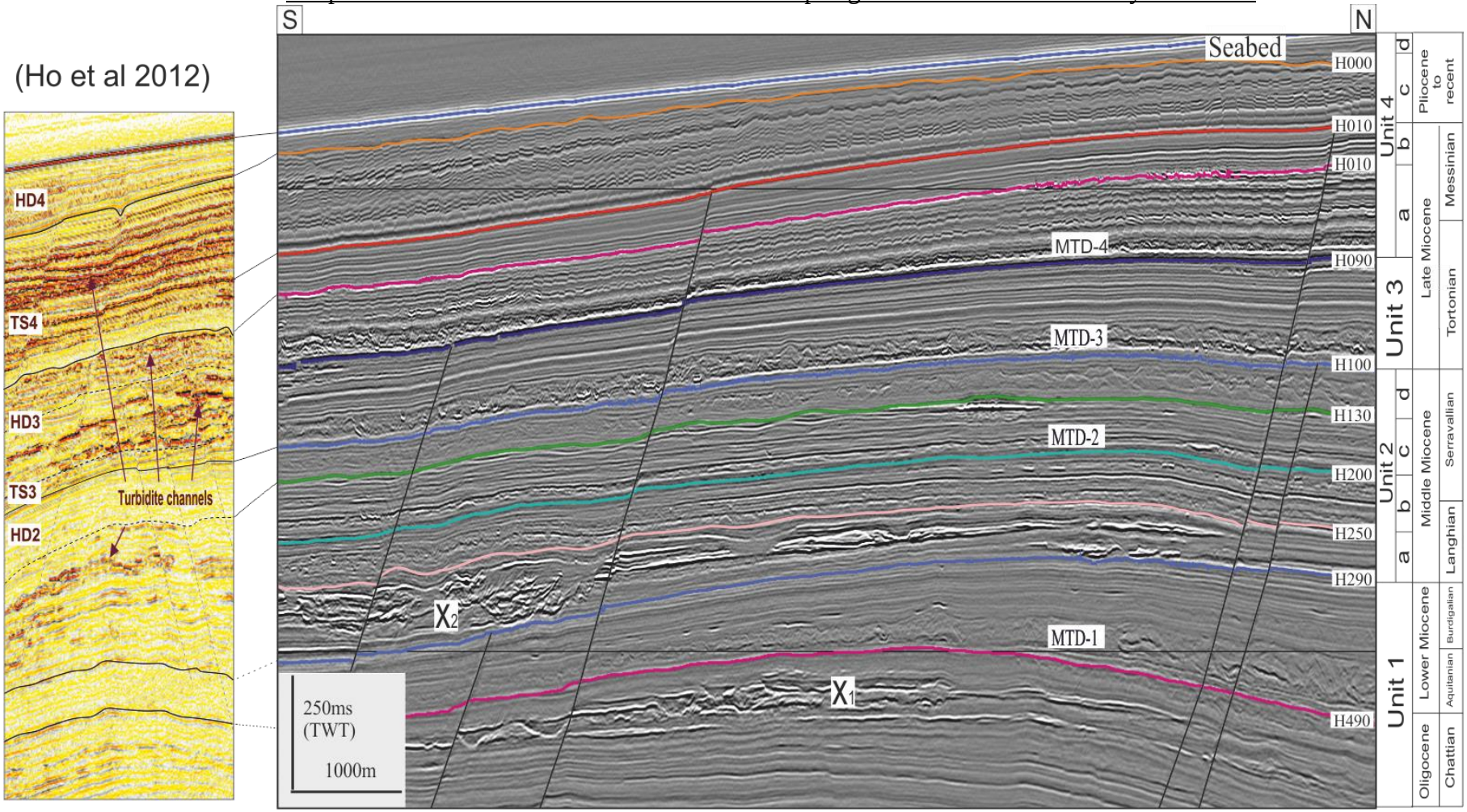

Figure 4.5: N-S Seismic profile showing main stratigraphic subdivision of the study area and the main interval of interest i.e. the Waste zone between horizons H130 to H250, 1 to 4 are the regional seal units (modified from Broucke et al., 2004), TS: Turbiditic sequence; HD: Hemipelagic sequence, and MTD: Mass transport deposit.X1: Oligocene Turbidite channel, X2: Miocene turbidite channel.

Table 4.1: Seismic stratigraphy of the study area with detailed geological and seismic features.

Unit		Age		Horizon	Geological Features	Seismic observation	Lithology	Average Thickness (m)
4	d	Pliocene to recent		Seabed	Burrows, pock marks	No HAAs	Shales dark and green in colour, sometimes laminated beds, loose sediments	85
	c			H000	Tier-2 polygonal fault system	High amplitude anomalies, PFS	Very fine, mud rich sediments	100
	b	Upper Miocene	Messinian	H010	Transparent and continues laminated beds	No HAAs	Claystone interbedded with siltstone	146
	a			H045	Tier-1 polygonal fault system, pock marks, small scale channels. MTD at base.	HAAs but not in MTD-5	Claystone interbedded with siltstone	218
3			Tortonian	H090	Transparent and continues laminated beds. MTD at base.	Few HAAs observed in MTD-3	claystone/fine-grained sand stone beds interbedded	200
2	d	Middle Miocene	Serravallian	H100	Transparent and continues laminated beds. MTD at base.	No HAAs	Claystone, interbedded with siltstone	125
	c			H130	Mud waves. MTD at base.	HAAs along faults and stratigraphic traps	Claystone olive grey to greenish colour, slightly silty and calcareous	150
	b			H200	Complex turbidite channels	HAAs in Channel levees	Claystone brown in colour. More silty to very fine sand, strings of siltstone. Turbidite channels	220
	a		Langhian	H250	Complex turbidite channels	HAAs in sand with turbidite system	Sand, fine to medium, bad to moderated sand in turbidite and claystone in the back ground	165
1		Lower Miocene		H290	Transparent and continues laminated beds. MTD at base	Hard reflections and HAAs along the faults	Claystone interbedded with siltstone	500
		Late Oligocene		H490				

4.3.4 Seismic stratigraphy of the study area

A generalized stratigraphic column produced by the operator for the study area is shown in (Fig. 4.5). The seismic interval is subdivided into several units (Table 4.1) based on the occurrence of two different seismic signatures: (1) moderate amplitude, parallel, continuous reflections interpreted as hemipelagic deposits as interpreted by Ho et al (2012) and Broucke et al 2004 in the data from same basin (HD3, 2); and (2) high amplitude, low continuity packages encased in low-amplitude intervals interpreted as turbidite systems (TS4, 3) (Fig. 4.3 and 4.5) (Ho et al., 2012; Broucke et al., 2004). In accordance with the 3D seismic data cube and stratigraphic column, 10 seismic horizons have been identified that separate packages with hemipelagite deposits and turbidite systems. The hemipelagite deposits are composed of four transparent and continuously mapable intervals and are interpreted as regional seal units by the operator and similarly by Ho et al, 2012 and Broucke et al., 2004 (Fig. 4.3 and 4.5). These seal units are between the seabed and seismic horizon H000, Horizon H090 to H100, Horizon H100 to H130 and Horizon H290 to H490. The detailed lithostratigraphy for the Neogene is based on Vignau et al. (2000). The studied interval is subdivided as follows (Fig. 4.5) and all the ages are corrected through calibrating with following the confidential well data and Gradstein et al (2005).

4.3.4.1 Unit 1

This unit is an approximately 500ms TWT-thick interval of hemipelagite and turbidite deposits (H490 to H290) of Late Oligocene to Lower Miocene age (28.1-15.97Ma). The interval is composed of claystone and well bedded fine-grained sandstone (confidential well reports).

4.3.4.2 Unit 2

The Middle Miocene (15 Ma– 11.008 Ma) comprises the unit between H290 to H100, and is subdivided into four sub-units, very continuous clay-rich sediments,. There are two seismically-prominent mass transport deposits. Lithological description of the interval took from confidential well reports.

The scope of research comprises in the following studied intervals from base of regional seal unit 4 (H490) to the overlying strata at the base of regional seal unit 3 (H130) (Fig. 4.3). The interval H130 to H250 is termed as "Waste Zone" (Fig. 4.5). A waste zone in this chapter is defined as the zone that contains high amplitudes which are possibly related to hydrocarbon but not up to commercial discovery. The detailed stratigraphy of these subunits is as follows;

a. This sub interval is between seismic horizons H130 to H100 of approximately 150ms TWT thick sediments. The top of this unit is composed of transparent and continues seismic reflection and mass transport deposit at its base and interpreted as a regional seal 3 (Fig. 4.3).
b. The stratigraphy of the waste zone (H200 to H130) is composed of greenish to grey clay stone have some glauconitic, specks of pyrites, traces of forams and some sand lenses of sub-round to sub-angular grain size, loose sand lenses are cemented with silica.
c. The interval between seismic horizons H250 to H200 has four different storeys of channel levee complex of turbidite composed of alternativing less than one meter to ten of meters thick beds of sands of brown to dark brown in colour. The channel levee complexes are greenish claystone to silty sandy very sine sediments with beds of well sorted sand of medium fine grain size with sand lenses.

d. The stratigraphy of this unit (H290 to H250) is composed of turbidite channel levee complexes of lower Miocene age. Mainly clay stone to sand stone alternative beds. The claystone beds are of greenish colour with siltstone grain size from fine to medium. The sand beds are composed of colourless sand, sub-rounded to angular with some shaly lens.

4.3.4.3 Unit 3

This unit (H100-H090) is comprised of transparent and continues seismic reflections with continues lamination of different sedimentary layers. Lithology of these layers is claystone/fine-grained sand stone beds interbedded. Mass transport (MTD-3) deposit is observed at the base of this interval of late Miocene age (11.63 to 7.25 Ma).

4.3.4.4 Unit 4

Seismic horizon H090 to seabed has been assigned an age from Lower Miocene to recent (7.25Ma– 0Ma); comprises of hemipelagic sequence and turbidite system. This unit is further divided into four sub units (Fig. 4.5) on the bases of continuous seismic reflection. Two polygonal sub-units have also been observed in the study interval and reported by Ho et al., (2012), Gee et al., 2006, Gay et al., 2006. The unit (H000-Seabed [U4d]) overlying the polygonal fault tier (H010-H000 [U4c]) contains continuous internal reflections with low-to-moderate acoustic amplitudes. The interval U4d has been reported to comprise hemipelagite (Vignau et al., 2000) until the base of the unit which occurs at the top of a polygonal fault tier-1 as defined by Ho et al., (2012), Andresen et al., (2010), Gay et al., (2006) and Cartwright and Dewhurst, (1998). The base of polygonal fault tier-1 is observed at the seismic horizon H010 (U4b) at approximately 200ms TWT below the seafloor. The unit U4b

underlying the polygonal fault tier contains continuous internal reflections with low-to-moderate acoustic amplitudes. Another polygonal fault tier- interpreted between seismic horizons H090 and H045 approximately 500ms TWT below seabed.

In figure 4.5, the Tertiary fan sediments are characterised by discontinuous and continuous high amplitude reflections, complex geometries, with numerous terminations and lateral discontinuity in the channel levee complexes which suggests the deposition and erosion of turbidite deposits. The high amplitude anomalies within these different storeys of channel levee complexes are possibly due to the presence of hydrocarbon (confirmed from confidential well reports).

Abrupt changes in channel geometry are often observed as channels enter slope depressions flanking salt intrusions. Channels approaching salt diapirs are observed to rapidly broaden and thicken, often forming distinctively-shaped structures in planview. These broad, depositional systems are characterised by high seismic amplitudes and relatively high sand contents. They form a recently and poorly defined slope reservoirs class described as a weakly confined channels. Transitions between the two types of channel style are often characterised by weaker seismic amplitudes and steeper channel gradients which indicate erosional flow behaviour typical of hydraulic jumps (Gee et al, 2006).

4.3.5 Seismic acquisition artefacts

The vertical stripes on the seabed two-way time map in the inline direction are interpreted as seismic acquisition footprints (Fig. 4.6) which mimick the acquisition track. Footprints are commonly seen as amplitude stripes in time slices produced from a seismic data volume (Marfurt et al., 1995, 1998). Vertical stripes are normally removed during the processing of seismic data through different filtering techniques e.g. time-slice enhancement using dip filtering in FK domain, and median filtering of amplitudes from slices (Vishnoi et al, 2012).

There is evidence of fluid flow manifested on the seabed from few meters-to-few kilometres wide and comprise pockmarks, seep mounds, acoustic flares (Judd and Hovland, 2007), mounded structures (Anka et al., 2012), gas chimneys and seismic pipes (Cartwright et al., 2007; Løseth et al., 2009). Figure 4.7 illustrates a few pock marks on the seabed whilst Fig. 4.7A and 4.7B shows a close relationship of these pockmarks with deep-seated reservoirs of Miocene turbidite channels and a bottom simulating reflector (BSR) (Ho *et al.*, 2012).

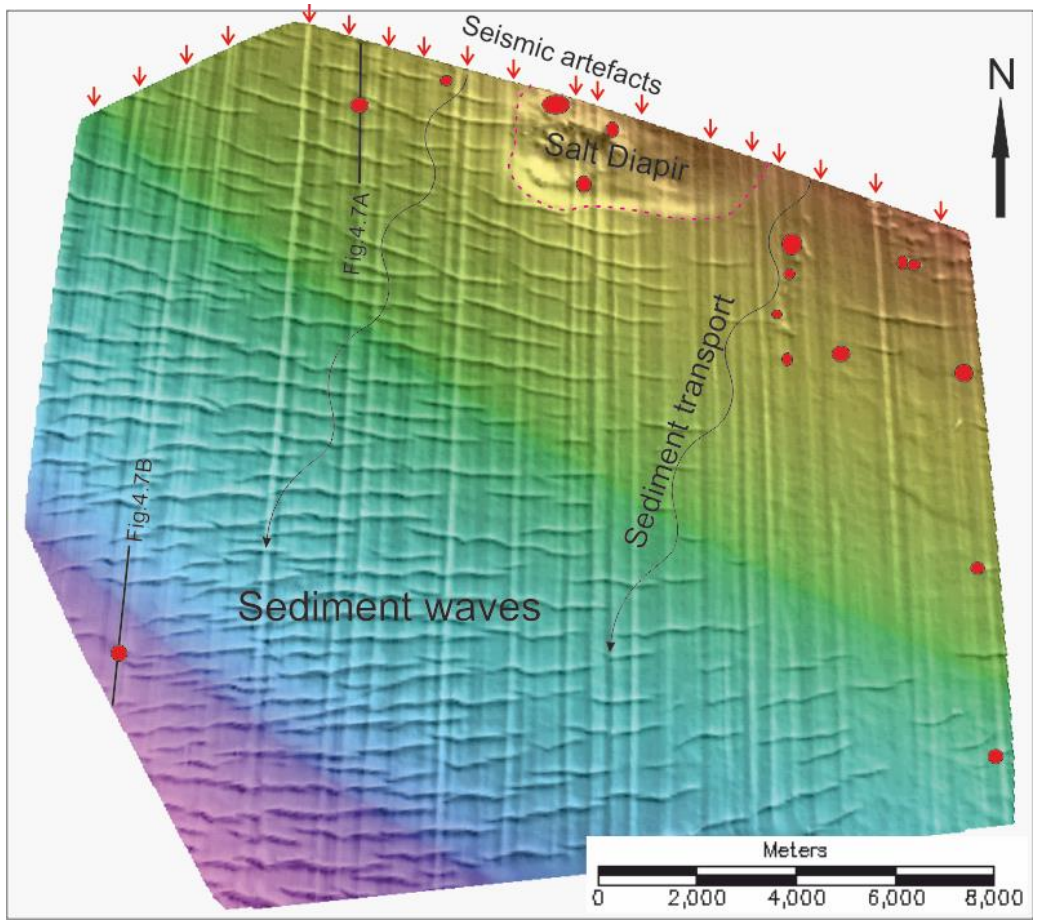

Figure 4.6: Seabed time structure map overlain with time derivated dip map with main geological elements such as sediment waves, pockmarks and salt diapirs. Seabed pockmarks are mostly rounded have direct or indirect relationship with deepseated reservoirs or hydrocarbon related high amplitude anomalies. The sediment transport direction (Slope direction) is NNE-SSW. Almost E-W furrows are sediment waves perpendicular to the slope direction. Blue dotted line shows extent of salt diapir. The red arrows at top of the map indicated seismic acquisition footprints, Red dot are pockmarks.

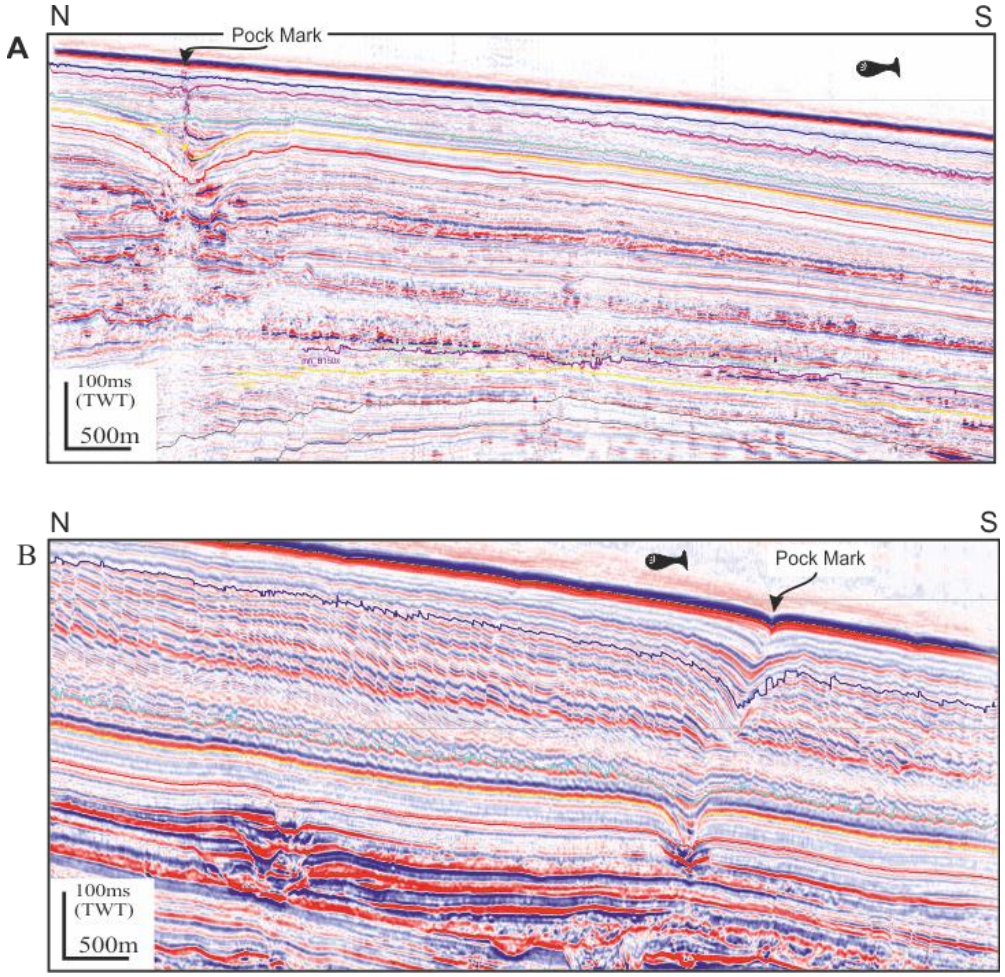

Figure 4.7: Seismic profile showing current seabed pockmarks (A, B).For location Fig. 4.6

Sixteen pockmarks were interpreted at the present day seabed (Fig. 4.6). These pockmarks are typically isolated but are aligned in a NE oriented trail. All these pock marks are originated at different sedimentary levels, interpreted as positive high amplitude anomalies. Two seismic profiles passing through isolated pockmarks that originated from channel and high amplitude anomaly respectively (Fig. 4.7A and Fig.4.7B). The detailed interpretation about formation and development of these pockmarks is beyond the scope of my research but the presence of these pockmarks leads to draw a conclusion that the fluid flow is still active in the study area and these faults developed due to high pressure in the study interval (Gay et al, 2006).

Shallow marine ocean bottom currents are observed and reported in many basins world widely (Stoker et al., 2005.). These current mostly influences both sediment deposition and erosion on continental margins and also in deep ocean basins (Gee and Gawthorpe, 2006b). The effects of these contour varies from geostrophic currents, slope dips and particularly marked on slopes and basin plains within and adjacent to continental margins, where a variable sea-floor bathymetry may locally intensify and focus current activity. Sediment drifts are anomalous, sediment bodies that commonly form positive features on the seabed and typically accumulate in areas swept by bottom currents and where there is a change in gradient of the sea bed, such as at the base of continental slopes. These types of ocean bottom currents are observed at the current seabed (Fig. 4.6) and paleo seabed (Fig. 4.14) at the deep margins from 500 to 1500 meter water depth.

4.3.6 Structural setting of the area

The study area can be divided into structural domains associated with features such as salt diapirs, structural anticline, pockmarks, chimney, turbidite channels and mass transport deposits (Ho et al., 2012, Anderson et al., 2010; Gay et at., 2004; Charlou et al., 2004). Oluboyo et al (2013) described three major structural domains of Lower Congo Basin (1) dominated by normal faults, (2) containing predominantly isolated salt diapirs and normal faults and (3) dominated by series of linear NEE-SSW trending elongate salt walls. The study area straddles the post-salt structural domain boundary separating up-dip extension and mid slope translational features (Ho et al., 2012).

The extension/translation domain boundary is defined by the downslope transition from the most distal of a series of NW-SE striking and seaward dipping roller faults and down built salt stocks and walls (Broucke et al., 2004; Andresen et al., 2000).

4.3.6.1 Polygonal Faults

Over large areas of the Lower Congo Basin, mud-dominated upper Miocene to lower Quaternary sequences, 700m (+-50m) thick, are affected by closely spaced small extensional faults displaying a polygonal pattern in planview (Ho et al., 2012 and Gay et al., 2006 and 2007). Two tiers of polygonal faults are observed in Unit 4 of study area that consist of small scaled normal faults with throws from 5 to 20m and small spacing of 100 to 500m (Gay et al., 2006). The presence of polygonal fault systems seems to be controlled by the fine grained nature of the faulted sediments and their mineralogy; in particular a high smectite content is considered to play an important role in the development of such structures (Dewhurst et al., 1999, Cartwright et al., 2011 and Cartwright 2007).The faults are often arranged in

stratigraphycally bound layers characterized by a distinct spacing between faults (Lonergan et al., 1998), which could be due to different lithologies within the layers (Dewhurst et al., 1999).

4.3.6.2 Fault Patterns

Faults are the main possible conduits for fluid flow in many sedimentary basins worldwide especially in the deeper subsurface where more lithified rocks are present (Ligtenberg, 2005). To understand the relation of faults and possibly related fluid flow expressions in the term of high amplitude anomalies, I reviewed all the faults in the study area, and based on our result, I have recognised three distinct types of fault system:

1. Tectonic faults related to salt tectonics e.g. crestal collapse fault above salt anticlines and synclinal fault within withdrawal basins.
2. Polygonal faults organised into two distinct tiers (beyond the scope of research).
3. Radial faults arranged around salt diapir in the northern part of the study area (beyond the scope of research).

The tectonic faults are grouped into four sets: (a) Group 1, NNW oriented faults located in north eastern portion of the study area (b) Group 2, NE oriented faults oriented normal to group 1 faults (c) Group 3, NW oriented faults that are isolated set of faults and (d) Group 4, WNW oriented faults merging with radial faults near salt diapirs. The four sets are illustrated with reference to a coherence slice (amplitude extraction of the coherence volume) at the H290 horizon (Fig. 4.8). The faults that belong to group 1 and 4 have curving plan form trajectory and coincide with radial faults near salt diapir. They are all normal faults with throws ranging from a few metres to c. 50m.

The relationship between the four tectonic fault sets and the salt-related folds in the study area will be discussed in the next Chapter 5. The trends of the fault sets have a strong correlation between the main fold axes and flanks. However, the growth histories of the various folds have not been established because of the limited coverage of the survey, and the link between the timing of the faults and the development of structural relief of the folds has not been undertaken yet.

The radial faults are regarded as a separate fault set because they have markedly contrasting characteristics to the tectonic faults. They are notable for displaying a curving planform trajectory, with intersection against the salt body in a near-orthogonal intersection (Fig 4.8). They have very low throw to length ratios (0.004-0.005), maximum throws 10-15m and were active during the Plio-Pleistocene.

The H290 coherence time slice illustrates the orthogonal intersection of the radial faults and the salt margin. The radial faults define the local $\sigma 2$ direction and there is clearly a zone of interaction some 3km away from the salt margin. The arrows indicate the position of onset of curvature on tectonic faults that have been bent by the zone of influence of the salt structure.

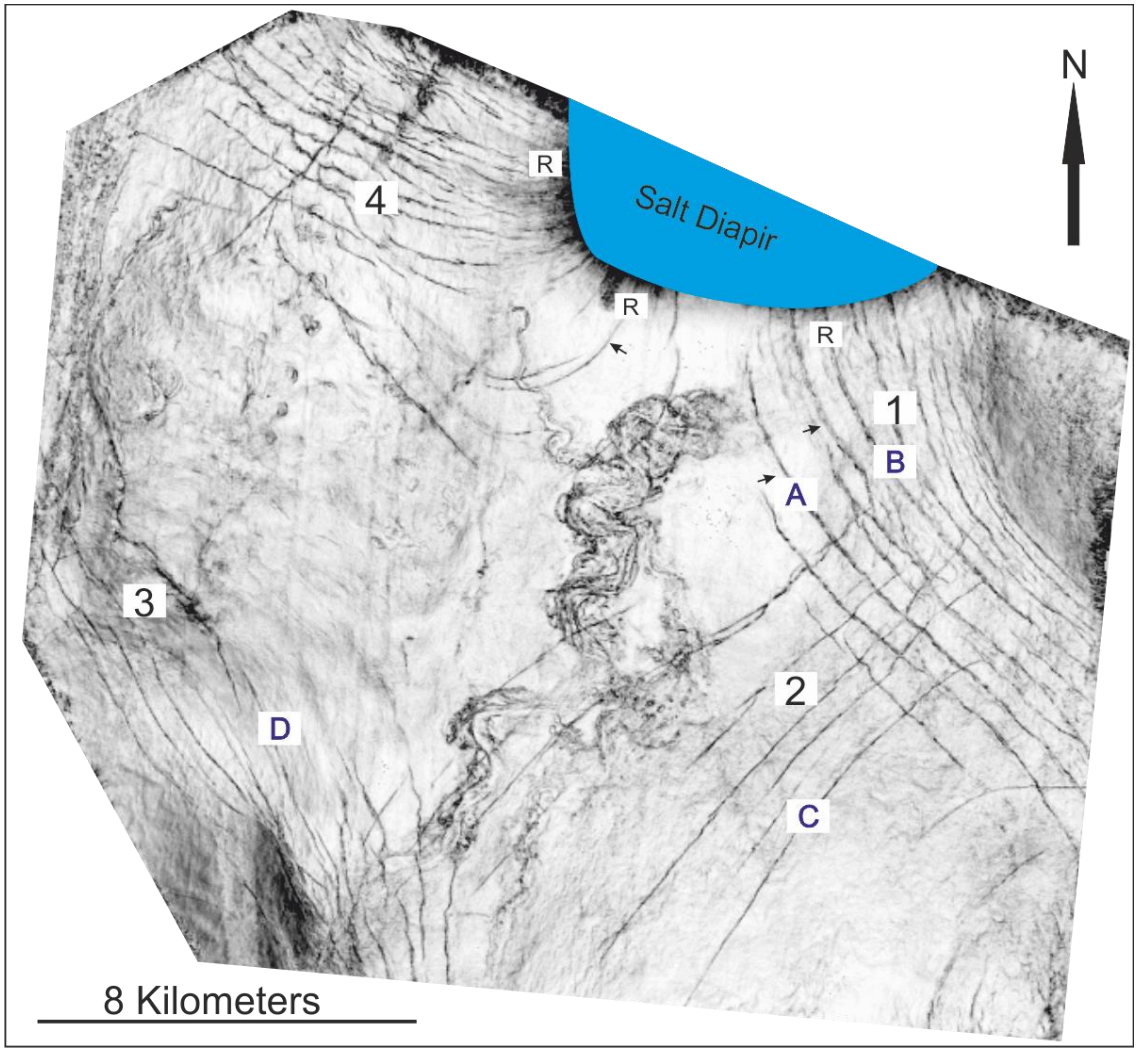

Continue at next page

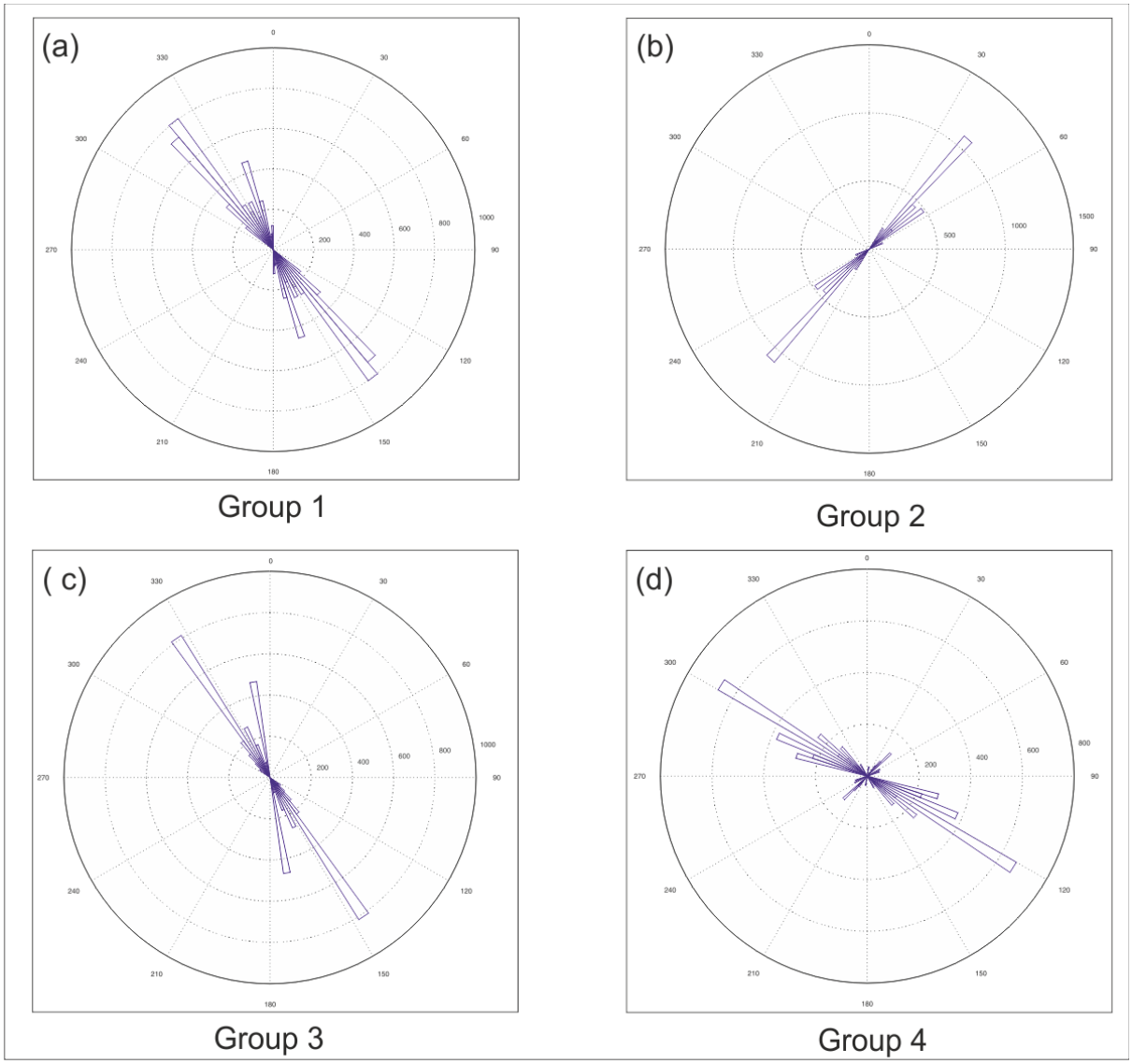

Figure 4.8: Dip map of top of regional seal unit 4 (H290) showing different local and regional (Tectonic) faults in the study area. Four types of normal faults are interpreted on the basis of their orientation and associated feature (salt diapir) indicated by numbers 1-4. (1) NW-SE fault, (2) SW-NE fault, (3) NNW-SSE fault and (4) WNW-ESE fault. Lower Miocene channels are affected by type 1 faults. The small arrows indicate curvilinear nature of fault types 1 and 4 that merging with radial faults developed due to salt activity. R= Radial faults.

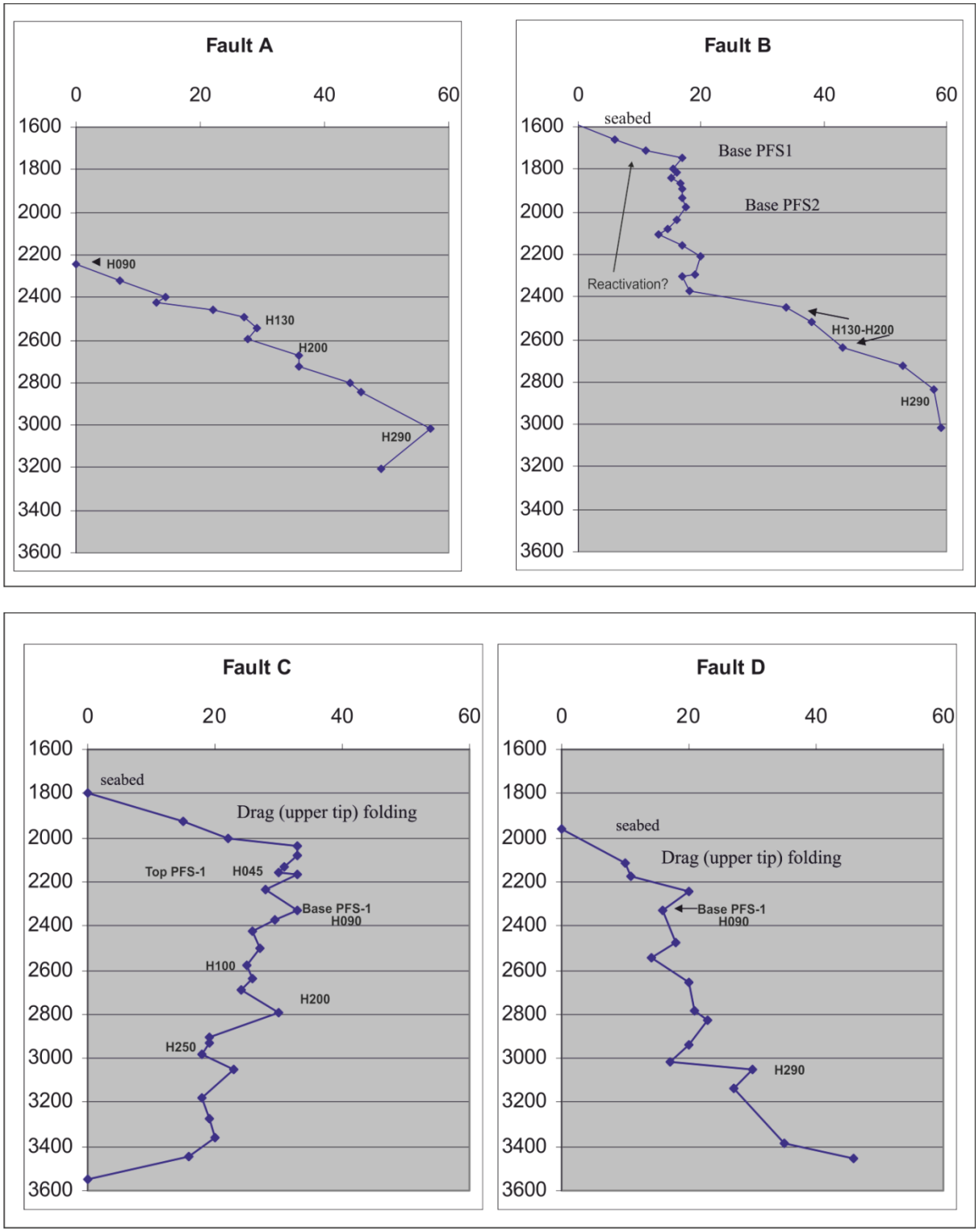

Figure 4.9: Throw-depth (T-Z) plots for representative faults from the three groups defined. The position of the faults is marked as A, B , C and D in Fig. 4.8.

4.4 Well calibration

High amplitude anomalies are identified and mapped in different layers of Unit 2 and particularly in the waste zone [(H130 to H290) Fig. 4.10]. Calibration of these mapped high amplitude anomalies with the available well data is performed.

Due to limited seismic data and relative distribution of seismic high amplitude anomalies with their fluid flow features, high amplitude anomalies are generally avoided during well planning due to risk hazards (Andresen, 2012; Cartwright, 2007). Six exploration wells drilled in the study area; however, only three of the wells were made available for this study. Only one well name W41 out of these three well, penetrates through seismic high amplitude anomaly.

High amplitude anomaly in seismic interval U2b (seismic horizon H200) related to channel levee complex (CLC) is calibrated with exploratory well W-41 as an interval of 2-3m fine sand/silts, thin bedded, with gas shows (Fig. 4.10A). W-71 shows no obvious levee facies, but the erratic Gamma ray (GR) may indicate thin beds of silt/fine sand, generally below GR resolution. We have not conducted a detailed petrophysical analysis of the channel levee complex interval, and this calibration is based on operator well reports. The levees clearly extend for >1km from the channel and the seismic facies suggests that there are local thickness and facies variations within the levee, as might be expected (Gee et al., 2006).

A zoomed-in section (Fig. 4.10B) of the calibration at the W41-1 well shows the clay-dominated interval in which the levee occurs. The levee facies is represented by two GR

spikes, and these probably match the soft reflection. However, a shift of 10ms due to stretching errors on well depth-to-time conversion will exactly match with seismic data (Fig. 4.10B). The synthetic trace is too low frequency to give a good match to real seismic traces. The uppermost reservoir is seen as striking blocky sand just beneath the seismic horizon H200.

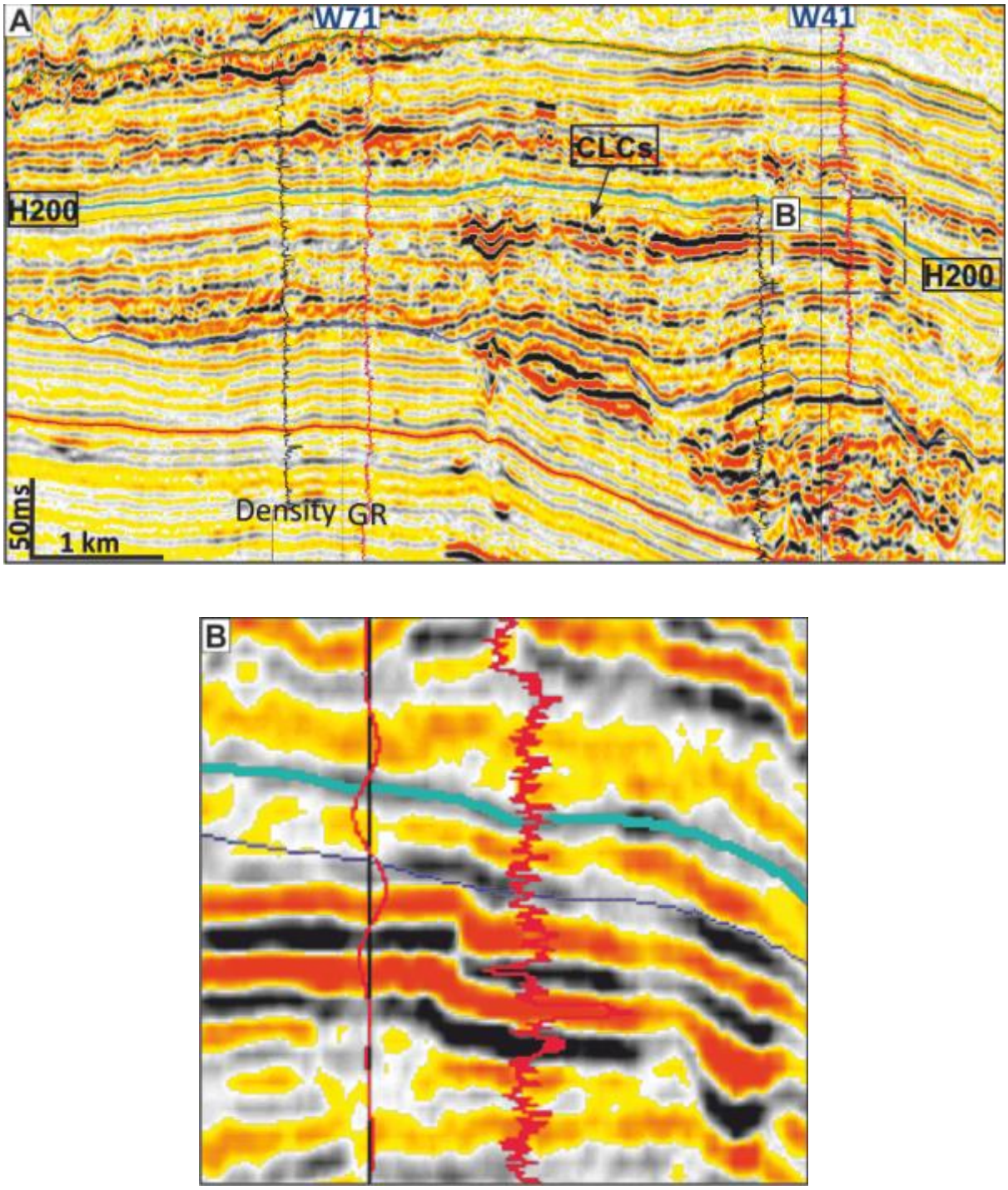

Figure 4.10: (A) High amplitude anomaly calibrated with well W41 showing the clay-dominated interval in which the levee occurs. (B) The levee facies is represented by two GR spikes, and these probably match the soft reflection, with a shift of 10ms (due to stretching errors on well depth-to-time conversion). The synthetic trace is too low frequency to give a good match to real seismic traces. See Fig. 4.14 for location of seismic profile

4.5 Classification of high amplitude anomalies

Detailed mapping indicates a pronounced concentration of high amplitude anomalies in the waste zone (Fig. 4.5) and seismic interval between H130 to H250. The high amplitude anomalies are widely distributed in six depositional elements in the study area (see section 4.3.2 Local setting for more detail). HAAs are developed above the main accumulations in Oligocene-Miocene turbidite channel complexes. There are many examples of HAAs illustrating the different local structural and stratigraphic contexts. Many of them are located on crest of an anticline but there are a significant number associated with levees that do not conform exactly to structure. Many HAAs are associated with large faults (Fig. 4.8).

High amplitude anomalies are classified on the basis of their plan form geometry, extent, morphology and seismic characteristics. Therefore, HAAs have been grouped into four different types:

1. Linear anomalies
2. Sub-Circular anomalies
3. Patchy anomalies
4. Discrete filamental anomalies

The nomenclatures of the high amplitude anomalies are representing the type of anomaly, stratigraphic unit and number of anomaly in that interval. For example P1b where *P* indicates for patchy anomalies, *1* represent the interval and *b* is anomaly.

4.5.1 Linear high amplitude anomalies

Linear, high amplitude anomalies are defined as isolated, long, and narrow features on amplitude maps (Fig. 4.11). They have aspect ratios (max. length: max. width) of > 6, are ten(s) to hundreds of meters long and less than 30 m wide. Linear anomalies are associated

with faults, along the turbidite channel, lithological barrier. These types of anomalies are occurring in the northwest to western part of the study area (Fig. 4.16). L2d and L2f linear anomalies were interpreted beneath seismic horizon H200 (Fig. 4.11) and are acoustically soft anomalies.

4.5.2 Sub-Circular high amplitude anomalies

Sub-circular high amplitude anomalies can be regular or irregular, near circular or elliptical in planform. They can be morphologically flat but most of the time they are associated with near-circular depressions. A representative example of sub-circular amplitude anomalies (C2a anomaly) is presented in figure 4.12. This amplitude anomaly is located at the top of horizon H200.

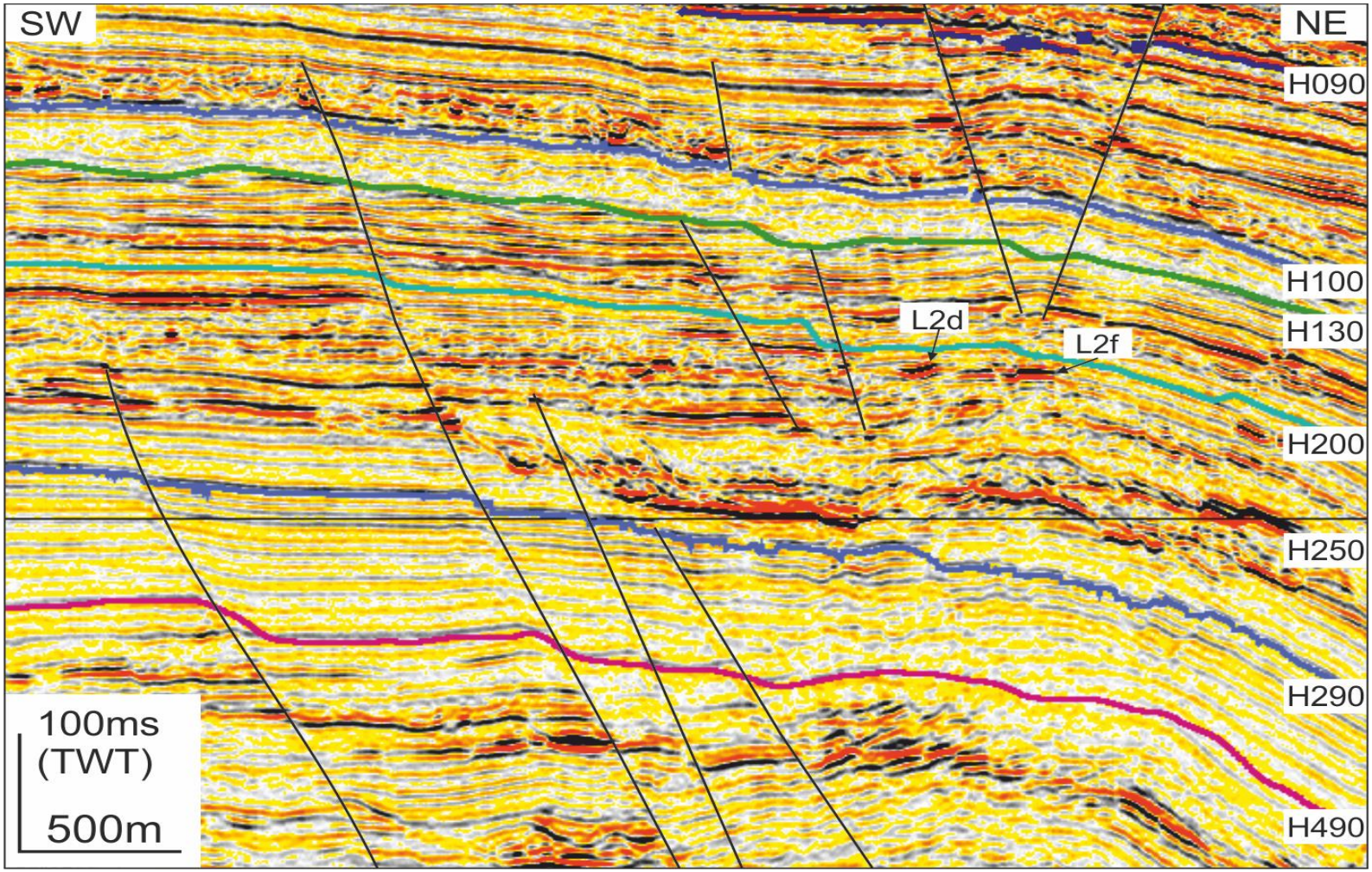

Figure 4.11: NE-SW oriented seismic profile showing example of linear anomalies. These anomalies are soft HAAs. See Fig. 4.16 for location of seismic profile

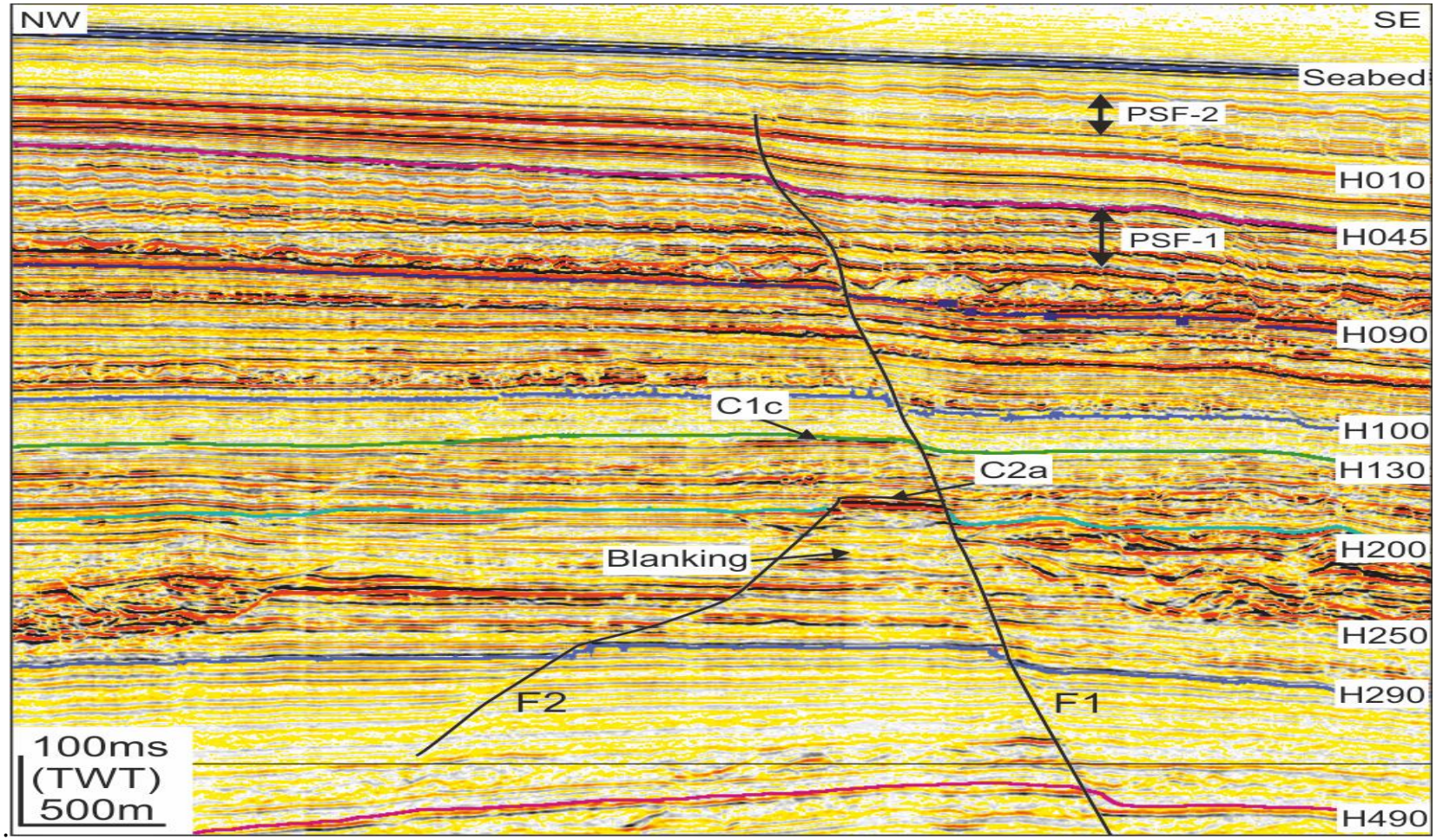

Figure 4.12: Example of sub-circular high-amplitude anomalies identified in the waste zone. The seismic profile shows C2a anomaly developed along faults F1 and F2. F1 fault cut through the waste zone and merged at the base of polygonal fault system tier-2. See Fig. 4.14 for location of seismic profile

4.5.3 Patchy anomalies

Patchy high-amplitude anomalies are defined here as anomalies which are isolated, irregularly shaped, patchy, and with rough geometry on map view. Twenty-two patchy anomalies are identified in the waste zone but they are more prominent in the interval between U2d and U2c (Table 4.1). The planform geometry of patchy anomalies is not symmetric, detailed observations showed finger like features that emerges from the main anomaly e.g. P1a and P2a (Fig. 4.14 and Fig. 4.16). In addition the patchy anomalies are associated with incised turbidite channel levee complex systems. Furthermore, the Patchy anomalies vary from a few tens of meters to hundreds of meter in length and with diameter from hundred meters up to two kilometres. Patchy anomalies are often limited to structural highs, regional faults and the Oligocene and Miocene turbidite channel levee systems (Fig. 4.8).

4.5.4 Discrete filamental anomalies

Discrete filamental anomalies are positive high amplitude anomalies observed at the northwest side of regional seal unit 4 (Fig. 4.3). On RMS amplitude maps, they sub-circular anomalies linked by curvi-linear lower amplitude anomalies. The pattern is clustered in two groups, curvi-linear and patchy. The curvi-linear anomalies are emergent from patchy anomalies or originated from patchy anomalies. These anomalies do not follow any fault trend (Fig. 4.13). Rather, they cluster on N-S trend, suggesting a close spatial relationship between the anomaly forming process and the stratigraphic heterogeneities. The suggestion here is that fluid ascent to the interval may have been through a network of porous bodies.

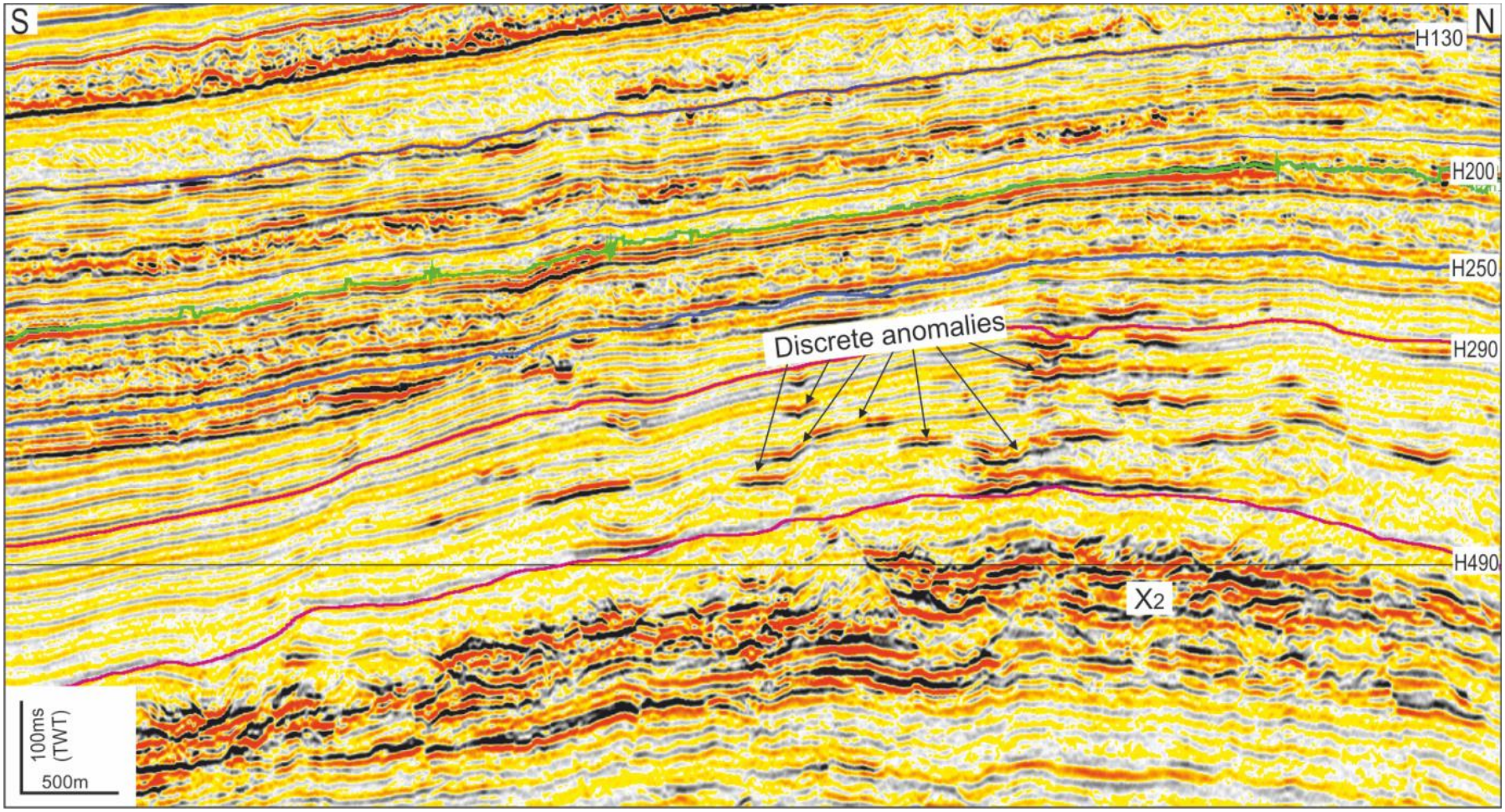

Figure 4.13: N-S seismic line across filamental anomalies shows positive paired seismic reflection. The anomalies are cuspate or conical and scattered. Anomalies are developed at the crest of anticline and above Oligocene channel levee systems (X_2). The smallest anomalies are the filaments, and the larger anomalies are the sub-circular anomalies. See Fig. 4.21 for location of seismic profile

4.6 Root Mean Square (RMS) amplitude maps

Root-Mean-Square seismic attribute maps are computed in order to visualise the stratigraphic features associated the anomalies. The RMS maps were computed for interval such as H130-H200, H200-H250, H250-H290 and H290-H490. High amplitude anomalies are typically manifested as subtle variations in amplitude strength, phase shift, or polarity reversal and are easily overlooked (for more detail see chapter 3).Interpretation of these RMS amplitude maps provided additional information on the spatial distribution and depositional pattern of the anomalies. For example, the sinuous geometry of some of the anomalies can only be visualised in time/horizontal slices rather than vertical seismic sections

4.6.1 HAAs in H130-H200

Anomalies in this interval include disseminated and patchy anomalies. The patchy anomalies include circular (P1a and P1b), elongate/tabular (P1f and P1g) and concave-shaped anomalies (P1c). The average perpendicular distances between the anomalies are c. 6 km, c. 22 km and c. 4 km between P1a and P1b, P1f and P1g, and P1d and P1f.

The patchy anomalies are restricted to the interval to the east of the map (H130–H200) and are associated with NNE-SSW oriented channels and individual faults of NW-SE strike (type 1) and NE-SW strike (Type 2) (Fig. 4.8). On the contrary, disseminated anomalies at the west side of the map are sandwiched within the Mass-transport deposits units where they are randomly distributed. These anomalies are interpreted as being in coarse units associated with remobilised and slumps of channel levee deposits. An obvious N-S clustering of the anomalies is observed closest to the MTD boundary.

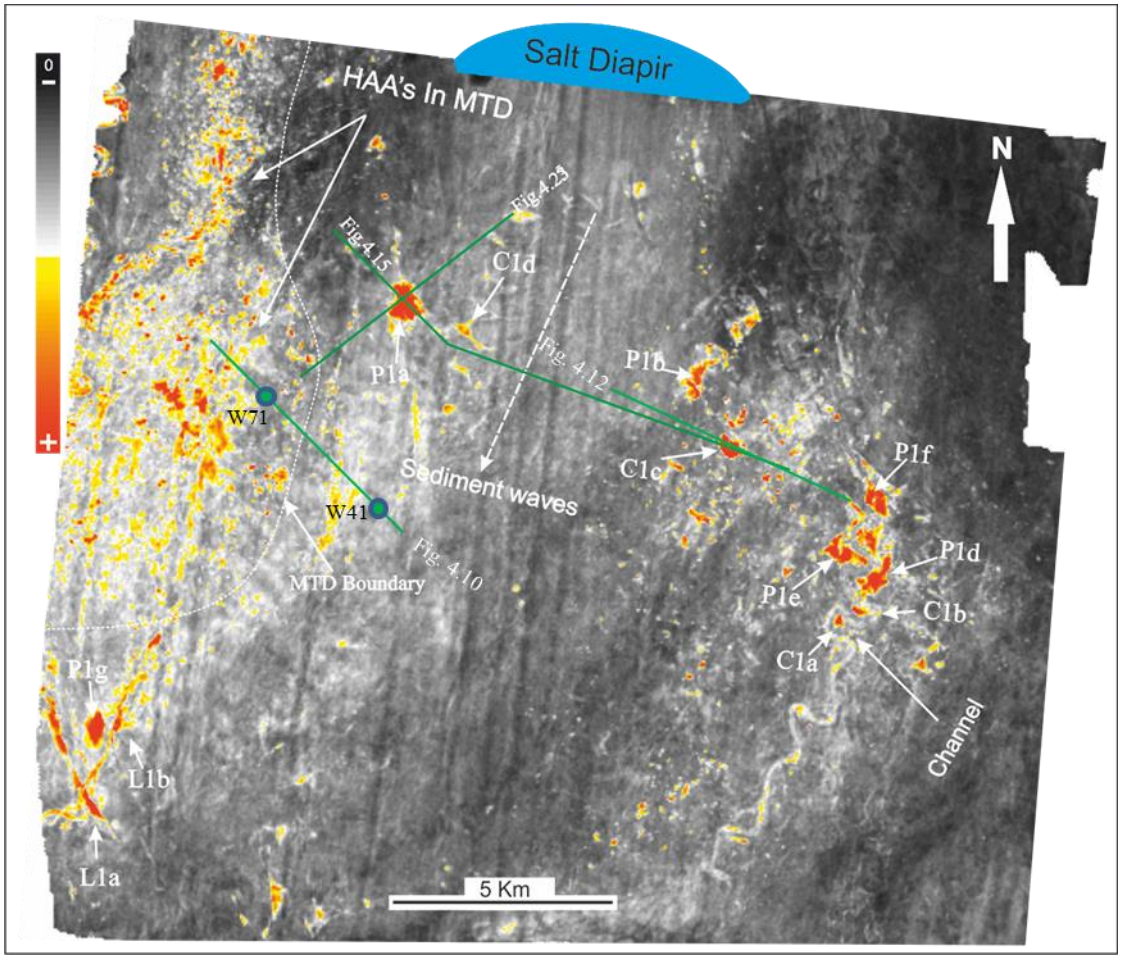

Figure 4.14: RMS amplitude extraction map in the waste zone below regional seal unit 3 below H200-H130 interval. Low amplitude values are in black and high-amplitude values are from yellow to red. Patchy, linear and sub-circular amplitude anomalies are developed in this interval. Location of high-amplitude anomalies is marked as P1a, L1a and C1a for patchy, linear and curve anomalies respectively.

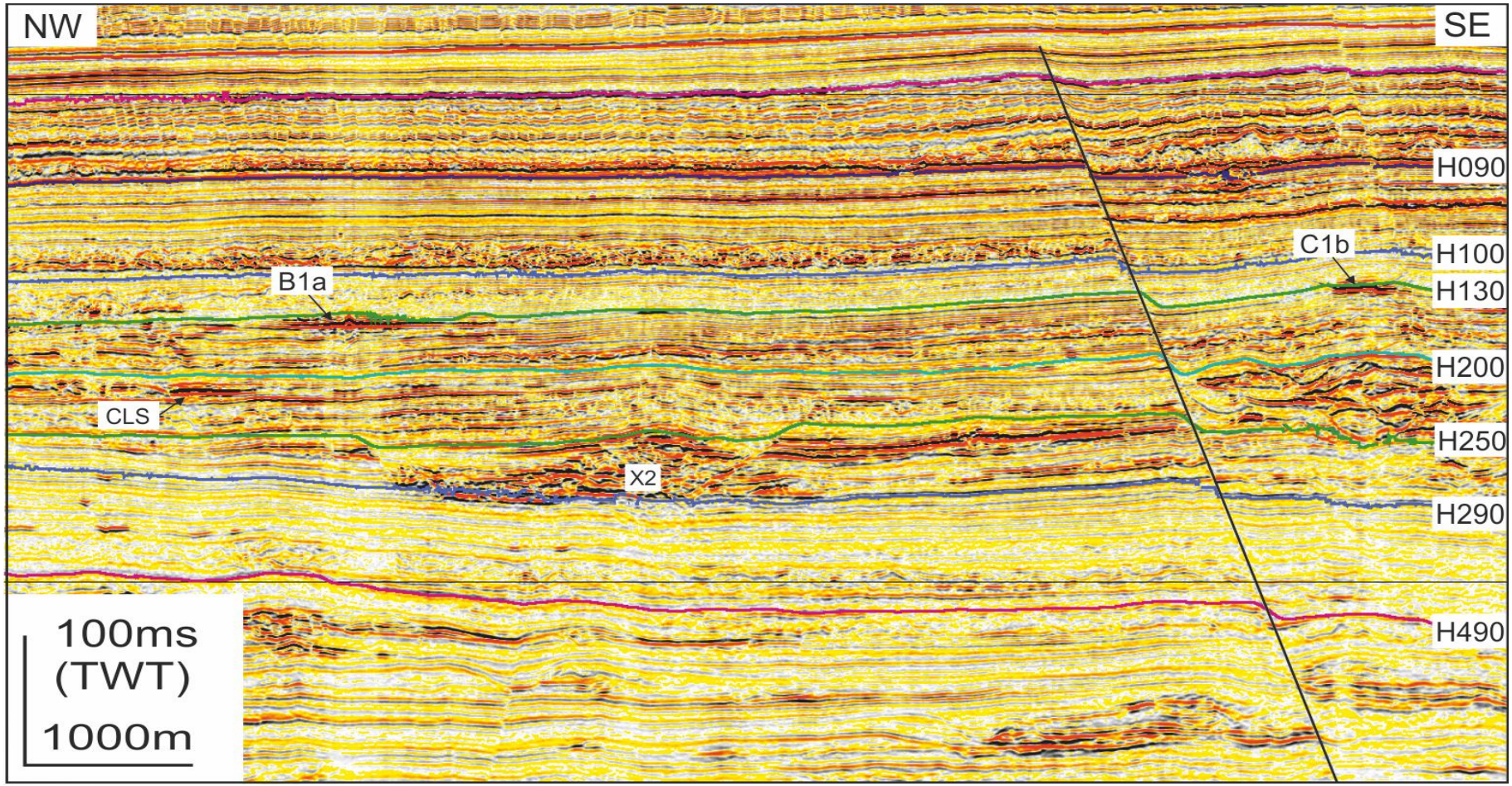

Figure 4.15: NW-SE oriented seismic profile passing through type 3 and type 2 anomalies P1a and C1b respectively. Both anomalies are laid above the upper-middle Miocene turbidite channels system (ca. 12 Ma) and developed below base of regional seal unit 3.There is no HAA observed above this interval. X2 is turbidite channel. For line location figure 4.14.

4.6.2 HAAs in H200-H250

Observed HAAs developed in this interval are linear (Type 2) and patchy (Type 3). These two types of anomalies are interpreted along the main middle Miocene turbidite channels except linear anomalies (type 1). Patchy amplitude anomalies (P2a, P2b, P2c, P2d and P2e) are hosted in levees of the mud filled NNE-SSW oriented channel (Fig. 4.17 and Fig. 4.18). In terms of orientation relative to the north, the anomalies trend 0^0 to 45^0. Patchy anomalies are also observed along the two NE-SW channels and channel lobes. Only C2a is bounded by faults F1 and F2 (Fig. 4.12). C1c anomaly is bounded by F1 and it is located at the top of C2a. On the contrary, linear anomalies (L2a, L2b, L2c, L2d, L2e and L2f) at the south and west side of the map are observed at the southern end of channel levee system (Fig. 4.16). The northwest oriented linear anomalies are possibly associated with group 3 faults (Fig. 4.11).

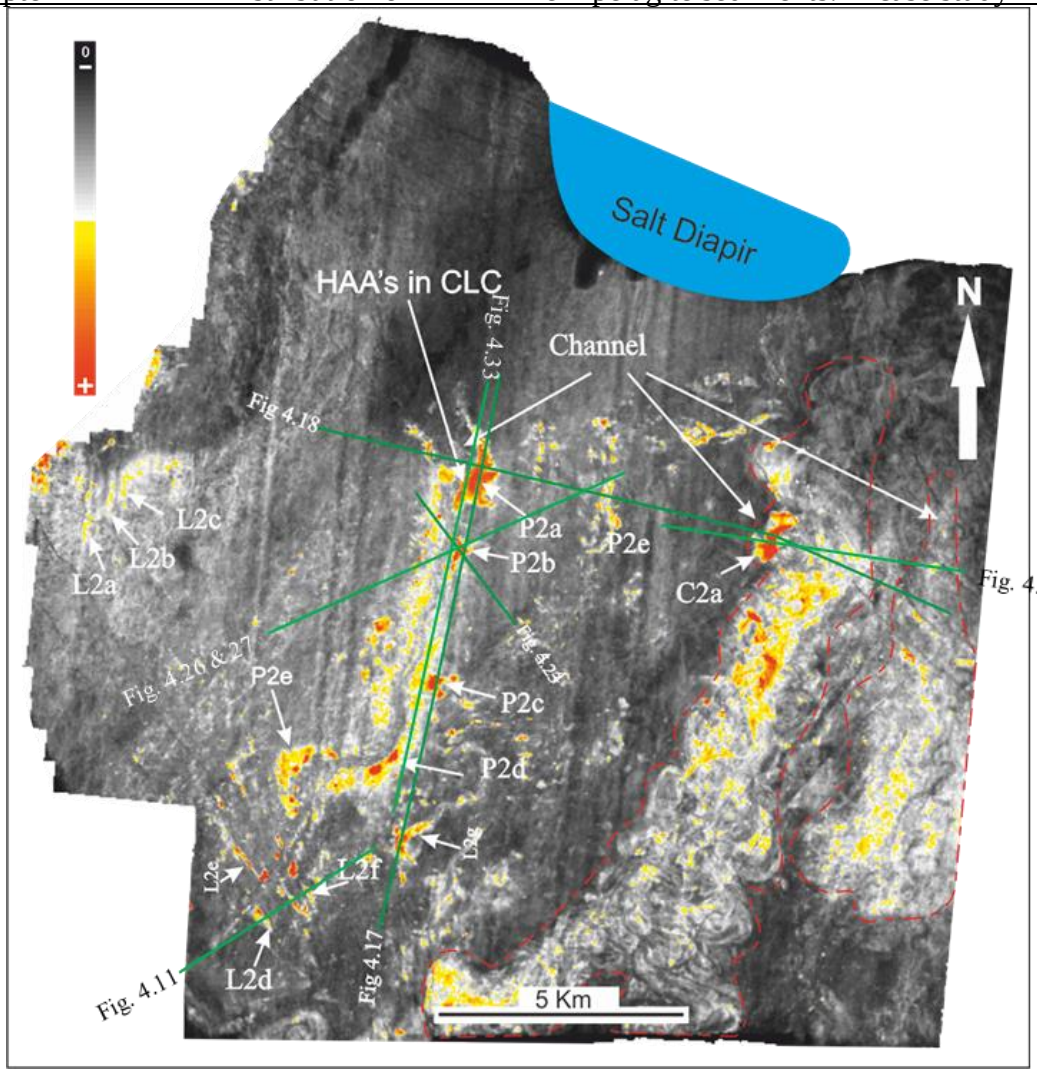

Figure 4.16: RMS amplitude extraction map between H250 and H200 in Unit 2b. The map shows positive cluster of linear and patchy high amplitude anomalies. Low amplitude values are in black and high-amplitude values are yellow to red. Location of high-amplitude anomalies is named P2, L2 and C2.The red dotted line shows extend of main reservoir turbidite channels.

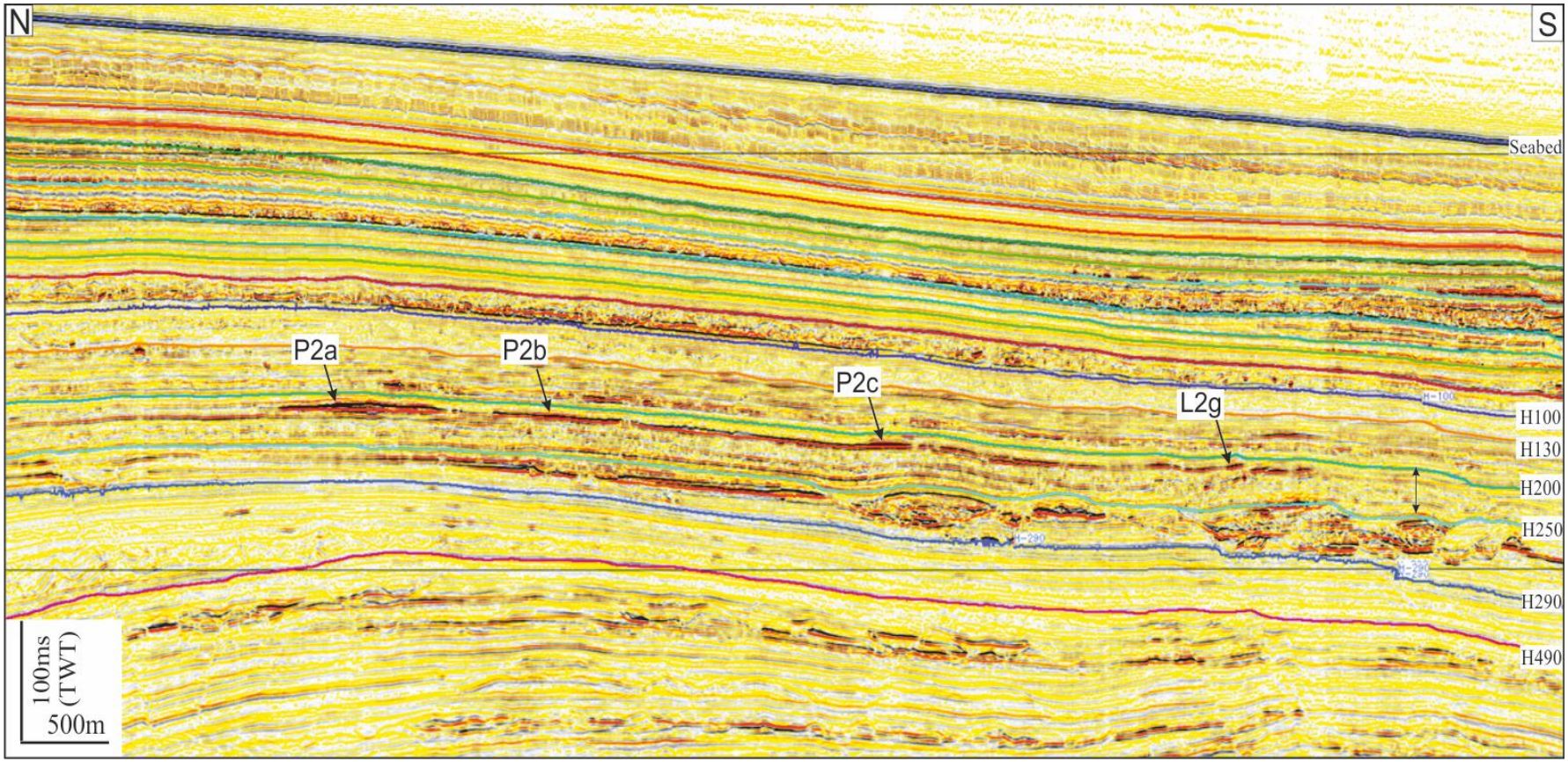

Figure 4.17: N-S oriented seismic profile passing through patchy and linear high amplitude anomalies that directly lies above the upper middle Miocene turbidite channels system (ca. 12 Ma). For line location figure 4.16.

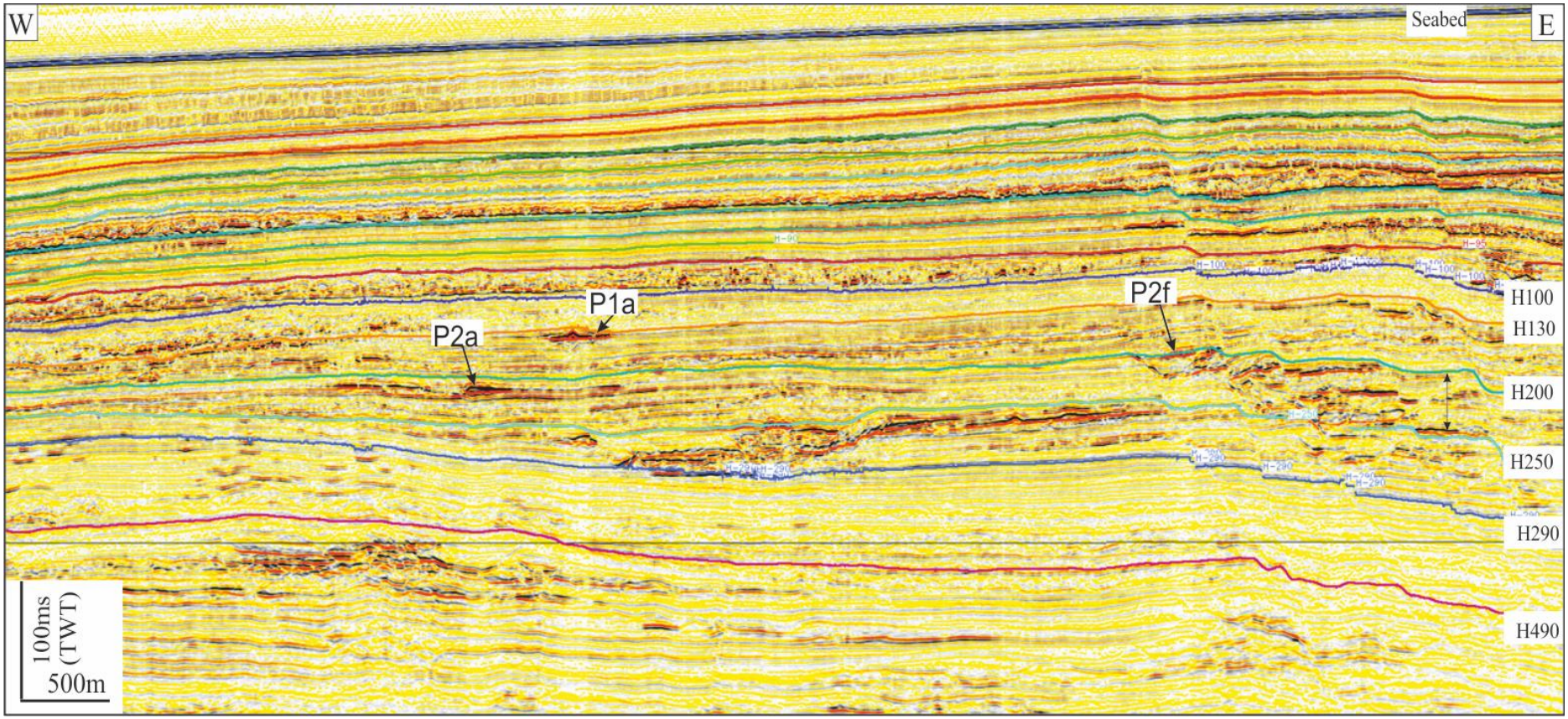

Figure 4.18: E-W oriented seismic profile showing through patchy high amplitude anomalies lies above upper middle Miocene turbidite channels system (ca. 12 Ma). For line location figure 4.16.

4.6.3 HAAs in H250-H290

This interval is composed of seven (1 to 7) NE oriented and parallel turbidite channels. Linear and patchy anomalies are developed along the levees of channel 4, 6 and 7 (Fig. 4.19). The other channels (1, 2, 3 and 5) are not associated with any HAAs. Discrete amplitude anomalies are developed between two channel 4 and 6 (Fig. 4.19). The sand bodies in these turbidite channels are main producing reservoirs in the LCB (Andresen et al., 2011; Anka et al., 2012). Due to the complexity of the turbidite channels, it was not possible to differentiate high amplitude anomalies in these channel sands more precisely; however, the RMS amplitude map shows the spatial distribution of the channel sand geometry (Fig. 4.19).

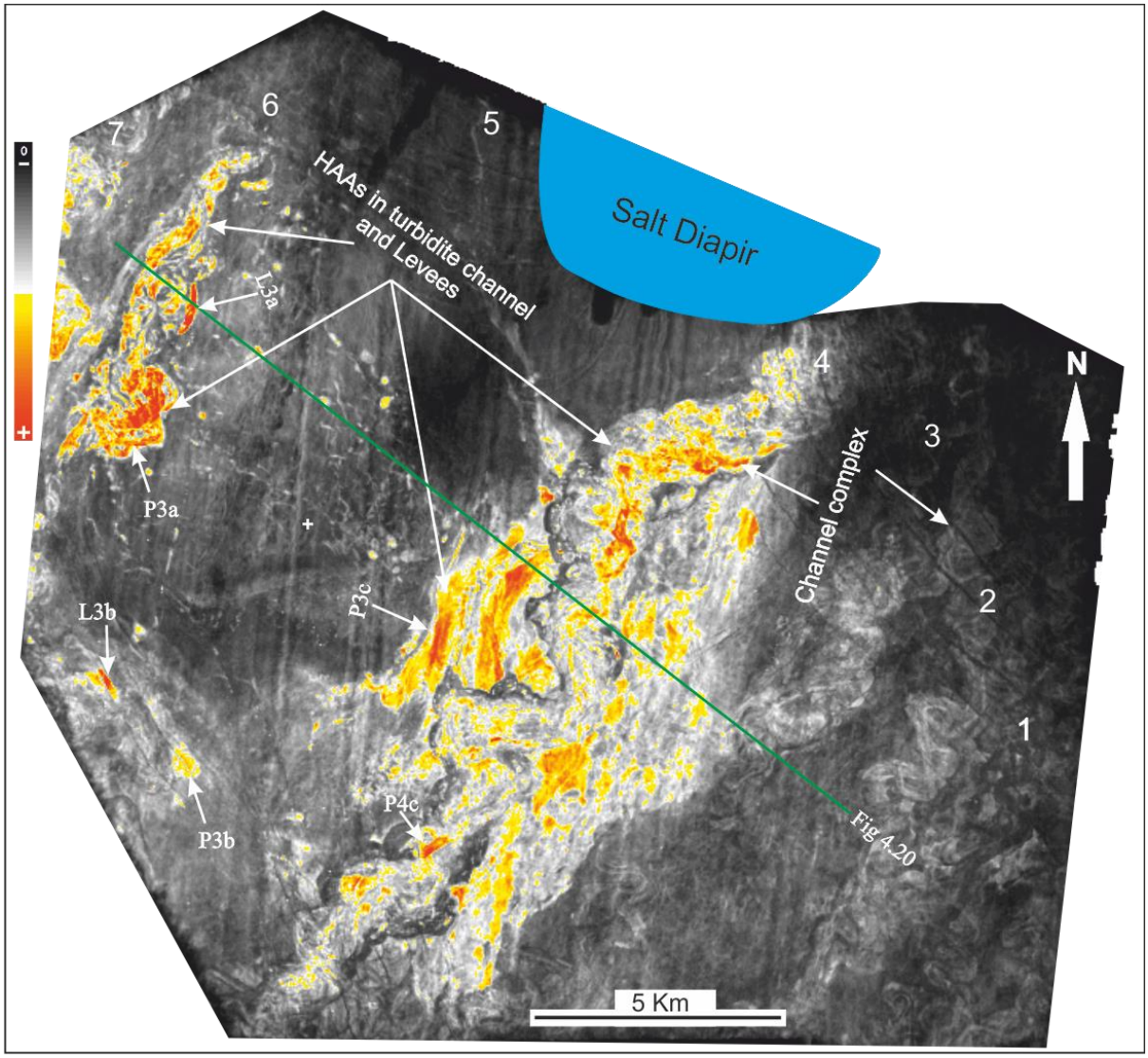

Figure 4.19: RMS amplitude map extracted between H250 and H290 (Top of regional seal unit 4). The map shows positive cluster of linear (L3a) and patchy (P3a) anomalies. Curve shaped HAAs are observed along the lower Miocene channel levee system. High amplitude anomalies are associated with only channel 4 to 7 and no amplitude along channel 1 to 3. The red-yellow colour indicates HAAs.

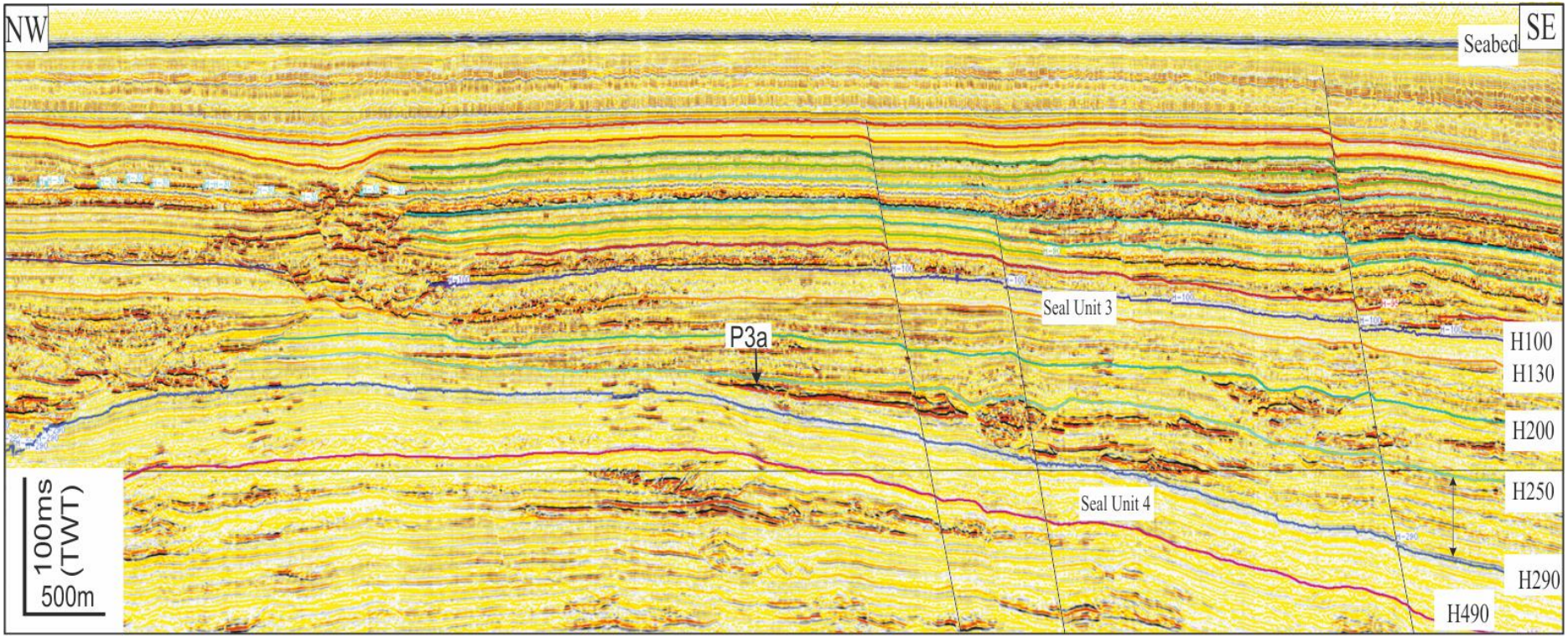

Figure 4.20: Northwest- southeast seismic profile shows different hemipelagite deposits. There is high amplitude anomalies associated with lower Miocene channel levee system, only Patchy HAAs developed into the levees or lobes of turbidite channels.4 and 6. See Fig. 4.19 for location.

4.6.4 HAAs in H290-H490

Anomalies are found in the central and NW portion of the study area. These anomalies are discrete group of linear and patchy anomalies in plan form (Fig. 4.20). All the linear anomalies are developed in cluster on N-S trend that following direction of major turbidite channels (Fig. 4.19). Patchy anomalies are mixed with linear but they are only developed above Oligocene turbidite channels (Fig. 4.22).

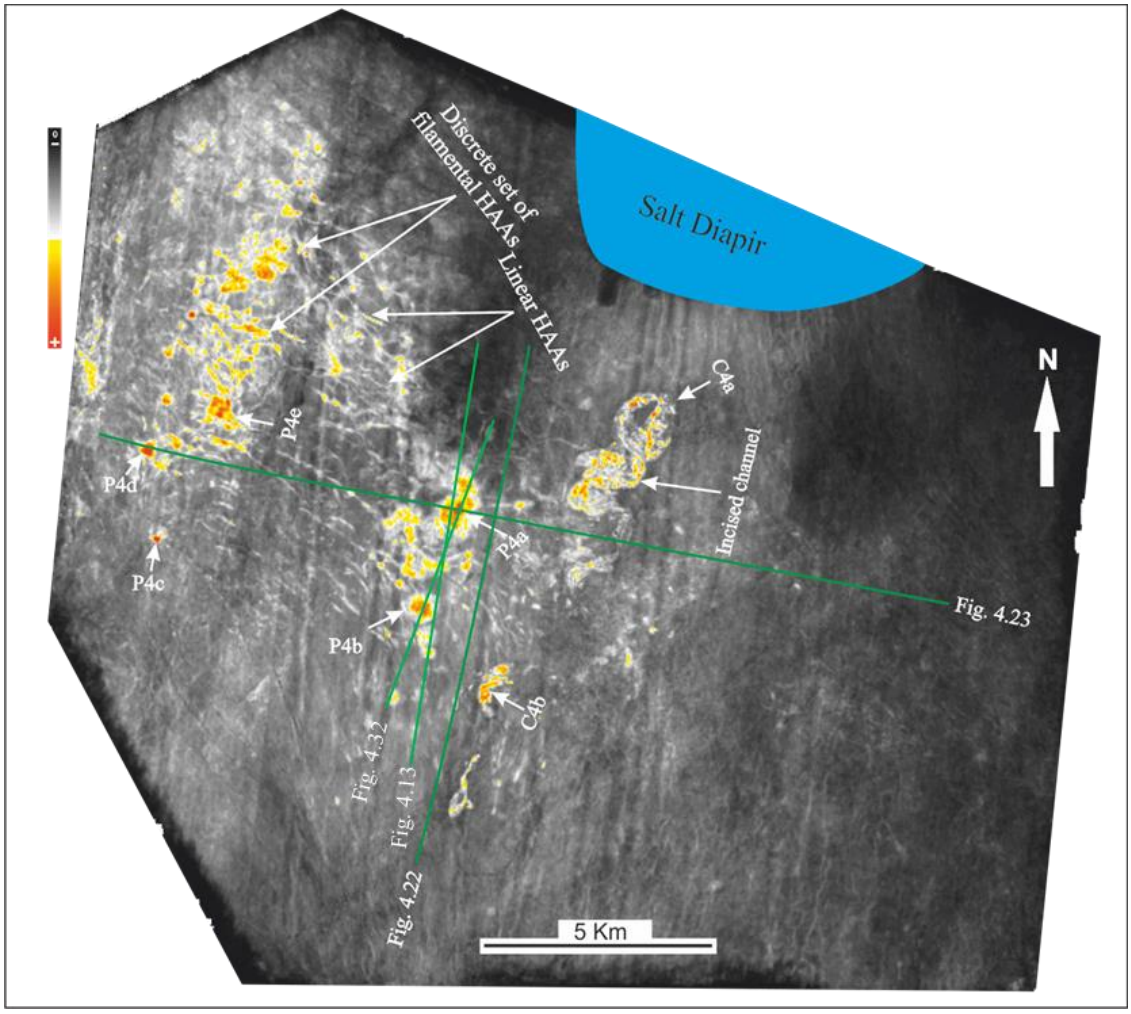

Figure 4.21: RMS amplitude map computed between horizon H290 and H490 (Regional seal unit 4). The map shows positive cluster of linear (LH4a) and patchy (P4a) high amplitude anomalies. Curve shaped (C4a) HAAs are observed along the channel. The discrete or filamental HAAs are at the north –west part of the study area. The red-yellow colour indicates HAAs.

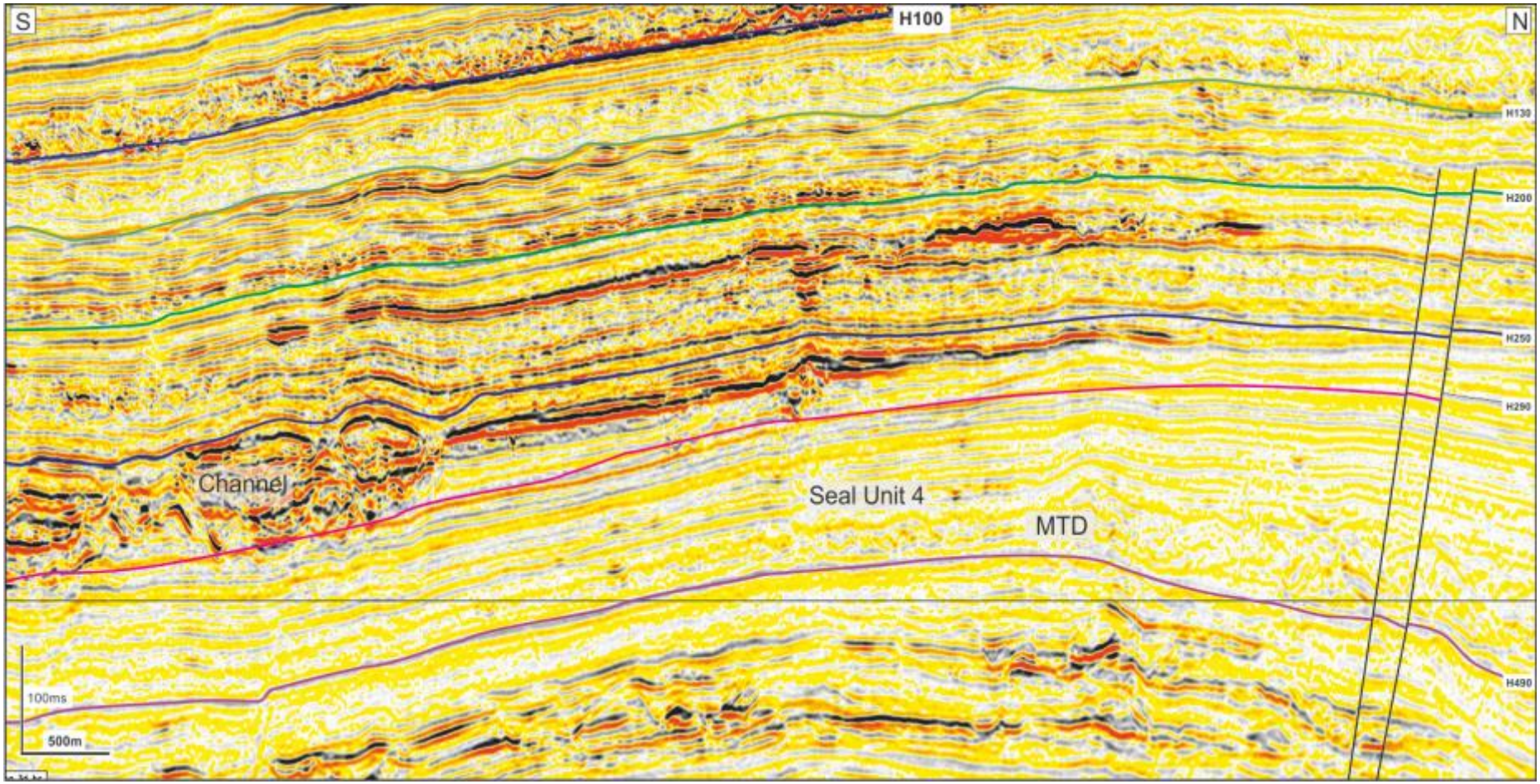

Figure 4.22: North South oriented seismic profile shows transparent hemipelagite deposits of regional seal unit 4. There is no high amplitude anomalies refer in the perfect seal. The top of Seal unit 4 (H290) is high-amplitude channel systems and a heterogeneous Mass-Transport Deposit (MTD) occurring at bottom of the succession (H490), Location of seismic line is shown in Fig. 4.21.

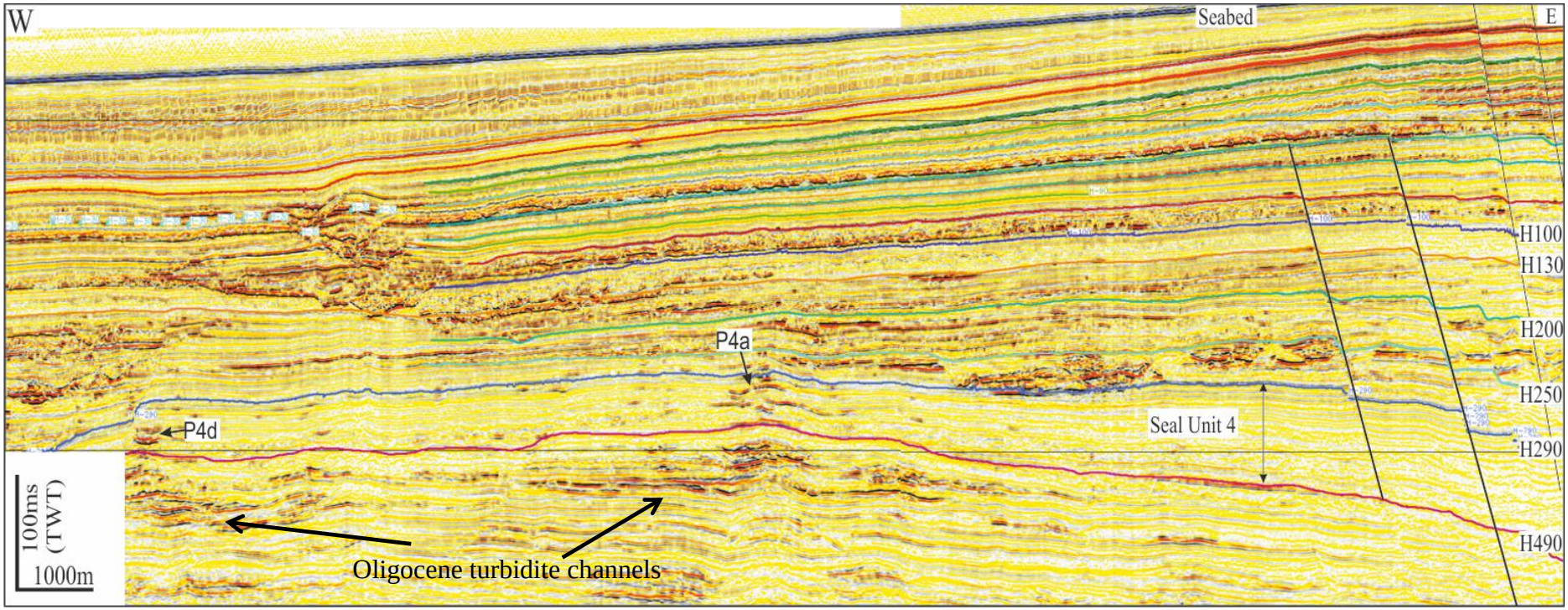

Figure 4.23: Northeast and west oriented seismic profile passing through two patchy high amplitude anomalies in the regional seal unit 4. South oriented line shows different interpreted horizons. P4a and P4d are the patchy HAAs. Paired reflections are disseminated in this unit. The back ground of these HAAs shows no amplification of seismic reflection possibly represents a seal unit. Location of seismic line is shown in Fig. 4.21.

4.7 Seismic observation and characterization of HAAs

Hydrocarbon indicators observed in the Lower Congo Basin includes flat spots, amplitude anomalies, dim spots, velocity push down effects, seismic acoustic blanking and polarity reversals (Fig. 4.24) Pockmarks are also observed on current seabed (Fig. 4.6) and paleo pockmarks are also reported by many researchers in the area (Ho et al., 2012; Gay et al., 2006; Andresen et al., 2012). The presence of hydrocarbon in the porous sediments cause changes in the acoustic properties and thus leads to developed DHIs that can be easily identified on seismic section (Brown 2010, 2004).

4.7.1 Flat spots

The term "flat spot" is used here for the reflective boundary between different fluids, either gas-oil, gas-water or water-oil. Two different flat spots were recognised in the study area. The Flat spots are associated with a channel levee and a stratigraphic trap that developed at the top of horizon H130 (Fig. 4.24 and Fig. 4.25).

Flat spot shows a high amplitude anomaly (P2b) accompanied by local compaction in sand units of mud-filled mid Miocene channels (Fig. 4.24). This high amplitude anomaly may be developed due to a porous sand layer in the levee and charged with hydrocarbons leaked from Oligocene-Miocene turbidite channels that are proven main reservoirs in the LCB. A lowering of acoustic amplitude immediately below the flat spot resulted in low frequency shadow zone. Such low frequency or acoustic blanking are commonly reported under gas accumulations and confined to a couple of cycles below the gas accumulations (Loseth 2009; Cartwright et al., 2007; Lee and Watkins., 1998; Sheriff and Geldart., 1983)

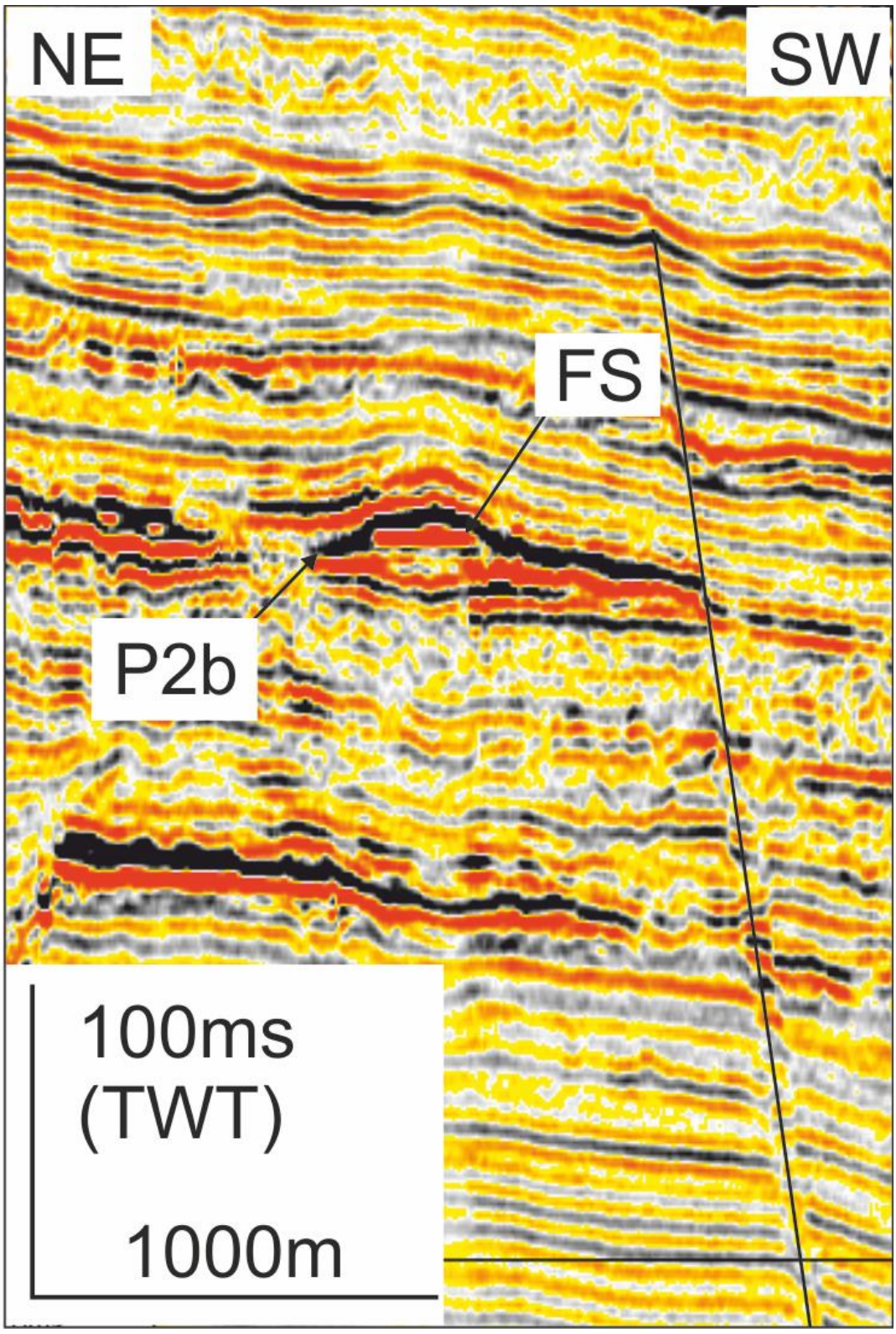

Figure 4.24: Seismic profile passing through patchy anomaly P2b showing flat spot (FS) that developed in levees of mud filled late Miocene channel. See Fig. 4.15 for location of seismic profile.

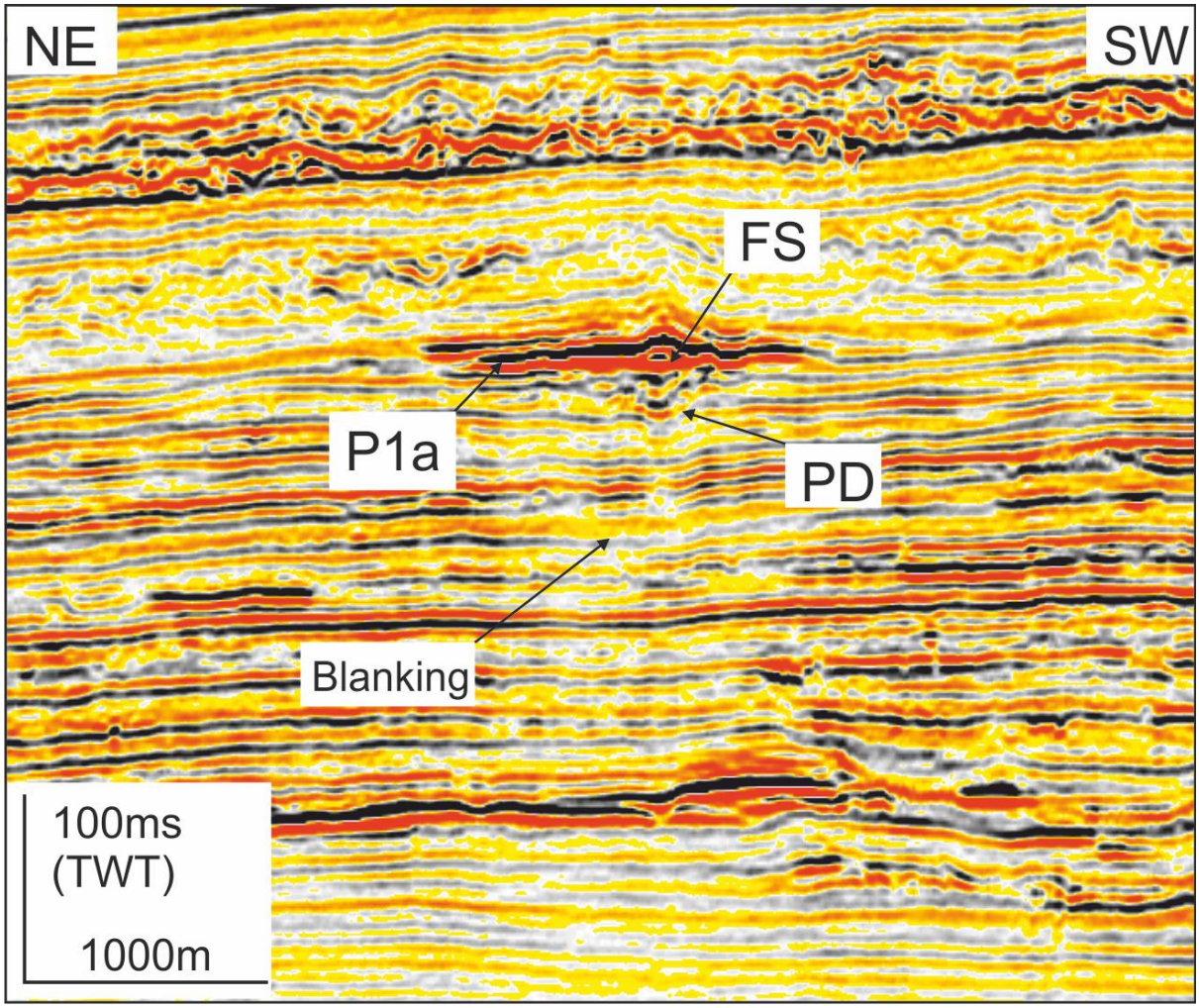

Figure 4.25: NE-SW seismic profile showing patchy anomaly (P1a) developed in a stratigraphic trap developed above main turbidite Miocene channel. MTD above the anomaly is possibly a good seal as there is no amplitude anomalies observed in it. See Fig. 4.14 for location of seismic profile

4.7.2 Velocity push downs

Down-bending of stratal reflections occurs beneath high amplitude anomaly P2b (Fig. 4.24) and P1a (Fig. 4.25) but similar down-bending does not occur beneath the other anomalies. Down bent reflections are generally lower in amplitude than their lateral continuations. The down-bending interval typically persists vertically for >20ms TWT beneath the P2a anomaly (e.g. Fig. 4.24) and for anomaly P1a is >50ms TWT (Fig. 4.25). From the geometry and the close spatial relationship between the anomalies and the downbent zone, the downbent regions is interpreted as being due to a velocity push down effect (Brown, 2011), resulting from the cumulative low velocity effect of the vertical stack of seismic traces. An alternative explanation that the down bending is real was discounted because the down bending is exclusively observed beneath well-developed anomalies. Similar association of pronounced acoustically-soft amplitude anomalies and velocity push down has been described from regions of shallow gas accumulation or CO_2 storage (Arts et al., 2004a; Boait et al., 2011).

4.7.3 Blanking or dimming

Attenuation of seismic signals, termed here as “blanking” (Brown, 2011; Sun et al., 2009), or “acoustic distortion” (Andresen et al., 2012) are commonly observed beneath high amplitude anomalies (Fig.2.4A and B, Chapter 2 for detailed). Dimming of signals begins immediately beneath extent of amplitude anomalies, and the background amplitude response is regained immediately outside of this zone of dimming. According to Sun et al (2012), Andresen (2012) and Løseth et al. (2009), dimming can be attributed to gas accumulation in the sediments and is widely observed in association with gas chimneys and other gas-charged structures (Sun et al., 2012, Heggland et al., 2005).

Seismic blanking or dimming observed beneath high-amplitude anomalies (P2b and P1a), may result from accumulation of free gas in these anomalies which trap seismic signals (e.g. Foschi et al., 2014; Cartwright et al., 2007; Loseth et al., 2009; Berndt, 2005; Heggland, 1998; Huuse et al., 2010; Judd and Hovland, 2007). Presence of hydrocarbons, particularly gas saturation in amplitude anomaly as low as 1–5% often produces seismic amplitude reflection of more than 30% saturation (Judd and Hovland, 1992) and causes scattering and absorption of the seismic signal, producing dimming beneath their locations. Seismic blanking was only observed below patchy anomaly (Fig. 4.25). About more than 20 meters thick and 1000 meters wide anomaly P1a generated 200ms TWT seismic blanking effect. In contrast, the P2b anomaly which is about 40 meters thick and more than few thousand meters wide generated more than 200ms TWT seismic blanking. The dimming phenomenon is only in the thickest part of the high amplitude anomaly which is usually associated with free gas saturation (Fig. 4.26). Seismic blanking is interpreted as indicators of the presence of free gas in any system (Loseth et al., 2009; Brown, 2004). Blanking is not visible below the other anomalies P2a, P1b, P1c and L2a. Although seismic dimming is not only the indicator of free gas in the anomaly, in some cases blanking actually represents homogeneity in lithology, reflected as lack of strong acoustic impedance contrasts between layers.

4.7.4 Seismic attributes

Seismic attributes helped to understand and classify seismic events within seismic traces based on their frequency and amplitude content. These attributes are helpful to differentiate seismic events that are not possible on normal seismic data.

4.7.4.1 Instantaneous frequency

Instantaneous frequency is useful for identifying abnormal attenuation that may be due to gas accumulation and for identifying thin-bed tuning effect on seismic data (Chopra and Marfurt, 2007). The seismic profile from instantaneous frequency volumes display low frequencies which produced by high-amplitude anomalies P1a and P2b (Fig. 4.27). As the gas reservoirs attenuate high frequencies more than in the rock without gas saturation (Brown, 2004). The low instantaneous frequencies immediately below these anomalies are possibly due to presence of gas in the observed anomalies.

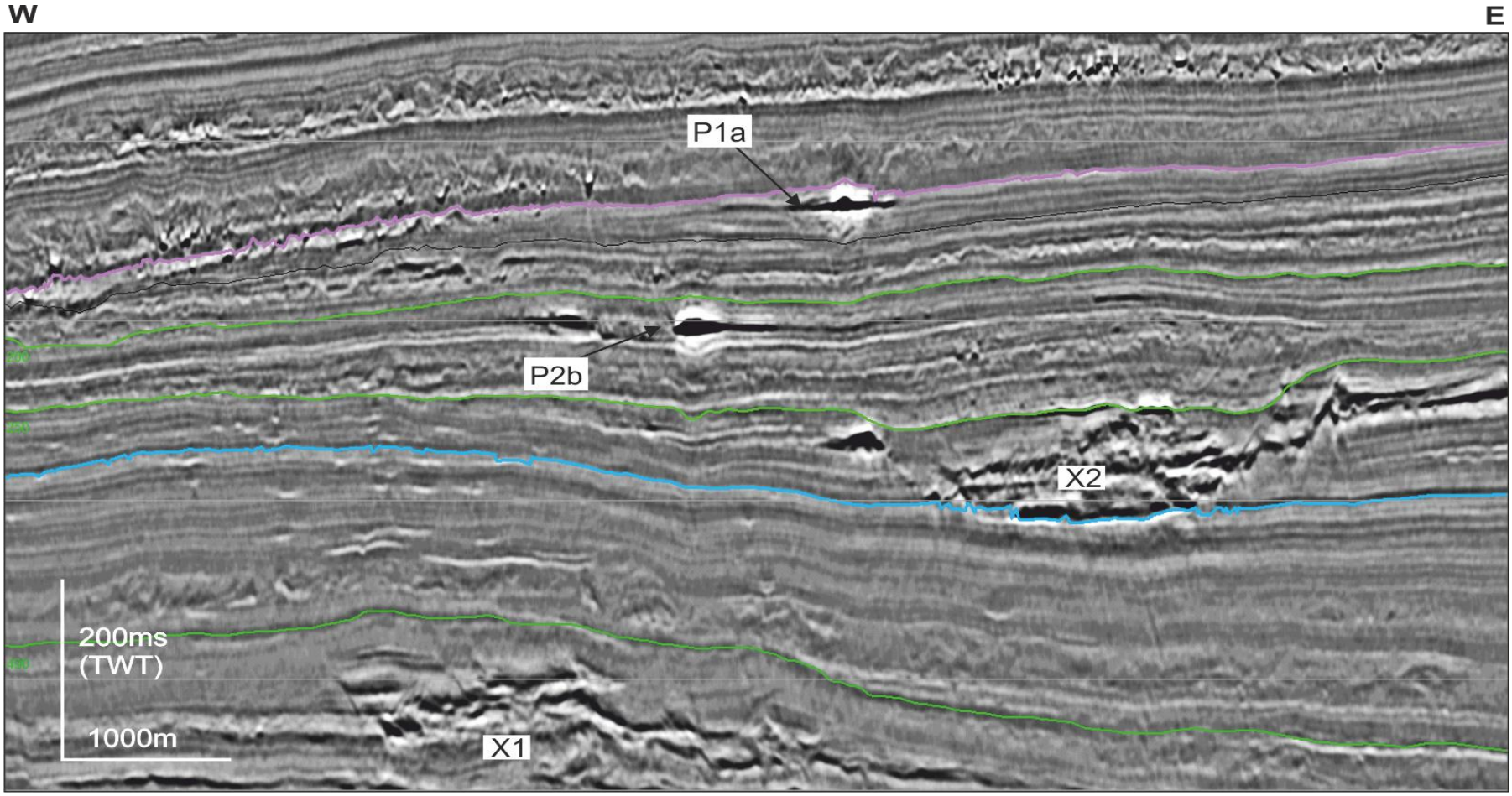

Figure 4.26: Cross line seismic profile passing through two representative high-amplitude anomalies P1a and P2b that developed immediately above the main Miocene (X2) and Oligocene (X1) turbidite channels. See Fig. 4.16 for location of seismic profile

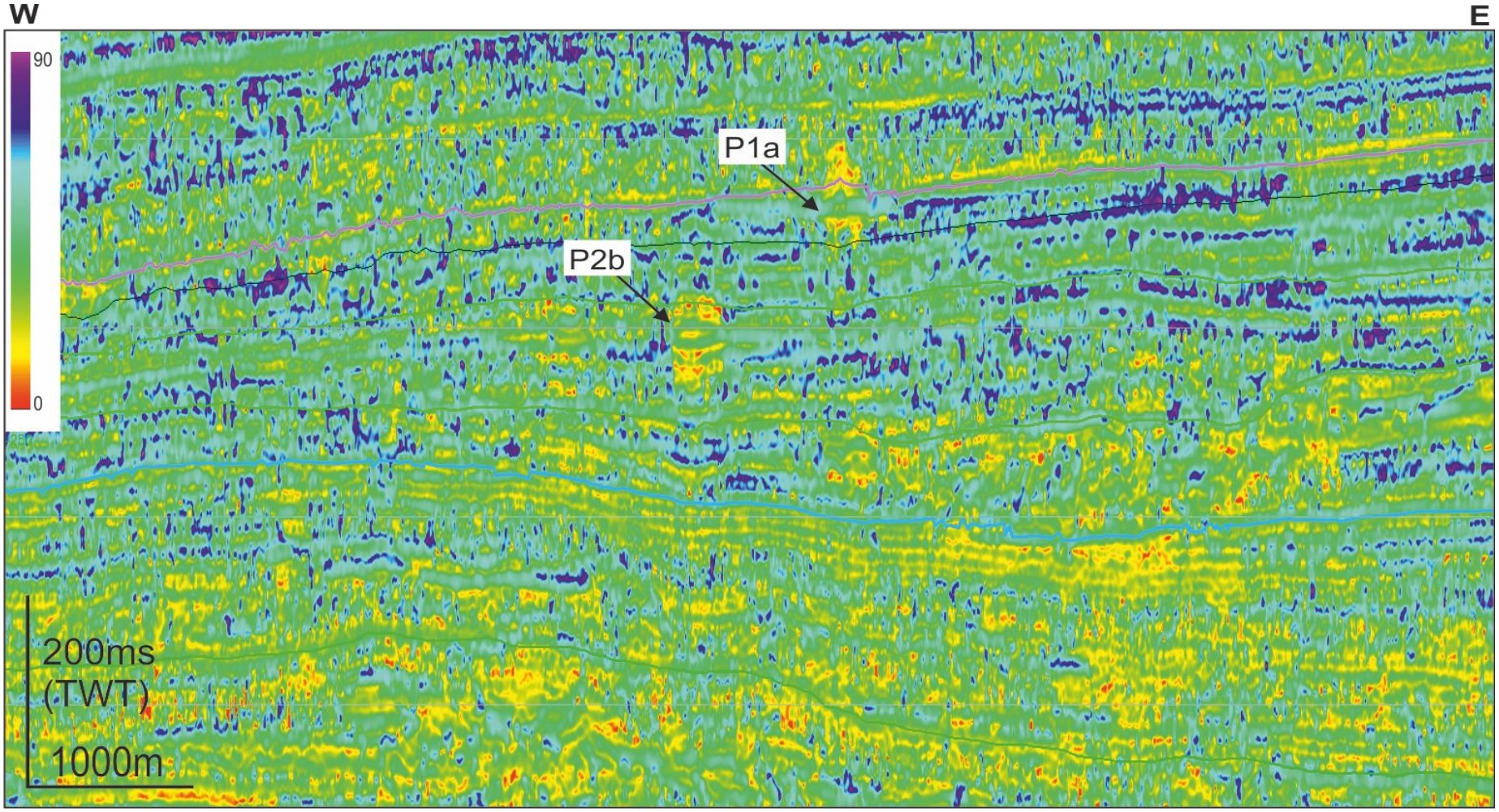

Figure 4.27: Seismic instantaneous frequency profile computed on seismic volume. Seismic profile passing through high-amplitude anomalies P1a and P2b. Low frequencies displayed in and below these anomalies are associated with velocity drop in the presence of gas. See Fig. 4.16 for location of seismic profile

4.8 Discussion

The discussion begins with a summary of the key observations followed by a discussion of uncertainties in the interpretation and the main implications for hydrocarbon exploration in this region. Since the wells available for the study did not penetrate the HAAs, interpretation rely solely on the acoustic expression, geometry, and the regional context provided by published works.

4.8.1 High amplitude anomalies related to Hydrocarbon

4.8.1.1 Structural and stratigraphic control on HAAs

Four types of high-amplitude anomalies are occur in the waste zone. Pockmarks on the seabed formed in response to an active phase of fluid flow. Their distribution is influenced by salt diapirs and associated minibasins and fault systems (Fig. 4.6 and 4.7) (Gay *et al.*, 2007; Andresen and Huuse, 2011; Anka *et al.*, 2012; Ho *et al.*, 2012). The deep, high-amplitude anomalies in the waste zone are also controlled by an anticlinal fold and faults (Ho et al., 2012). Patchy anomalies P1a, P1b and C1c are controlled by northwest-to-southeast elongated anticlines whose crests sit at approximately 1.2 kilometres depth (Fig. 4.28). P1a and C1c are controlled by deep-seated Group 1 normal faults (Fig. 4.8). The concentration of sub-circular anomalies, e.g anomaly C2a is also associated with an anticlinal structure in the deeper stratigraphy (Fig. 4.29). Discrete or filamental anomalies developed in the regional seal Unit 4 are only confined to the anticline (Fig. 4.30 and Fig. 4.31).

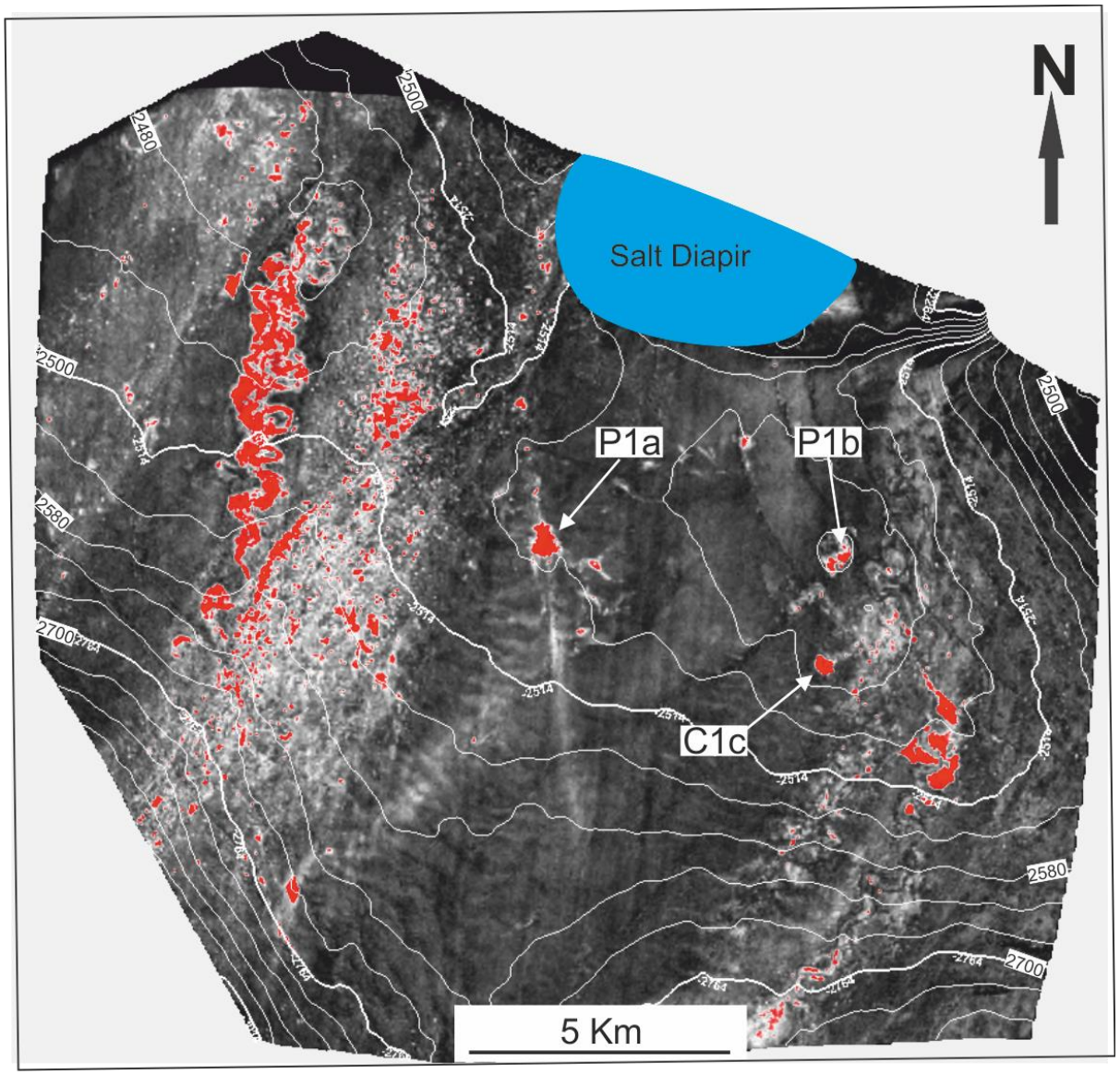

Figure 4.28: RMS amplitude map between H1200 and H130 overlain with TWTT structure contour. P1a, P1b and C1c anomalies are confined to an anticlinal structure. Contour interval 20 ms in TWT.

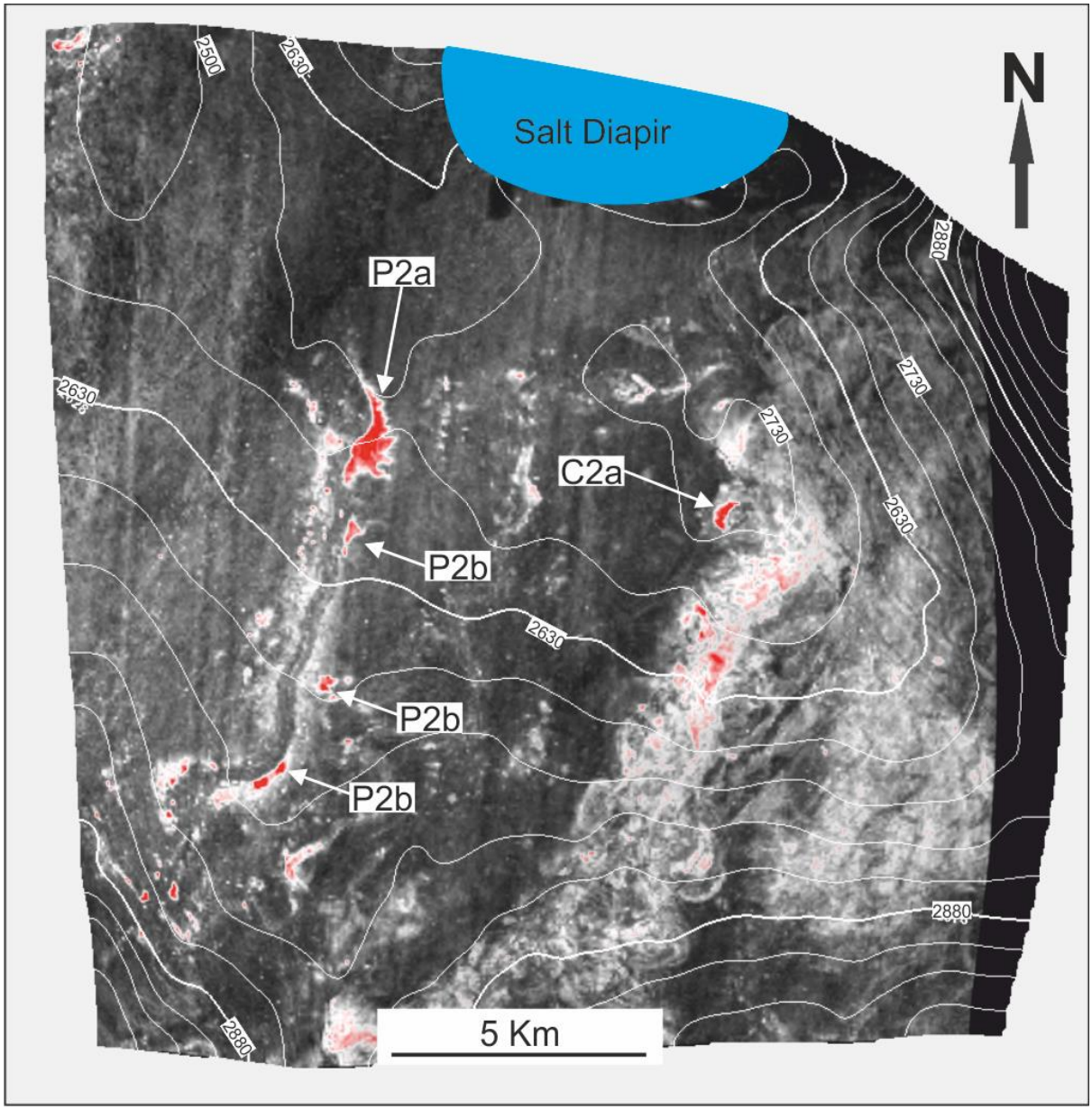

Figure 4.29: Two way travel time contours overlay on RMS amplitude map of seismic interval between H250 and H200. Map show that P2a anomaly is developed at the flank of shallow structure. Contour interval 50 ms in TWT.

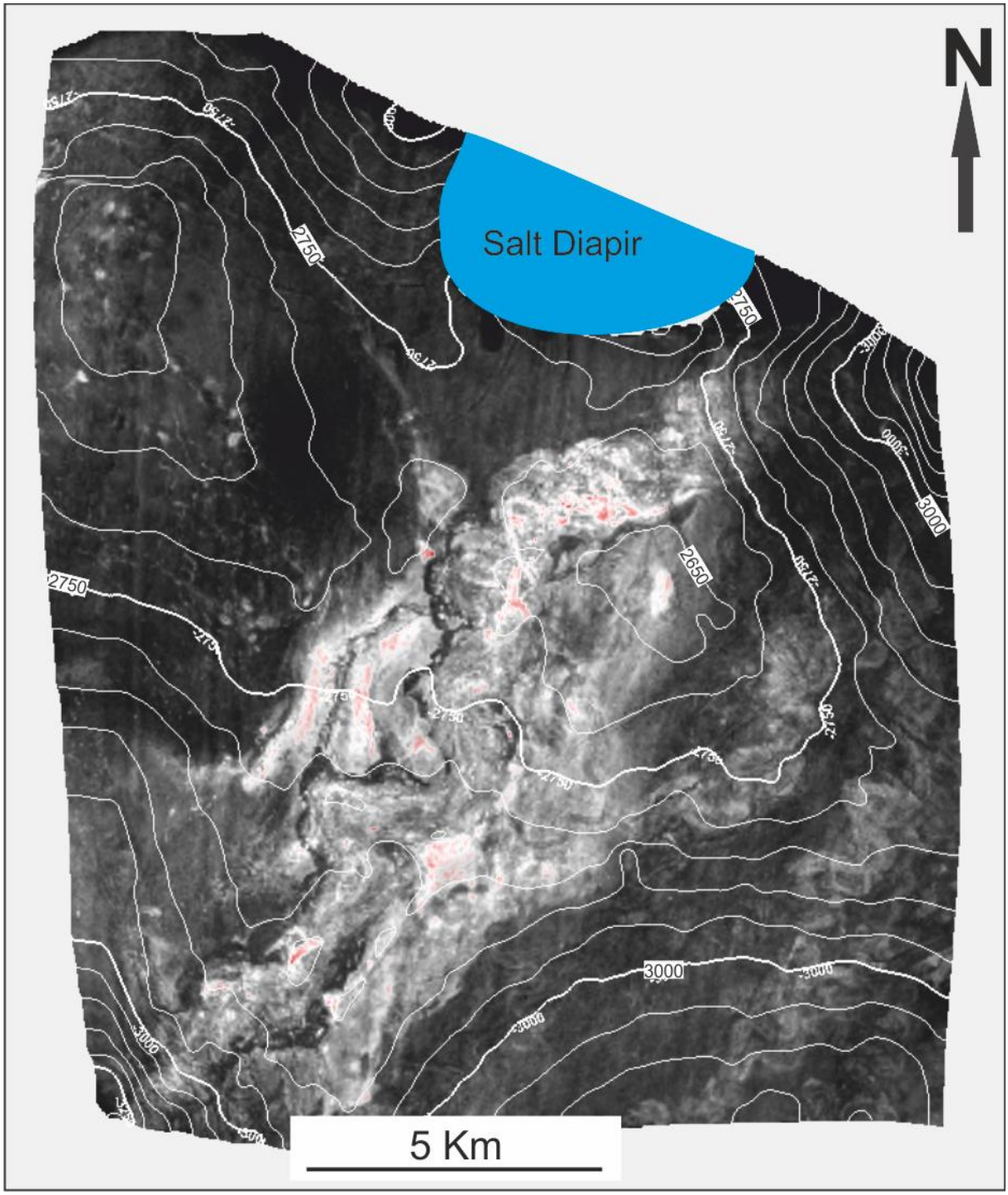

Figure 4.30: Two way time contour map overlay on RMS amplitude map of interval H290 and H250. Contour interval 20 ms in TWT.

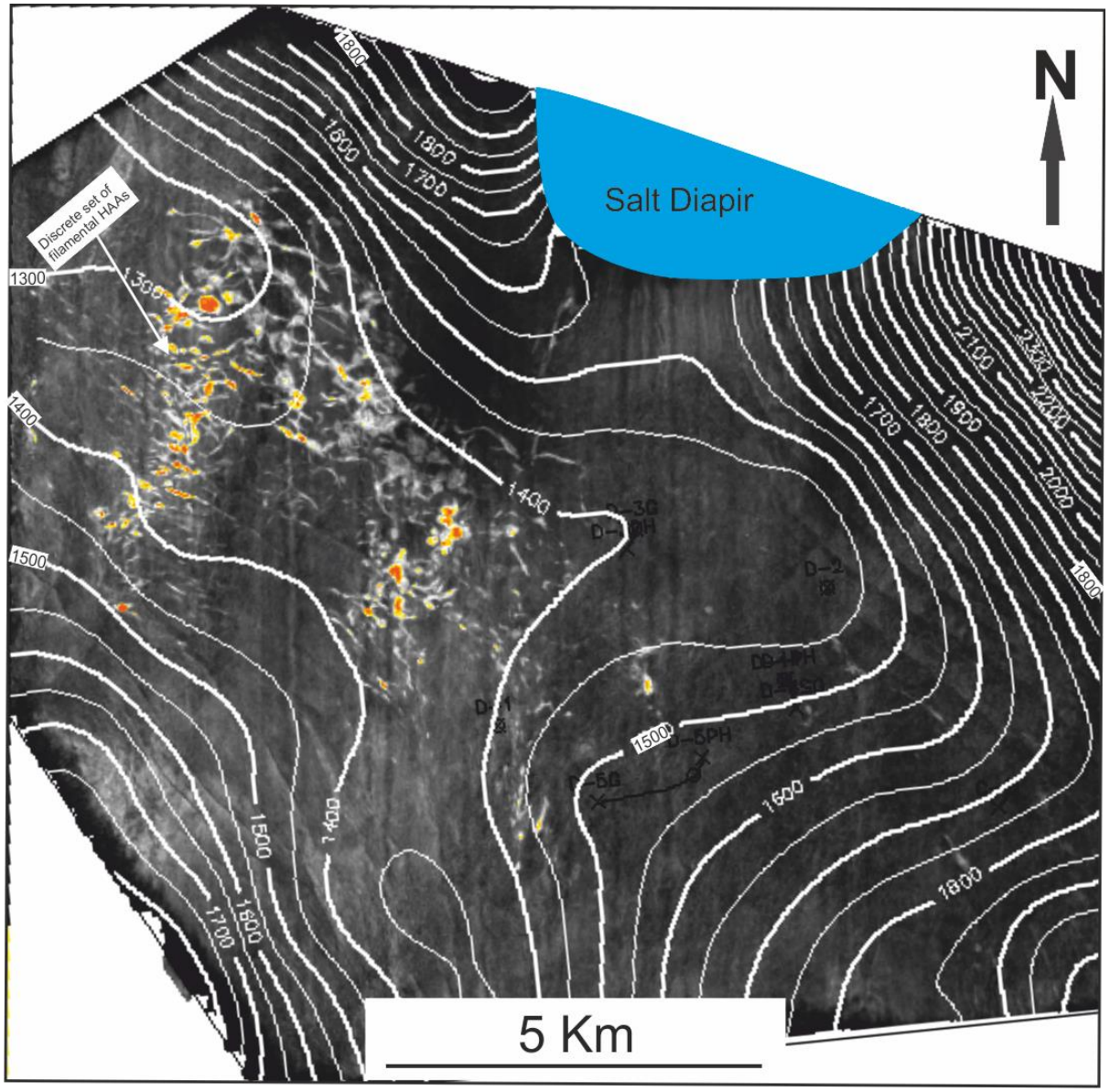

Figure 4.31: Two way time contours H200 overlay on RMS amplitude map of interval H490 and H290. Contour interval 50 ms in TWT.

4.8.1.2 Orientation of anomalies

High-amplitude anomalies show different long-axis orientations as illustrated on the RMS amplitude maps in Fig. 4.14, 4.16, 4.19 and 4.21. The majority of the anomalies are oriented in a northerly direction but most of patchy anomalies are oriented NNE to SSW along the trend of the turbidite channels (Fig. 4.16). A similar NNE trend exists for the majority of sub-circular anomalies. The sub-circular anomalies are possibly developed along sand units of the Miocene turbidite channels (patchy anomaly C2a, Fig. 4.16). The linear and discrete filamental anomalies do not follow any particular trend (Fig. 4.21). These anomalies are possibly, not associated with hydrocarbons as their acoustic behaviour is different from the other anomalies. In this study, the anomalies show a predominant NNE to SSW trending orientation that is the same orientation of present seabed sediment deposition, which suggest a similar dynamic relationship between anomalies and turbidite channels.

4.8.1.3 HAAs related to channel levee complex

The turbidite reservoirs in the study area are indicators that thermogenic fluids ascended from deeper source rocks and migrated from one channel to the next and are progressively concentrated in the upper Miocene channels (Andresen and Huuse, 2011; Andresen *et al.*, 2011; Anka *et al.*, 2012; Ho *et al.*, 2012). In general, most deepwater reservoirs are turbidite sands, channels, and sand lobes originally deposited in a slope or basin setting (Mike, 2012). The acoustic properties of seismic anomalies observed in the study interval are directly associated with underlying Oligocene and Miocene turbidite channels (Berndt *et al.*, 2003; Stuevold *et al.*, 2003). Possibly the presence of hydrocarbon in turbidite sands caused a change in the acoustic properties, and thus direct hydrocarbon indicators like flat spot,

velocity push down, acoustic blanking are identified. Curvy and patchy anomalies occur at different stratigraphic levels in the waste zone (Fig. 4.5) but are only associated with turbidite channels possibly because they tend to have a high net-to-gross ratio (Mayall *et al.*, 2006). The clustering of high-amplitude patchy anomalies in in the channel levees is due to the erosive nature of the channels. Therefore, anomalies are only developed where there is high net to gross ratio.

4.8.1.4 HAAs related to mass transport deposits

Four (MTD1 to MTD4) mass transport deposits were interpreted to understand the distribution of high-amplitude anomalies. RMS amplitude maps between different seismic horizons H130-H200) and H290-H490 were computed for key intervals to highlight the internal character of MTDs. The computed maps showed a cluster of high amplitude anomalies (Fig. 4.14) included four patchy anomalies. In the contrast there is no high amplitude anomalies developed in MTD1 at the base of regional seal unit 4 (Fig. 4.22). The presence of high amplitude anomalies was depicted only in MTD2 inferred as presence of siliciclastic emanating from the sand bed/sheets of channel levees.

4.8.1.5 HAAs related to faults

In many basins of the world Syn-depositional major faults located above turbiditic sand bodies may periodically act as main vertical fluid escape pathways (Lonergan et al., 2000, R). The study area is affected by different type tectonic and salt related radial faults during the Cenozoic era. The polygonal faults are developed in two discrete tiers, separated by a thin

interval, with no faulting other than the tectonic sets. The faults are organised into conjugate pairs, which is uncommon amongst polygonal fault systems globally. They have throws ranging from 1-10m. They commonly cross-cut the master faults, but do not extend across the entire tier. They are considered to be a space-filling system of faults, whose propagation ensures the most complete fragmentation of the volume into fault blocks. Earlier work suggesting that polygonal faults do not degrade seal integrity, but can be reactivated under external agents and form fluid ascent routes (Bunz *et al.*, 2003; Stuevold *et al.*, 2003).

Only patchy anomalies are developed in the study interval between seismic horizons H130-H200, H200-H250 and H250-290 along those tectonic faults that were passing through the main turbidite channel reservoir of Oligocene-Miocene age. The migration of fluids through the impermeable Oligocene–present cover leads to high amplitude anomalies development, free gas accumulation beneath hydrates, occurrence of HAAs over turbiditic channels and pockmark formation at the seabed.

4.8.2 Positive high-amplitude anomalies

Paired seismic reflections, termed here as filamental anomalies, are observed in Seal Unit 4. Linear and filamental anomalies occur as a tuned, positive-negative reflection amplitude doublets. This character suggests: a) accumulations below the minimum seismic resolution for Seal Unit 4; b) anomalies are larger than the minimum seismic resolution but are highly tuned into positive-negative wavelet doublets particularly when dealing with vertically clustered anomalies. Concave-shaped type-2 anomalies and marginal areas of type 3 anomalies may also reflect a significant seismic tuning effect. The associated velocity push down which occurred preferentially in the centre of the imaged anomalies may give important leads on their nature and development (Fig. 4.32).

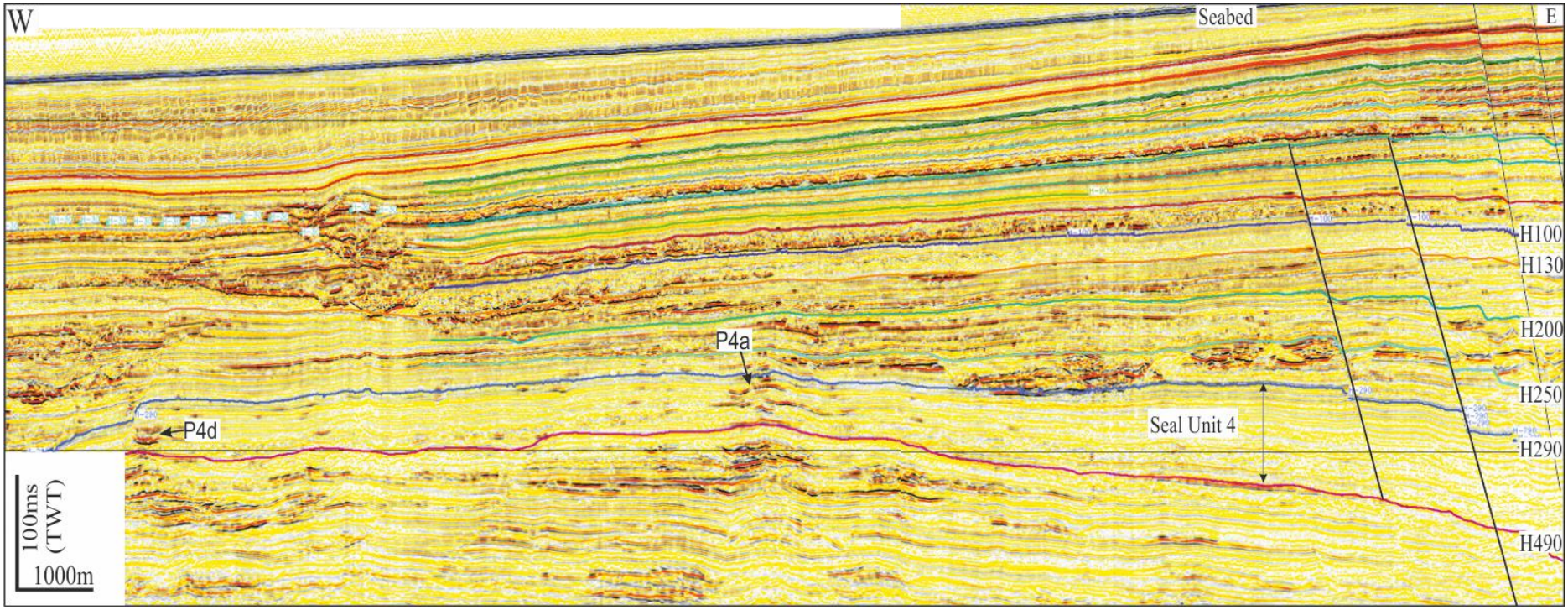

Figure 4.32: Discrete set of filamental high amplitude anomalies are only observed northwest part of the study area. The two Patchy anomalies (P4a and P4d) observed in this interval are associated with faults and channels. See Fig. 4.21 for location of seismic profile.

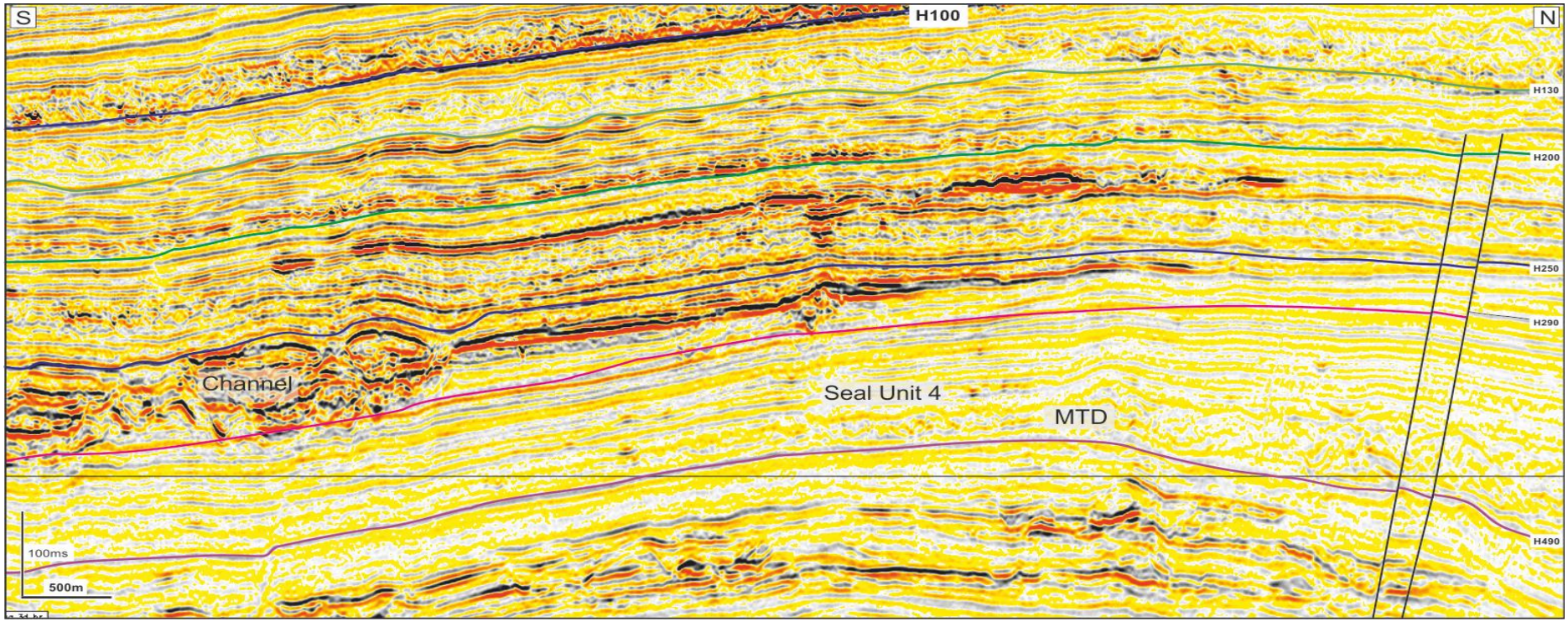

Figure 4.33: Discrete filamental anomalies have strong relations with underlying and overlying reservoir units, which include channels, associated levee deposits and Mass Transport Complexes. See Fig. 4.16 for location of seismic profile

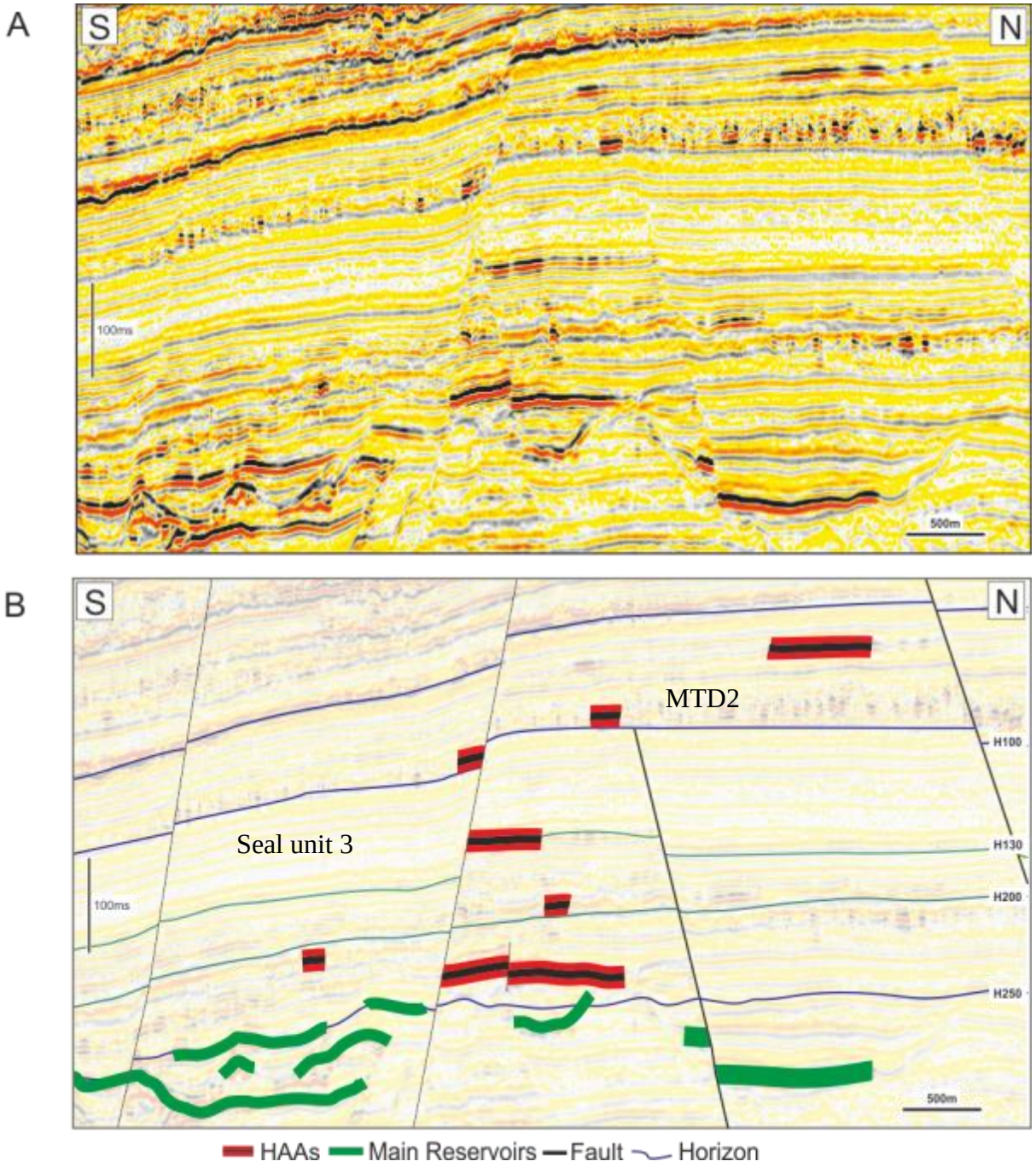

Figure 4.34: Seismic profile showing distribution of high amplitude anomalies through interval between H130 and H290. (A) North south seismic section has high amplitude anomalies associated with Stratigraphically and faults with relation to underlying Miocene turbidite channels. (B) Interpreted section of seismic profile. See Fig. 4.16 for location of seismic profile

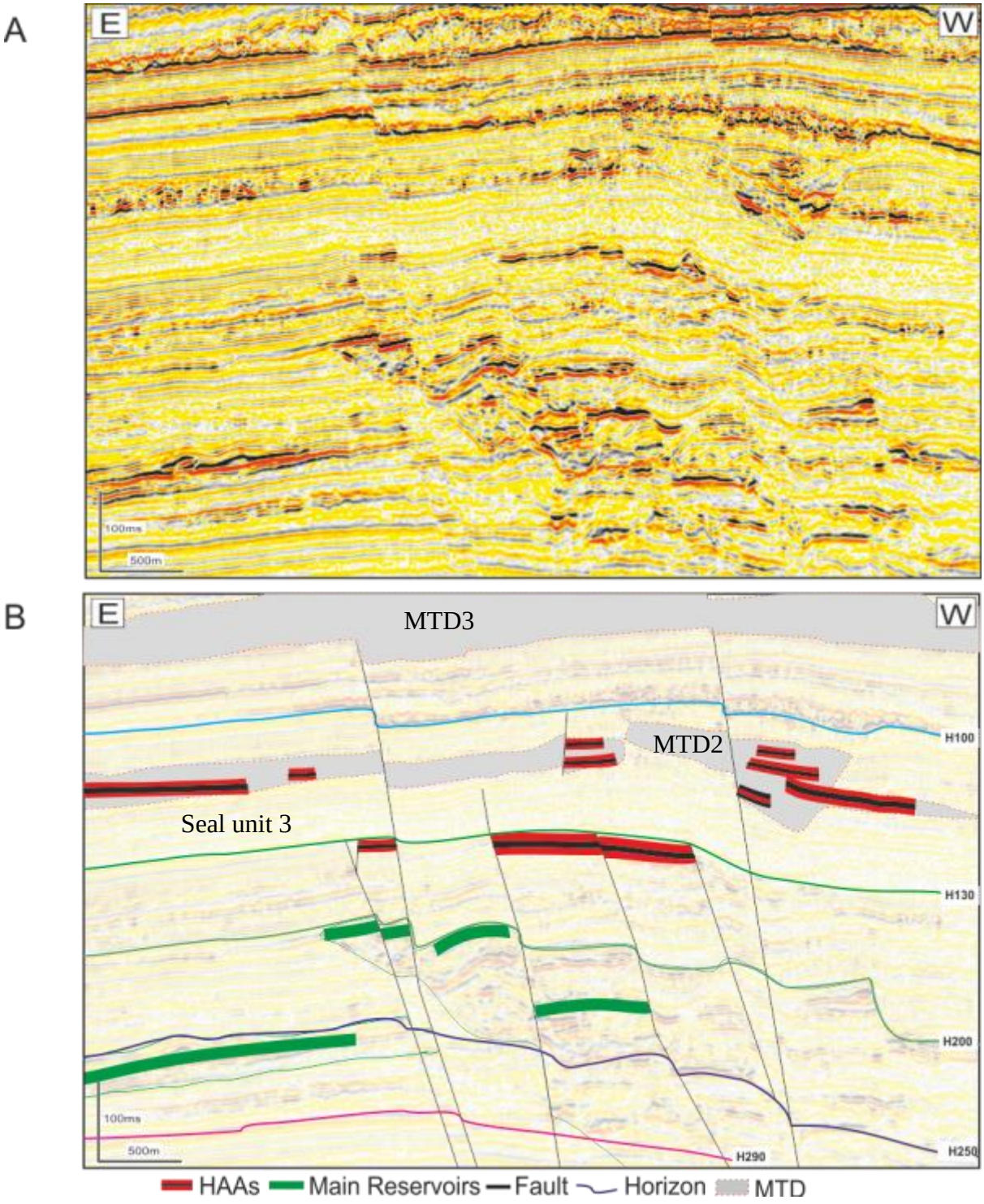

Figure 4.35: Seismic profile showing distribution of high-amplitude anomalies through interval H130 and H290. (A) East west seismic line shows high-amplitude anomalies associated with faults and MTDs. HAAs have strong relation to underlying Miocene turbidite channels. (B) Interpreted section of seismic profile See Fig. 4.16 for location of seismic profile.

4.9 Conclusion

Careful analysis of 3-D seismic data has revealed the occurrence of different types of high-amplitude anomalies in the overburden succession (Miocene to Holocene) of the study area. The four types of high-amplitude anomalies include linear, sub-circular, patchy and discrete filamental anomalies developed in the Miocene sediments. The high-amplitude anomalies generally occur in the middle and upper Miocene successions and represent shallow gas accumulations and/or diagenetic features associated with fluid flow through the sediments.

The main conclusions are:

1. The documented high-amplitude anomalies distributed in the Lower Congo Basin are developed in hemipelagite sediments and accumulated in to porous sediments and trapped against faults (Fig. 4.33 and Fig. 4.34).
2. The anomalies are direct hydrocarbon indicators.
3. High-amplitude anomalies associated with push down effects indicate the presence of gas and mostly type 1, 2 and 3are related to gas and typefour are possibly not related with any hydrocarbon.
4. Present day seabed pockmarks reflect the dynamic fluid flow in the system. I attribute the development of VACs to dominantly vertical gas migration across a multilayered low permeability reservoir interval (Fig. 4.35), where individual layers are filled successively from bottom-to-top, and where small normal faults provide conduits for cross-stratal migration.

CHAPTER 5

Hydrocarbon plumbing system: in the Lower Congo Basin

CHAPTER FIVE

5.1 Introduction

The study area for this chapter is a continuation of the previous chapter. The amplitude anomalies observed in the waste zone reveal a systematic, upward leakage of hydrocarbons (particularly gas) in a fine-grained sedimentary succession. The hydrocarbons leaked from a main Oligocene and Miocene turbidite channel levee system that is a proven reservoir in this basin. The main aim of this chapter is to determine the mechanisms by which fluids migrated from deep reservoirs and led to the development of HAAs. A second aim is to establish the hydrodynamic behaviour of identified hydrocarbon-related anomalies through their shape.

High amplitude anomalies as pockmark belts, giant pockmarks and gas chimneys in the shallow part from the basin are evidence of past and present-day leakage of liquid and gaseous hydrocarbon from deep-seated reservoirs (Cunningham and Lindholm, 2000; Pilcher and Argent, 2007; Kuhlmann *et al.*, 2011) and in particular offshore the Congo margins, where evidence of direct leakage from the reservoirs to the seafloor have been found in the Lower Congo Basin (LCB) (Gay *et al.*, 2006; Gee *et al.*, 2006; Andresen and Huuse, 2011; Anka *et al.*, 2012; Ho *et al.*, 2012).

The primary objectives of this chapter are to establish the formation processes of high-amplitude anomalies that were selected for further analysis at different levels of stratigraphic intervals for hydrocarbon leakage mechanism from main Oligocene-Miocene reservoir to waste zone in the Lower Congo Basin. These results are used to provide to explain leakage mechanism in the basin.

5.2 Mini case studies

Four types of high amplitude anomalies are observed in the study interval and particularly in to waste zone. Only patchy and sub-circular anomalies are selected for further fluid flow analysis because these anomalies have few ten meters in thickness and hundreds of meters in width where these high-amplitude anomalies are developed into channel levees, stratigraphic and faults traps (Fig. 5.1, Fig. 5.2 and 5.3). All these anomalies are linked with different styles of plumbing. The plumbing system of hydrocarbons has involved HAAs that have vertical and/or laterally direct or some evidences of connection with deepseated reservoirs. The connectivity between HAAs and the reservoir was established through various bypass systems that developed in low permeable, fine-grained sedimentary layers. The study area presents strong evidence that high-amplitude anomalies associated with channels levee system and gully have leakage pathways that associated with vertical cluster anomalies.

Analyses of three dimensional seismic data gave a better understanding of distribution of high-amplitude anomalies in the waste zone. On the basis of their plain view shape and geometry, location and lateral extent, the following three examples from hydrocarbon-related amplitude anomalies are selected for further analysis to better understand the hydrocarbon plumbing mechanism and formation of anomalies.

The selected mini case studies (CS) are;

1. CS-1: High amplitude anomalies developed along the channel levee complex in seismic interval H200-H250 (Fig. 5.1)

2. CS-2: Patchy high amplitude anomaly (P1a) developed as a linear future at seismic interval H130-H200 (Fig. 5.2)
3. CS-3: Patchy high amplitude anomalies developed along the faults in the northeast side of the study area between seismic horizons H130 to H200 (Fig. 5.2).

5.3 Stratigraphy of the study area

An overview of the regional geology is given in Chapter 4 Section 4.2.

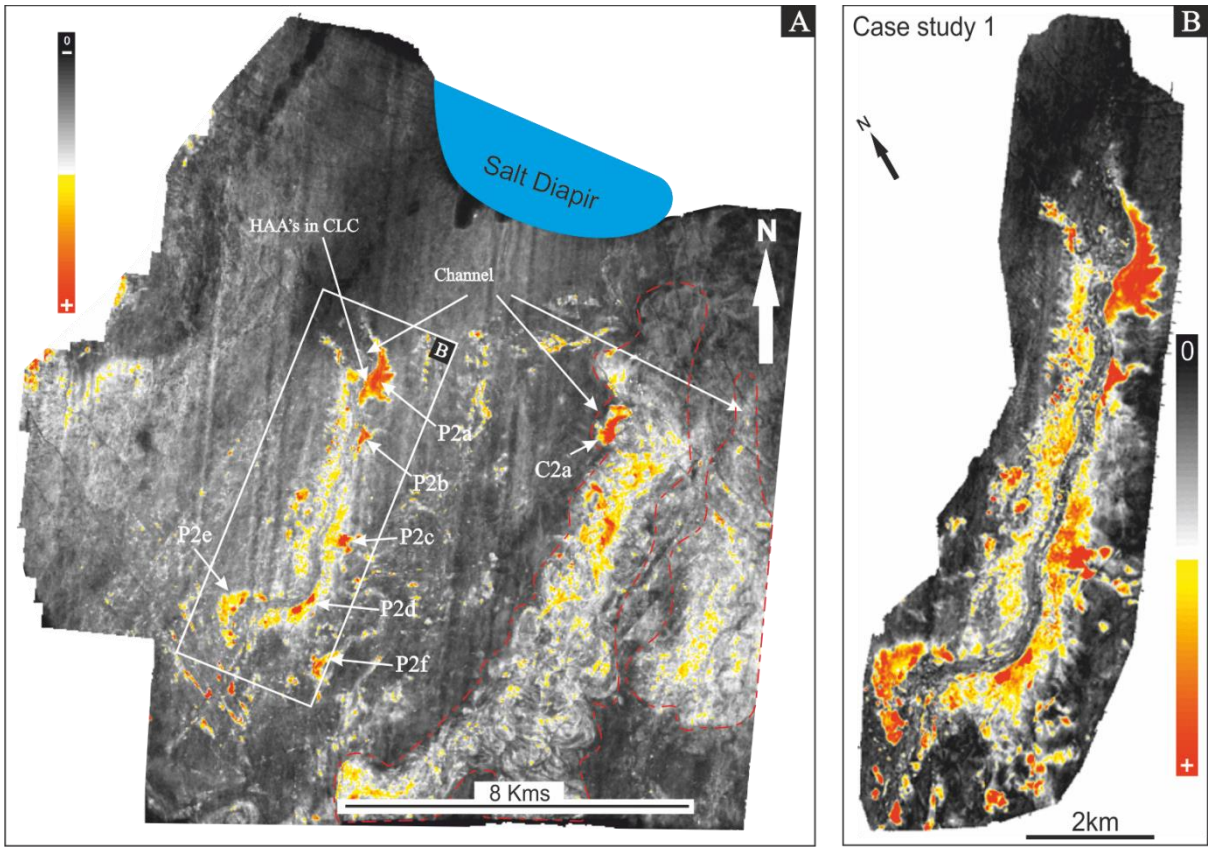

Figure 5.1: Root mean square amplitude map extracted between seismic horizon H200 and H250 (A) Shows high amplitude anomalies in the channel levee system of middle Miocene and Early-Mid Miocene erosive channel levee complex (red dotted boundary) with its flood plane extend (B) zoomed section of Channel levee system selected as a mini case study 1.

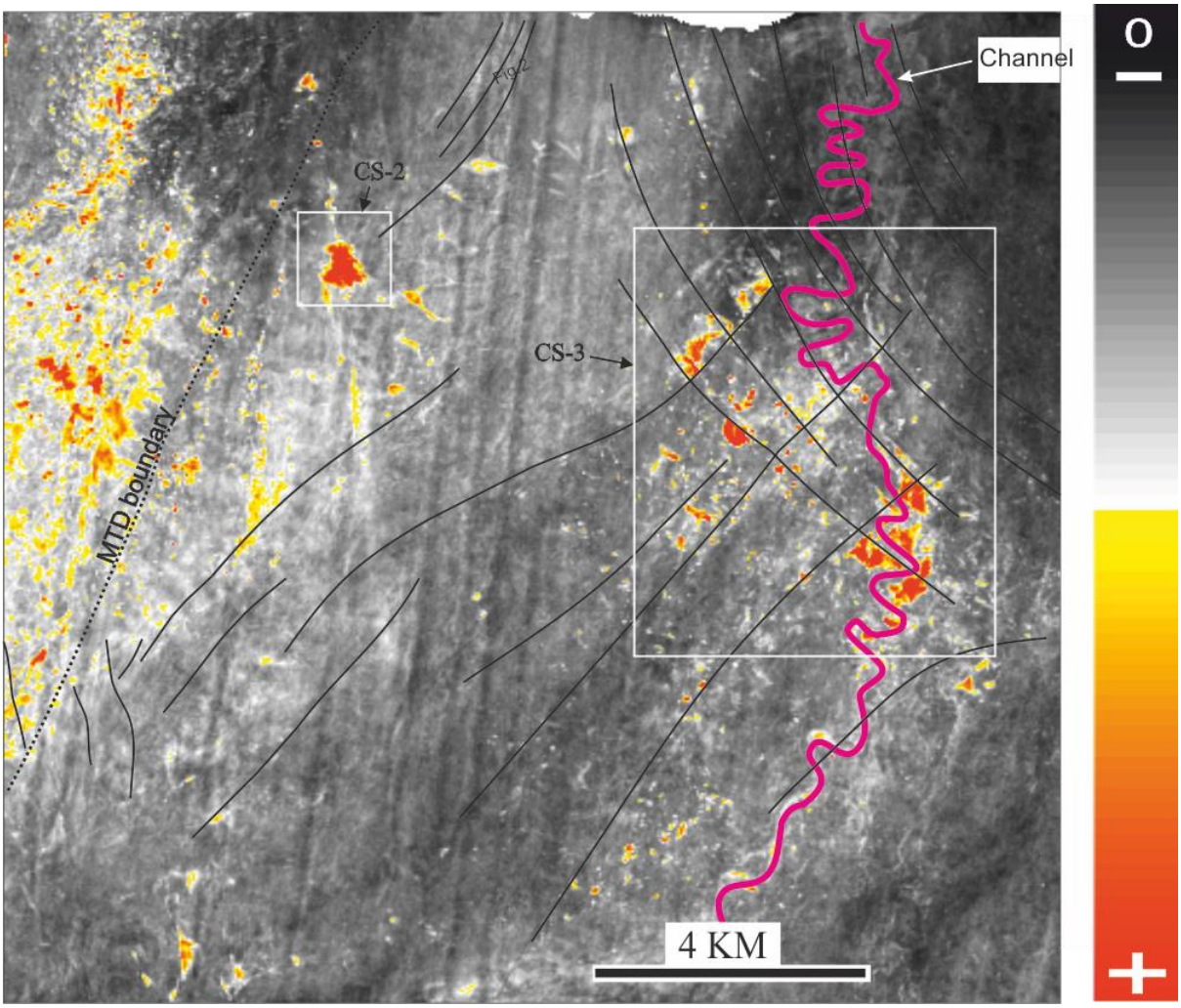

Figure 5.2: Root mean square amplitude map extracted between seismic horizons H130 and H200. The map shows high amplitude anomalies associated with mass transport deposit (MTD) on the west, linear anomaly in the middle and with fault bounded high amplitude anomalies on east part of the area. Linear anomaly and fault bounded high amplitudes are selected for further understanding fluid flow migration mechanism as a case study 2 and 3 respectively. White rectangles indicate mini case studies, pink curve is turbidite channel and black lines are faults.

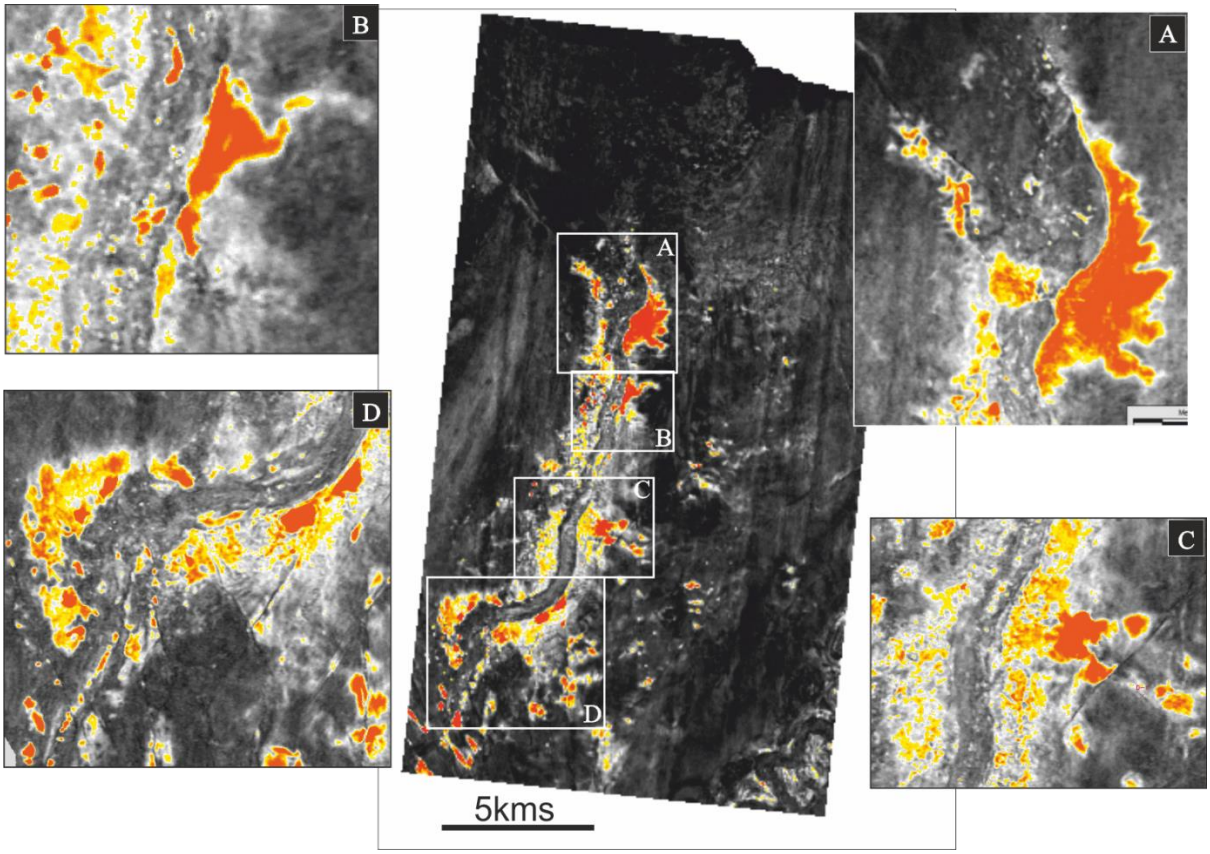

Figure 5.3: Root mean square amplitude map extracted between seismic horizon H130 and iso proportional slice H130_3 to shows mini case study 1. Case study is further divided from north to south into four different portions A, B, C and D. Amplitude anomalies developed into levees of turbidite channel system. Anomaly in c-portion terminated against fault.

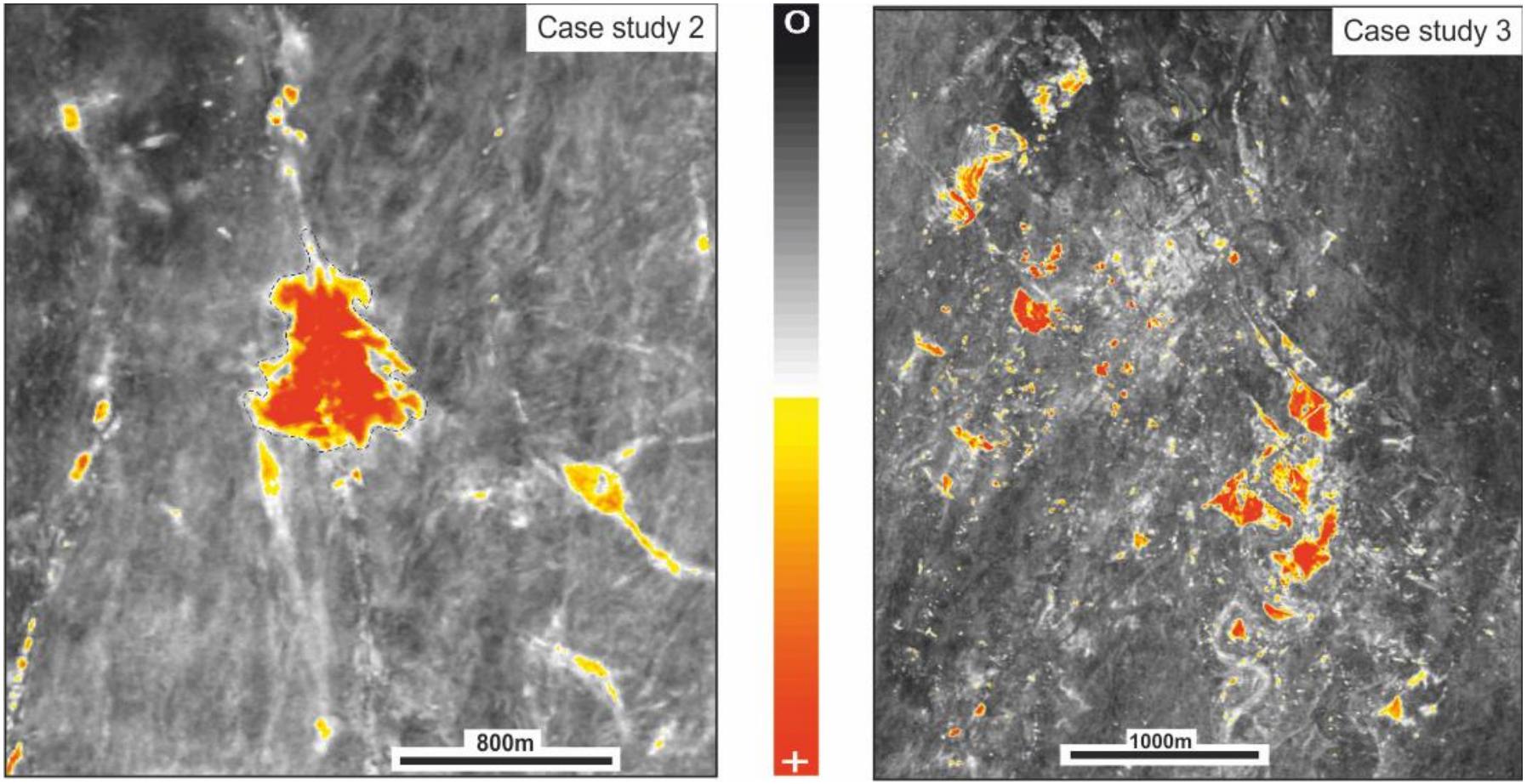

Figure 5.4: Zoomed RMS amplitude map shows extend of mini case studies 2 and 3. For location Fig. 5.2

5.4 Distribution of amplitude anomalies

High-amplitude anomalies observed at different stratigraphic intervals of middle Miocene successions are termed as the "waste zone" (Fig. 4.5). The waste zone was selected to understand the development of amplitude anomalies and their associated various types of fluid flow features. The overburden of the study area is composed of a 1.5 to 2 km thick interval of late Miocene to recent hemipelagite sediments which are above proven reservoirs of the Oligocene-Miocene turbidite channel levee system (Fig. 4.3 and 4.5) (Broucke *et al.*, 2004; Andresen and Huuse, 2011; Andresen *et al.*, 2011; Andresen, 2012; Anka *et al.*, 2012; Ho *et al.*, 2012).

A variety of hydrocarbon-related high-amplitude anomalies (Fig. 4.11 to fig. 4.13) occur in the middle Miocene interval including two types of anomalies; (1) Sub-circular and (2) Patchy anomalies. Patchy and sub-circular anomalies are developed in the waste zone of middle Miocene succession; a thick interval of hemipelagite sediments with turbidite channels and mass transport deposits (Fig. 4.5).

Three different mini case studies have been selected for further analysis of high-amplitude anomalies to establish fluid flow mechanism that formed them (Fig. 5.1 and 5.4).

5.4.1 Patchy anomalies along channel

A small channel runs north to south and deflects around a salt structure in the northeast. Amplitude anomalies are observed only along 12 kilometers section in the levees of the mud-filled channel (Fig. 5.5). The central channel is acoustically dim and interpreted as a mud-plugged whereas the levees are bright and are probably hydrocarbon-filled sandbodies. Amplitude anomalies along the channel (Fig. 5.5) are developed in a northwest-south oriented anticline. The structure map in depth shows that the anomalies in the levees (mud

plugged channel) are only bright in the area of structural closure. This led to the conclusion that; masking of non-bright sandstones/porous units may have further lead to underestimates of the connectivity and hampered a correct seal assessment but may also provide a classic example of a DHI. A structural contour map in depth has been computed over the H200 horizon with 50m interval to confirm location of channel levee complex. High amplitude anomalies lie between contour values 1350-1400 (Fig. 5.5).

The extent of the amplitude anomalies from the axis of channel vary from a few hundreds of meters to two kilometers (especially amplitude anomaly P2a in fig. 4.1) (Fig. 5.6). The thickest amplitude anomaly (P2b) is measured as being 21ms thick and has a 7ms TWT push down effect. In general, at the margins of anomalies, there is a tuned and paired response with a subjacent hard event, but where thickest, the levee unit has a separation into the soft event, and an underlying flat hard event interpreted as the HWC. The vertical resolution of the data is c. 7m, so the separation occurs where the thickness of the reservoir unit in the levee (HC filled) is > than c. 8-10m.

Amplitude anomalies observed along the channel have a strong spatial relationship with the underlying Late Oligocene and Early Miocene main turbidite reservoirs (upper and lower reservoir) (Fig. 5.7). The sharp, lateral margins imply a rapid cut-off of fluid content (indicated by arrows in Fig. 5.8), from hydrocarbon-filled to pore water. If the HC are gas, as seems likely, then low saturations consider as a CS-3 could result in the amplitude response. The sharp cut-off may not be a dramatic change of saturation but could indicate only a few percent of saturation difference (Knight *et al.*, 1998).

Seismic acoustic features like soft reflections, flat spots, velocity pushdown effect, and blanking below anomalies leads us to conclude that patchy anomalies are developed due to presence of gas in the porous and permeable layers of sand units in the levee.

5.4.2 Patchy anomaly in gully feature

The selected high amplitude anomaly observed in middle Miocene stratigraphic Unit 2b (Fig. 4.5) is in porous sediments beneath the regional MTD/Seal Unit 3 (Unit 2d). The anomaly is developed in porous and permeable sediments deposited in the gully (Fig. 5.11) that cross cut mud-wave features (Fig. 5.2). The linear feature is below the MTD so it is not due to sliding blocks of the MTD (Fig. 5.9). No direct leakage evidence is observed above amplitude anomaly which implies that the MTD above the anomaly is a regional seal Unit 3 and is acting as a prefect seal (Fig. 5.10).

The polarity of the anomaly is opposite of the seabed and is interpreted as a soft event. Seismic acoustic features like flat spots, velocity push down effect and dimming of seismic reflections (Fig. 5.12B C, and F) below anomalies are interpreted as being due to the presence of gas in the host sediments. Finger-type features (labelled 1 to 9) emerge from the anomaly on RMS amplitude map extracted between seismic horizon H130 and iso-startal horizon H130_3 about 30ms two way time interval (Fig. 5.12A). The zoomed RMS amplitude maps of the anomaly illustrate the imbibition effect and help us to understand its development (Chapter 6 for more details). The representative seismic profiles (B to F) display seismic blanking, soft anomalies (HAAs) that surround the main anomaly and are directly above the main turbidite reservoir channel.

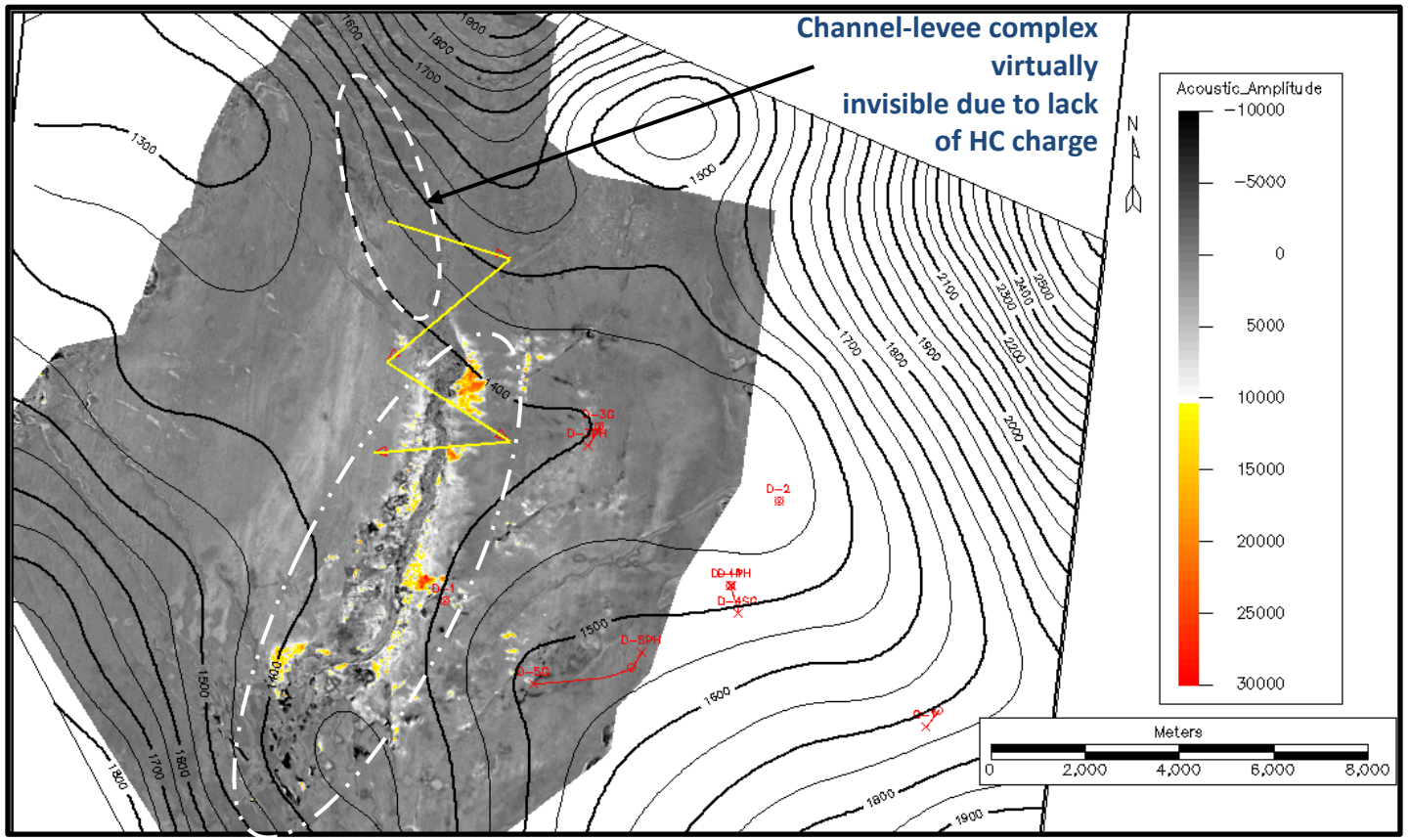

Figure 5.5: Structure contour map in depth showed that high-amplitude anomalies in the levees (mud plugged channel levee system) only bright at structural closure. High amplitude anomalies lies are confined at crest of anticlinal structure. The channel is virtually invisible at deeper side due to lack of hydrocarbon accumulation. Structural contour map in depth computed over H200 horizon with 50m interval to confirm location of channel levee complex. High amplitude anomalies lie between contour values 1350-1400 meter of c. I 50 meter thick

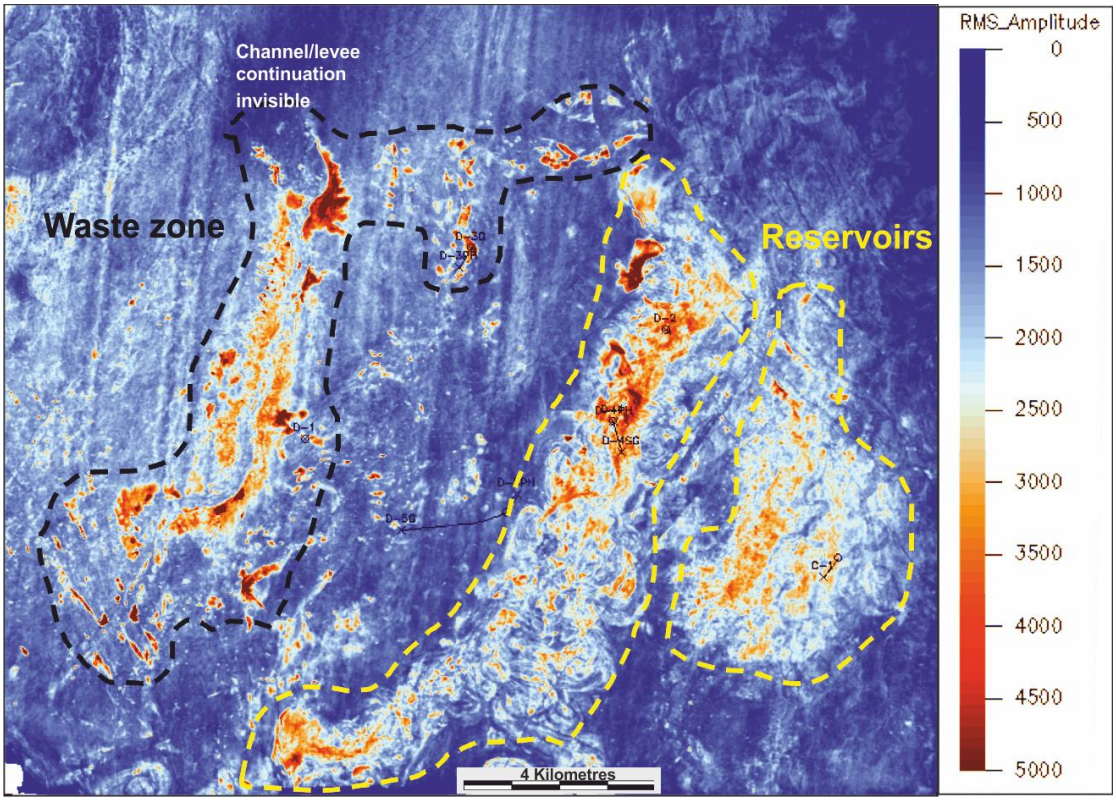

Figure 5.6: RMS extracted between 20ms thick interval from iso-proportional seismic horizon H200_2 (30ms below from H200) and Iso-propportional seismic horizon H200_5 (50ms below from H200) , showed a extent of mud filled channel levee system (black dotted line) in the waste zone and related Early Miocene turbite channels (yellow dotted line). Black dotted line marked the boundary of bright amplitude that developed in the levees. Channel continuation is invisble on north and south side due to hrdrocarbon charging limit (Fig. 5.5)

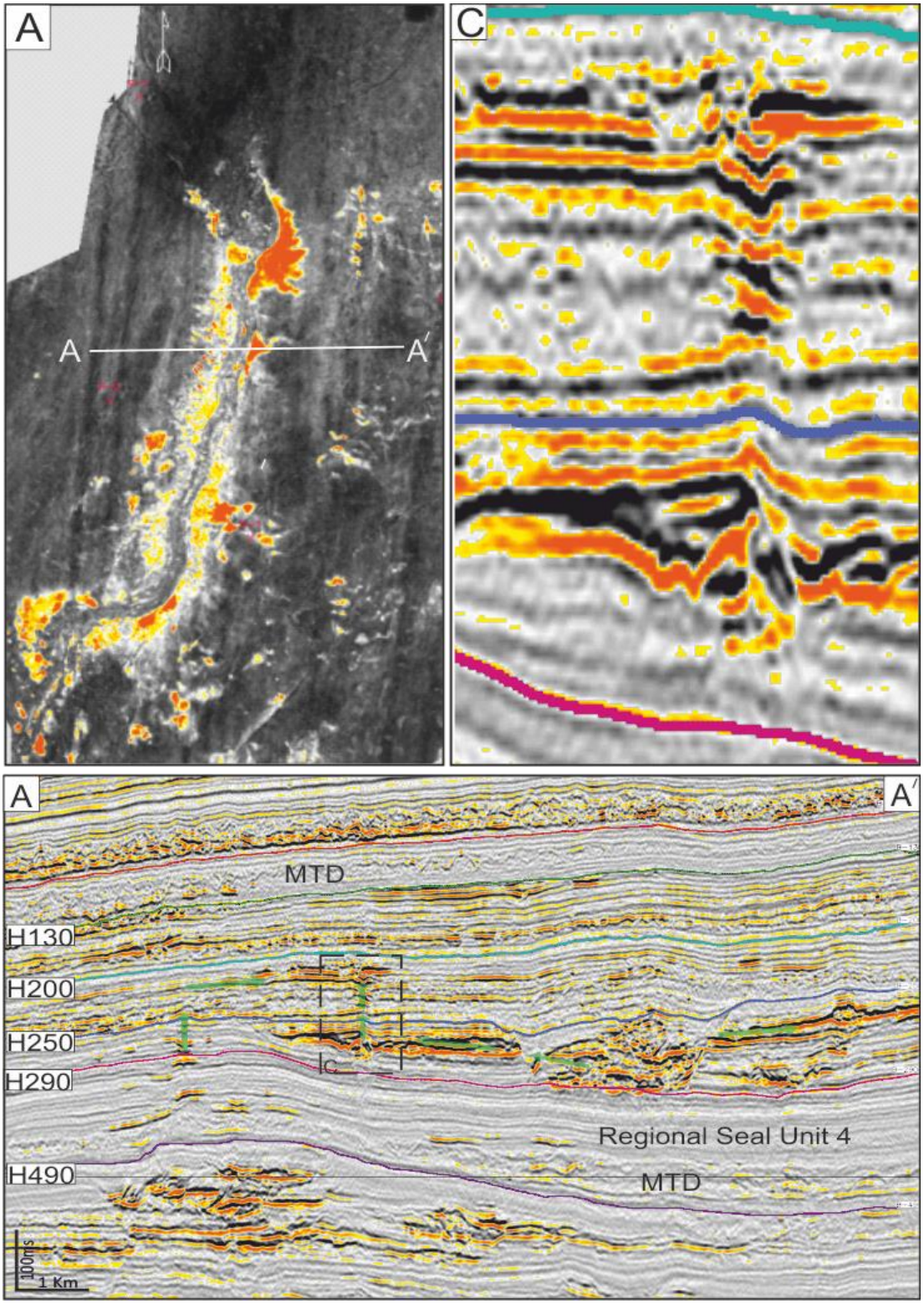

Figure 5.7: Overview of amplitudes along Channel Levee Complex: A) RMS amplitude map computed from mapped horizon H130 to 30ms below showing amplitude distribution along the channel. B) E-W seismic profile shows possible migration path from overlying the Lower Miocene turbidite channel. C) Zoomed section of seismic profile shows amplitude variation through VACs. MTD: Mass transport deposit

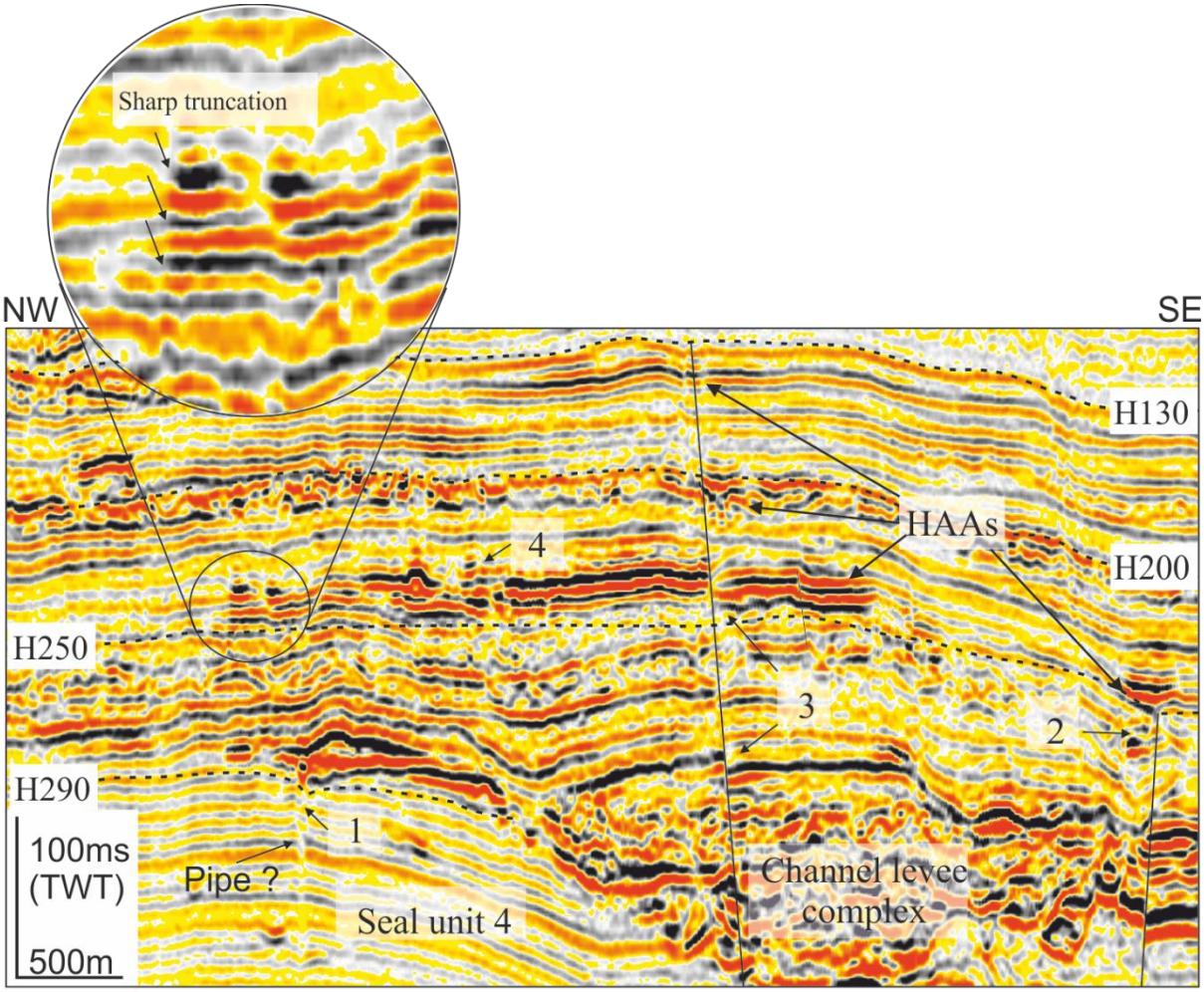

Figure 5.8: High-amplitude anomalies associated with CS-1 that developed above the main turbidite reservoir. Local compaction observed at the thickest part of anomaly. Possible four pathways are mentioned here and labelled 1 to 4. Amplitude anomaly truncated very small fault.

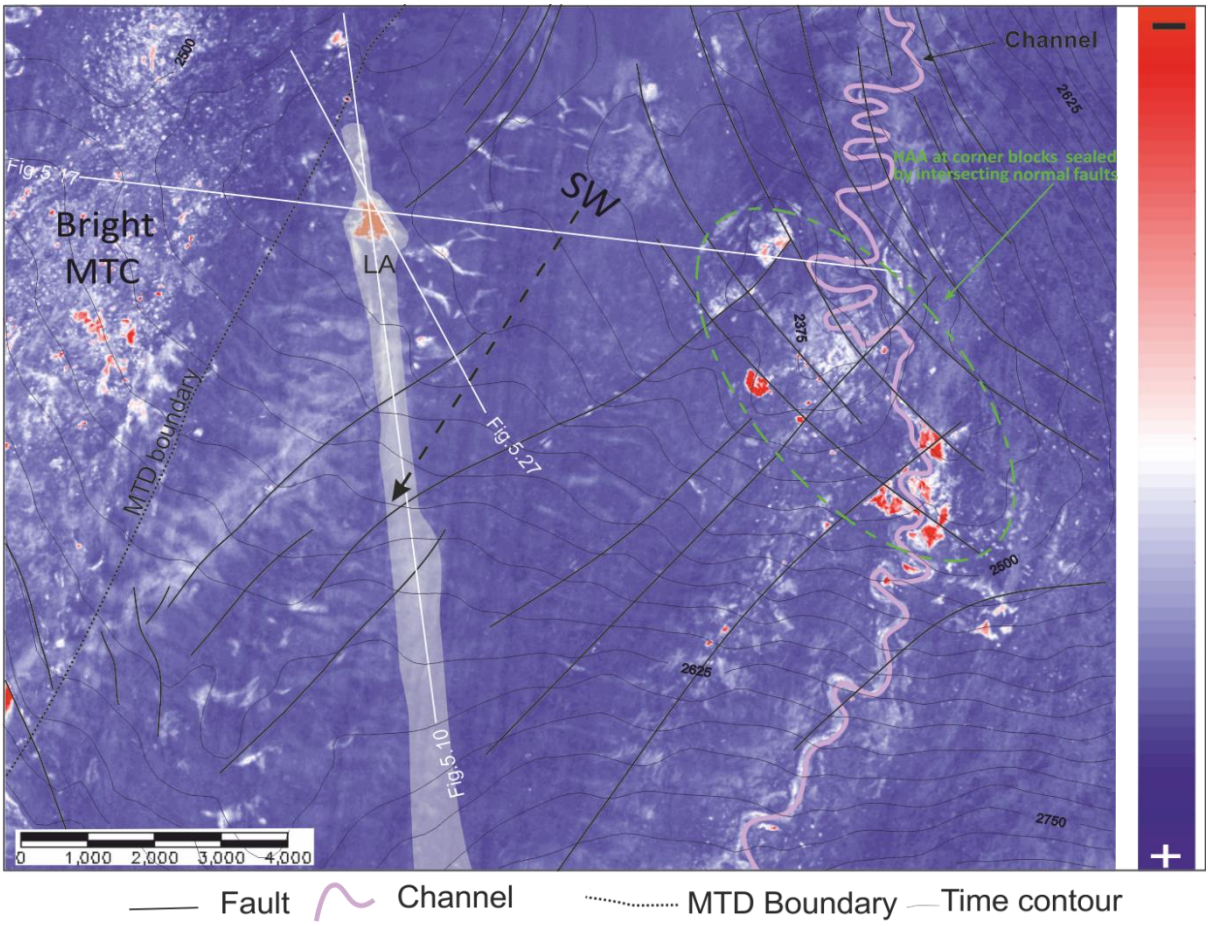

Figure 5.9: A minimum amplitude map computed between horizon H130 to iso-stratal horizon H130_3 about 30ms thick time interval showing orientation of channel and faults. Linear feature of high amplitude is developed at the mapped horizon H130. A channel is mapped from North south cross cut by faults. Time structure contour of Horizon H130 showing local highs (25ms contour interval). SW: Sediment waves; LA: Linear Anomaly; MTC: Mass Transport Complex; MTD: Mass Transport Deposit.

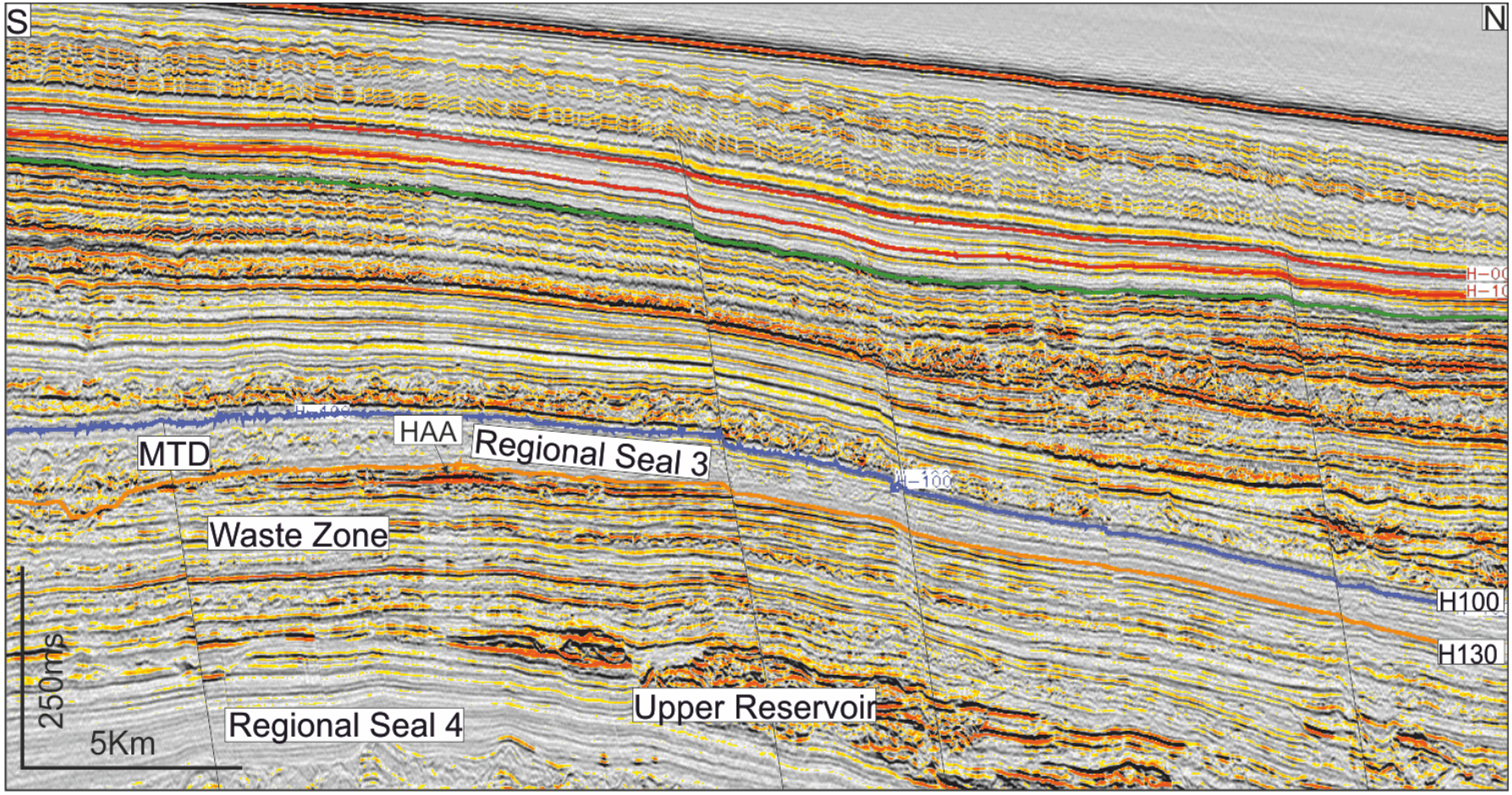

Figure 5.10: N-S seismic profile showing LA developed at north south closure. The MTD is acting like as a seal. HAA: High amplitude anomaly; MTD: Mass transport deposits. For location Fig. 5.9

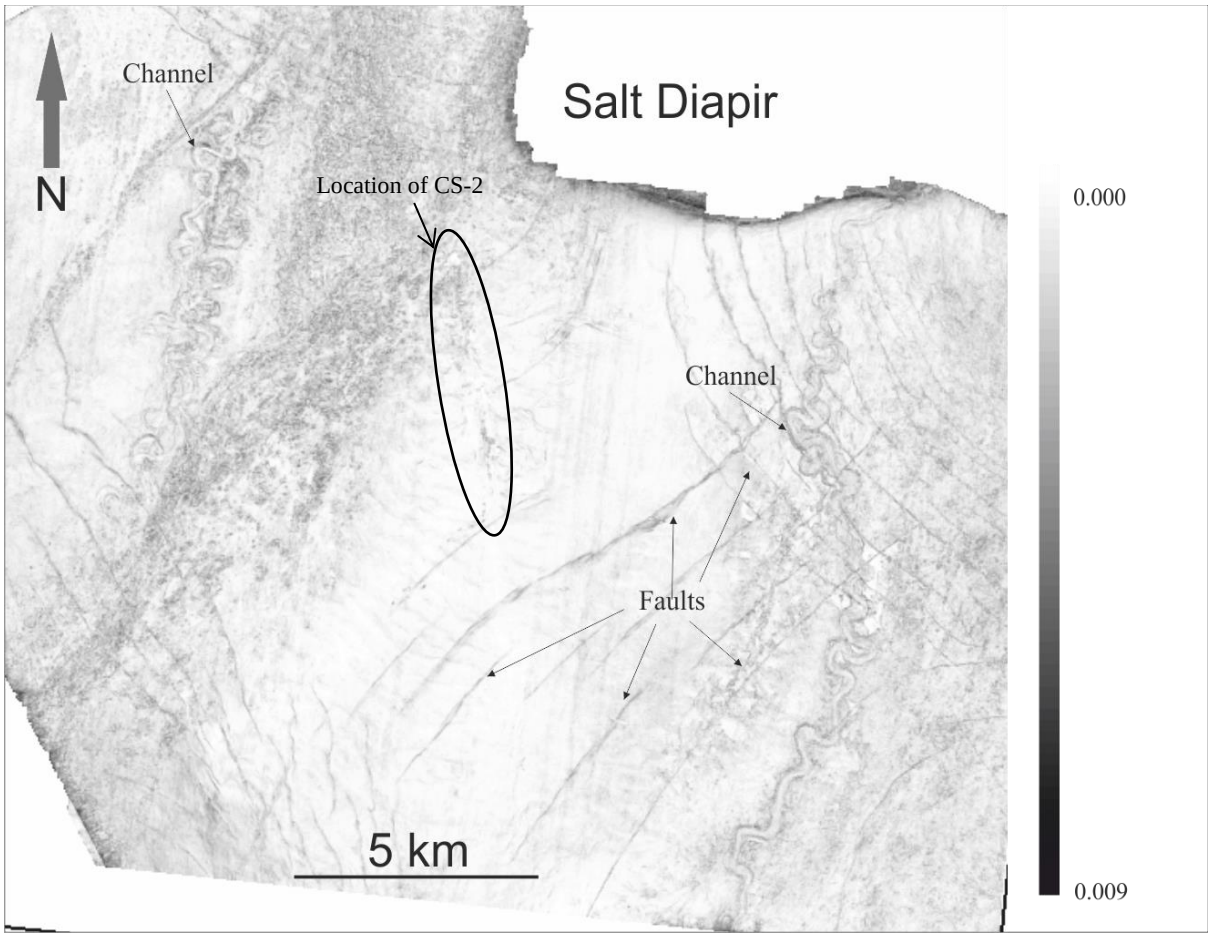

Figure 5.11: Time-dip map of seismic horizon H130 showed geological features, faults and north-south oriented turbidite channels. The parabola is indicating location of P1a patchy anomaly that is independent mini case study 2.

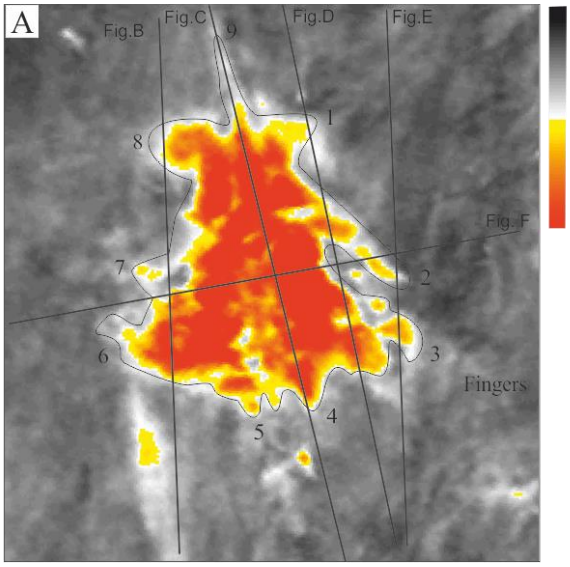
A
Fig.B
Fig.C
Fig.D
Fig.E
Fig. F
1
2
3
4
5
6
7
8
9
Fingers
500 meters

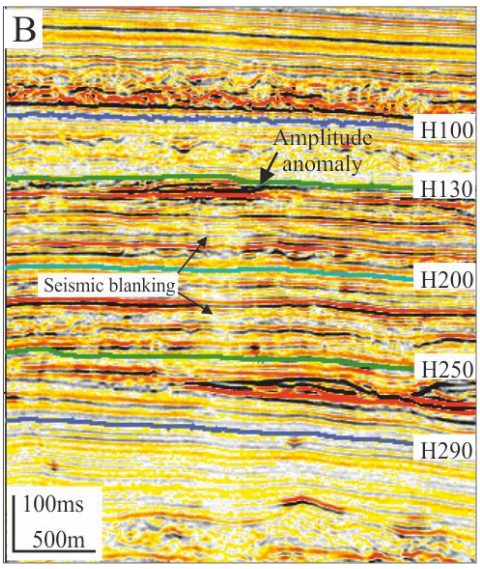
B
Amplitude anomaly
H100
H130
H200
H250
H290
Seismic blanking
100ms
500m

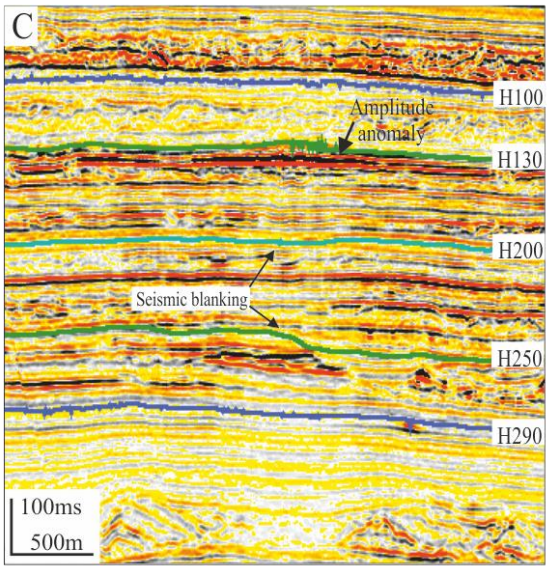
C
Amplitude anomaly
H100
H130
H200
H250
H290
Seismic blanking
100ms
500m

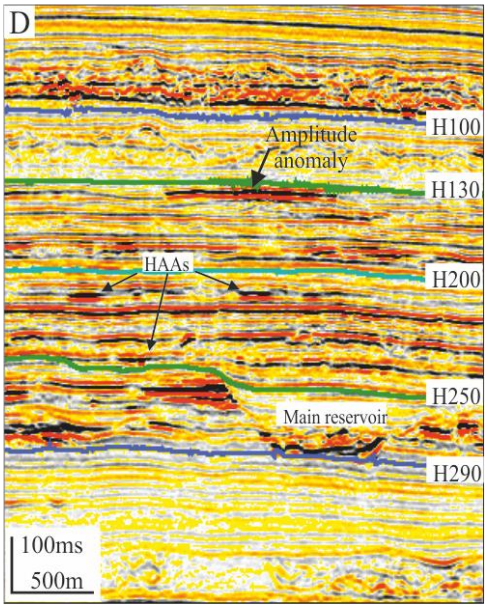
D
Amplitude anomaly
H100
H130
H200
H250
H290
HAAs
Main reservoir
100ms
500m

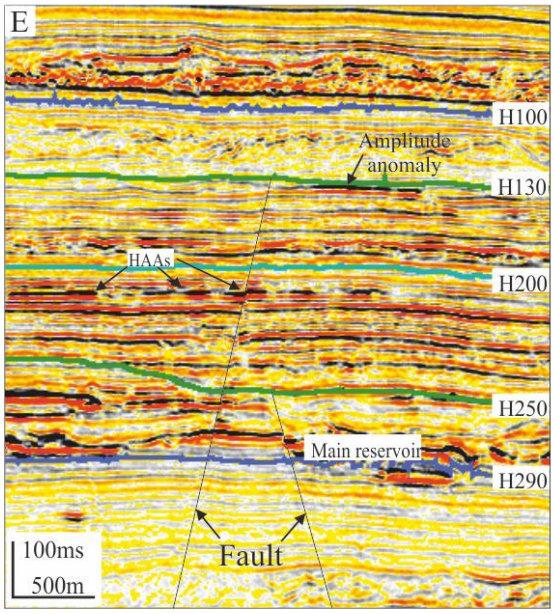
E
Amplitude anomaly
H100
H130
H200
H250
H290
HAAs
Main reservoir
Fault
100ms
500m

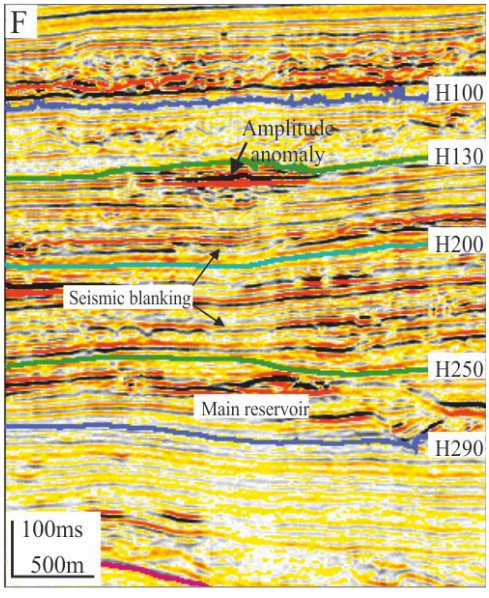
F
Amplitude anomaly
H100
H130
H200
H250
H290
Seismic blanking
Main reservoir
100ms
500m

Figure 5.12: The selected high amplitude anomaly observed at early Pliocene sediments below a regional MTD/Seal unit 3. Linear feature of the linear anomaly is still under research but interpreted as a gully cross cutting mud wave features. The linear feature is below the MTD so it is not due to sliding block of MTD. NW-SE seismic profile showing the flat spot and the anomaly is a soft reflection. A) The zoomed RMS amplitude maps of the anomaly illustrating the imbibition effect and help us to understand its development. The representative seismic profiles (B to F) are displaying/showing seismic blanking, soft anomalies (HAAs) that are observed in the surroundings of main anomaly and directly above the main turbidite reservoir channels.

5.4.3 Fault bounded anomalies

The near-offset, time-migrated three-dimensional seismic volume was interpreted in great detail over the northeast structural domain. The northeast domain has two fault arrays; type-1 faults which strike NW-SE, and type-2 faults which strike NE-SW (for more detail chapter 4 section .4.3, Fig. 4.14 and Fig. 5.9). In CS-3, the lateral terminations of gas-related patchy and sub-circular anomalies are bound by normal faults. NNE to SSW oriented turbidite channels are displaced by normal faults. High amplitudes are bound by faults and locally conform to structure (Fig. 4.28). Hydrocarbons are only trapped by those faults passing through the deep turbidite channels (Fig. 5.13, Fig. 5.15 and 5.17).

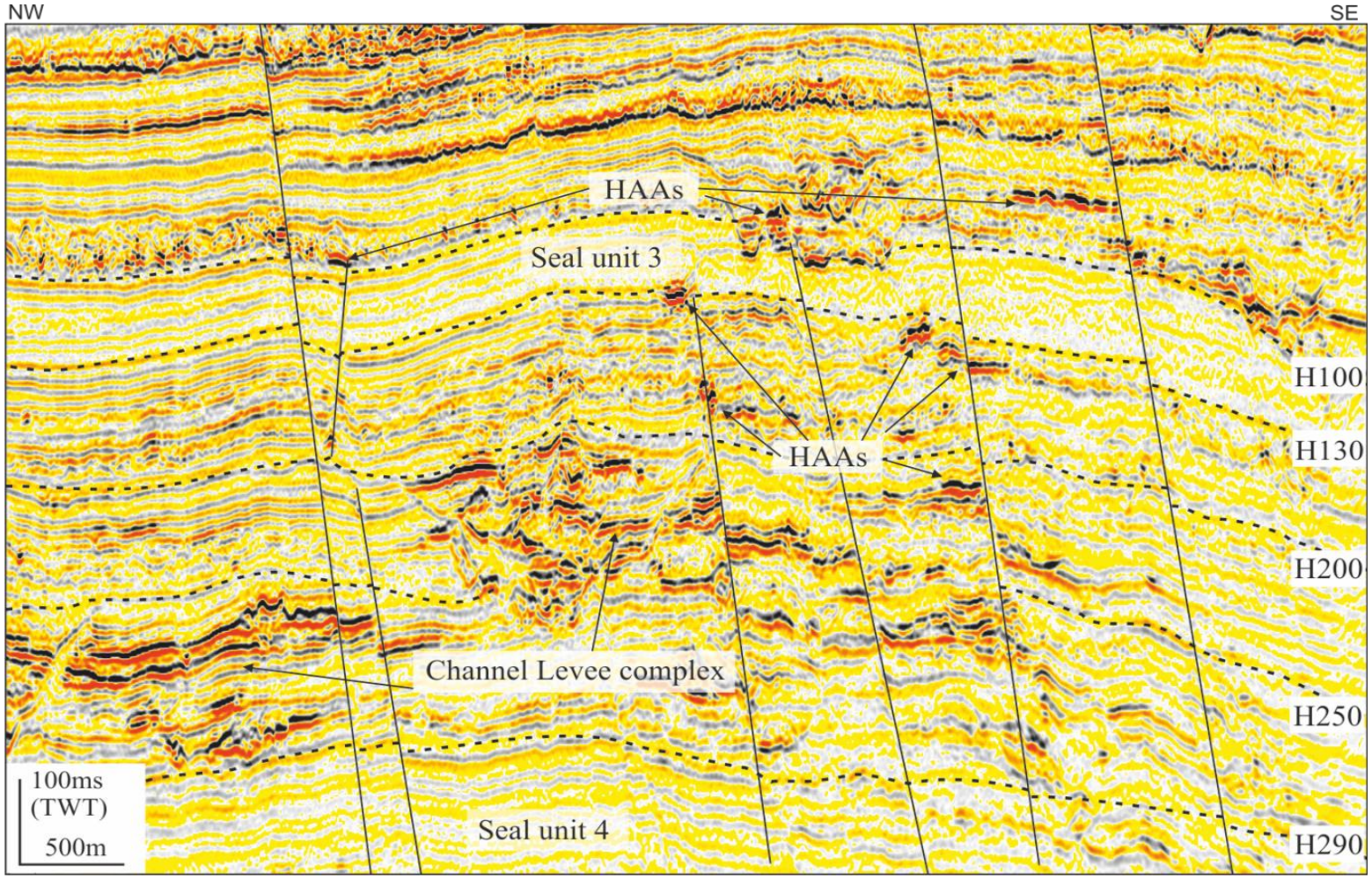

Figure 5.13: Example of distribution of high amplitude anomalies in the waste zone (H290 to H130). Amplitude anomalies observed above Miocene Turbidite main reservoir. All these anomalies developed in stratigraphic interval between H220 and H130 and trapped against normal faults have few meters throw.

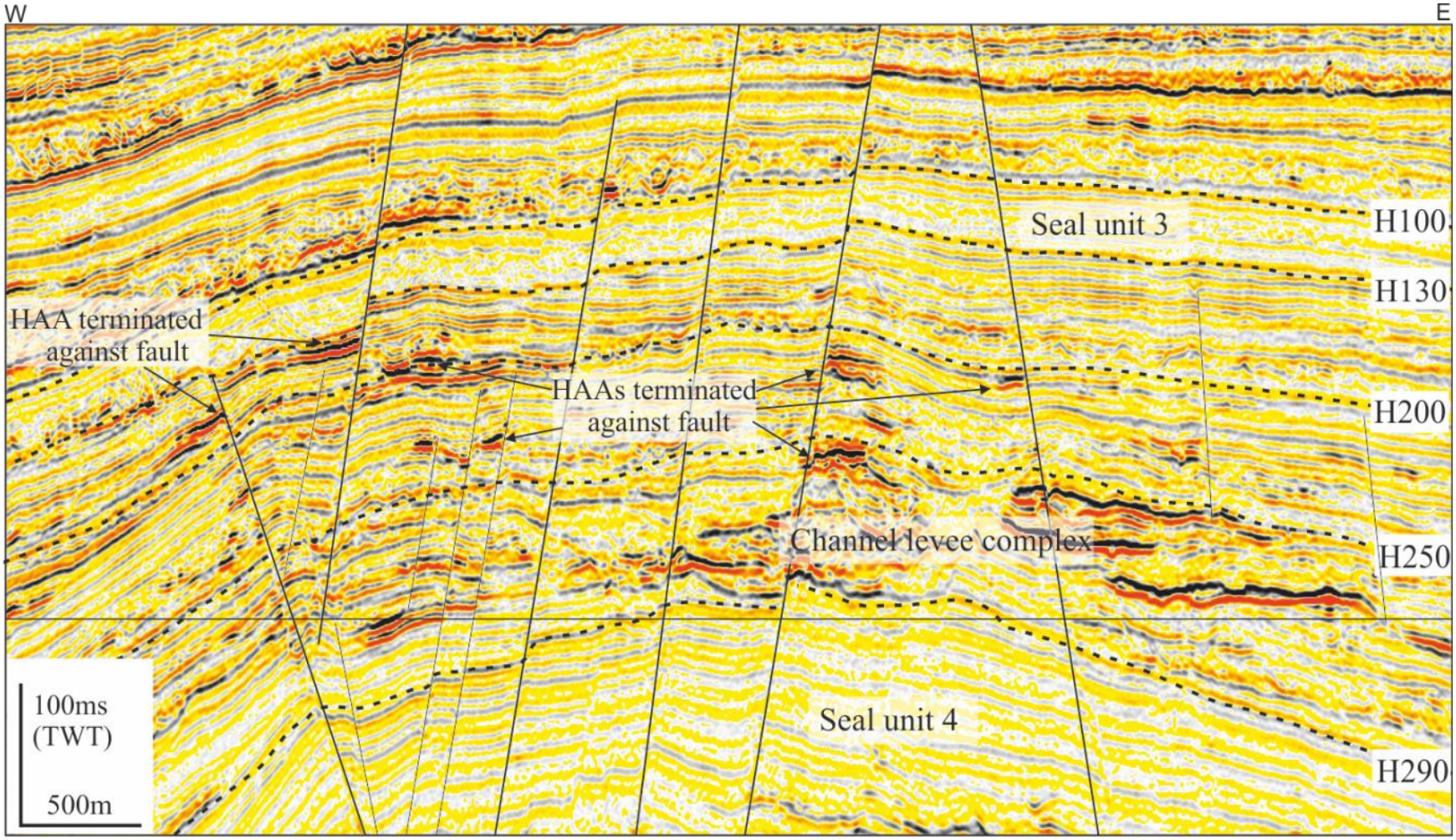

Figure 5.14: seismic line showing examples of high-amplitude anomalies developed against normal faults between stratigraphic interval between H250 and H130 in the waste zone.

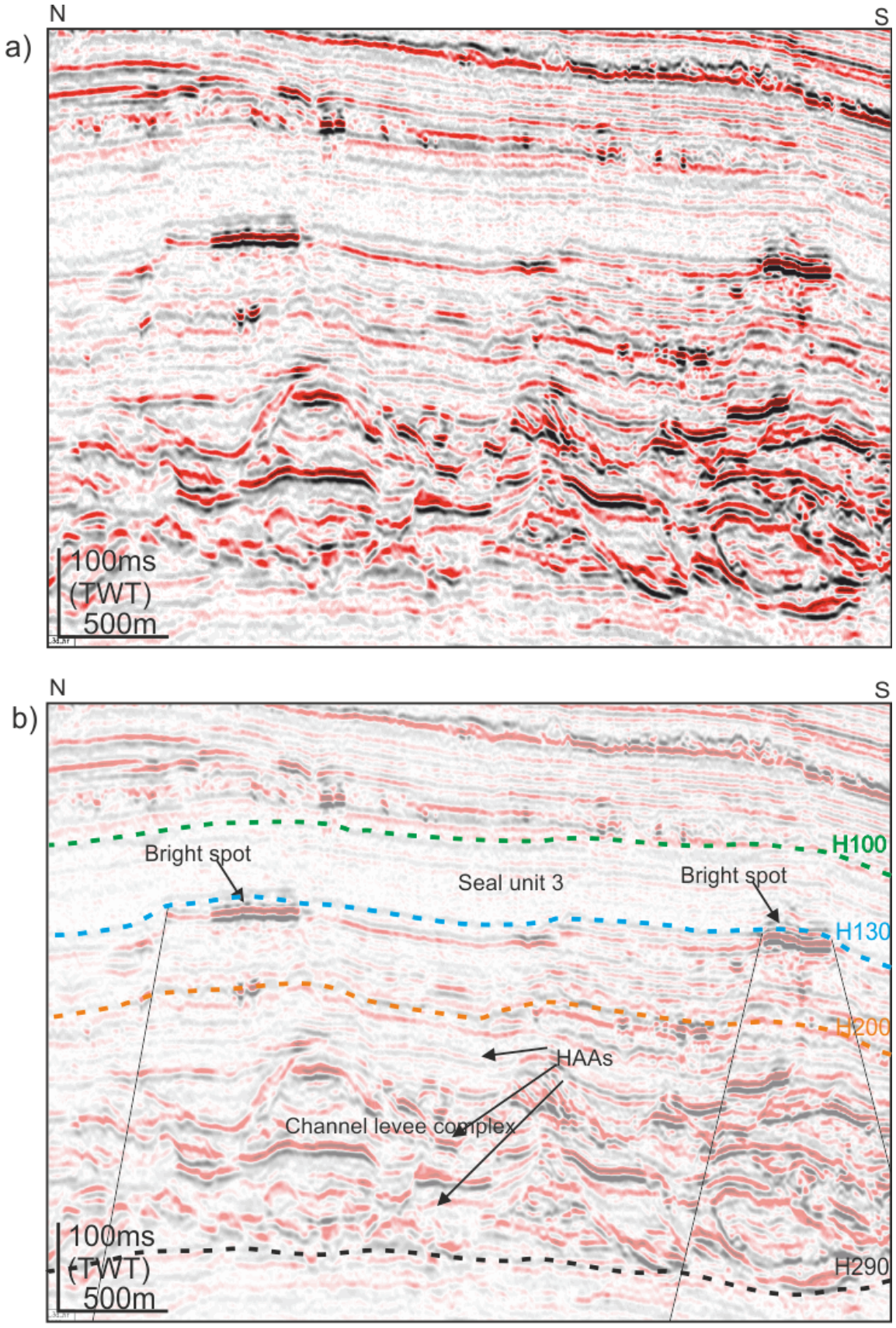

Figure 5.15: seismic line showing examples of high-amplitude anomalies developed against normal faults between stratigraphic interval between H250 and H130 in the waste zone.

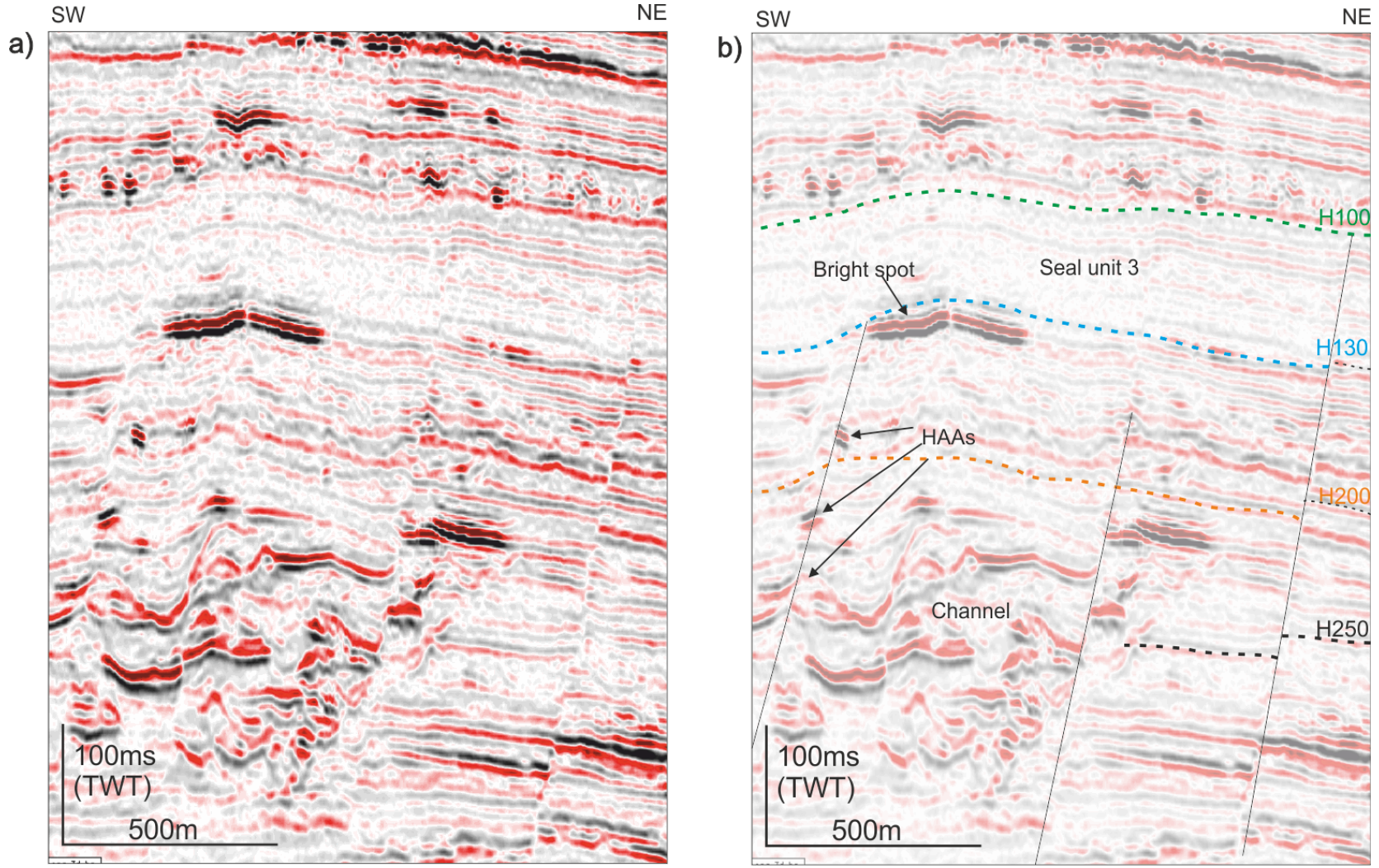

Figure 5.16: Seismic profile show amplitude anomalytrapped against a normal fault tjhat pass through deeper main turbidite reservoir.

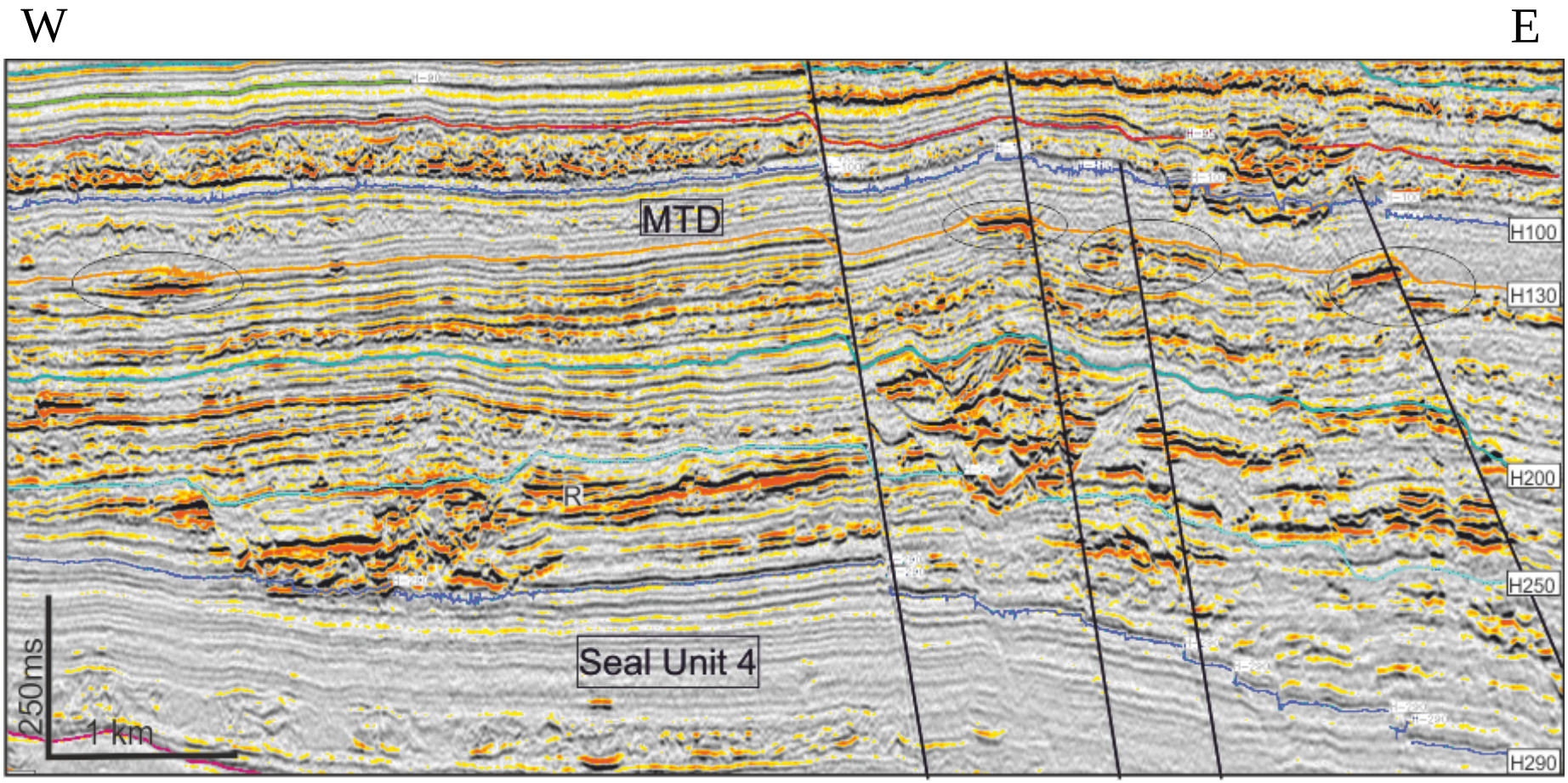

Figure 5.17: E-W seismic section passing through LA and fault bounded HAAs showing possible feeding points from the deeper reservoirs possibly through faults and stratal paths for migration of hydrocarbon. For location Fig. 5.9

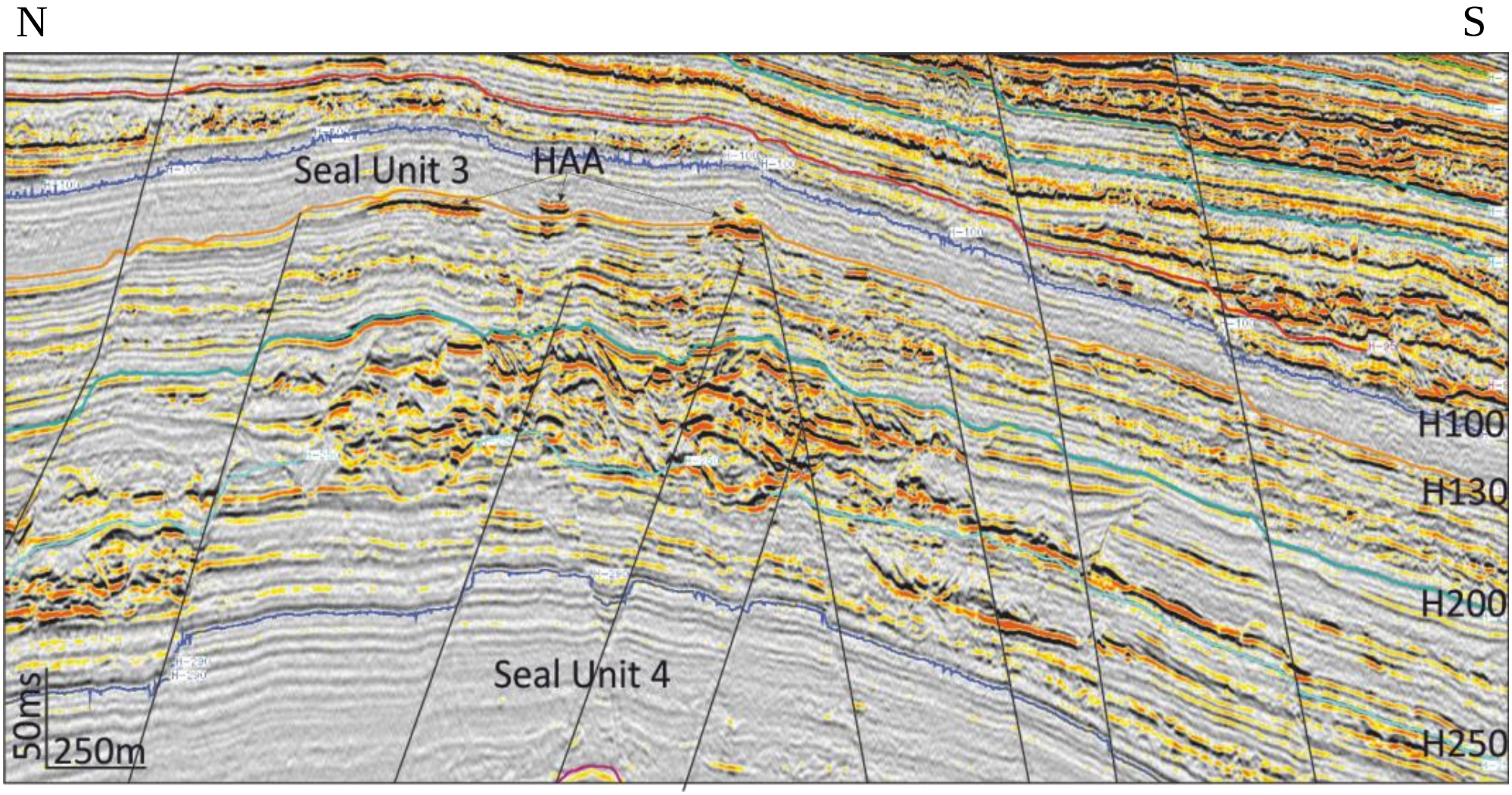

Figure 5.18: N-S seismic profile showing accumulation of high amplitude anomalies confirming the local structural high and associated with faults.

5.5 Discussion

5.5.1 Fluid flow features in Waste Zone

The waste zone succession comprises a 1.0 km thick interval of Late Oligocene to Middle Miocene hemipelagic sediments (Fig. 4.5 and Table 4.1). The overlying sediments are about the same thickness of 1.0 Km from the Late Miocene to recent. The overlying sediments comprises two tiers of polygonal faults with focused fluid flow features including; present day sea floor pockmarks, Pliocene-Pleistocene stacked pockmarks, and Miocene pockmarks (Giresse, 2005; Gee *et al.*, 2006; Gay *et al.*, 2007; Andresen and Huuse, 2011; Andresen *et al.*, 2011; Vemba *et al.*, 2011; Anka *et al.*, 2012). These fluid flow features commonly affect the stratal reflections in the both sedimentary successions. High density three dimensional seismic data reveal numerous types of fluid flow features related to amplitude anomalies in the waste zone. Mostly patchy and sub-circular anomalies are observed in the thicker part of waste zone. The interval is mainly composed of fine-grained sediments embedded within Oligocene and Miocene turbidite channel levee complexes (Séranne and Nzé Abeigne, 1999; Anderson *et al.*, 2000; Cole *et al.*, 2000) that are proven hydrocarbon reservoirs in the Lower Congo Basin (Gay *et al.*, 2006; Andresen, 2012; Anka *et al.*, 2012; Ho *et al.*, 2012). The waste zone is bounded by continuous, seismically transparent intervals of few meter thickness which are interpreted here as regional seal unit because no high-amplitudes are observed in the interval.

Andresen (2012) observed fluid flow features in the Lower Congo Basin and described a variety of fluid flow features like high amplitude pies, paleo and present day pockmarks, high-reflectivity zones, and seismic chimneys. Many other authors have presented work on fluid flow in Lower Congo Basin (Gay *et al.*, 2007; Anka *et al.*, 2012). Ho *et al.* (2012) presented conceptual model for the evolution of fluid venting structures in term of pipes and

pockmarks that developed due to slow and then fast fluid flow expulsion and which were sealed afterward with fine-grained sediments. All of the present day pockmarks at the seabed (Fig. 4.6); (Ho, et al 2012; Andresen, 2012; Gay, 2007) reflect current fluid flow activity in the study area.

Direct hydrocarbon indicators such as bright spots, flat spots, velocity push downs, polarity reversals, and seismic blanking are sporadically observed within the waste zone that developed within the turbidite mud-filled channel (Fig. 5.1 and 5.3), gullies (Fig. 5.2) and fault bounded traps (Fig. 5.4). DHI's in the Miocene succession indicate the presence of hydrocarbons (probably gas) in the system (for more details chapter 4, section 4.5.2).

The high resolution seismic profiles through high-amplitude anomalies reveal thick accumulation of acoustically semi-transparent to transparent reflection composed of different levels of mass transport deposits (MTDs) and single to multi-storey turbidite channel levee systems (Fig. 5.18). High-amplitude anomalies observed in the main channels and their extended levees that reach ten to a few hundred meters in width, for further understand hydrocarbon migration.

5.5.1.1 Vertical anomaly cluster: A new DHI?

The most dominant amplitude feature in the middle Miocene stratigraphic interval is a systematic, vertically-stacked group of stratigraphically-concordant amplitude anomalies termed here as Vertical Anomaly Clusters (VACs). Foschi *et al.* (2014) defined VACs as assemblage of high-amplitude anomalies or bright spots in the fine-grained sediments where the assemblage is demonstrably linked by the hydrocarbon migration process. VACs interpreted were based on regional 2D survey of the East Falkland Basin. VACs occur in the

stratigraphic intervals Unit2 b between seismic horizon H250 and H200 (Fig. 5.7) and Unit2 c between seismic horizon H200 and H130. The observed VACs developed between levees of Mid Miocene turbidite channels (Upper channel) to amplitude anomalies in CS-1 (stage-1) and then in later from CS-1 to amplitude anomaly developed in gully CS-2.

VACs in the waste zone are 100 meters thick and 100-500 meters wide bright reflection that stands out from the host reflections (Fig. 5.7B). Most of the anomalies have an extremely sharp cut-off in amplitude at their margins across few meters c.a 100 meters. Amplitude reflections are concordant with the background strata and have no sign of disturbance (Fig. 5.7C and Fig. 5.21) that would suggest that amplitude have same lithology for the anomalies (Løseth *et al.*, 2009; Foschi *et al.*, 2014). The length of individual amplitude anomaly increased in upper layers that suggest anomalies are charged from deep layer to shallow layers (Fig. 5.21C).

5.5.1.2 Fault bound anomalies

Faults are present in basically every sub-basin throughout the Lower Congo Basin (Anka *et al.*, 2012) and cause basin architecture and sedimentation to be mostly controlled by footwall uplift and hanging wall subsidence (Fig. 5.11). The faults feature a wide variety of lateral extents, depth, throw, and other properties. They have an important function for pressure development and fluid flow and may have considerable impact on migration. They can act as migration pathways (open faults) or as seals (closed faults), where they can trap petroleum and hold column heights depending on their sealing or leaking properties.

There is a suite of HAAs associated with faults in the northeast side of salt structure. Amplitude anomalies are observed against these normal faults (Fig. 5.13, 5.14 and 5.15). Clustering of amplitude anomalies on faults, with amplitude anomalies cross cutting the

structure without respecting the relative fault throw (Fig. 5.16 and 5.17). One noticeable observation has been made that faults cross cut the main reservoir units and have an association with the high amplitude anomalies and rest on the faults which have no amplitude anomalies associated with them (Fig. 5.13 to 5.15, Fig. 5.23 and 5.27).

5.5.2 Present day fluid flow features

Apart from observed gas-associated amplitude anomalies in the waste zone that are observed along channels, gullies and fault traps. The overlying sediments in waste zone are a Late Miocene-recent thick succession (about 1 to 1.5 kilometers) of hemipelagic sediments. Other fluid flow features are developed and also documents in the Late Miocene to recent sediments that developed along channels, polygonal and normal faults and stratigraphic traps (Giresse, 2005; Gay *et al.*, 2007; Andresen and Huuse, 2011; Andresen, 2012; Anka *et al.*, 2012; Ho *et al.*, 2012; Oluboyo *et al.*, 2014).

The pockmarks are typically circular and ranging in size from few hundred meters to one kilometer in diameter; depths of 100 to 150 ms TWT, and were formed above the two channel complexes (Fig. 5.19). Ho *et al.* (2012) summarised that pockmarks and pipes containing positive high amplitude anomalies always developed due to fluid flow in the shallow sediments and Andresen *et al.* (2011) concluded that the high-amplitude pipes generally occur in the shallow successions in offshore Angola represent shallow gas accumulations and/or diagenetic features associated with fluid flow through the sediments. The observed trail of pockmarks above channel complexes (Fig. 5.20) in the study area reflects the recent fluid flow activity in the Lower Congo Basin.

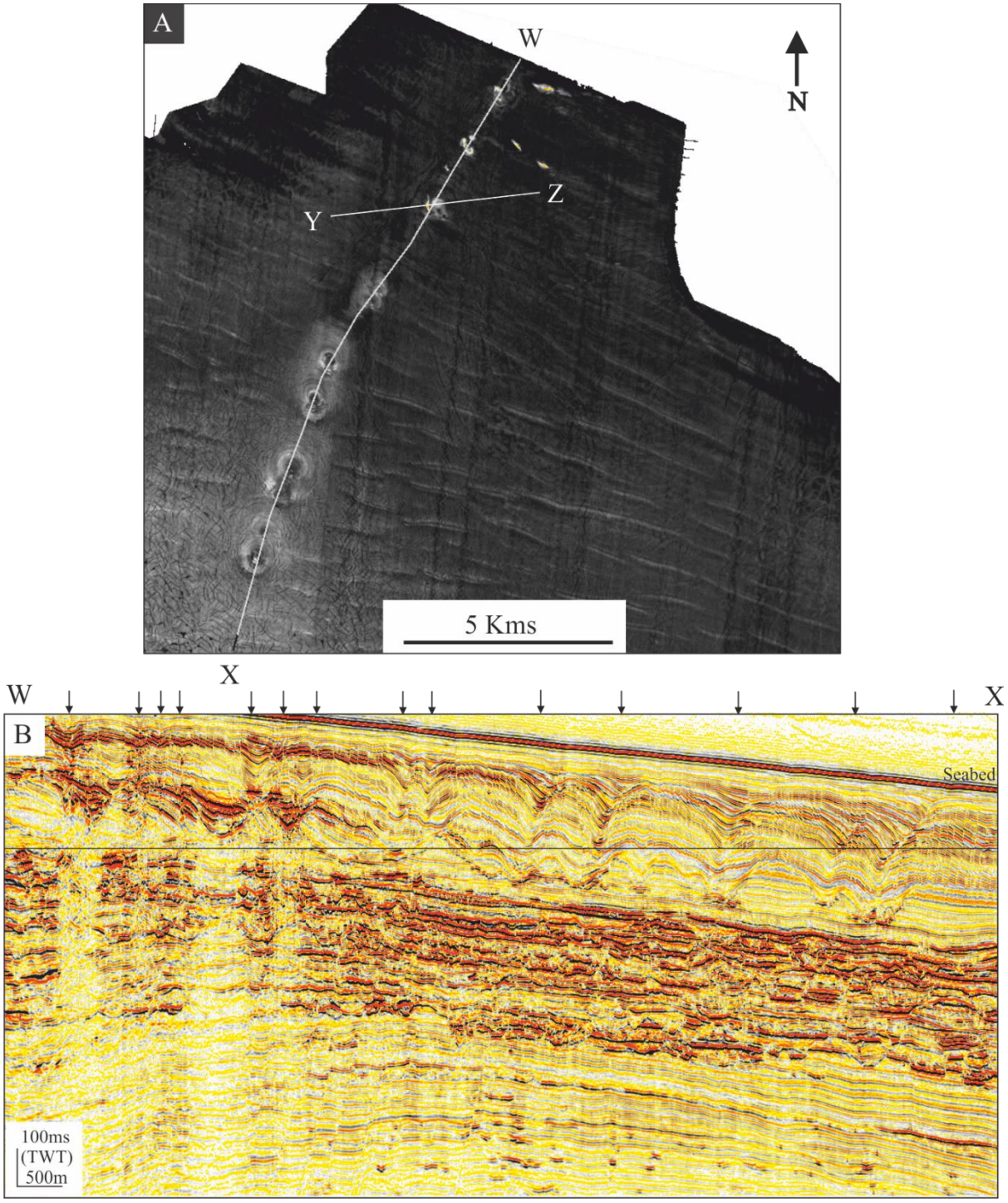

Figure 5.19: A) Base Pliocene acoustic map (base of PFS tier 1) showing major pockmarks above upper Miocene channel complex and a few isolated pocks. B) Fluid escape structure in up dip position within pockmark trail (indicated with arrows) feeding gas through the channel to seabed Note the stacked amplitude anomalies.

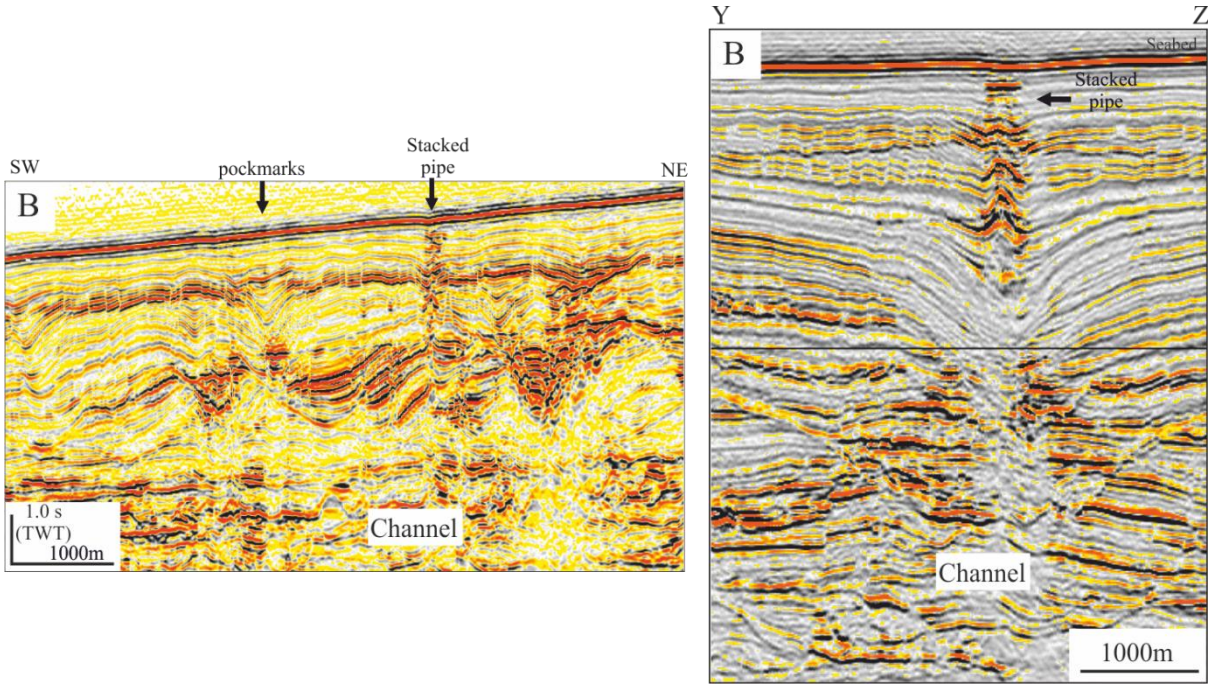

Figure 5.20: Pockmarks and pipe observed in the recent sediments above the upstream side of channel. B) Other example of fluid escape blowout pipe has several stages of cut and fill of the crater implying an episodic genesis.

5.6 Interpretation of hydrocarbon migration

Different types of fluid flow features and amplitude anomalies detected in the waste zone and shallow sediments were outlined in the preceding section. In this section, I assess possible migration pathways for hydrocarbons. Only two fluid flow features vertical anomaly clustering and through faults are observed in the waste zone. The origin of hydrocarbon in the study area is based from two types of sources rock in this region. The main source rock is bituminous shale of the Lower Cretaceous Bucomazi formation deposited during the rift phase (Burwood, 1999; Cole *et al.*, 2000). The rocks consist of clastics with intervals of high total organic content (TOC) and hydrogen index (HI), mostly oil prone type I kerogen of >5% TOC assemblage. The second source rock includes clastic and marls of the Albian-Cenomanian Moita Sceca formation with 2-3% of TOC mostly oil-gas prone (Burwood, 1999; Brownfield and Charpentier, 2006; Anka *et al.*, 2012).

The hydrocarbons in the study area are predominantly oil in the Middle Miocene turbidite channels complex system that are acting as a reservoirs in the west African margins (Broucke *et al.*, 2004; Gay *et al.*, 2006; Gee and Gawthorpe, 2006; Gee *et al.*, 2007; Savoye *et al.*, 2009). In the shallow section (Late Miocene to recent) gas leakage observed in the Lower Congo basin without know the origin (Gay *et al.*, 2007; Andresen and Huuse, 2011; Andresen, 2012; Anka *et al.*, 2012; Ho *et al.*, 2012). The previous section observed many amplitude anomalies in order to further conclude on the role of VACs and faults as preferential paths for the vertical migration of hydrocarbons. As previously mentioned, diagnostic parameters indicating modern fluid flow are investigated in detail and include: i) changes in the geometry of acoustic anomalies, ii) vertical and horizontal variations in the distributions of acoustic anomalies, iii) changes in the relationship amongst anomalies, reservoir rocks and adjacent faults.

5.6.1 Leakage through VACs

VACs features are observed in two stratigraphic intervals within the waste zone; first in the Middle Miocene turbidite channels (Upper channel) and mud-filled channel levee system at seismic interval Unit2 b between seismic horizons H250 and H200, and in the mud-filled channel levee system at seismic interval Unit2 c between seismic horizons H200 and H130 following by a regional seal unit 3 (Fig. 5.27).

This strike profile shows the amplitude response across the 'fingers' along the eastern levee margin (Fig. 5.3A). The background seismic facies is identical to the illuminated seismic character, implying that the amplitude response is due to presence of a substituting fluid (gas) and not due to lateral variations in levee sedimentary facies and/or thickness. The presence of vertical anomaly clustering at two different levels, few representative seismic profiles across VACs are shown in figure 5.24 and figure 5.27.

To understand development of VACs in the fine grain, low permeable sediment, and amplitudes are mapped at each continues reflection to assess development of anomalies. RMS amplitude maps were generated between each mapped reflection to evaluate gas migration. Six horizons were mapped and labelled 1 to 6 (Fig. 5.21B). Amplitude maps extracted between horizon1 and 10ms TWT below it shows two bright reflections and the boundary of these amplitudes are marked with a dotted line up to extend of bright reflection. Careful observation and interpretation of amplitude maps between interpreted horizons, bright reflection is consistent at one point that is interpreted as a feeding point for gas migration (indicated by green circle at Fig. 5.21C). This type of feeding point rarely seen before, and is imaged superbly here in this ultra-high resolution seismic cube. The sharpness of the lateral cut-off of amplitude means that it is truly image the amplitude migration/expension, not seismic artefacts due to tuning effects.

Lobate invasion geometry of these amplitudes is also observed in the upper layer between seismic horizon H200 and H130 (Fig. 5.27A) and again on these profiles, the low amplitude regions are of similar frequency to the illuminated portions, suggesting fluid substitution.

Sub-vertical to vertical stacking of HAAs (VACs) occur at all scales. Sub-vertical stacks can be taken to infer predominantly vertical flow paths involving ascent across quite thick intervening clay-dominated sections (Fig. 5.28 and 5.29). Figure 5.26 describes the leakage pathways and indicates that the CLC is not charged from the flanks. The detailed seismic interpretation was carried out to investigate how fluids migrated from the Middle Miocene channels to CLCs in the waste zone. Seismic cross sections passing the VACs feature are shown in figure 5.26 and figure 5.27. The central axis occurs directly above the fold seen just below horizon 1. The feeding point is crudely circular and visible at level 2, and this shape is then superimposed on shallower amplitude images to show the northward (up dip) invasion geometry, of presumably thin sands within the predominantly clay-rich, post reservoir interval. Critically, the identification of this VAC shows that H200 CLC is not charged from the flanks, at least here. It is charged by feeding points from the H250 main reservoir directly below (Fig. 5.21). This would be an obvious focal point for pressure and possible hydraulic fracturing. It is charged by feeding points from main reservoirs of Lower Miocene to Oligocene reservoirs seated below. There are other possible pathways for migrating hydrocarbon in the form of faults and stratal routings in despite of VACs for this CLCs anomaly because of the small data cube which is not enough to interpret the whole plumbing features.

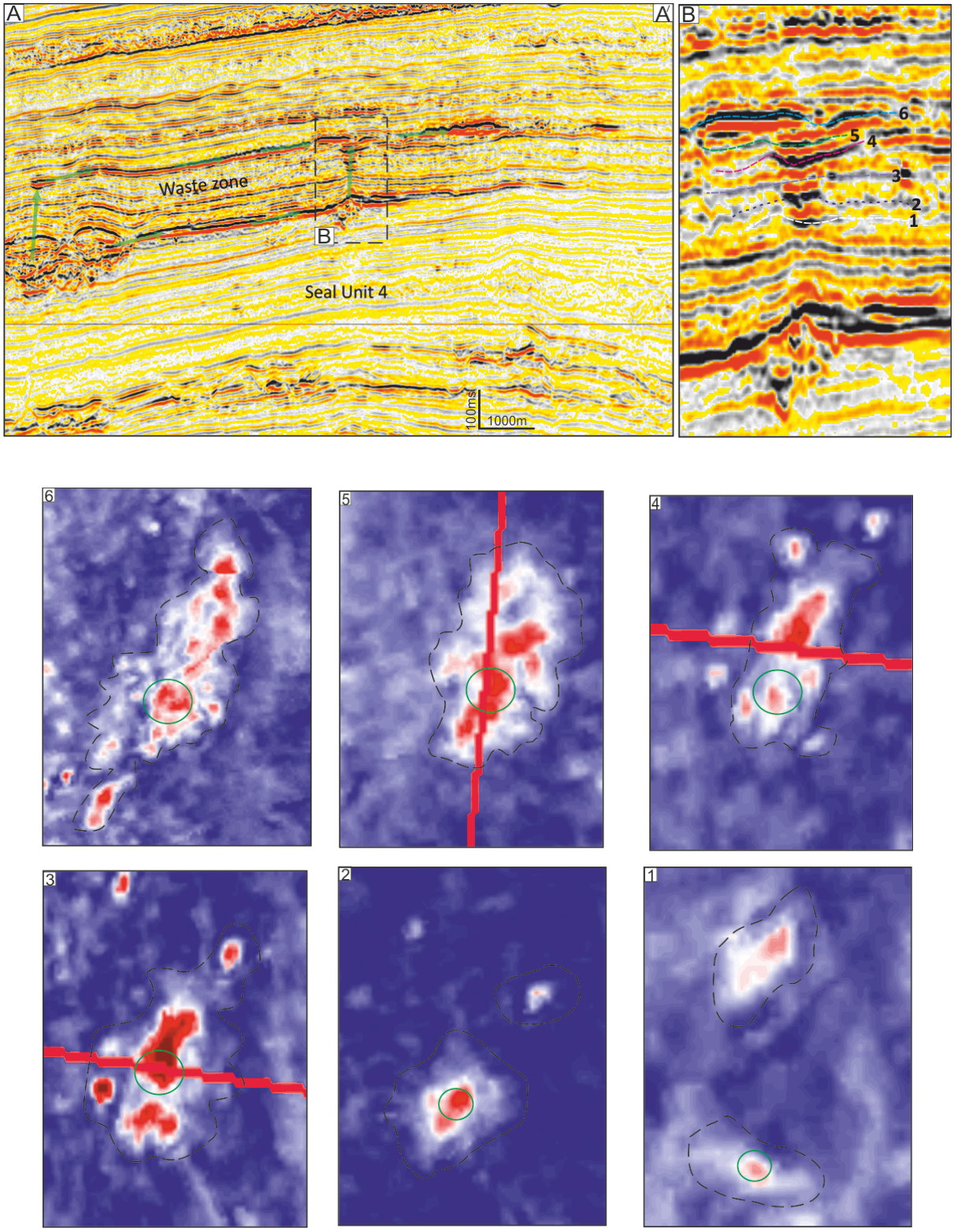

Figure 5.21: Seismic profiles and amplitude maps of circular to sub-circular HAAs. (A) N-S Cross-section through a circular to semi-circular Vertical Anomalies clusters (VACs) connected the Middle Miocene Channels to CLCs (Location fig. 4.26A). B) Zoomed section of cross section through VACs showing internal features of HAAs. C) RMS amplitude maps computed at mapped horizons 1 to 6 showing the geometry, orientation and spatial density of VACs.

5.5.2 Leakage through faults

Faults are often invoked as a mechanism to facilitate vertical or sub-vertical migration of fluids through sedimentary basins. In the context of the study area, normal faults are formed due to one of the following reasons; 1) extensional collapse of salt structures and minibasins due to thin-skinned gravity extension on the slope, 2) out-arc extension of salt-cored anticlinal structures, or 3) late-stage, inversion of folded structures due to landward propagation of downdip gravity-driven shortening. The shallow stratigraphy is further deformed by laterally extensive, layer-bound arrays of closely spaced normal faults called polygonal faults although these faults formed during volumetric contraction of discrete shale layers. Recent studies by Ho *et al.* (2012) and Andresen *et al.* (2011) showed that faults played an important role in the migration of fluids in the Tertiary succession in similar areas in the LCB. In this deeper section of the stratigraphy, there are many examples of amplitude anomalies either terminating abruptly against extensional faults (Fig. 5.13 and 5.14) or anomalies occurring above the upper tip of faults. It is tempting to link these amplitude anomalies to migration pathways parallel to the faults; however it is possible that some anomalies may have been present first and offset later (Fig. 5.15 and 5.16).

From the analyses presented in this chapter there is great inconsistency in which faults are associated with anomalies and which faults are not. For example, in figure 5.23, there are 3 faults which intersect the deep-seated turbidite source layer for the shallow amplitude anomalies. Only on one fault is there amplitude anomalies which are close to the fault or offset by the fault and it is possible that late-stage faulting offset pre-existing amplitude anomalies. I do not rule out the role of faults on fluid flow but given the limitations imposed by seismic data and a lack of sub-surface data such as wells and cores it was not possible to

do the required analysis to conclusively determine whether faults are permeable pathways for deep fluid flow from turbidite source layers (Fig. 5.14 and 5.16).

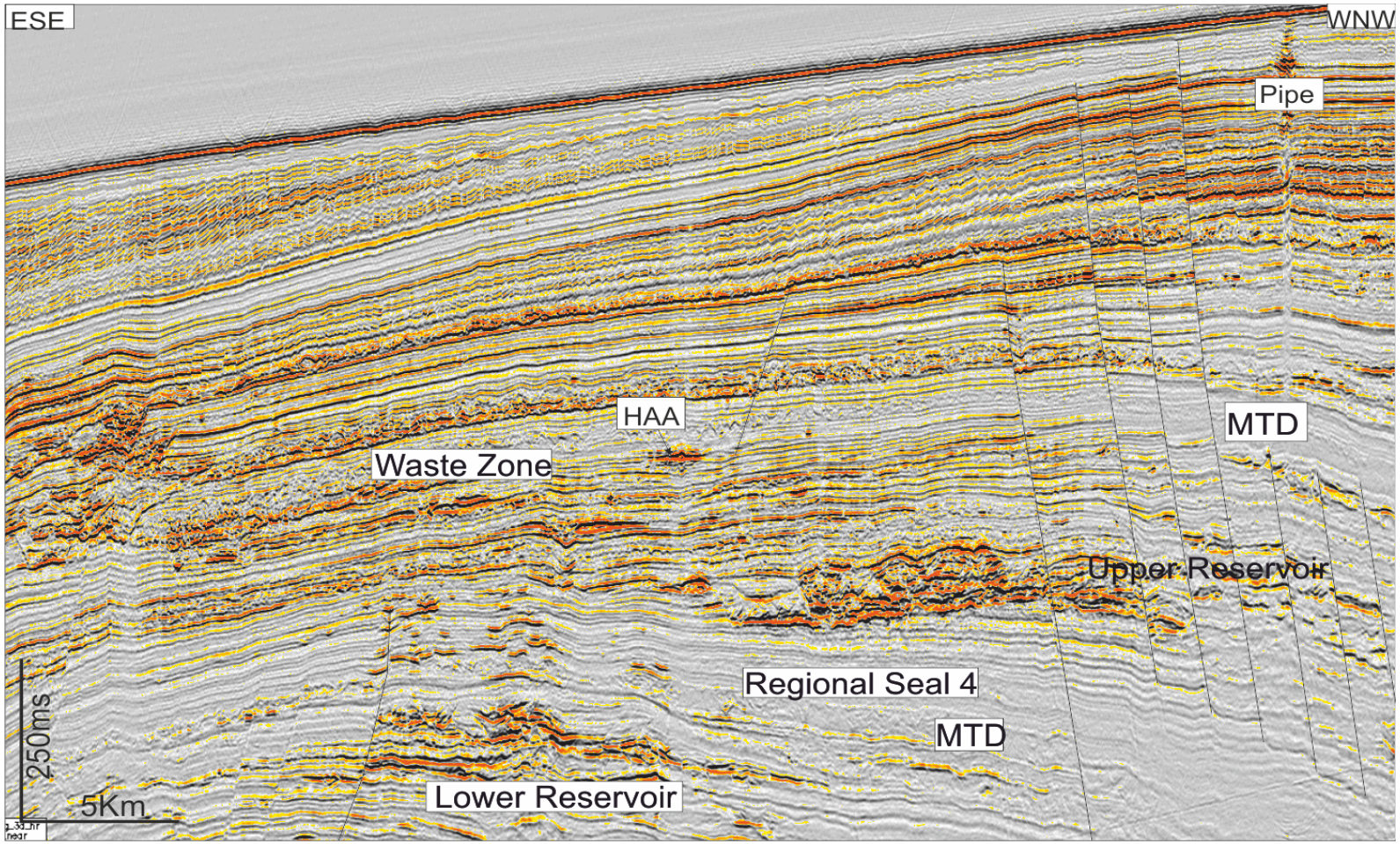

Figure 5.22: SE-NW seismic section passing through LA below MTD in waste zone. The La developed above the Middle Miocene turbidite channel reservoirs. The profile showing possible feeding points from the deeper reservoirs through vertical and stratal migration of hydrocarbon. HAA: High amplitude anomaly; MTD: Mass transport deposits.

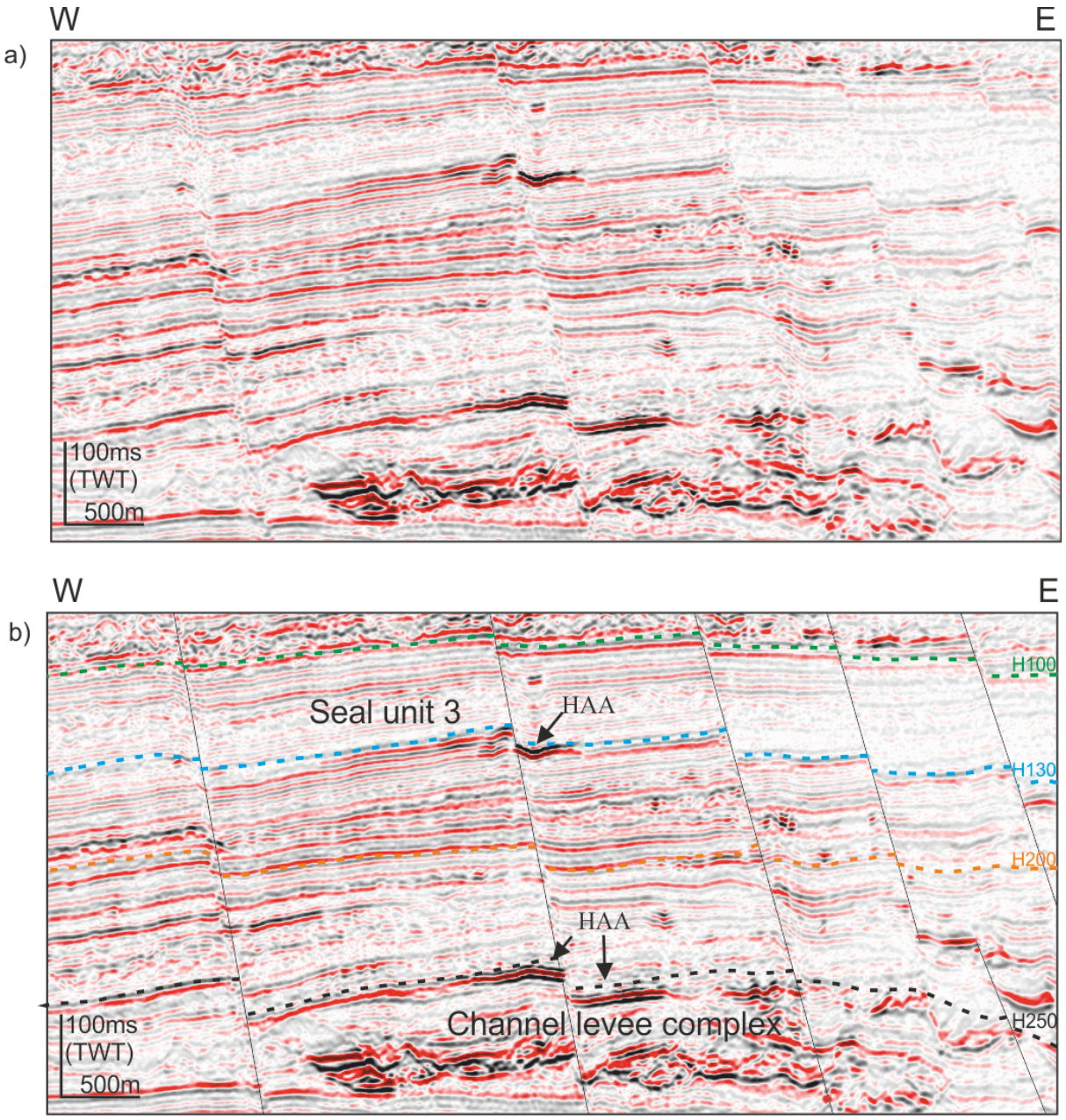

Figure 5.23: NW-SE seismic culmination of high amplitude anomaly trapped along the fault passing through Miocene turbidite reservoir. The fault cross cutting through reservoir have a culmination of amplitude anomaly and rest of the fault not show evidence of fluid flow.

5.7 Leakage mechanism

The leakage in the Middle Miocene sequence (waste zone) represented through high amplitude anomalies in VACs (Fig. 5.21A) and cluster of anomalies against tectonic faults (Fig. 5.23). These two possible pathways displays character of extensive and consistent fluid flow migration through hemipelagic sediments. Distribution of amplitude anomalies observed in widespread laterally in levees of turbidite channels and stratigraphically along the up dip strata (Fig. 5.28) throughout waste zone, but amplitude anomalies developed very closely in sediments over main turbidite reservoirs (Fig. 5.24, 5.25 and 5.26). These examples show the close vertical juxtaposition of the H130 and the underlying H200 channel levee complex. The connection path is above the up dip limit of the H200 levee.

The concentration of amplitude anomalies above the main Oligocene-Miocene turbidite reservoirs (Fig. 5.22) in the areas suggest that migration was probably dominated from levees of reservoir channels. The subtle correlation of amplitude anomalies with underlying reservoirs might suggest that anomalies were charged from deeper reservoirs as reported in the basin (Andresen *et al.*, 2011; Anka *et al.*, 2012; Ho *et al.*, 2012).

Three different stages of fluid flow migration levels are observed in the study area. a) Stage 1: Main turbidite reservoirs to CS-1 through vertical anomaly clusters (Fig. 5.24, 5.25 and 5.26) b) stage-2: CS-1 to CS-2 through vertical anomaly clusters (Fig. 5.27 and 5.28) and c) stage-3 Main reservoirs to upper sediments through faults and possibly through stratal pathways (Fig. 5.26).

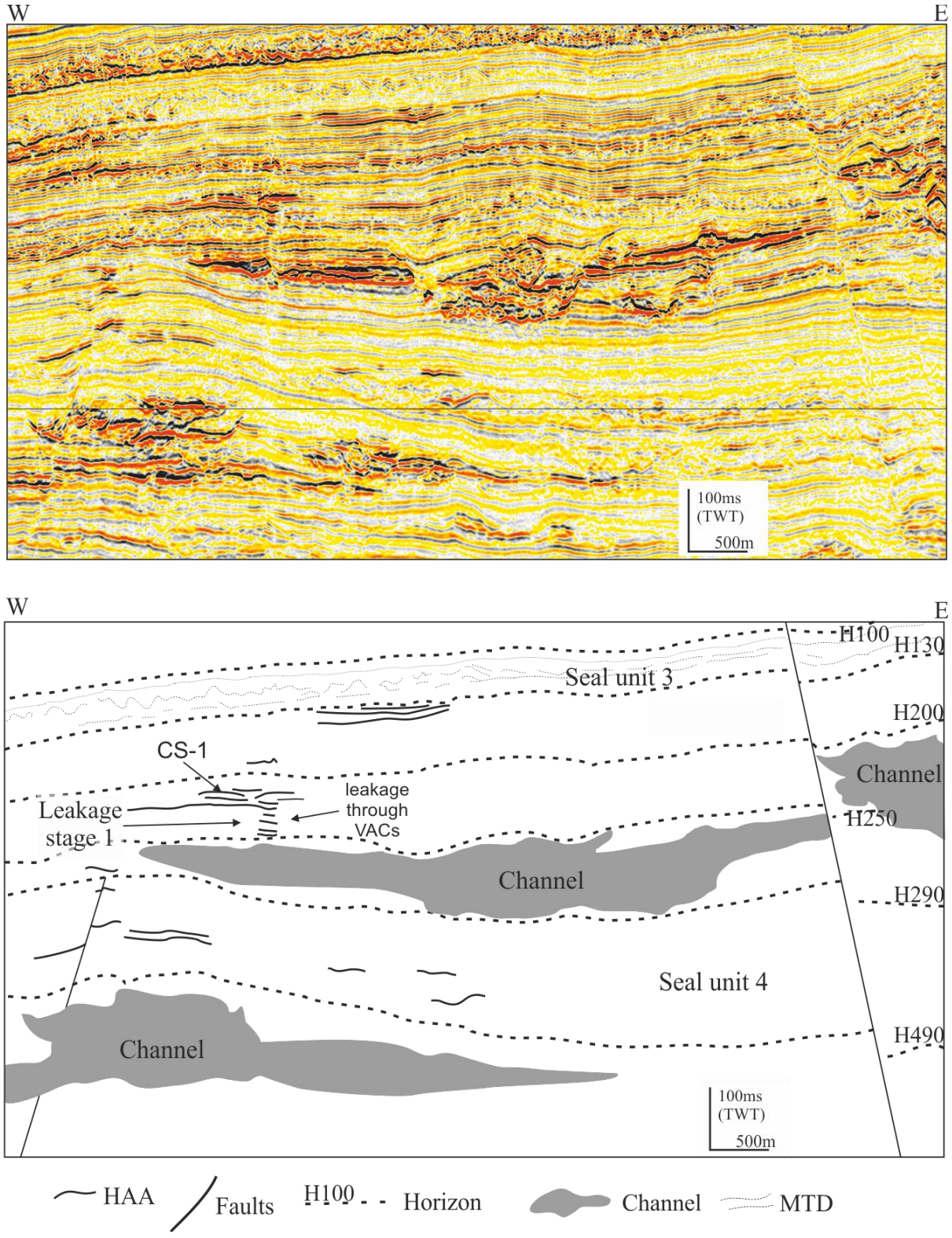

Figure 5.24: seismic profile showing different possible fluid flow pathways from Oligocene turbidite channels (Below H490 horizon) to upper reservoirs. Fluid migration is observed along VACs between CS-1 and underlying Miocene turbidite reservoir in stage 1.

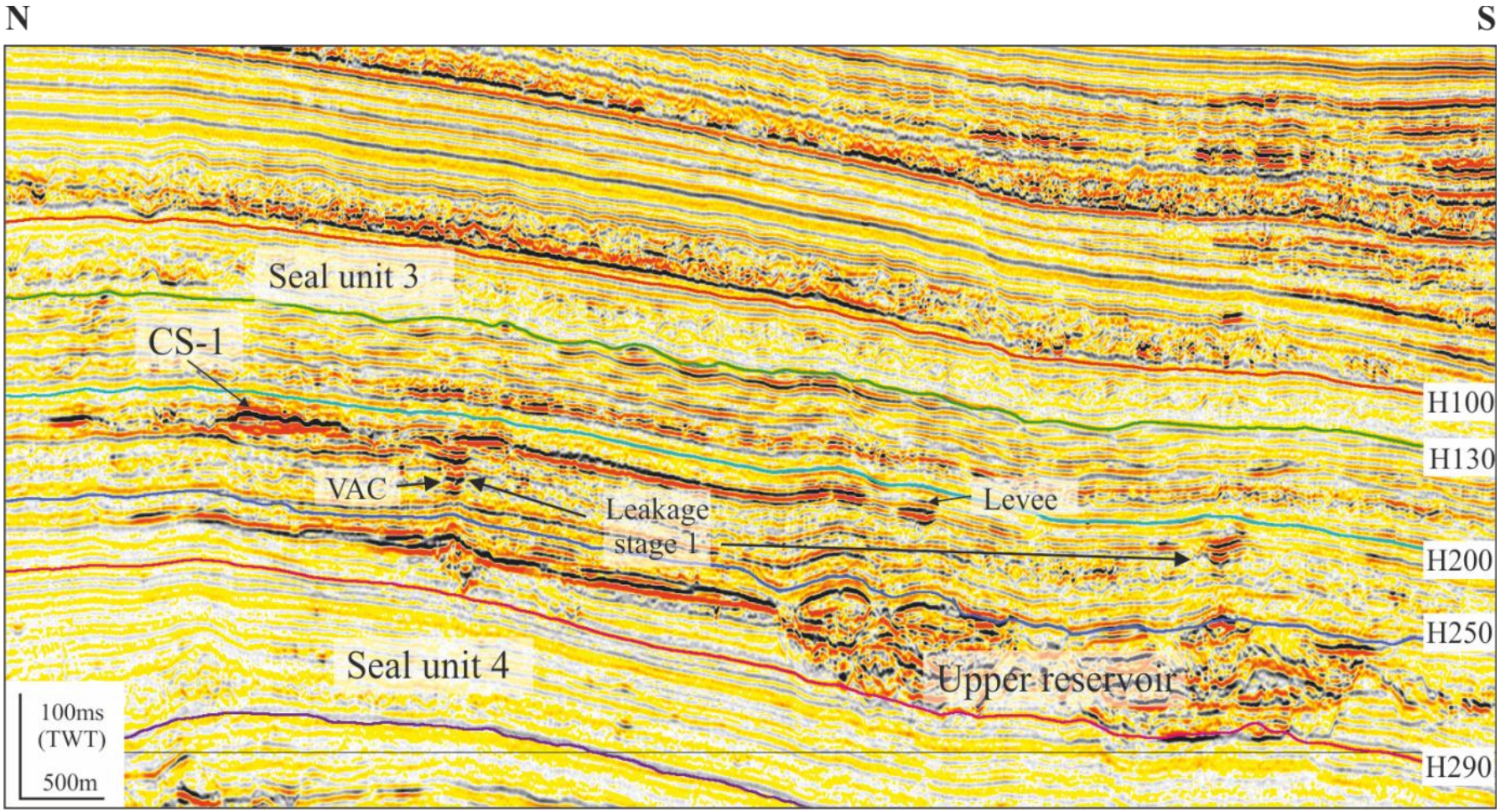

Figure 5.25: Amplitude anomalies in CS-1 developed in mud plugged channel levee in the waste zone below seismic horizon H200. Anomalies are connected with Miocene turbidite reservoir through vertical anomaly cluster that indicate fluid migration as stage 1. The extent of anomalies in CS-1 is following extent of lower reservoir.

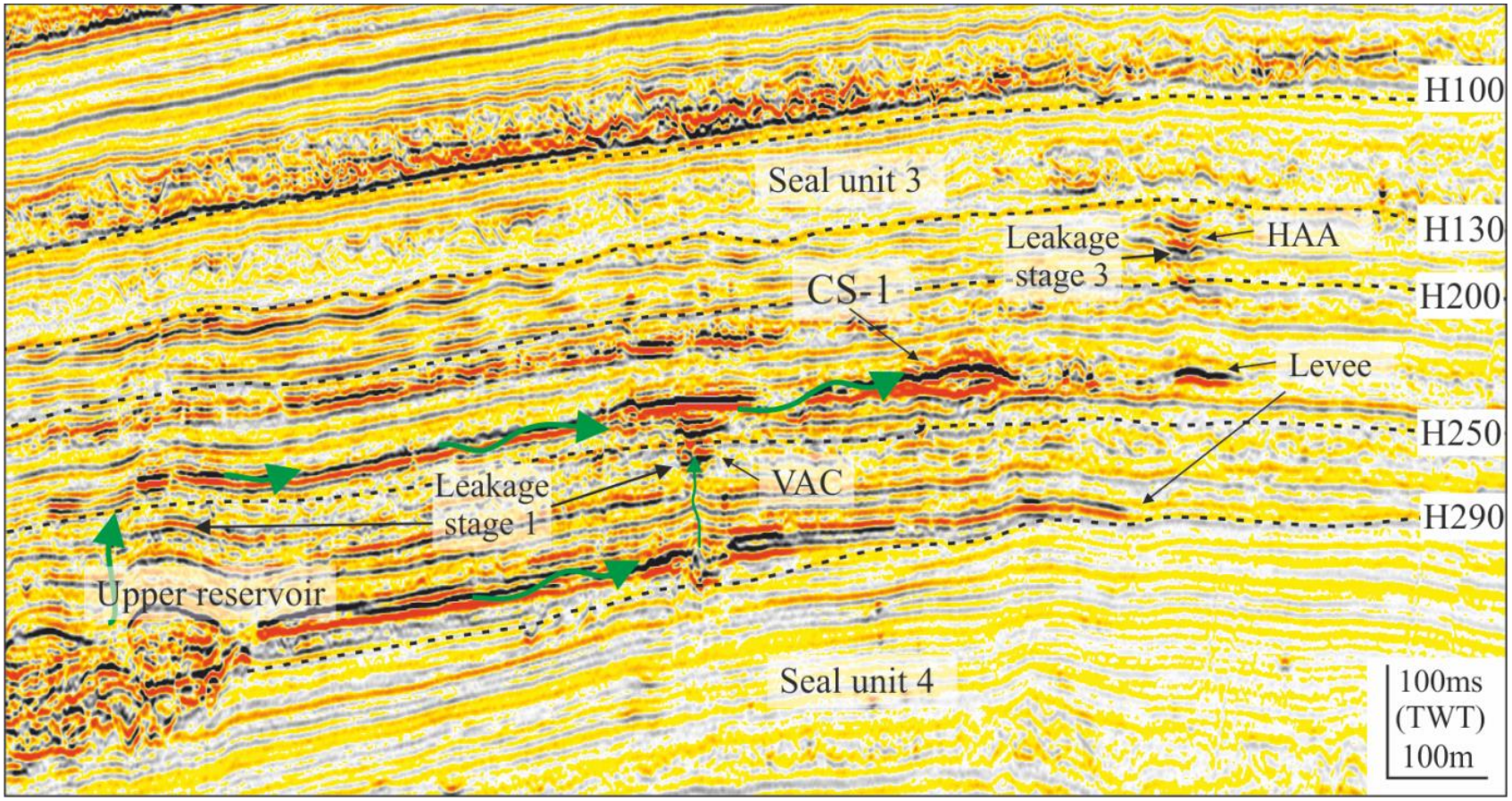

Figure 5.26: Another example shows amplitude anomalies in CS-1 developed in mud plugged channel levee in the waste zone below seismic horizon H200. Anomalies are connected with Miocene turbidite reservoir through vertical anomaly cluster that indicate fluid migration as stage 1 and further level stage 3 is observed, The extent of anomalies in CS-1 is following extent of lower reservoir.

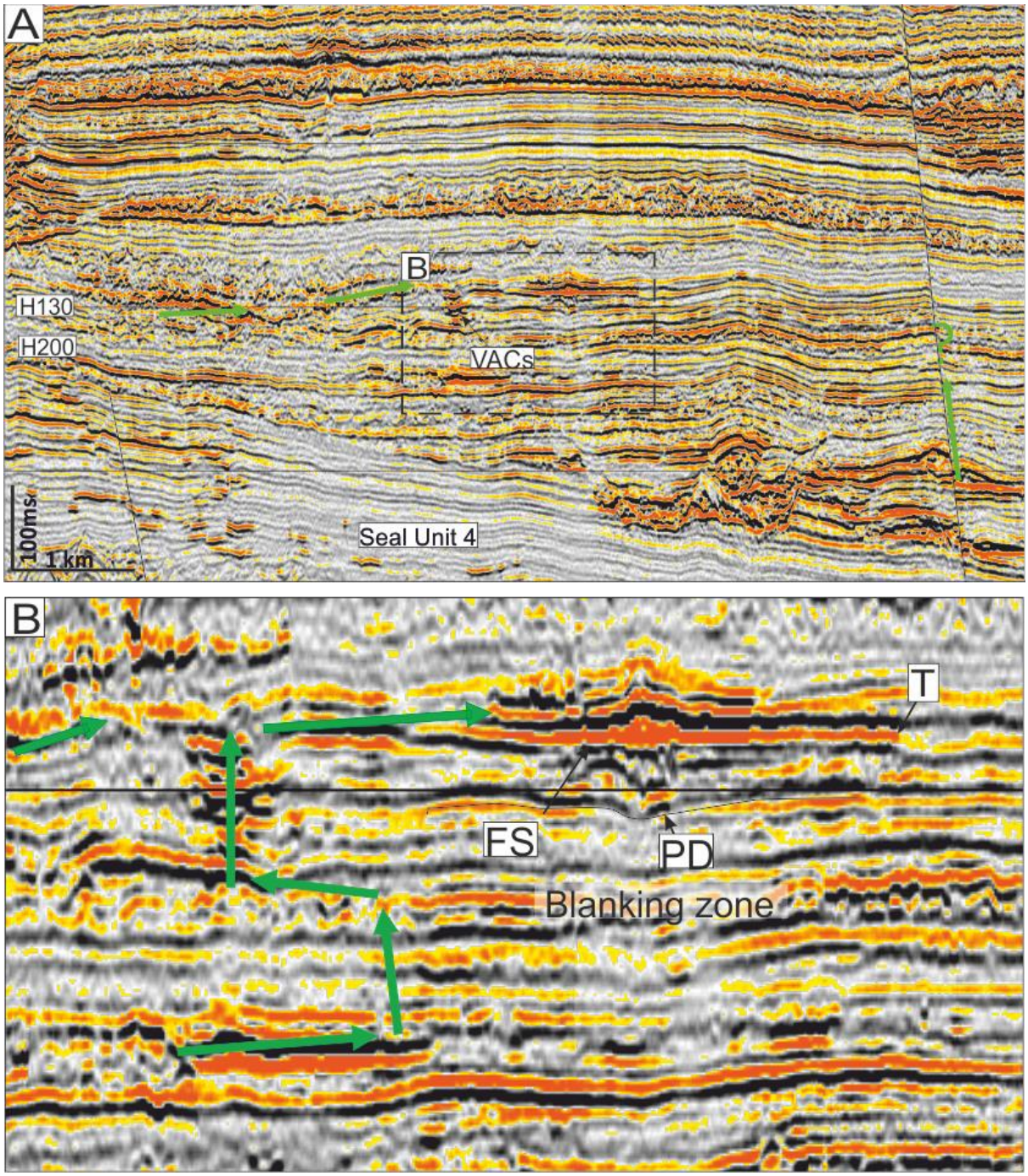

Figure 5.27: A) NW-SE seismic section passing through CS-2 showing possible feeding points from the deeper reservoirs through vertical and stratal paths for migration of hydrocarbon. B) Zoomed section shows the truncation (T), flat spot, velocity push down and blanking zone below the anomaly. HAA= High amplitude anomaly; MTD= Mass transport deposit; T= Truncation; FS= Flat spot; PD= Push down; and VACs= Vertical anomaly clusters.

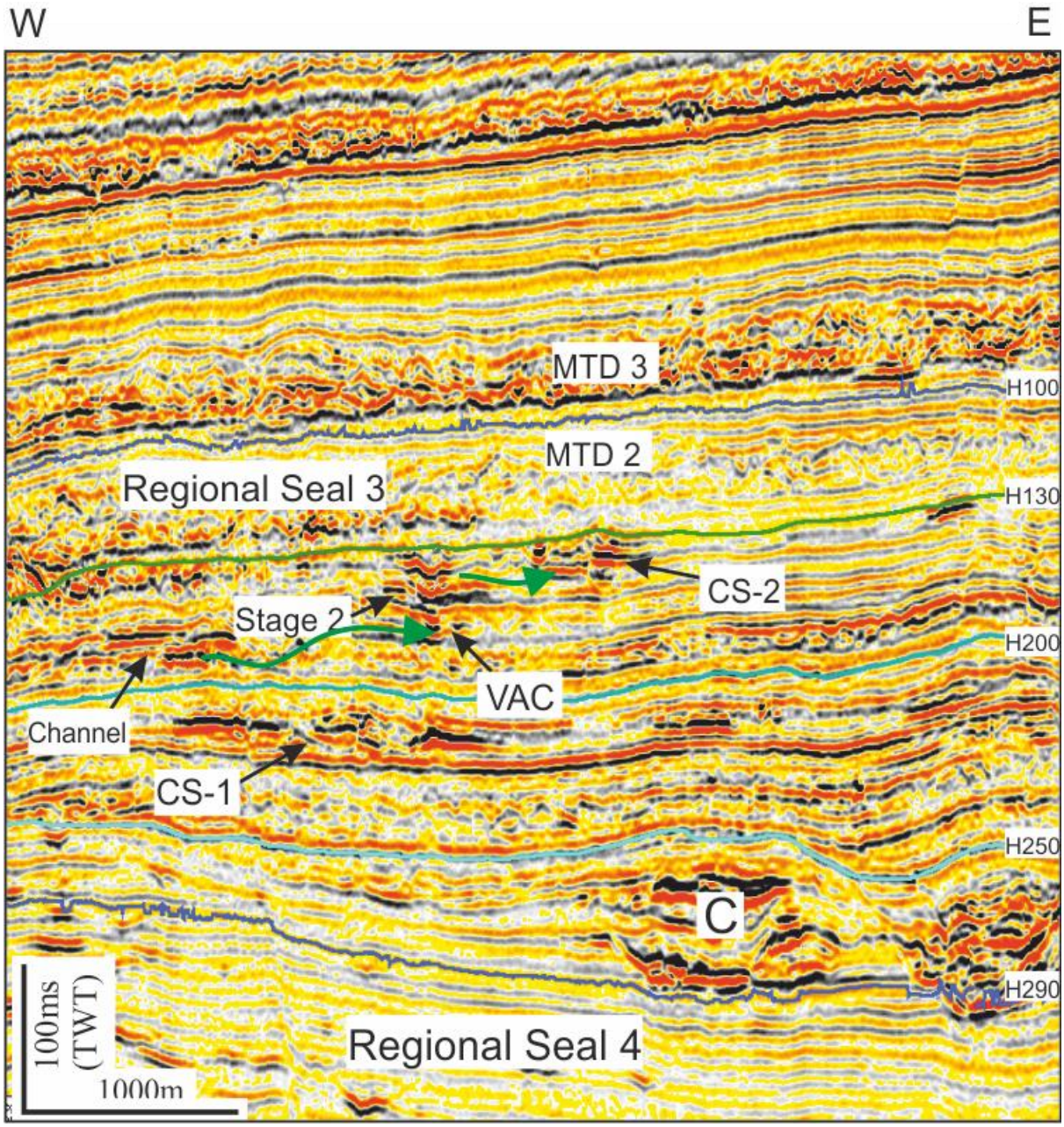

Figure 5.28: Another example of fluid flow migration from CS-1 to CS-2 through VACs in stage 2. The green arrows are indicating possible migration routes in the waste zone. C: upper turbidite channel.

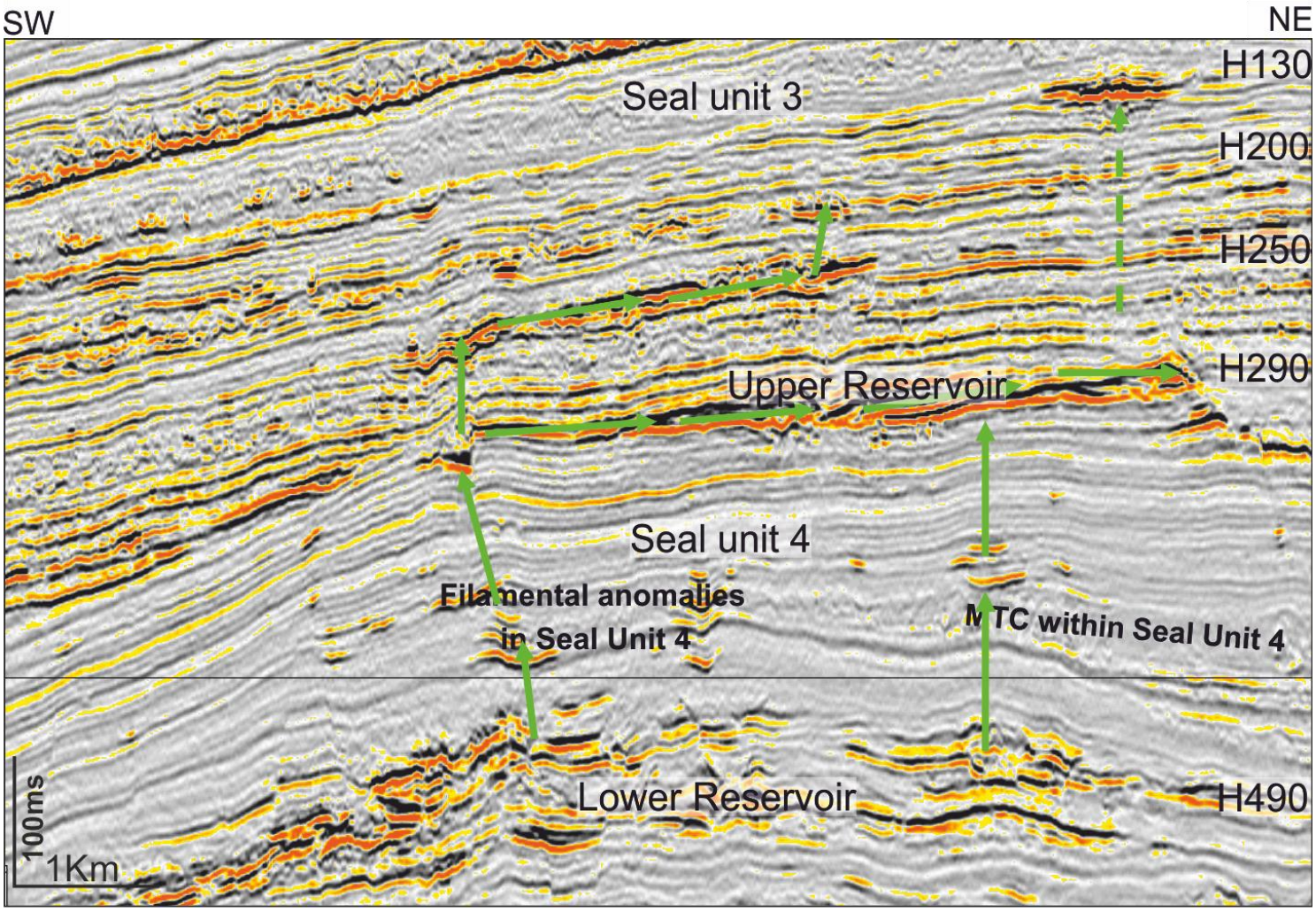

Figure 5.29:The depicted SW-NE seismic line shows the same bypass from Oligocene reservoirs through Seal Unit 4 and waste zone to base of Seal Unit 3.

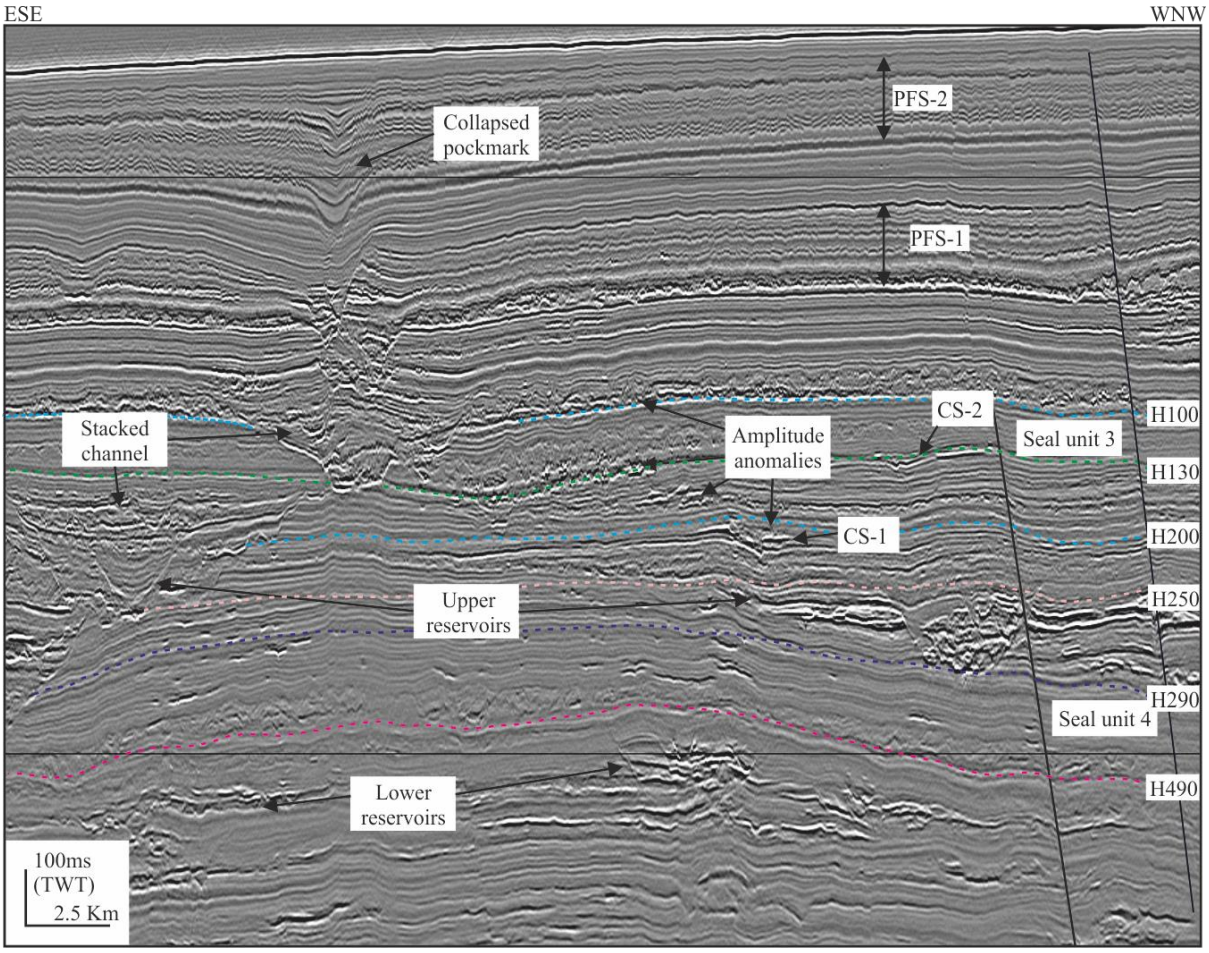

Figure 5.30: seismic profile displaying stratigraphic genetic units. Amplitude anomalies have a bypass system from Oligocene turbidite reservoir (Lower reservoirs) to Miocene turbidite channels (Upper reservoir). Upper reservoirs are directly connected with overlaying channels through VACs in CS-1 and CS-1 to upper straigraphic layer at H130 horizon. Stacked channels are connecting with top of waste zone and possibly provide a pathway for hydrocarbon migration through collapsed pockmarks.

5.8 Conclusion

Hydrocarbon migration from lower and upper reservoir units to different possible routes through thick hemipelagic sediment interval. Amplitude anomalies developed in the Middle Miocene succession have connect with upper and lower level anomalies (Fig. 5.29). Therefore anomalies have established bypass system from Oligocene turbidite reservoir (Lower reservoirs) to Miocene turbidite channels (Upper reservoir) through VACs. Upper reservoirs are directly connected with overlaying channels through VACs in CS-1 and CS-1 to upper stratigraphic layer at H130 horizon. Stacked channels are connecting with top of waste zone and possibly provide a pathway for hydrocarbon migration through collapsed pockmarks (Fig. 5.30)

The following are the conclusions;

- There are multiple possible routes for the leakage from main turbidite reservoirs to the waste zone. Seismic examples shows that CLC's are not charged from the flanks but instead are charged by feeding points from main reservoirs seated below them. There are other possible pathways to migrate hydrocarbon through faults and stratal routings.
- 3D distribution of HAAs, their geometries and context leads us a model where hydrocarbon exploit thin sands, faults, VACs, for cross-stratal migration at different genetic units
- But it is difficult to identify a precise rout for the leakage due to multiple options combining stratal and structural migration paths.

CHAPTER 6

Summary and discussion

CHAPTER SIX

6.1 Discussion

The preceding chapters presented a detailed seismic interpretation and geophysical analysis of high-amplitude seismic anomalies which were attributed to the presence of fluid (free gas). A case study of an anomalous zone within biosiliceous of the Eocene to Oligocene units in the Møre Basin was presented in Chapter 3. In Chapters 4-5, four different types of high amplitude anomalies from the Miocene succession of the Lower Congo Basin were shown.

This chapter begins with a summary of the key scientific results from preceding result chapters (Chapter 3 to 5). Following the summary is a discussion of particular elements of the results chapters which remain unanswered including; 1) controls on the distribution of high-amplitude anomalies and their acoustic features that are directly observed on seismic data, 2) how these controls result in the geometric characteristics of the anomalies, and 3) what the major controls are on the hydrocarbon plumbing system i.e. whether migration pathways are depositional or structural conduits. To conclude the chapter, the major limitations of the research project are outlined.

6.2 Summary of results

6.2.1 Chapter 3

The main aim of chapter 3 was to establish the nature and genesis of a suite of high-amplitude anomalies that are grouped as the anomalous zone are developed at the crest of Havsule Dome in

the Møre Basin, offshore mid-Norway. The chapter focused on the development of the anomalous zone and striking concave-upward basal contact (Fig. 3.5 and 3.6).

The high-amplitudes in the anomalous zone are interpreted to represent porous layers hosting fluid (free gas) beneath a sealing sedimentary layer (Base of the Naust Formation). The anomalous zone discussed here was located at the crest of Havsule Dome. The presence of free gas in the anomalous zone is responsible for the poor imaging of the polygonal faults below. Coherence time slices help to visualise the presence of faults inside and outside of the anomalous zone. Instantaneous phase attribute display enhanced the continuity of sedimentary layers inside the anomalous zone. The presence of polygonal faults and continuity of sedimentary layers implies that it was the same lithology of anomalous zone from background lithology.

The main findings of the Chapter 3 are; 1) The amplitude anomalous zone has a negative reflection and sharp change in amplitude at the boundary with the background reflections, 2) The anomaly is developed at the crest of Havsule Dome (Fig. 3.7), 3) The anomaly creates a significant velocity push-down effect of a few-to-tens of milliseconds and reduces the seismic reflection strength relative to the background by > 20% (Fig.3.5), 4) Seismic blanking or attenuation is observed below the anomalous zone (Fig. 3.13), 5) The interval velocity of the anomalous zone is less than interval velocity of the host sediments which is 1500 m/sec (Fig. 3.18), 6) Seismic data in the anomalous zone has a low frequency relative to the background data (Fig. 3.16), 7) Continuity of sedimentary layering through the anomalous zone suggests that the anomaly is developed in the same type of sediments as the background (Fig. 3.17). All these observations collectively support the interpretation that the high-amplitude anomalous zone is a

direct response to the presence of free gas within Opal-A-rich sediments of the Brygge Formation.

6.2.2 Chapter 4

Chapter 4 focused on the distribution of high-amplitude anomalies developed in the Late Neogene-to-Quaternary strata of the Lower Congo Basin (LCB). High-amplitude (HAA) anomalies were classified on the basis of their planform geometry, their lateral extent, morphology, and seismic character. HAA's were grouped into four types: 1) linear anomalies, 2) sub-circular anomalies, 3) patchy anomalies and 4) discrete filamental anomalies. Only sub-circular and patchy anomalies were found to conform to structures, were associated with channel levee system and are fault-bounded. A combination of seismic interpretation, attribute analyses and well ties were used to assess the likelihood of amplitude anomalies defining zones of hydrocarbon or non-hydrocarbon-bearing fluids. Three examples of the anomalies were selected for further study on focused flow and leakage mechanism for Chapter 5.

6.2.3 Chapter 5

Chapter 5 focused on the processes which resulted in the formation of 3 particular anomalies presented in Chapter 4. These include; semi-circular and patchy anomalies which were analysed at different stratigraphic levels within the Miocene-aged Waste Zone. These results were then used to establish the leakage mechanism in the LCB.

The 3D distribution of high-amplitude anomalies, their geometry and context leads to a plumbing model where hydrocarbon exploit thin sands, faults and pipes for cross-stratal migration at different genetic units. The main findings of these selected examples were as follows

1) Anomalies that developed along the mud-filled turbidite channels (example one) in the waste zone were charged from the Oligocene-Miocene mains reservoir comprising turbidite channels via vertical pipe-like features termed here as "vertical anomaly clusters" (VACs) see (Foschi *et al.*, 2014).

2) Multiple routes for leakage were identified.

3) Specific routes were found to be hard to prove since there were multiple options combining stratal and structural routing.

4) 3D distribution of high amplitude anomalies, geometries and context leads to a basic 'multi-storey car park' model where HC exploit thin sands, faults and pipes for cross-stratal migration at different levels (as example Fig. 1.39).

There are multiple possible routes for the gas leakage from main reservoirs into the waste zone but they are difficult to identify precisely because the extent of seismic data is not allows to analyse lateral migration through possible carrier beds/layers. Migration in the LCB is concluded through multiple options combining stratal and structural migration paths.

6.3 Origin of patchy and finger anomalies

The various two and three dimensional geometries of seismic amplitude anomalies presented in Chapters 3-5 illustrate the various ways in which fluids have infiltrated sedimentary layers. Fluids infiltrate sedimentary rocks through permeable and connected pore-spaces created either from grain-grain dimensions which in shallowly buried clastic deposits are most likely primarily inherited by the depositional environment (Løseth *et al.*, 2009; Plaza-Faverola *et al.*, 2010; Micallef *et al.*, 2011; Vadakkepuliyambatta *et al.*, 2013) or by fractures and shear zones formed during compaction and deformation of the units (Berndt, 2005; Cartwright *et al.*, 2007; Andresen, 2012; Foschi *et al.*, 2014). The directions in which fluids migrate into these pores are influenced by the head gradient and pressure gradient imposed on the fluid. Fluid flows from areas of high pressure to low pressure which is typically vertical but where heterogeneous sedimentary sections are tilted and folded fluids can flow horizontally (Cartwright *et al.*, 2007; Foschi *et al.*, 2014) and even downwards (Doyle *et al.*, 2003). It is likely that the various different styles and geometries of fluid-related anomalies are the result of a combination of one or more of these mechanisms. The purpose of this section is to explore how anomaly shape is related to mechanism of formation and properties of the sediment.

I focus on one particular group of patchy anomalies that had finger-type amplitude anomalies located along north-south trending turbidite channel in the Lower Congo Basin (Fig. 6.1and Fig 6.2). In Chapter 5 they were interpreted as representing gas. The part of the channel where anomalies are located is in the crest of an obliquely NNW-SSE striking anticlinal fold (Fig 5.5). This fold is cored at depth by a salt and was formed after the deposition of the channel. The most obvious explanation for the first-order location of the anomalies is that gas flowed from sources

(Oligocene-Miocene turbidite channels) at depth into the crest of the fold and infiltrated the most permeable and porous areas.

The strong association with the channel suggests that gas anomalies shown in figure 6.2, filled the most permeable and porous parts of the channel levee system. Conventionally these areas would occur along the axis of the channel (Kolla *et al.*, 2001; Broucke *et al.*, 2004) however in this case they are quite clearly restricted to the levees and are absent from the channel itself i.e. the channel is mud-plugged

The study area is primarily composed of turbidite deposits where channel levee complexes are stacked vertically and laterally (Broucke *et al.*, 2004; Nakajima *et al.*, 2009) and interbedded with depositional lobes (Anka *et al.*, 2009). Broucke *et al.* (2004) stated that turbidite channels found within the uppermost Lower Miocene and base Middle Miocene intervals are mainly consist of hemipelagic sediments with low amplitude facies with isolated turbiditic deposits. The erosive character of turbidite channels are filled by slide deposits, sandy elementary channel deposits and confined levees with sand sheets of a few meters thick (Fig. 6.3).

The first-order geometry and location of the anomalies with respect to the channel are consistent with the depositional pattern of channel-levee depositional model (Fig. 6.3), However, the fingering edges of the anomalies are more ambiguous. For example, are they also sand-filled parts of levee and overbank deposits, thus defining the lateral edge of the reservoir (Clark and Pickering, 1996), or are they the lateral edge of a currently under-filled trap with potential reservoir outboard which can be filled?

Few examples of finger-shaped anomalies exist in the literature. Dennis *et al.* (2005) showed examples of finger-shaped amplitude anomalies in channel deposits in the Arbroath and Montrose fields in the North Sea Basin. It was shown that these anomalies represented sands charged with oil. Dennis *et al.* (2005) suggested that oil preferentially migrated to the (direction) in a discrete zone forming the finger anomalies observed on seismic data. They interpreted this preferential flow due to the hydro-dynamic pressuring of the basin.

Evidence of finger-shaped fluid accumulations have also been observed in 4D time lapse seismic surveys over sites where CO_2 has been injected into the subsurface (Chadwick *et al.*, 2005). These studies have shown that CO_2 does not always invade the reservoir intervals at equal rate from the injection well but invades preferentially toward a certain direction creating a finger. There are a few explanations for why this may occur. 1) Preferential flow may occur in the direction of the head gradient which is commonly upslope or where there is the smallest load. 2) There is preferential flow parallel to fracture sets which are parallel or perpendicular to the paleo-or-present day strain and stress field. 3) There is preferential flow along discrete permeability zones such as sand-rich channels.

Based on these studies it appears that the finger geometry is not formed by a specific mechanism of fluid flow. In the absence of sub-surface well data it was not possible to ascertain the relative porosity and permeability of the levee systems. However, based on previous studies it is possible that the fingers could be sand-filled lobes of perpendicular-striking overbank channels.

Alternatively, there is growing evidence in this part of the Lower Congo Basin of late-stage fluid leakage from deeper traps into the overlying succession. There is also evidence of fluid-leakage at the seabed. Other fluid-related amplitude anomalies and features such as pockmarks and fluid-

related depressions (Fig. 6.5), strongly suggest fluid was overpressured and could breach and fracture hemipelagic sequences. Given this, it is also possible that the crest of the fold containing patchy and fingering anomalies was or is significantly pressured.

There is no direct seismic evidence for fluids leaking from the crest of the fold (Fig. 6.1, Fig. 6.2 and Fig. 6.4) which may be expected as the most likely place where failure would occur during overpressure. However, given that fluid-related anomalies are so distinctly absent from the channel axis, the crest of the fold in this case may actually be well-sealed. The more permeable levee systems could provide the most viable route for fluid migration. The finger elements to the patchy anomalies may therefore represent more recent phases of outward expansion of fluid volume in the reservoir.

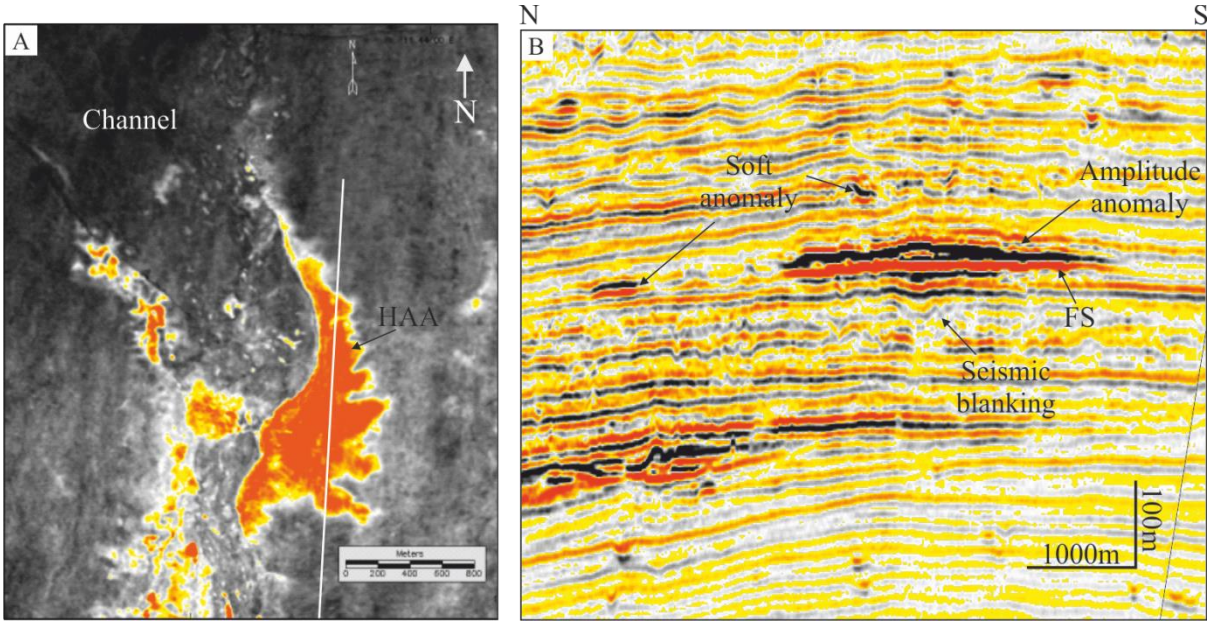

Figure 6.1: Amplitude anomaly developed in the fine grained sediments of mud filled channel. A) Root mean square amplitude map showing bright reflection in levees of mud filled channel. B) Representative seismic profile showing extent of amplitude anomaly. A hard reflection at the base of anomaly is interpreted as a flat spot (FS). Soft anomalies are observed on the left (1000 meters) and upside (100 meters) of high-amplitude anomaly.

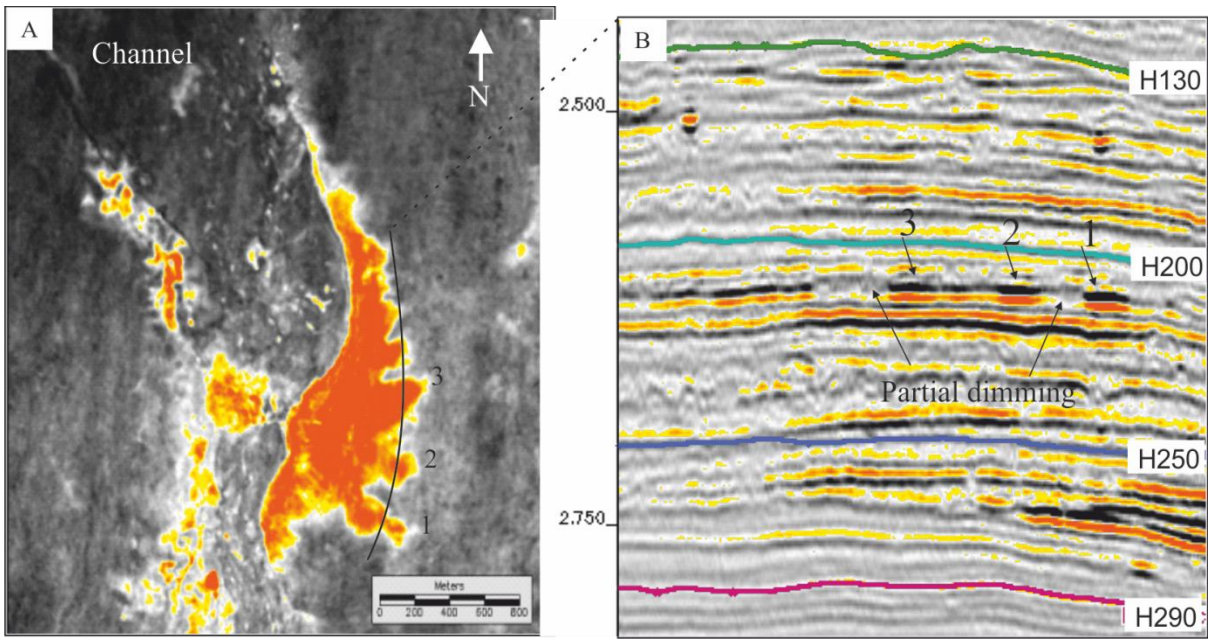

Figure 6.2: The lateral margins are highlighted here in detail from the northern margin. Strikingly, the high amplitude anomaly margin has a fingered geometry whose lateral limit does not correspond to the full lateral levee extent. The 'fingering' is due to fluids and not a facies effect. The question arising, is whether the fingering is by gas invasion eastwards during dynamic filling or due to water invasion westwards due to drainage. The partial dimming between these finger types geometries labelled with 1 to 3 is interpreted as partial gas saturation.

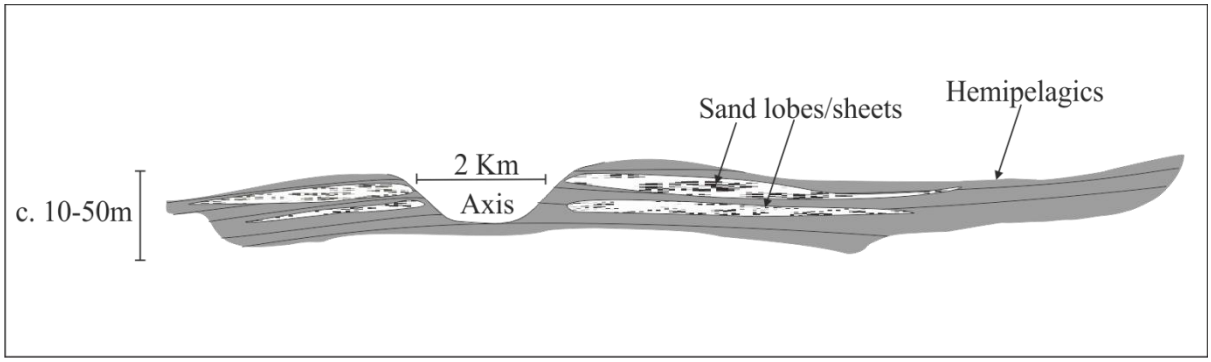

Figure 6.3: Turbidite channel levee complex model showing deposition of sand lobes/sheets in the confined levees (modified from Broucke *et al.*, 2004).

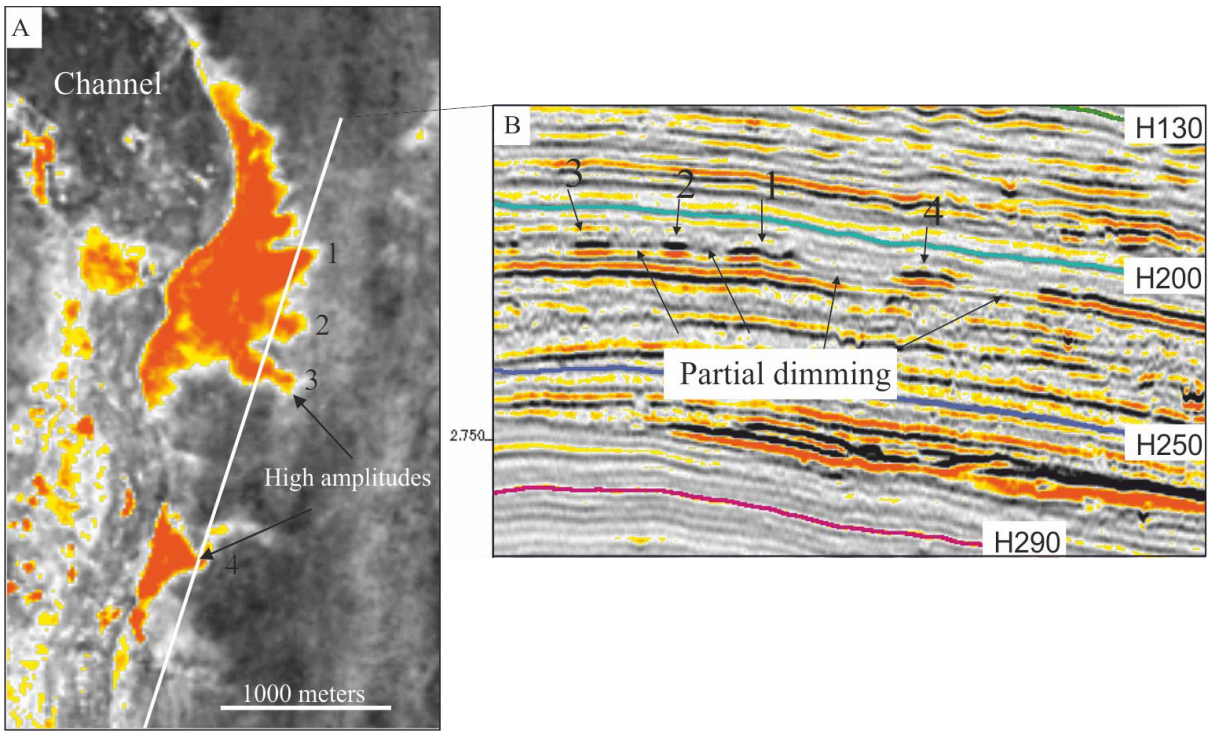

Figure 6.4: This strike profile shows the amplitude response across the 'fingers' along the eastern levee margin. The background seismic facies is identical to the illuminated seismic character, implying that the amplitude response is due to presence of a substituting fluid (most probably gas) and not due to lateral variations in levee sedimentary facies and/or thickness. We think this image is an outstanding example of 'fingering' rarely seen before, and imaged superbly here on this ultra-high resolution seismic cube. The sharpness of the lateral cutoff of amplitude means that we can truly image the 'fingers': they are not seismic artefacts due to tuning.

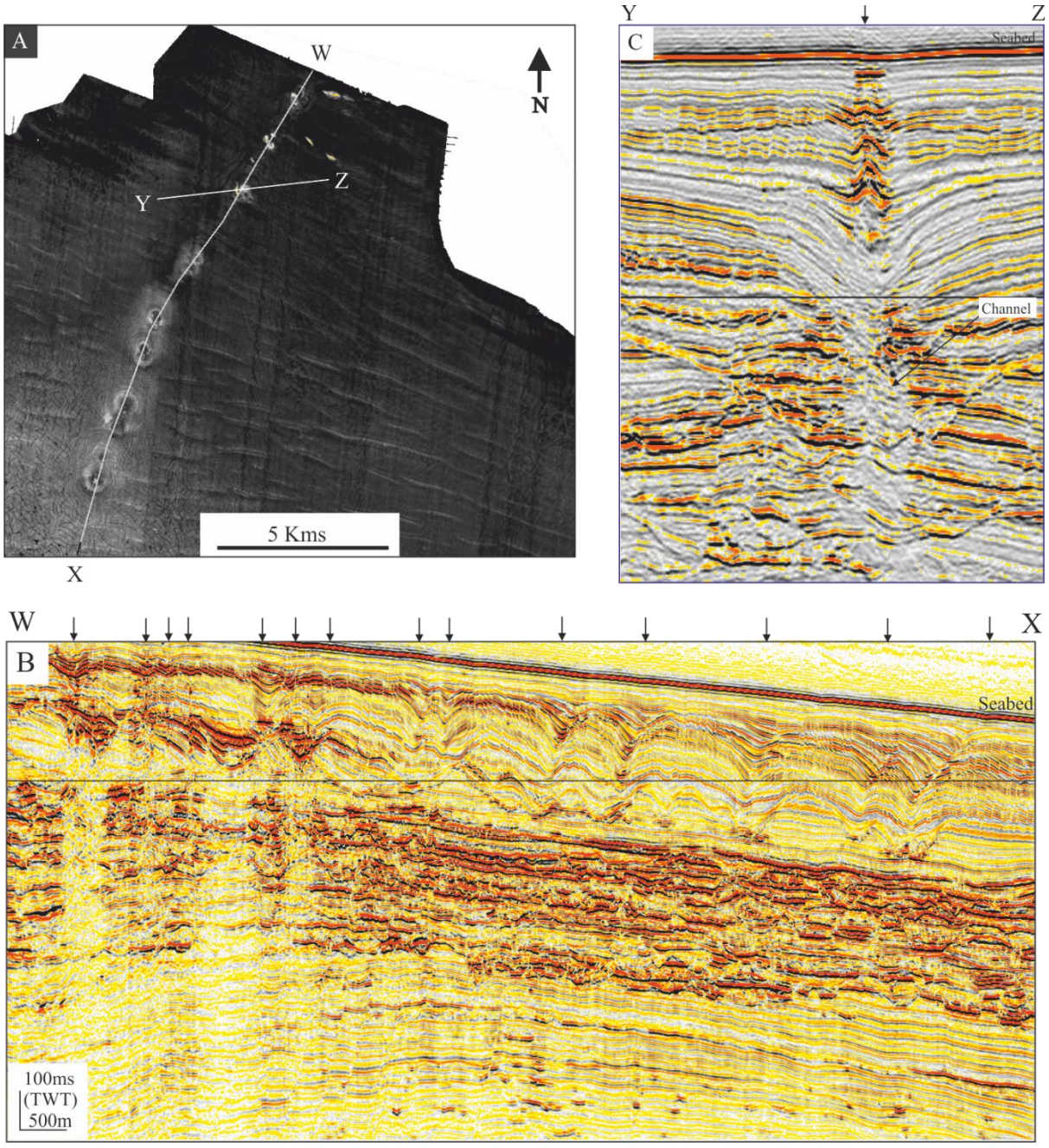

Figure 6.5: A) Base Pliocene acoustic map (base of PFS tier 1) showing major pockmarks above upper Miocene channel complex and a few isolated pocks. B) Fluid escape structure in up dip position within pockmark trail (indicated with arrows) feeding gas through the channel to seabed Note the stacked amplitude anomalies. C) other example of fluid escape blowout pipe have several stages of cut and fill of the crater implying an episodic genesis.

6.4 Geometry of anomalies: Origin of patchy anomalies

Seismic blanking is a phenomenon that is observed on the seismic data due to sound wave energy dispersions as they travel in rocks. The level of attenuation depends on the degree of fluid saturation, porosity of the rock, fluid pressure and the mineral content of the rock. Theoretical studies indicate (Müller and Gurevich, 2004; Mavko *et al.*, 2009) that increasing saturation up to a critical level will cause seismic attenuation that is directly related to the effect of gas on seismic wave velocities. The relationship between elastic wave velocities and water saturation in gas reservoirs depends on whether the saturation is heterogeneous (patchy) or homogeneous (Knight *et al.*, 1998). Two types of mechanisms for partial gas saturation are widely accepted; one is pressure dissolving (Han and Batzle, 2002), and the other is physical trapping such as patchy saturation due to spatial heterogeneity in the permeability of the medium (Dvorkin and Nur, 1998). A commonly accepted theory is that a small percentage of gas saturation, often within 10%, will result in a drop of P-wave velocity. The drop in P-wave velocity has a magnitude comparable to that under full gas saturation (Knight *et al.*, 1998). Consequently, partially gas-saturated reservoirs may be mistakenly drilled as a prospect. This study explores the lithological effect on partial gas saturation and its relationship with seismic rock properties. The partially saturated sequences observed in the Lower Congo basin (Fig. 6.2 and Fig. 6.4) and Møre Basin of Mid Norwegian continental margins (Fig. 6.7) reveals that anomalies are not fully saturated and did not reached the spill point of the structure (Knight *et al.*, 1998; Toms *et al.*, 2007; Raji, 2013).

Seismic attenuation beneath high-amplitude anomalies were observed in the Lower Congo Basin and Møre Basin of Mid Norwegian continental margins (Fig. 6.6 and Fig. 6.7). The anomalous zone in Møre Basin developed in a northward dipping Havsule Dome (Fig. 6.6). The anomalous zone is about 4 kilometers wide and eleven kilometers long. The anomalous

zone is oriented north-south Havsule dome and RMS amplitude map of anomalous zone reveals close conformity between orientation of anomalies and TWT structural map of the top Brygge Formation (Fig. 6.7). The anomalous zone is not confined to the structure contours of the top the Brygge Formation.

The anomalous zone thickness contour map of anomalous zone with contour interval of 20 meters overlay at root mean square amplitude map of the anomalous zone in the fine grained Brygge Formation. Trace of anomalous zone (red dotted line) following the trend of thickness map contours dipping from north to south (Fig. 6.11) that implies the anomalous zone is extending towards up dip direction this implies that the anomalous zone is still a active zone and has dynamic fluid mechanism.

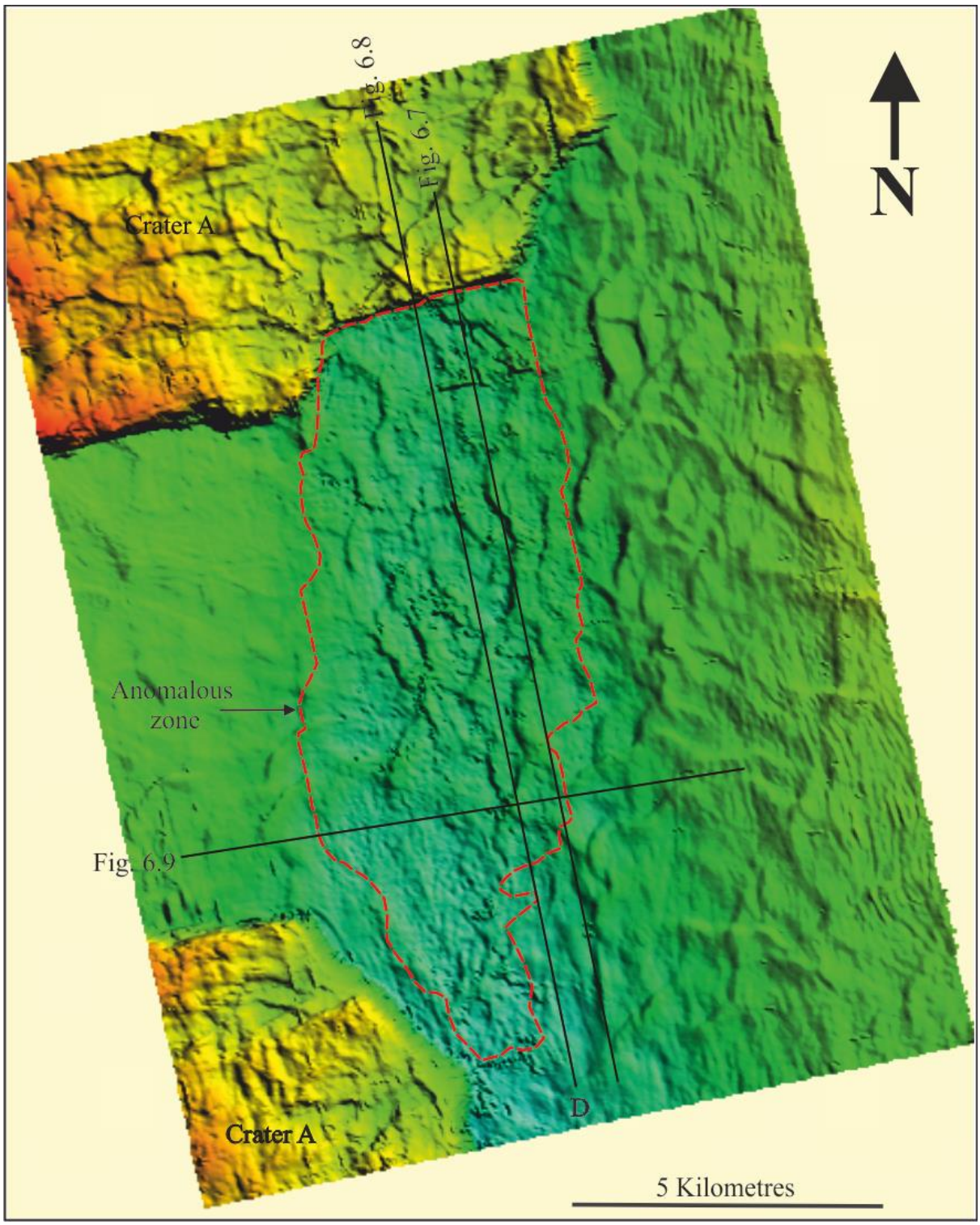

Figure 6.6: Time structure map top of the Brygge Formation, Red dotted line marked the boundary of the anomalous zone. High-amplitudes started to develop south side of crater A that act as a lateral seal.

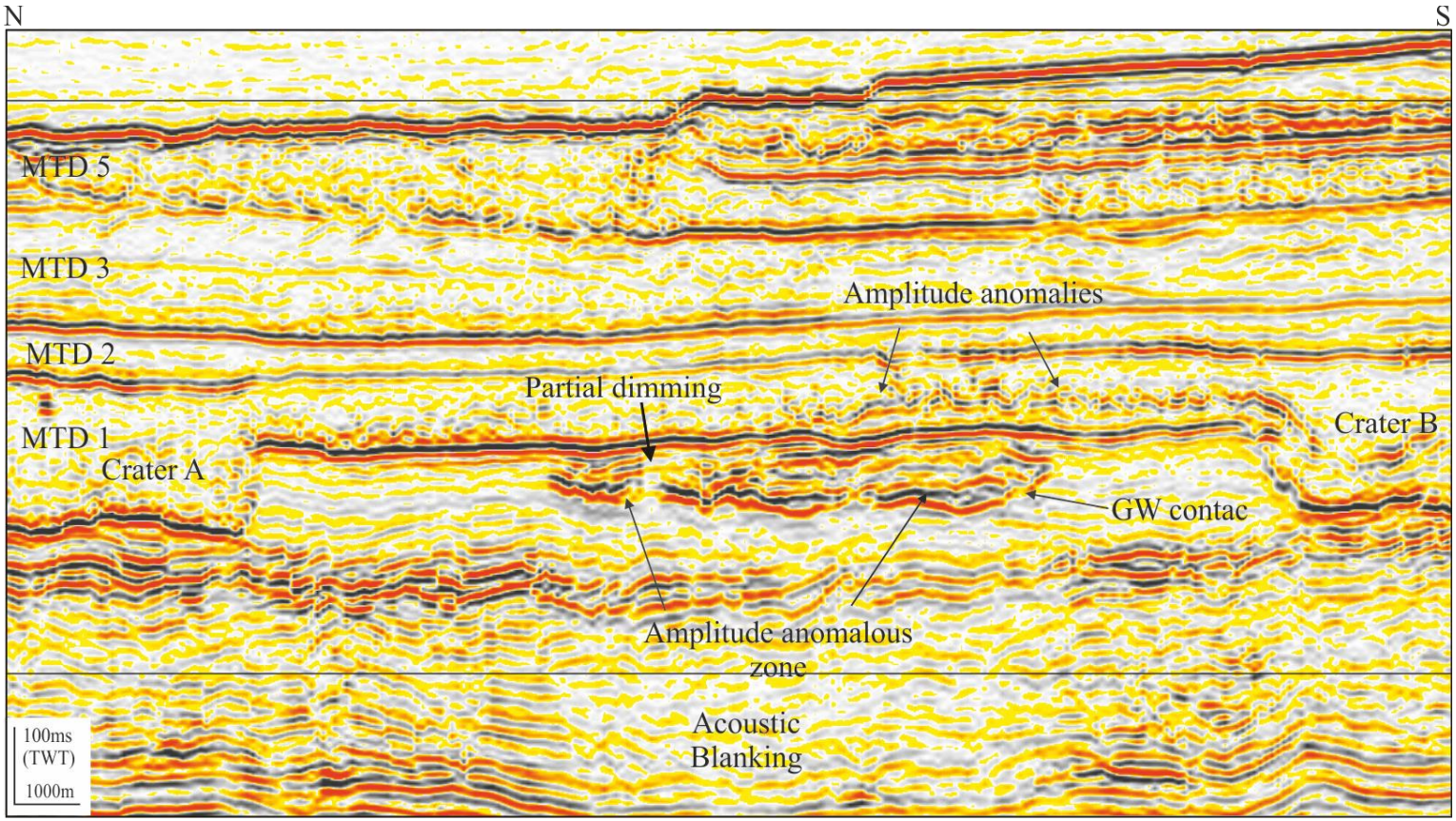

Figure 6.7: Seismic section (vertical exaggeration is approximately eight times) showing some high-amplitude anomalous zone developed between two carters (Crater A in north and carter B in south). Seismic blanking zone is also observed below up to the extent of this zone. Amplitudes are not laterally continues due to presence of polygonal faults that are acting as a barrier or leakage carrier for gas migration depending on juxtaposition with corresponding beds. Partial dimming is also observed on the amplitude anomalous zone. For location of line see Fig. 6.6.

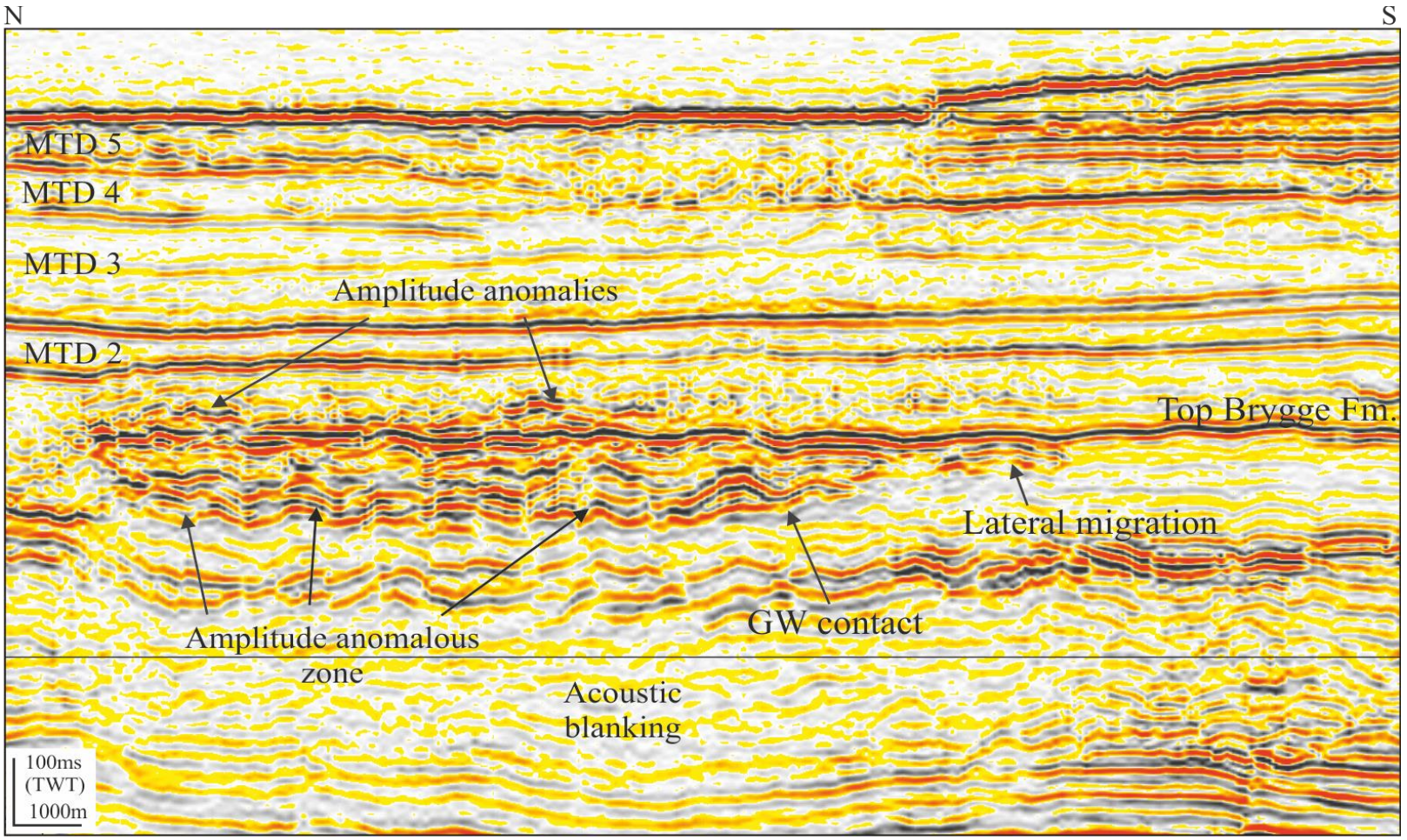

Figure 6.8: Seismic section showing high-amplitude anomalous zone developed between two carters (Crater A in north). Seismic blanking zone is also observed below up to the extent of this zone. Amplitudes anomalies are laterally migrate towards up dip direction (south). Gas water contact is undulated due to presence of polygonal faults. For location of line see Fig. 6.6.

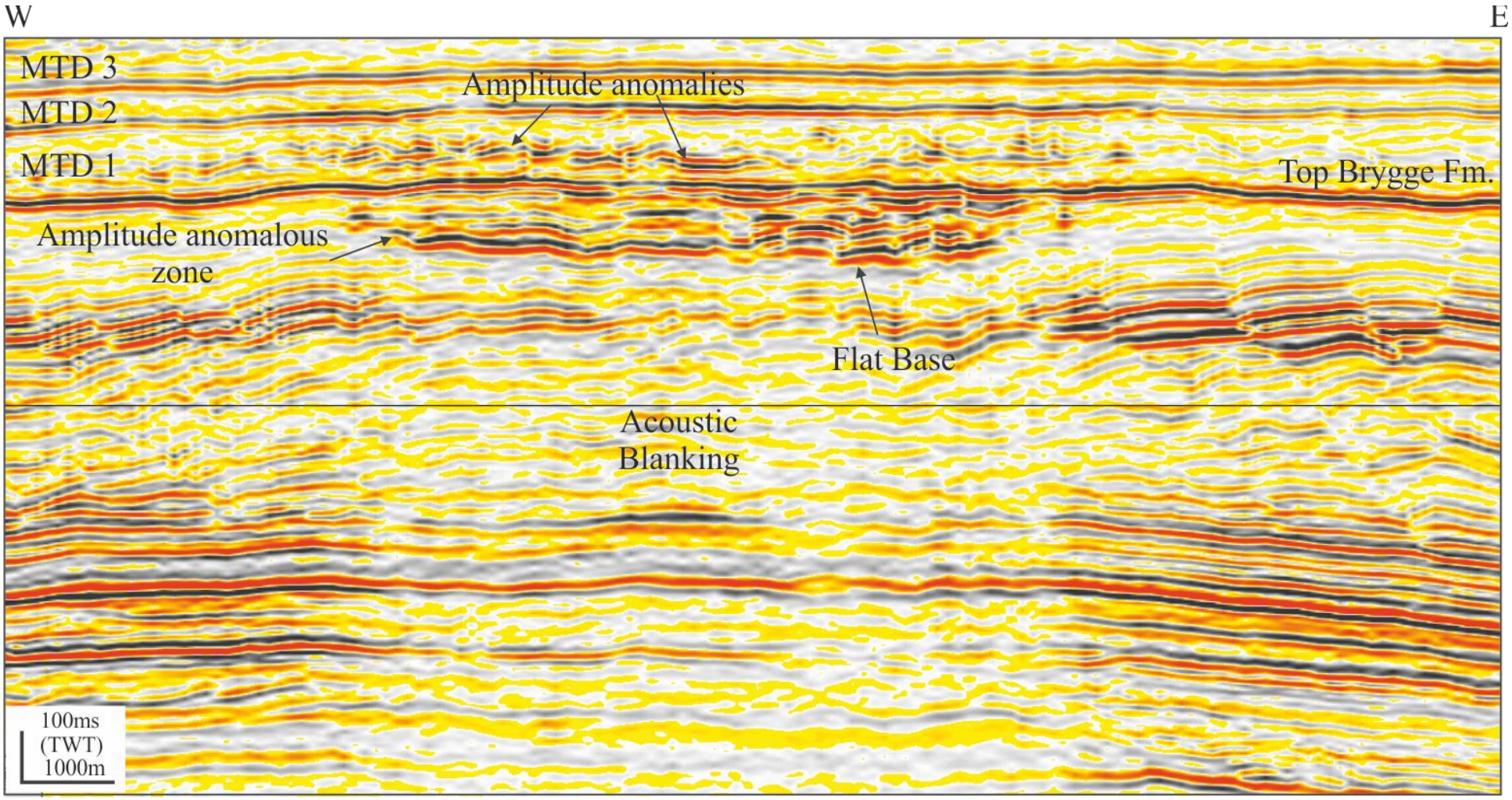

Figure 6.9: Seismic section showing high-amplitude anomalous zone developed between. Seismic blanking zone is also observed below up to the extent of this zone. Anomalies are observed in the Naust Formation. Gas water contact is undulated due to presence of polygonal faults. For location of line see Fig. 6.6.

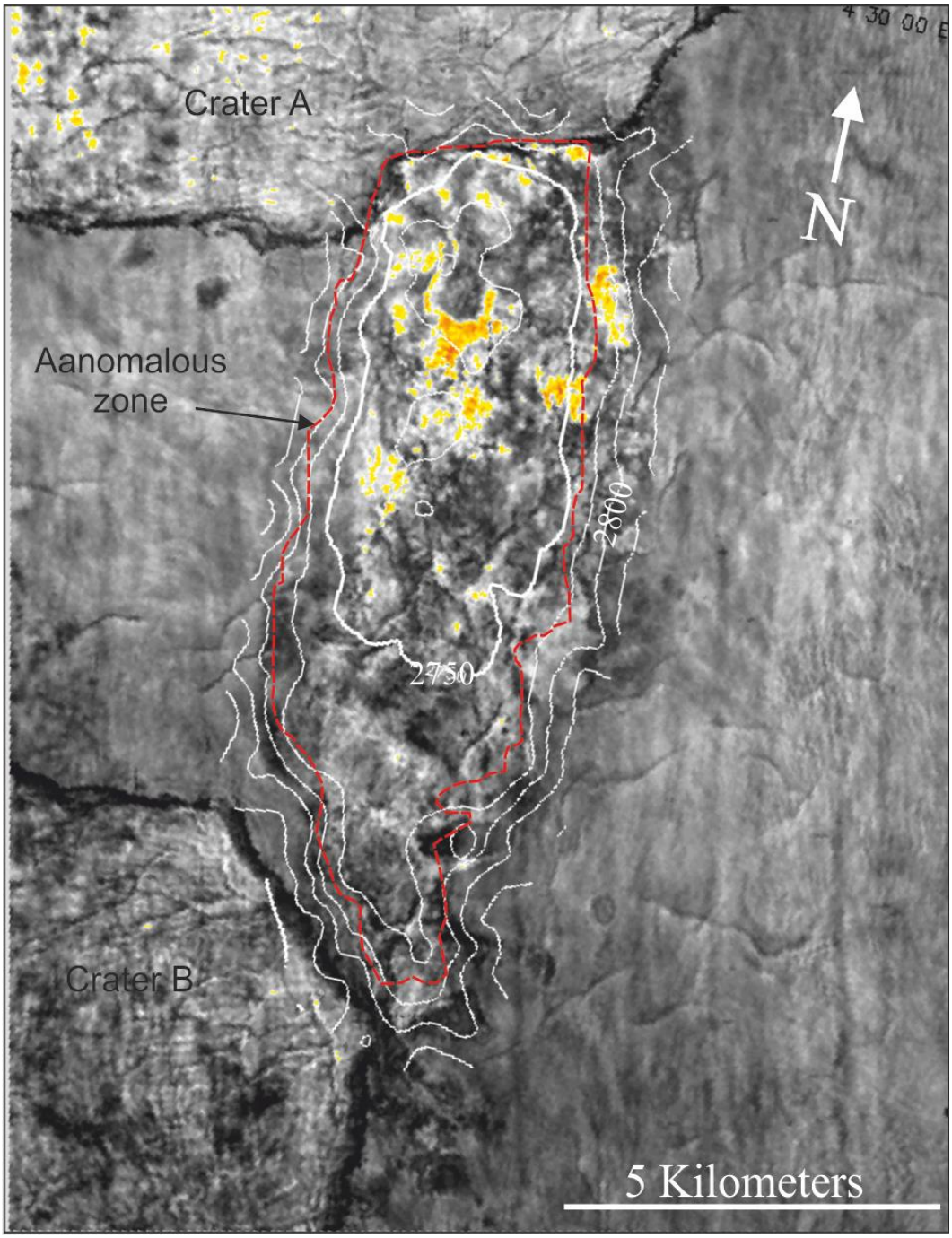

Figure 6.10: structural contour map of top Brygge Formation confirming that anomalous zone is developed at the crest of Havsule Dome. Trace of anomalous zone (red dotted line) following the trend of structural contours from dipping north to south but has irregular cross cutting geometry with time contours.

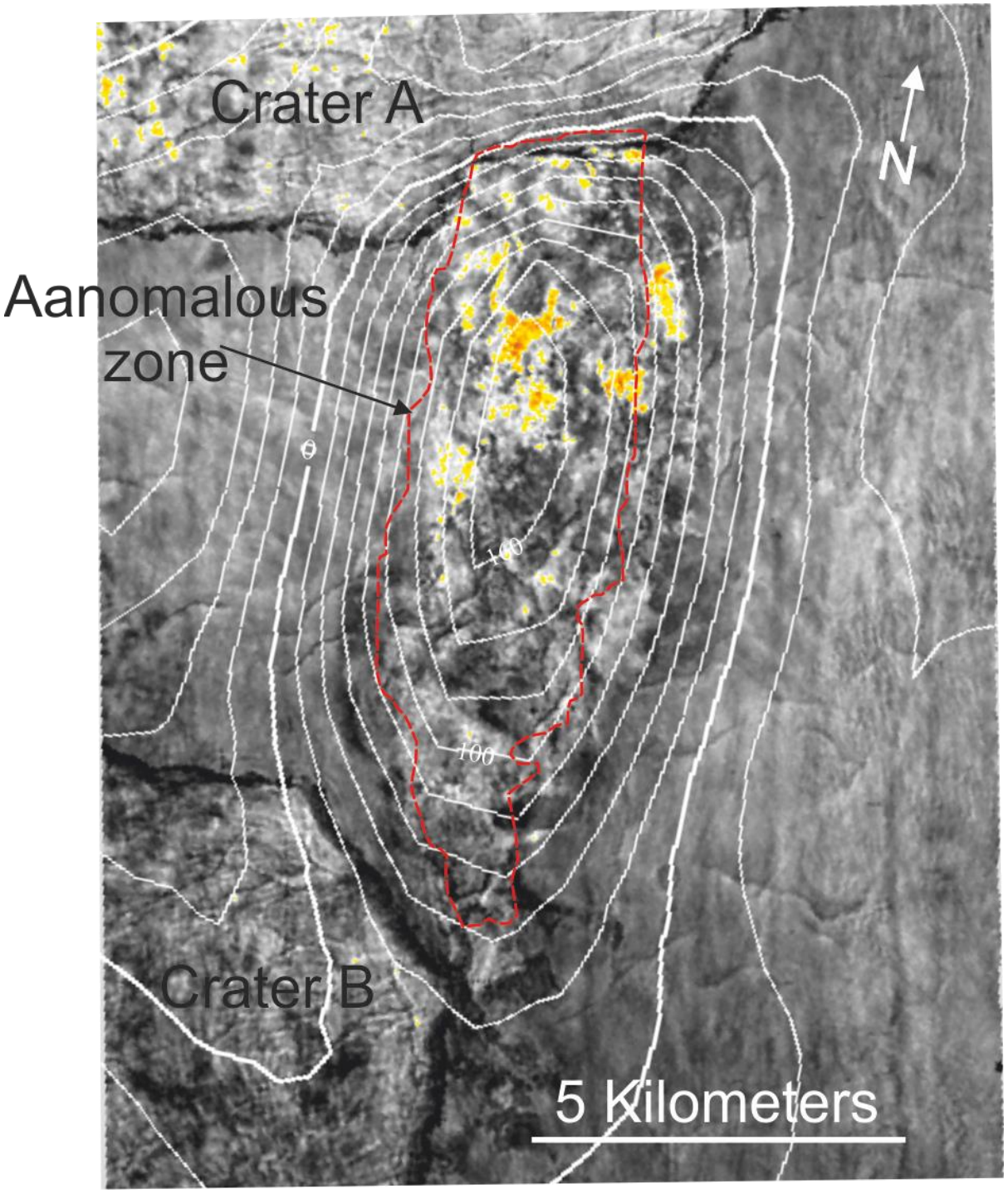

Figure 6.11: Thickness contour map of anomalous zone with contour interval of 20 meters overlay at rout mean square amplitude map of anomalous zone in fine grained Brygge Formation. Trace of anomalous zone (red dotted line) following the trend of thickness map contours from north to south up dipping.

6.5 Implication of the research

The findings of this research have important implications for oil and gas exploration. The research focused only on amplitude anomalies associated with hydrocarbons and particularly with gas. Each individual amplitude anomaly provides an insight into the geoplumbing system in two sedimentary basins. Implication of amplitude anomalies have already been discussed in detail in Chapter 4, 5 and 6 and are summarised here:

1) Careful seismic analysis of high-amplitude anomalous zone over a north-south oriented anticlinal structure in the Møre Basin explain how the vertical stacking of anomalies developed in calcareous siliciclastic sediments where vertical permeability of sediments are low as compared to horizontal permeabilities (Chapter 3).
2) The distribution of amplitude anomalies in the Møre Basin allow us to infer the specific migration mechanisms on small scale, for example, the cluster of amplitude anomalies implies a micro scale migration through capillary entry pressure and macro scale processes of gas migration through faults.
3) There is a distinct gas-water contact (GWC) in the Møre Basin which is concave-upward which implies flat spots due to hydrocarbons are not always flat, which also leads us to conclude that the GWC is a dynamic contact.
4) Distributions of high-amplitude anomalies in hemipelagite sediments in the waste zone of the Lower Congo Basin suggest that fluid migration from Oligocene-Miocene turbidite main reservoirs through vertical anomaly clusters (VACs), stratal and possibly through faults. All these possibilities of fluid flow migration implies that in the active basin like the LCB.

5) Geometries and orientations of amplitude anomalies over a structure (for example amplitude anomalies developed in the levees of mud filled channel levee complex system) have been identified as an indicator of further migration of fluid away from channel.

6) Mass transport deposits (MTDs) are characterised by composition and structural heterogeneity which may incite their capability as a hydrocarbon reservoirs (Gamboa *et al.*, 2012; Omosanya and Alves, 2014). In chapter 4 and 5 was shown that homogeneous and heterogeneous nature of the MTD described the potential of it as a hydrocarbon carrier or seal. In LCB, the MTDs observed transparent above the patchy anomaly which implies the MTDs in the waste zone were acting as a seal.

6.6 Limitation of the research

The work produced for this research was benefited from of the 3D seismic data from the Lower Congo Basin and the Møre Basin. The high quality seismic data from LCB allied to a very low number of artefacts in shallow section, allowed a very good visualisation and interpretation of the seismic amplitude anomalies and associated structures present in the studied stratigraphic intervals. The limitations of the research in this thesis are summarised as follows;

The availability of well data would have allowed a much greater calibration of the seismic horizons, a more precise dating of horizons, calculation of sedimentations rates which could have been correlated with timing and positions of fluid-related amplitude anomalies. Porosity and density measurements would provide information on physical properties of the host formations to explain the origin of amplitude anomalies. Pore pressure measurements within main reservoirs, hemipelagic units and MTDs would have helped to determine the fluid flow behaviour and allow a better understanding on the geo-plumbing history in

different lithologies. Furthermore, sonic logs across the studied stratigraphic units would also have enabled me to constrain the effect of downward increasing velocity on apparent bed thickness in time-domain data.

A high resolution seismic survey would have been helpful for better illustrating the internal structures of high-amplitude anomalies and associated plumbing features that were possibily below seismic resolution and increase the accuracy of geometrical measurements. It would have been especially useful for determining the height of anomalies associated with gas and could have been used to better constrain the contact position between gas anomalies and their lateral extents.6.6.1 Chapter 3

1. The plumbing system of the study area was not properly outlined in as much detail because the seismic data was truncated at 4 ms TWT, and for that reason it was not possible to comment on whether deep-seated features exist that could help to explain specific position and development of the anomalous zone.
2. There was limited well data to calibrate lithology of the interval where anomalous zone is developed.
3. The vertical resolution of 3D seismic data limited the extent at which anomalies could be interpreted and classified in cross-section.

6.6.1 Chapter 4 and 5

1. Near-angle-stack 3D seismic data suffers from decreasing image quality with depth and thus limited the extent at which anomalies could be analysed.
2. This research would also have also benefited from well data but the provided well data files were not correct and not able to load on the work station due to problem in

check shot data file. Due to this reason correlation of amplitude anomalies with well data was not possible for detailed study.

3. Seismic acquisition foot prints are observed on the shallow section of the Late Miocene-recent sediments

6.7 Future work

The work done in this thesis provided a number of answers to better understand development and distribution of high-amplitude anomalies in offshore basins but many other open questions remain. As such, going further in our general understanding about development, distribution and associated fluid migration mechanism requires a detailed research with calibration results from well data.

The key point for understanding high-amplitude anomalies is to establish the timing of geoplumbing in the study area. The proposed leakage model in Møre Basin case study needs to be recalibrated with well data for two reasons; first, layers within the Brygge Formation are a few meters thick which is below the vertical seismic resolution to explain geological heterogeneities and second, throw of polygonal faults were too far below the seismic resolution to properly understand leakage mechanism through faults. Therefore; further detailed studies of the proposed leakage model will lead to a better understanding of development of anomalous zone which may provide a better insight to the origin on the concave upward gas-water contact.

The leakage mechanism proposed in Lower Congo Basin through vertical anomaly clusters presented by Foschi *et al.* (2014) to dominantly vertical gas migration across the multilayers of low permeable hemipelagic sediments; need more detailed work with calibration with well data.

CHAPTER 7

Conclusions

CHAPTER SEVEN

7.1 Conclusions

The purpose of this chapter is to summarise the main results and conclusions drawn throughout this work. The core themes of this research have important implications for the wider topic of seal integrity and hydrocarbon migration through fine-grained sedimentary series. The main conclusions of this work are as follows;

7.2 Conclusions from Chapter 3: the Møre Basin

1. A 165-meter-thick high amplitude anomalous zone, 4 kilometers wide and 11 kilometers long, is developed in a succession of biosiliceous sediments that are deformed intensely by compaction-derived polygonal faults.
2. The anomalous zone developed at the crest of a structure called the Havsule Dome.
3. Continuity of seismic reflections through the anomaly on instantaneous phase profiles indicate the anomalous zone is developed in the same stratigraphy and therefore lithologies as is regarded regionally in that interval.
4. Although poorly imaged, it is also likely that pervasive polygonal faults are also developed in the anomalous zone as is observed regionally in the stratigraphic interval.
5. The amplitude anomaly is attributed to the presence of free gas. This interpretation was based on several observations:
    a) The location of the anomaly at the crest of the dome structure,
    b) The geometry of the host sediments,
    c) The presence of a pronounced velocity push down,

d) Interval velocities calculated inside the anomalous zone are about 1500 m/sec which is much less (1700 m/sec to 2300 m/sec) than the interval velocity of the regional host lithology in the Brygge Formation.

e) The presence of anomalies in the seal immediately above the amplitude anomaly cluster.

6. Gas leakage was attributed to capillary entry pressure and through polygonal faults that happened due to development of column height in calcareous rich oozes sediment. Their thickness varies from less than meter to maximum 8 meters with following clay/silt layers.
7. Crater A in north is acting as a seal unit as dot observed any amplitude anomaly and amplitude is expanding towards Anomaly is not charged up to spill point so that is why anomaly is propagating towards south direction.
8. The reason for the curved shape of the basal gas/water contact is due to the fact that different layers of high amplitude anomalies within the anomalous zone exist and every layer acts like a separate reservoir.
9. This is the first description of a hydrocarbon fluid contact with this shape with a dynamics of hydrocarbon trapping.

7.3 Conclusion from Chapter 4

There are number of different amplitude anomalies in the waste zone above deep-seated turbidite reservoirs.

1 Amplitude anomalies are classified into different groups on the basis of their plan-form geometry, their lateral extent and include;

a. Linear anomalies: Anomalies that are isolated, long and narrow features on

amplitude map with aspect ratios (maximum length to maximum width) > 6.

b. Sub-circular anomalies: Amplitude anomalies that have regular to semi-irregular, and circular to elliptical plan-view geometries.

c. Patchy anomalies: groups of amplitude anomalies that are isolated and have irregular plan form geometries with rough edges. Some of the patchy anomalies have finger-like features that emerge out from the main anomaly.

d. Discrete, filamental anomalies: positive, high amplitude anomalies. These anomalies are observed in seal Unit 4 and occasionally in MTDs.

2. A combination of seismic interpretation, attribute analyses and well ties were used to assess the likelihood of amplitude anomalies defining zones of hydrocarbon or non-hydrocarbon-bearing fluids.

    a. Only the sub-circular and patchy anomalies were found to be hydrocarbon-bearing.

3. An analysis of acoustic properties and seismic attributes of the high-amplitude anomalies indicates that they attributed to the presence of gas.

7.4 Conclusion from Chapter 5

1. There are multiple possible routes for the leaking fluids sources from the main turbidite reservoirs to the waste zone.

    a. CLC's are not charged from the flanks but instead are charged by feeding points from main reservoirs seated below them.

    b. There are other possible pathways to migrate hydrocarbon through faults and stratal routings.

2. The 3D distribution of HAAs, their geometry and geological context suggest hydrocarbon leaked through thin sands, faults, VACs, and strata routings.
3. I attribute the development of VACs to dominantly vertical gas migration across a multi-layered low permeability reservoir interval, where individual layers are filled successively from bottom-to-top, and where small normal faults provide conduits for cross-stratal migration.

REFERENCES

Alvarado, J. M., Aminzadeh, F. and Connolly, D. (2003). Application of Gas Chimney Technology in the Lamprea area offshore GOM. In: AAPG 2003 National Convention Abstracts.

ALVARADO, J. M., AMINZADEH, F. and CONNOLLY, D. (2003). Application of Gas Chimney Technology in the Lamprea area offshore GOM. In: AAPG 2003 National Convention Abstracts.

AMINZADEH, F., CONNOLLY, D. and DE GROOT, P. (2002). Interpretation of gas chimney volumes. In: SEG Annual Meeting, October. p. 6-11.

Aminzadeh, F., Connolly, D., Heggland , R., Meldahl, P. and De Groot, P. (2002b). Geohazard detection and other applications of chimney cubes. The Leading Edge, Vo. 21, p. 681.

Aminzadeh, F., Groot, P., Berge, T., Oldenziel, T. and Ligtenberg, H. (2002c). Determining Migration path from seismically derived gas chimney. Near-Surface Hydrocarbon Migration: Mechanisms and Seepage Rates, Vo., p. 7–10.

Anderson, J., Cartwright, J., Drysdall, S. and Vivian, N. (2000). Controls on turbidite sand deposition during gravity-driven extension of a passive margin: examples from Miocene sediments in Block 4, Angola. Marine and Petroleum Geology, Vo. 17, p. 1165-1203.

Andresen, K. J. (2012). Fluid flow features in hydrocarbon plumbing systems: What do they tell us about the basin evolution? Marine Geology, Vo. 332, p. 89-108.

Andresen, K. J. and Huuse, M. (2011). 'Bulls-eye'pockmarks and polygonal faulting in the Lower Congo Basin: Relative timing and implications for fluid expulsion during shallow burial. Marine Geology, Vo. 279, p. 111-127.

ANKA, Z., ONDRAK, R., KOWITZ, A. and SCHØDT, N. (2013). Identification and numerical modelling of hydrocarbon leakage in the Lower Congo Basin: Implications on the genesis of km-wide seafloor mounded structures. Tectonophysics, Vo. 604, p. 153-171.

Anka, Z., Séranne, M. and Primio, R. d. (2010). Evidence of a large upper-Cretaceous depocentre across the Continent-Ocean boundary of the Congo-Angola basin. Implications for palaeo-drainage and potential ultra-deep source rocks. Marine and Petroleum Geology, Vo. 27, p. 601-611.

Anka, Z., Séranne, M., Lopez, M., Scheck-Wenderoth, M. and Savoye, B. (2009). The long-term evolution of the Congo deep-sea fan: A basin-wide view of the interaction between a giant submarine fan and a mature passive margin (ZaiAngo project). Tectonophysics, Vo. 470, p. 42-56.

Arntsen, B., Wensaas, L., Løseth, H. and Hermanrud, C. (2007). Seismic modeling of gas chimneys. Geophysics, Vo. 72, p. SM251-SM259.

Avseth, P., Mukerji, T. and Mavko, G. (2005). Quantitative seismic interpretation: applying rock physics tools to reduce interpretation risk, Cambridge University Press

Bahorich, M. and Farmer, S. (1995). The coherence cube. The Leading Edge, Vo. 14, p. 1,053-58.

Barth, G. A., Scholl, D. W. and Childs, J. R. (2004). Quantifying the methane content of natural gas and gas hydrate accumulations in the deep-water basins of the Bering Sea. In: Extended abstract, AAPG Hedberg Conference, Vancouver. p. 16.

Berg, K., Solheim, A. and Bryn, P. (2005). The Pleistocene to recent geological development of the Ormen Lange area. Marine and Petroleum Geology, Vo. 22, p. 45-56.

Berggren, W. A., Hilgen, F., Langereis, C., Kent, D. V., Obradovich, J., Raffi, I., Raymo, M. and Shackleton, N. (1995). Late Neogene chronology: new perspectives in high-resolution stratigraphy. Geological Society of America Bulletin, Vo. 107, p. 1272-1287.

Berndt, C. (2005). Focused fluid flow in passive continental margins. Philosophical Transactions of the Royal Society A: Mathematical, Physical and Engineering Sciences, Vo. 363, p. 2855-2871.

Blystad, P., Brekke, H., Færseth, R., Larsen, B., Skogseid, J. and Tørudbakken, B. (1995). Structural elements of the Norwegian continental shelf. Part II: The Norwegian Sea region. Norwegian Petroleum Directorate Bulletin, Vo. 8, p. 45.

Bøen, F., Eggen, S. and Vollset, J. (1984). Structures and basins of the margin from 62–69 N and their development. Petroleum Geology of the North European Margin, Vo. 271, p. 284.

Brekke, H. and Riis, F. (1987). Tectonics and basin evolution of the Norwegian shelf between 62 N and 72 N. Norsk Geologisk Tidsskrift, Vo. 67, p. 295-322.

Brice, S. E., Cochran, M. D., Pardo, G. and Edwards, A. D. (1982). Tectonics and sedimentation of the South Atlantic rift sequence: Cabinda, Angola. Studies in continental margin geology: AAPG Memoir, Vo. 34, p. 5-18.

Broucke, O., Temple, F., Rouby, D., Robin, C., Calassou, S., Nalpas, T. and Guillocheau, F. (2004). The role of deformation processes on the geometry of mud-dominated turbiditic systems, Oligocene and Lower–Middle Miocene of the Lower Congo basin (West African Margin). Marine and Petroleum Geology, Vo. 21, p. 327-348.

Brown, A. R. (2001). Calibrate yourself to your data! A vital first step in seismic interpretation. Geophysical prospecting, Vo. 49, p. 729-733.

Brown, A. R. (2004). Interpretation of three-dimensional seismic data, Soc of Exploration Geophysicists, No. 42

Brown, A. R. (2005). Pitfalls in 3D seismic interpretation: Keynote presentation at the 11th Annual 3-D Seismic Symposium, Denver. The leading edge, Vo. 24, p. 716-717.

Brown, A. R. (2012). Dim spots: Opportunity for future hydrocarbon discoveries? The Leading Edge, Vo. 31, p. 682-683.

Brown, A. R., Wright, R. M., Burkart, K. D. and Abriel, W. L. (1984). Interactive seismic mapping of net producible gas sand in the Gulf of Mexico. Geophysics, Vo. 49, p. 686.

Brownfield, M. E. and Charpentier, R. R. (2006). Geology and Total Petroleum Systems of the West-Central Coastal Province (7203), West Africa. Vo.

Bryn, P., Berg, K., Stoker, M., Haflidason, H. and Solheim, A. (2005). Contourites and their relevance for mass wasting along the Mid-Norwegian Margin. Marine and Petroleum Geology, Vo. 22, p. 85-96.

Bukovics, C. and Ziegler, P. A. (1985). Tectonic development of the Mid-Norway continental margin. Marine and Petroleum Geology, Vo. 2, p. 2-22.

Bunz, S., Mienert, J. and Berndt, C. (2003). Geological controls on the Storegga gas-hydrate system of the mid-Norwegian continental margin. Earth and Planetary Science Letters, Vo. 209, p. 291-307.

Bunz, S., Mienert, J. and Berndt, C. (2003). Geological controls on the Storegga gas-hydrate system of the mid-Norwegian continental margin. Earth and Planetary Science Letters, Vo. 209, p. 291-307.

Burwood, R. (1999). Angola: source rock control for Lower Congo Coastal and Kwanza Basin petroleum systems. Geological Society, London, Special Publications, Vo. 153, p. 181-194.

Calvès, G., Huuse, M., Schwab, A. and Clift, P. (2008). Three-dimensional seismic analysis of high-amplitude anomalies in the shallow subsurface of the Northern Indus Fan: Sedimentary and /or fluid origin. Journal of Geophysical Research, Vo. 113, p. B11103.

Carruthers, D. and de Lind van Wijngaarden, M. (2000). Modelling viscous-dominated fluid transport using modified invasion percolation techniques. Journal of Geochemical Exploration, Vo. 69, p. 669-672.

Cartwright, J. A. (1997). Polygonal extensional fault systems: a new class of structure formed during the early compaction of shales. Fluid Flow and Transport in Rocks-Mechanisms and Effects, Vo., p. 35-56.

Cartwright, J. and Dewhurst, D. (1998). Layer-bound compaction faults in fine-grained sediments. Geological Society of America Bulletin, Vo. 110, p. 1242.

Cartwright, J., Huuse, M. and Aplin, A. (2007). Seal bypass systems. AAPG bulletin, Vo. 91, p. 1141-1166.

Cartwright, J., James, D. and Bolton, A. (2003). The genesis of polygonal fault systems: a review. Geological Society, London, Special Publications, Vo. 216, p. 223-243.

Castagna, J. P., Sun, S. and Siegfried, R. W. (2003). Instantaneous spectral analysis: Detection of low-frequency shadows associated with hydrocarbons. The Leading Edge, Vo. 22, p. 120.

Chadwick, R., Arts, R. and Eiken, O. (2005). 4D seismic quantification of a growing CO2 plume at Sleipner, North Sea. In: Geological Society, London, Petroleum Geology Conference series. Geological Society of London, p. 1385-1399.

Chopra, S. and Marfurt, K. J. (2007). Seismic attributes for prospect identification and reservoir characterization, Society of Exploration Geophysicists

Chopra, S. and Larsen, G. (2000). Acquisition footprint its detection and removal. CSEG Recorder, Vo. 25, p. 16.

Chopra, S., Castagna, J. and Portniaguine, O. (2006). Seismic resolution and thin-bed reflectivity inversion. CSEG Recorder, Vo. 31, p. 19-25.

Clark, J. D. and Pickering, K. T. (1996). Architectural elements and growth patterns of submarine channels: application to hydrocarbon exploration. AAPG bulletin, Vo. 80, p. 194-220.

Cole, G., Requejo, A., Ormerod, D., Yu, Z. and Clifford, A. (2000). AAPG Memoir 73, Chapter 23: Petroleum Geochemical Assessment of the Lower Congo Basin. Vo.

Cunningham, R. and Lindholm, R. M. (2000). AAPG Memoir 73, Chapter 8: Seismic Evidence for Widespread Gas Hydrate Formation, Offshore West Africa. Vo.

Dalland , A., Worsley, D., Ofstad, K. and Oljedirektoratet, N. (1988). A Lithostratigraphic Scheme for the Mesozoic and Cenozoic and Succession Offshore Mid-and Northern Norway, Oljedirektoratet

Davies, R. J., Stewart, S. A., Cartwright, J. A., Lappin, M., Johnston, R., Fraser, S. I. and Brown, A. R. (2004). 3D seismic technology: are we realising its full potential? Geological Society, London, Memoirs, Vo. 29, p. 1.

Deangelo, M. V. and Wood, L. J. (2001). 3-D seismic detection of undrilled prospective areas in a mature province, South Marsh Island , Gulf of Mexico. The Leading Edge, Vo. 20, p. 1282.

Deegan, C. t. and Scull, B. J. (1977). A stand ard lithostratigraphic nomenclature for the Central and Northern North Sea, HMSO, No. 1

Dennis, H., Baillie, J., Holt, T. and Wessel-Berg, D. (2000). Hydrodynamic activity and tilted oil-water contacts in the North Sea. Norwegian Petroleum Society Special Publications, Vo. 9, p. 171-185.

Doré, A. and Lundin, E. (1996). Cenozoic compressional structures on the NE Atlantic margin; nature, origin and potential significance for hydrocarbon exploration. Petroleum Geoscience, Vo. 2, p. 299.

Doyle, E., Berry, J. and McCormack, N. (2003). Plan for surprises: Pore pressure challenges during the drilling of a deepwater exploration well in mid-winter in Norway. In: SPE/IADC Drilling Conference.

Duval, B., Cramez, C. and Jackson, M. (1992). Raft tectonics in the Kwanza basin, Angola. Marine and Petroleum Geology, Vo. 9, p. 389-404.

Dvorkin, J. and Nur, A. (1998). Acoustic signatures of patchy saturation. International Journal of Solids and Structures, Vo. 35, p. 4803-4810.

Enachescu, M. (1990). Structural setting and validation of direct hydrocarbon indicators for Amauligak oil field, Canadian Beaufort Sea. AAPG bulletin, Vo. 74, p. 41-59.

Evans, B. J. and Dragoset, W. H. (1997). A hand book for seismic data acquisition in exploration, Society of exploration geophysicists

Fink, P., Zimmer, W. and Punch, S. (2012). A Mediterranean petroleum province on the North Africa Plate margin: The Sicily Channel. The Leading Edge, Vo. 31, p. 794-801.

Forsberg, C. F. and Locat, J. (2005). Mineralogical and microstructural development of the sediments on the Mid-Norwegian margin. Marine and Petroleum Geology, Vo. 22, p. 109-122.

Foschi, M., Cartwright, J. A. and Peel, F. J. (2014). Vertical anomaly clusters: Evidence for vertical gas migration across multilayered sealing sequences. AAPG Bulletin, Vo. 98, p. 1859-1884.

Frey-Martnez, J., Cartwright, J., Hall, B. and Huuse, M. (2007). Clastic intrusion at the base of deep-water sand s: A trap-forming mechanism in the eastern Mediterranean. Vo.

Gabrielsen, R. (1984). Long-lived fault zones and their influence on the tectonic development of the southwestern Barents Sea. Journal of the Geological Society, Vo. 141, p. 651-662.

Gamboa, D., Alves, T. M. and Cartwright, J. (2012). A submarine channel confluence classification for topographically confined slopes. Marine and Petroleum Geology, Vo. 35, p. 176-189.

Gay, A. and Berndt, C. (2007). Cessation/reactivation of polygonal faulting and effects on fluid flow in the Vøring Basin, Norwegian Margin. Journal of the Geological Society, Vo. 164, p. 129.

Gay, A., Lopez, M., Berndt, C. and Séranne, M. (2007). Geological controls on focused fluid flow associated with seafloor seeps in the Lower Congo Basin. Marine Geology, Vo. 244, p. 68-92.

Gay, A., Lopez, M., Cochonat, P. and Sermondadaz, G. (2004). Polygonal faults-furrows system related to early stages of compaction–upper Miocene to recent sediments of the Lower Congo Basin. Basin Research, Vo. 16, p. 101-116.

Gay, A., Lopez, M., Cochonat, P., Levaché, D., Sermondadaz, G. and Seranne, M. (2006). Evidences of early to late fluid migration from an upper Miocene turbiditic channel revealed by 3D seismic coupled to geochemical sampling within seafloor pockmarks, Lower Congo Basin. Marine and Petroleum Geology, Vo. 23, p. 387-399.

Gay, A., Lopez, M., Cochonat, P., Séranne, M., Levaché, D. and Sermondadaz, G. (2006). Isolated seafloor pockmarks linked to BSRs, fluid chimneys, polygonal faults and stacked Oligocene–Miocene turbiditic palaeochannels in the Lower Congo Basin. Marine Geology, Vo. 226, p. 25-40.

Gay, A., Lopez, M., Cochonat, P., Sultan, N., Cauquil, E. and Brigaud, F. (2003). Sinuous pockmark belt as indicator of a shallow buried turbiditic channel on the lower slope of the Congo Basin, West African Margin. Geological Society, London, Special Publications, Vo. 216, p. 173-189.

Gay, A., Lopez, M., Ondreas, H., Charlou, J. L., Sermondadaz, G. and Cochonat, P. (2006b). Seafloor facies related to upward methane flux within a Giant Pockmark of the Lower Congo Basin. Marine Geology, Vo. 226, p. 81-95.

Gee, M. and Gawthorpe, R. (2006). Submarine channels controlled by salt tectonics: Examples from 3D seismic data offshore Angola. Marine and Petroleum Geology, Vo. 23, p. 443-458.

Gee, M., Gawthorpe, R. and Friedmann, S. (2006). Triggering and evolution of a giant submarine land slide, offshore Angola, revealed by 3D seismic stratigraphy and geomorphology. Journal of Sedimentary Research, Vo. 76, p. 9-19.

Gee, M., Gawthorpe, R., Bakke, K. and Friedmann, S. (2007). Seismic geomorphology and evolution of submarine channels from the Angolan continental margin. Journal of Sedimentary Research, Vo. 77, p. 433-446.

Giresse, P. (2005). Mesozoic–Cenozoic history of the Congo Basin. Journal of African Earth Sciences, Vo. 43, p. 301-315.

Gjelberg, J., Martinsen, O., Charnock, M., Møller, N. and Antonsen, P. (2005). The reservoir development of the Late Maastrichtian–Early Paleocene Ormen Lange gas field, Møre Basin, Mid-Norwegian Shelf. In: Geological Society, London, Petroleum Geology Conference series. Geological Society of London, p. 1165-1184.

Gluyas, J. and Swarbrick, R. (2009). Petroleum geoscience, John Wiley and Sons

Grunnaleite, I. and Gabrielsen, R. H. (1995). Structure of the Møre Basin, mid-Norway continental margin. Tectonophysics, Vo. 252, p. 221-251.

György Marton, L., Tari, G. C. and Lehmann, C. T. (2000). Evolution of the Angolan Passive Margin, West Africa, With Emphasis on Post-Salt Structural Styles. Atlantic rifts and continental margins, Vo., p. 129-149.

Haflidason, H., Lien, R., Sejrup, H. P., Forsberg, C. F. and Bryn, P. (2005). The dating and morphometry of the Storegga Slide. Marine and Petroleum Geology, Vo. 22, p. 123-136.

Han, D. H. and Batzle, M. (2002). Fizz water and low gas-saturated reservoirs. The Leading Edge, Vo. 21, p. 395.

Haskell, N. L., Nissen, S. E., Lopez, J. A., and Bahorich, M. S., (1995). 3-D seismic coherency and the imaging of sedimentological features in predictive high resolution sequence stratigraphy. Norwegian Petrol. Soc. Conf.

Heggland , R. (2004). Definition of geohazards in exploration 3-D seismic data using attributes and neural-network analysis. AAPG bulletin, Vo. 88, p. 857-868.

Heggland , R. (2005). Using gas chimneys in seal integrity analysis: A discussion based on case histories. Evaluating fault and cap rock seals: AAPG Hedberg Series, Vo., p. 237-245.

Hilterman, F. J. (2001). Seismic amplitude interpretation: 2001 Distinguished Instructor Short Course, Distinguished Instructor Series, No. 4, Soc. of Expl. Soc. Expl. Geophys, Vo.

Hjelstuen, B. O., Eldholm, O. and Skogseid, J. (1997). Vøring Plateau diapir fields and their structural and depositional settings. Marine Geology, Vo. 144, p. 33-57.

Hjelstuen, B. O., Sejrup, H. P., Haflidason, H., Nygård, A., Berstad, I. M. and Knorr, G. (2004). Late Quaternary seismic stratigraphy and geological development of the south Vøring margin, Norwegian Sea. Quaternary Science Reviews, Vo. 23, p. 1847-1865.

Ho, S., Cartwright, J. and Imbert, P. (2012). Vertical evolution of fluid venting structures in relation to gas flux, in the Neogene-Quaternary of the Lower Congo Basin, Offshore Angola. Marine Geology, Vo. 332, p. 40-55.

Hovland , M. and Svensen, H. (2006). Submarine pingoes: Indicators of shallow gas hydrates in a pockmark at Nyegga, Norwegian Sea. Marine Geology, Vo. 228, p. 15-23.

Hurst, A. and Cartwright, J. (2007). Relevance of sand injectites to hydrocarbon exploration and production. MEMOIRS-AMERICAN ASSOCIATION OF PETROLEUM GEOLOGISTS, Vo. 87, p. 1.

Hustoft, S., Bünz, S. and Mienert, J. (2010). Three dimensional seismic analysis of the morphology and spatial distribution of chimneys beneath the Nyegga pockmark field, offshore mid Norway. Basin Research, Vo. 22, p. 465-480.

Hustoft, S., Mienert, J., Bünz, S. and Nouzé, H. (2007). High-resolution 3D-seismic data indicate focussed fluid migration pathways above polygonal fault systems of the mid-Norwegian margin. Marine Geology, Vo. 245, p. 89-106.

Huuse, M., Jackson, C. a. L., Van Rensbergen, P., Davies, R. J., Flemings, P. B. and Dixon, R. J. (2010). Subsurface sediment remobilization and fluid flow in sedimentary basins: an overview. Basin Research, Vo. 22, p. 342-360.

Imbert, P. (2009). Seismic-scale Expression of Fluid Sourcing Circulation and Expulsion in Sedimentary Series. In: International Petroleum Technology Conference. International Petroleum Technology Conference.

Jansen, J., Giresse, P. and Moguedet, G. (1984). Structural and sedimentary geology of the Congo and southern Gabon continental shelf; a seismic and acoustic reflection survey. Netherland s journal of sea research, Vo. 17, p. 364-384.

Jarvie, D. M., Hill, R. J., Ruble, T. E. and Pollastro, R. M. (2007). Unconventional shale-gas systems: The Mississippian Barnett Shale of north-central Texas as one model for thermogenic shale-gas assessment. AAPG bulletin, Vo. 91, p. 475-499.

Jørgensen, F. and Navrestad, T. (1981). The geology of the Norwegian shelf between 62 N and the Lofoten Island s. Petroleum geology of the continental shelf of NW Europe. Institute of Petroleum Geologists, London, Vo., p. 407-413.

Kearey, P., Brooks, M. and Hill, I. (2002). An introduction to geophysical exploration, Wiley-Blackwell

Knight, R., Dvorkin, J. and Nur, A. (1998). Acoustic signatures of partial saturation. Geophysics, Vo. 63, p. 132-138.

Kolla, V., Bourges, P., Urruty, J. M. and Safa, P. (2001). Evolution of deep-water Tertiary sinuous channels offshore Angola (west Africa) and implications for reservoir architecture. AAPG bulletin, Vo. 85, p. 1373-1405.

Kuhlmann, G., Adams, S., Anka, Z., Campher, C., Di Primio, R. and Horsfield, B. (2011). 3D petroleum systems modelling within a passive margin setting, orange basin, blocks 3/4, offshore south africa–implications for gas generation, migration and leakage. South African Journal of Geology, Vo. 114, p. 387-414.

Laberg, J. S., Stoker, M. S., Dahlgren, K., Haas, H., Haflidason, H., Hjelstuen, B. O., Nielsen, T., Shannon, P. M., Vorren, T. O. and van Weering, T. C. E. (2005). Cenozoic alongslope processes and sedimentation on the NW European Atlantic margin. Marine and Petroleum Geology, Vo. 22, p. 1069-1088.

Larson, R. L. and Ladd, J. W. (1973). Evidence for the opening of the South Atlantic in the Early Cretaceous. Vo.

Lavier, L. L., Steckler, M. S. and Brigaud, F. (2001). Climatic and tectonic control on the Cenozoic evolution of the West African margin. Marine Geology, Vo. 178, p. 63-80.

Lawrence, G. W. M. and Cartwright, J. A. (2010). The stratigraphic and geographic distribution of giant craters and remobilised sediment mounds on the mid Norway margin, and their relation to long term fluid flow. Marine and Petroleum Geology, Vo. 27, p. 733-747.

Lawrence, G. W. M. and Cartwright, J. A. (2009). The initiation of sliding on the mid Norway margin in the Møre Basin. Marine Geology, Vo. 259, p. 21-35.

Lawrence, G. W. M. and Cartwright, J. A. (2010). The stratigraphic and geographic distribution of giant craters and remobilised sediment mounds on the mid Norway margin, and their relation to long term fluid flow. Marine and Petroleum Geology, Vo. 27, p. 733-747.

Lee, M., Collett, T. and Inks, T. (2010). Seismic attribute analysis for gas-hydrate and free-gas prospects on the North Slope of Alaska. Natural Gas Hydrates--Energy Resource Potential and Associated Geologic Hazards: American Association of Petroleum Geologists Memoir, Vo. 89.

Leynaud, D., Sultan, N. and Mienert, J. (2007). The role of sedimentation rate and permeability in the slope stability of the formerly glaciated Norwegian continental margin: the Storegga slide model. Land slides, Vo. 4, p. 297-309.

Lie, Ø. and Trayfoot, M. (2009). Seismic characterization of the first 3D surveys offshore Cyprus and Lebanon. Search and Discovery Article, Vo.

Ligtenberg, J. H. (2005). Detection of fluid migration pathways in seismic data: implications for fault seal analysis. Basin Research, Vo. 17, p. 141-153.

Løseth, H. and Henriksen, S. (2005). A Middle to Late Miocene compression phase along the Norwegian passive margin. In.: Geological Society of London, p. 845.

Løseth, H., Gading, M. and Wensaas, L. (2009). Hydrocarbon leakage interpreted on seismic data. Marine and Petroleum Geology, Vo. 26, p. 1304-1319.

Marfurt, K. J., Kirlin, R. L., Farmer, S. L. and Bahorich, M. S. (1998). 3-D seismic attributes using a semblance-based coherency algorithm. Geophysics, Vo. 63, p. 1150-1165.

Mavko, G., Mukerji, T. and Dvorkin, J. (2009). The rock physics hand book: Tools for seismic analysis of porous media, Cambridge university press

Mayall, M., Jones, E. and Casey, M. (2006). Turbidite channel reservoirs—key elements in facies prediction and effective development. Marine and Petroleum Geology, Vo. 23, p. 821-841.

Meldahl, P., Heggland , R., Bril, B. and de Groot, P. (2001). Identifying faults and gas chimneys using multiattributes and neural networks. The Leading Edge, Vo. 20, p. 474.

Micallef, A., Berndt, C. and Debono, G. (2011). Fluid flow systems of the Malta Plateau, central Mediterranean Sea. Marine Geology, Vo. 284, p. 74-85.

Möller, N. K., Gjelberg, J. G., Martinsen, O., Charnock, M. A., Færseth, R. B., Sperrevik, S. and Cartwright, J. A. (2004). A geological model for the Ormen Lange hydrocarbon reservoir. Norwegian Journal of Geology/Norsk Geologisk Forening, Vo. 84.

Mulder, T., Hüneke, H. and Van Loon, A. (2010). Progress in Deep-Sea Sedimentology. Deep-Sea Sediments. Developments in SedimentologyElsevier, Amsterdam, Vo., p. 1-24.

Müller, T. M. and Gurevich, B. (2004). One-dimensional rand om patchy saturation model for velocity and attenuation in porous rocks. Geophysics, Vo. 69, p. 1166-1172.

Nakajima, T., Peakall, J., Mccaffrey, W. D., Paton, D. A. and Thompson, P. J. (2009). Outer-bank bars: a new intra-channel architectural element within sinuous submarine slope channels. Journal of Sedimentary Research, Vo. 79, p. 872-886.

Nichols, R. J. (1995). The liquification and remobilization of sand y sediments. Geological Society, London, Special Publications, Vo. 94, p. 63-76.

Nombo-Makaya, N. L. and Han, C. H. (2009). Pre-Salt Petroleum System of Vand ji-Conkouati Structure (Lower Congo Basin), Republic of Congo. Research Journal of Applied Sciences, Vo. 4, p. 101-107.

O'brien, J. (2004). Seismic amplitudes from low gas saturation sand s. The Leading Edge, Vo. 23, p. 1236.

OLUBOYO, A., GAWTHORPE, R., BAKKE, K. and HADLER-JACOBSEN, F. (2014). Salt tectonic controls on deep-water turbidite depositional systems: Miocene, southwestern Lower Congo Basin, offshore Angola. Basin Research, Vo. 26, p. 597-620.

Pilcher, R. and Argent, J. (2007). Mega-pockmarks and linear pockmark trains on the West African continental margin. Marine Geology, Vo. 244, p. 15-32.

Plaza-Faverola, A., Bünz, S. and Mienert, J. (2010). Fluid distributions inferred from P-wave velocity and reflection seismic amplitude anomalies beneath the Nyegga pockmark field of the mid-Norwegian margin. Marine and Petroleum Geology, Vo. 27, p. 46-60.

PRSKALO, S. (2004). Application of relations between seismic amplitude, velocity and lithology in geological interpretation of seismic data: Journal of Hungarian Geomathematics, v. 2. ndash, Vo. 68, p. 51.

Raji, W. (2013). The use of seismic attenuation to indicate saturation in hydrocarbon reservoirs: Theoretical study and modelling approach. Advances in Applied Science Research, Vo. 2, p. 45-53.

Ren, H., Hilterman, F. J., Zhou, Z. and Kumar, M. (2006). Seismic Rock-Property Transforms for Estimating Lithology and Pore-Fluid Content. Vo.

Riis, F., Berg, K., Cartwright, J., Eidvin, T. and Hansch, K. (2005). Formation of large, crater-like evacuation structures in ooze sediments in the Norwegian Sea. Possible implications for the development of the Storegga Slide. Marine and Petroleum Geology, Vo. 22, p. 257-273.

Rise, L., Ottesen, D., Berg, K. and Lundin, E. (2005). Large-scale development of the mid-Norwegian margin during the last 3 million years. Marine and Petroleum Geology, Vo. 22, p. 33-44.

Robinson, E. S. (1988). Basic exploration geophysics. Vo.

Rønnevik, H. and Navrestad, T. (1977). Geology of the Norwegian Shelf between 62 N and 69 N. Geojournal, Vo. 1, p. 33-46.

Rønnevik, H., Bergsager, E., Moe, A., Øvrebø, O., Navrestad, T. and Stangenes, J. (1975). The geology of the Norwegian continental shelf. Petroleum and the Continental Shelf of North-West Europe, Vo. 1, p. 117–129.

Rønnevik, H., Eggen, S. and Vollset, J. (1983). Exploration of the Norwegian Shelf. Geological Society, London, Special Publications, Vo. 12, p. 71.

Satyavani, N., Thakur, N. K., Aravind Kumar, N. and Reddi, S. I. (2005). Migration of methane at the diapiric structure of the western continental margin of India — insights from seismic data. Marine Geology, Vo. 219, p. 19-25.

Savoye, B., Babonneau, N., Dennielou, B. and Bez, M. (2009). Geological overview of the Angola–Congo margin, the Congo deep-sea fan and its submarine valleys. Deep Sea Research Part II: Topical Studies in Oceanography, Vo. 56, p. 2169-2182.

Schoellkopf, N. B. and Patterson, B. A. (2000). AAPG Memoir 73, Chapter 25: Petroleum Systems of Offshore Cabinda, Angola. Vo.

Schroot, B. and Schuttenhelm, R. (2003). Expressions of shallow gas in the Netherland North Sea. Netherland s Journal of Geosciences, Vo. 82, p. 91-106.

Selnes, A., Strommen, J., Lubbe, R., Waters, K. and Dvorkin, J. (2013). Flat Spots-True DHIs or False Positives? In: 75th EAGE Conference and Exhibition incorporating SPE EUROPEC 2013.

Séranne, M. and Anka, Z. (2005). South Atlantic continental margins of Africa: a comparison of the tectonic vs climate interplay on the evolution of equatorial west Africa and SW Africa margins. Journal of African Earth Sciences, Vo. 43, p. 283-300.

Séranne, M. and Nzé Abeigne, C.-R. (1999). Oligocene to Holocene sediment drifts and bottom currents on the slope of Gabon continental margin (West Africa): Consequences for sedimentation and southeast Atlantic upwelling. Sedimentary Geology, Vo. 128, p. 179-199.

Seranne, M., Seguret, M. and Fauchier, M. (1992). Seismic super-units and post-rift evolution of the continental passive margin of southern Gabon. Bulletin de la Société Géologique de France, Vo. 163, p. 135-146.

Sheland er, D., Dai, J. and Bunge, G. (2010). Predicting saturation of gas hydrates using pre-stack seismic data, Gulf of Mexico. Marine Geophysical Researches, Vo. 31, p. 39-57.

Sheriff, R. E. (1975). Factors affecting seismic amplitudes. Geophysical Prospecting, Vo. 23, p. 125-138.

Sheriff, R. E. (1980). Nomogram for Fresnel-zone calculation. Geophysics, Vo. 45, p. 968-972.

Sheriff, R. E., Brown, A. R. and Lansley, R. M. (2010). Fundamentals of Reservoir Geophysics. Methods and Applications in Reservoir Geophysics, Vo., p. 101.

Sikkema, W. and Wojcik, K. (2000). 3D visualization of turbidite systems, Lower Congo Basin, offshore Angola. In: Deep-Water Reservoirs of the World, SEPM, Gulf Coast Section, 20th Annual Research Conference. SEPM, p. 928-939.

Skogseid, J. and Eldholm, O. (1989). Vøring Plateau continental margin: seismic interpretation, stratigraphy and vertical movements. In., p. 993-1030.

Skogseid, J., Planke, S., Faleide, J., Pedersen, T., Eldholm, O. and Neverdal, F. (2000). NE Atlantic continental rifting and volcanic margin formation. Dynamics of the Norwegian margin, Vo. 167, p. 295-326.

Smith, R. and Møller, N. (2003). Sedimentology and reservoir modelling of the Ormen Lange field, mid Norway. Marine and Petroleum Geology, Vo. 20, p. 601-613.

Smythe, D., Chalmers, J., Skuce, A., Dobinson, A. and Mould, A. (1983). Early opening history of the North Atlantic—I. Structure and origin of the Faeroe—Shetland Escarpment. Geophys. JR astr. Soc, Vo. 72, p. 373-398.

Solheim, A., Berg, K., Forsberg, C. and Bryn, P. (2005). The Storegga Slide complex: repetitive large scale sliding with similar cause and development. Marine and Petroleum Geology, Vo. 22, p. 97-107.

Storvoll, V., Bjrlykke, K. and Mondol, N. H. (2005). Velocity-depth trends in Mesozoic and Cenozoic sediments from the Norwegian Shelf. AAPG bulletin, Vo. 89, p. 359-381.

Storvoll, V., Bjrlykke, K. and Mondol, N. H. (2005). Velocity-depth trends in Mesozoic and Cenozoic sediments from the Norwegian Shelf. AAPG bulletin, Vo. 89, p. 359-381.

Stuevold, L. M., Faerseth, R. B., Arnesen, L., Cartwright, J. and Möller, N. (2003). Polygonal faults in the Ormen Lange field, Møre basin, offshore mid Norway. Geological Society, London, Special Publications, Vo. 216, p. 263-281.

Sun, Q. L., Cartwright, J., Wu, S. G. and Chen, D. X. (2013). 3D seismic interpretation of dissolution pipes in the South China Sea: Genesis by subsurface, fluid induced collapse. Marine Geology, Vo. 337, p. 171-181.

Taner, M. T. (2001). Seismic attributes. CSEG Recorder, Vo. 26, p. 48–56.

Taner, M. T., Koehler, F. and Sheriff, R. E. (1979). Complex seismic trace analysis. Geophysics, Vo. 44, p. 1041-1063.

Toms, J., Müller, T. M. and Gurevich, B. (2007). Seismic attenuation in porous rocks with rand om patchy saturation. Geophysical Prospecting, Vo. 55, p. 671-678.

Vadakkepuliyambatta, S., Bünz, S., Mienert, J. and Chand , S. (2013). Distribution of subsurface fluid-flow systems in the SW Barents Sea. Marine and Petroleum Geology, Vo. 43, p. 208-221.

Vågnes, E., Gabrielsen, R. and Haremo, P. (1998). Late Cretaceous-Cenozoic intraplate contractional deformation at the Norwegian continental shelf: timing, magnitude and regional implications. Tectonophysics, Vo. 300, p. 29-46.

Van Rensbergen, P. and Morley, C. K. (2003). Re-evaluation of mobile shale occurrences on seismic sections of the Champion and Baram deltas, offshore Brunei. Geological Society, London, Special Publications, Vo. 216, p. 395-409.

Van Rensbergen, P., Hillis, R. R., Maltman, A. J. and Morley, C. K. (2003). Subsurface sediment mobilization: introduction. Geological Society, London, Special Publications, Vo. 216, p. 1-8.

Vemba, J., Cunha, F., Brechet, E., Maultsch, S. and Toinet, S. (2011). 4D Monitoring: Example of 4D Interpretation In Lower Flanks Systems, Dalia-Angola. In.

Watts, N. (1987). Theoretical aspects of cap-rock and fault seals for single-and two-phase hydrocarbon columns. Marine and Petroleum Geology, Vo. 4, p. 274-307.

Weibull, W., Mienert, J., Bünz, S. and Hustoft, S. (2010). Fluid migration directions inferred from gradient of time surfaces of the sub seabed. Marine and Petroleum Geology, Vo. 27, p. 1898-1909.

Weimer, P. and Slatt, R. M. (2004). Petroleum systems of deepwater settings, Society of Exploration Geophysicists

Wood, W., Gettrust, J., Chapman, N., Spence, G. and Hyndman, R. (2002). Decreased stability of methane hydrates in marine sediments owing to phase-boundary roughness. Nature, Vo. 420, p. 656-660.

Yilmaz, Ö. and Doherty, S. M. (1987). Seismic data processing, Society of Exploration Geophysicists Tulsa, No. 2

Zeng, H. and Backus, M. M. (2005). Interpretive advantages of 90-phase wavelets: Part 1—Modeling. Geophysics, Vo. 70, p. C7-C15.

Zühlsdorff, L. and Spiess, V. (2004). Three-dimensional seismic characterization of a venting site reveals compelling indications of natural hydraulic fracturing. Geology, Vo. 32, p. 101-104.

http://www.open.edu/openlearn/science-maths-technology/science/environmental-science/earths-physical-resources-petroleum/content-section-3.2.1 on 08-09-2014

http://www.open.edu/openlearn/science-maths-technology/science/environmental-science/earths-physical-resources-petroleum/content-section-3.2.1 on 08-09-2014